VNIVERSITAT DE VALÈNCIA

UNIVERSITAT DE VALÈNCIA

PHD DISSERTATION

Programa de Doctorado en Física

The Origin of Flavor in Physics Beyond the Standard Model

Author:
Aurora MELIS

Thesis Director:
Prof. Óscar Manuel VIVES GARCÍA
Thesis Co-Director:
Dra. Maria Luisa LÓPEZ IBÁÑEZ

A thesis submitted in fulfillment of the requirements for the degree of Doctor of Philosophy in Physics

in the

FACULTAT DE FÍSICA

Departament de Física Teòrica

Deposito: September 3, 2020

Declaration of Authorship

I, Aurora MELIS, declare that this thesis titled, "The Origin of Flavor in Physics Beyond the Standard Model" and the work presented in it are my own. I confirm that:

- This work was done wholly or mainly while in candidature for a research degree at this University.
- Where any part of this thesis has previously been submitted for a degree or any other qualification at this University or any other institution, this has been clearly stated.
- Where I have consulted the published work of others, this is always clearly attributed.
- Where I have quoted from the work of others, the source is always given. With the exception of such quotations, this thesis is entirely my own work.
- I have acknowledged all main sources of help.
- Where the thesis is based on work done by myself jointly with others, I have made clear exactly what was done by others and what I have contributed myself.

Signed: 

Prof. **Óscar Manuel VIVES GARCÍA**, catedrático del Departamento de Física Teórica de la Universidad de Valencia,

CERTIFICA:

Que la presente memoria, "The Origin of Flavor in PhysicsBeyond the Standard Model", ha sido realizada bajo su dirección y la de la Dra. Maria Luisa LÓPEZ IBÁÑEZ en la Universidad de Valencia, por Aurora Melis, y constituye su Tesis para optar al grado de Doctor en Ciencias Físicas.

Y para que así conste, en cumplimiento de la legislación vigente, presenta en el Departamento de Física Teórica de la Universidad de Valencia la referida Tesis Doctoral, y firman el presente certificado.

Firma:

"Ora tu pensa: un pianoforte. I tasti iniziano. I tasti finiscono.
Tu sai che sono 88, su questo nessuno può fregarti. Non sono infiniti, loro.
Tu, sei infinito, e dentro quei tasti, infinita è la musica che puoi fare.
Loro sono 88. Tu sei infinito. "

— Novecento, A. Baricco.

UNIVERSITAT DE VALÈNCIA

Abstract

Facultat de Fisica

Departament de Física Teorica

Doctor of Philosophy

The Origin of Flavor in Physics Beyond the Standard Model

by Aurora MELIS

In this dissertation, we investigate the interplay between Supersymmetry and models based on different flavor symmetry groups: A_4, S_3, A_5 and $\Delta(27)$. The use of flavor symmetries is the most popular tool for model builders to tackle the Standard Model's flavor puzzle. A plethora of possible choices for the flavor symmetry and its breaking are consistent with the existing flavor data. A well-known problem of the SM is that we can not fully recover the fundamental flavor parameters of the SM Lagrangian, the Yukawa matrices. This problem is especially critical in the neutrino sector, where the Seesaw mechanism entangles the neutrino Yukawa couplings and the right-handed neutrino Majorana masses. Hence, we may never be able to detect which flavor symmetry lies behind the Origin of Flavor. Physics Beyond the Standard Model, which predicts new flavor interactions, like, for example, Supersymmetry, is probably the only opportunity to sort out the flavor puzzle. We show that the combination of bounds over lepton flavor violating processes, especially $\mu \to e\gamma$, can significantly restrict the parameter space of Supersymmetry well beyond direct searches and, at the same time, provide detached testable predictions to be (dis) proven by the upcoming flavor violation searches. For the most promising of these models, we also investigate the possibility of viable Leptogenesis. Finally, we discuss the constraints imposed by the anomalous magnetic moment $(g-2)_{\mu,e}$ and $\mu \to e\gamma$ on the leptonic Yukawa structure and propose a radiative flavon correction to the lepton masses as a possible solution.

Acknowledgements

First of all, I want to express my deepest gratitude to my thesis director, *Prof. Óscar Manuel Vives García*, for guiding me through this PhD-journey with his profound experience, endless patience and admirable humbleness. I am deeply indebted to my thesis co-director, *Dra. Maria Luisa López Ibáñez* for advising, inspiring and helping me as a big sister in so many different ways.

I was given a chance to make enriching visits to international institutes. My most sincere thanks goes to *Prof. Ivo de Medeiros Varzielas*, who warmly hosted me at the Instituto Tecnico de Lisboa, as well as to *Prof. Jinmin Yang*, who welcomed me at the Institute of Theoretical Physics of Beijing.

I much appreciated that *Prof. Lorenzo Calibbi* and *Prof. Ivo de Medeiros Varzielas* suggested corrections to this thesis. A special thanks to their kindness and invaluable insights on particle Physics.

Many heartfelt thanks go to my fantastic fellows at the Department of Theoretical Physics of the University of Valencia who shared with me many days of this journey and made them wonderful: *Nuria Carrasco Vela, Matteo Rinaldi, Manuel Martinez Quesada, Alberto Aparici Benages, Viníçius Rodrigues Debastiani, Michele Ronco, Leonardo Coito Pereyra, Silvia Pla García, Pablo Arnault, Fei Gao, Isabel Oldengott, Pablo Martínez Miravé, Roberto Bruschini, Clara Figueiredo, and Flavio Bombacigno*. There will never be enough pages to thank each one of them properly.

I could never forget to acknowledge the support of my lifelong friends, *Elisabetta Arcieri* and *Alessia Sarra*. They have the power to make any physical distance disappear.

Finally, I feel blessed by the existence of my beloved family — my parents, *Roberto and Emanuela*, and my lovely sister *Ambra* — who remind me every day of all the magnitudes we can not measure.

Thanking You.

Aurora MELIS

Contents

Abstract **ix**

Acknowledgements **xi**

Resumen de la tesis **xix**

Introduction **1**

I.1 Overview . . . 1
I.2 The Flavor puzzle . . . 9
I.2.1 Yukawa sector of the Standard Model . . . 11
I.2.2 Neutrino masses and mixings . . . 14
I.2.3 Sequential Dominance . . . 21
I.3 Leptogenesis . . . 23
I.4 Flavor Symmetries . . . 27
I.4.1 Froggatt-Nielsen mechanism . . . 27
I.4.2 Residual symmetries in model building . . . 30
I.4.3 Generalized CP symmetry . . . 35
I.5 The Origin of Flavor . . . 36
I.5.1 Supersymmetry . . . 37
I.5.2 Soft terms and the supersymmetric flavor problem . . . 41
I.5.3 Planck-scale-mediated soft terms . . . 44
I.5.4 Supersymmetry and Flavor Symmetries . . . 46
I.6 Flavor and CP Observables of interest . . . 48
I.6.1 Anomalous Magnetic Moment . . . 48
I.6.2 Lepton Flavor Violation . . . 51
I.6.3 Neutral Kaon Mixing . . . 56

1 Slepton non-universality in the flavor-effective MSSM **63**

1.1 Introduction . . . 64
1.2 A Review of the Mechanism . . . 66

1.3 A $\Delta(27)$ Model . . . 72
1.4 An A_4 Model . . . 77
1.5 An S_3 Model . . . 82
1.6 Conclusions . . . 86

2 Controlled flavor violation in the MSSM from a unified $\Delta(27)$ 89
2.1 Introduction . . . 90
2.2 A $\Delta(27)$ model for quarks and leptons . . . 91
2.3 Analysis of FV-effects . . . 94
2.3.1 Soft breaking terms . . . 94
2.3.2 Phenomenological results . . . 100
2.3.3 Comparisons with other models . . . 102
2.4 Conclusions . . . 103

3 LFV and neutrino masses from A_5 and CP in the non-universal MSSM 107
3.1 Introduction . . . 108
3.2 Flavor symmetries in supersymmetric theories . . . 109
3.3 Lepton masses and mixing from A_5 and CP . . . 112
3.3.1 Charged-lepton masses . . . 114
3.3.2 Neutrino masses . . . 117
3.3.3 Lepton Mixing . . . 121
3.3.4 Next-to-Leading Order Corrections . . . 122
3.4 Kähler Potential and Soft Terms . . . 124
3.4.1 Kähler corrections . . . 124
3.4.2 Soft-breaking Masses . . . 127
3.5 Predictions on flavor observables . . . 128
3.5.1 Neutrinos . . . 129
3.5.2 Charged Leptons . . . 131
3.5.3 Relations among observables . . . 135
3.6 Conclusions . . . 136

4 Leptogenesis in $\Delta(27)$ with a universal texture zero 141
4.1 Introduction . . . 142
4.2 Overview of the $\Delta(27)$ Model . . . 143
4.3 The UTZ seesaw mechanism . . . 147
4.4 Leptogenesis . . . 148
4.4.1 Boltzmann equations . . . 148
4.4.2 Decay factors and CP asymmetries . . . 150

4.5 Analysis and results . . . 152
4.5.1 Numerical results . . . 152
4.5.2 N_2 leptogenesis and comparison with other models . . . 155
4.6 Conclusions . . . 158

5 Muon and electron g-2 and lepton masses in flavor models 161
5.1 Introduction . . . 162
5.2 General Idea . . . 165
5.2.1 Lepton masses and $g-2$ contribution . . . 168
5.3 A $U(1)_f$ toy model . . . 172
5.3.1 Mass generation and $(g-2)_\ell$ . . . 175
5.4 Phenomenological implications . . . 176
5.5 Conclusions . . . 180

Appendix A 183
A.1 Rotations to the Physical basis . . . 183
A.1.1 Canonical rotation . . . 183
A.1.2 Yukawa diagonalization . . . 184
A.1.3 Canonical normalization and rotation to CKM basis . . . 185
A.2 Gaugino-slepton-lepton interaction . . . 186
A.3 Mass Insertion Approximation . . . 187

Appendix B 191
B.1 A_4 Group . . . 191
B.2 S_3 Group . . . 192
B.3 A_5 Group . . . 194

Appendix C 195
C.1 Boltzmann equations . . . 195
C.2 Seesaw with rank-one matrices . . . 197
C.3 Analytic expression for the leptogenesis parameters . . . 199

Appendix D 203
D.1 $V_{\rm PMNS}$ parametrization . . . 203
D.2 Bounds on Mass Insertions . . . 204

Appendix E 205
E.1 Minimization of the potential . . . 205

Resumen de la tesis

Contexto de investigación

El *Modelo Estándar* (SM), el modelo propuesto por Glashow, Salam y Weinberg a mediados de los años sesenta, es actualmente el modelo teórico que describe las interacciones electromagnéticas, débiles y fuertes de las partículas elementales conocidas. La descripción se implementa matemáticamente mediante una *teoría de gauge* basada en el grupo de simetría $SU(3)_C \otimes SU(2)_L \otimes U(1)_Y$ bajo el cual el lagrangiano queda invariante. Esta simetría se rompe espontáneamente en $SU(3)_C \otimes U(1)_{\text{em}}$ a través del mecanismo de Higgs. El contenido en partículas del SM puede dividirse en *fermiones* de materia (quarks y leptones), *bosones de gauge* que transportan la fuerza y el *bosón de Higgs*.

La física del sabor ha desempeñado un papel crucial en el desarrollo del SM, que se ha demostrado complementaria a las búsquedas directas para detectar nuevas partículas. El concepto de ***sabor*** es esencialmente la existencia de tres réplicas de cada fermión elemental. Podemos rastrear el origen del concepto a principios de 1947, cuando el experimento de Conversi, Pancini y Piccioni mostró que los muones μ de los rayos cósmicos no eran los mediadores de la fuerza nuclear, los piones predichos por Yukawa, sino, más bien, partículas parecidas a electrones pero 200 veces más pesadas. Ya en ese momento se propuso buscar la desintegración del muón a un electrón más un fotón $\mu \to e\gamma$.

En 1955, el límite superior de esta tasa de desintegración (BR) se estableció en 2×10^{-5}. Esto condujo a la hipótesis de "los dos neutrinos" en la cual dos neutrinos diferentes aparecen en la desintegración $\mu \to e\nu_\mu\overline{\nu}_e$, de forma que, dos números cuánticos adicionales se conservan: los ***números leptónicos*** L_μ y L_e. En consecuencia, la desintegración $\mu \to e\gamma$ debería estar prohibida, ya que, viola el número leptónico.

En 1947 también se descubrió el kaon, la primera partícula que contenía un quark extraño, aunque la existencia del quark extraño en sí (y la de los quarks up y down) solo se postularía en 1964 por Murray Gell-Mann y George Zweig. En el *Modelo de Quarks*

sugirieron que los hadrones no son partículas elementales y, por tanto, pueden clasificarse como estados ligados de sus quark y antiquarks de valencia up u, down d y extraños s.

A partir del mecanismo Glashow-Iliopoulos-Maiani (GIM) , que explica la pequeñez de la tasa de desintegración $K_L \to 2\mu$, el quark encanto c se predijo con éxito en 1970, antes de su descubrimiento en 1974 en Stanford Linear Accelerator Centro (SLAC) , contemporáneo al Brookhaven National Laboratory (BNL). La segunda generación de cada familia de partículas, μ, ν_μ, s y c, se había completado.

La observación inesperada de la violación de CP en la desintegración de los kaones neutros estableció la hipótesis de una tercera generación de quarks, que ganó fuerza después del descubrimiento en 1974-77 en SLAC de un tercer leptón, el τ. Se necesitaron unos años más para obtener una imagen completa, pues el quark b, inferior, no hizo su aparición hasta 1977 en Fermilab, mientras que, el quark superior t lo hizo en 1995. Notablemente su pesadez ya se predijo a partir del tamaño de la violación de CP en los kaones neutros y de las oscilaciones de mesones B neutros.

Los bosones de gauge W, Z se identificaron a principios de la década de 1980 en el Super Proton Synchrotron (SPS). Finalmente, el ν_τ apareció en 2000. La última pieza faltante del SM, el bosón de Higgs H, fue descubierta por los experimentos ATLAS y CMS en el Gran Colisionador de Hadrones (LHC) en 2012.

Hoy estamos acostumbrados a incluir la existencia de las tres generaciones en el SM: (e, μ, τ), (u, c, t) y (d, s, b), donde los únicos términos que distinguen entre las diferentes generaciones son las ***interacciones Yukawa*** de los fermiones con el Higgs. Se aprecia una gran redundancia innecesaria en el SM, pues la mayor parte de su contenido en partículas está formado por tres copias pesadas de las partículas más ligeras e, u y d.

En los siguiente años, el rol de la física del sabor derivó del descubrimiento de los componentes básicos del SM a la medición de sus parámetros. De hecho, la mayoría de ellos están relacionados con el sector del sabor y, por lo tanto, pueden determinarse en las descomposiciones que lo violan (FV). Con el desarrollo experimental y teórico, su determinación ha alcanzado una precisión impresionante y los procesos FV ahora se utilizan para imponer restricciones a la física de los Modelos más allá del Estándar (BSM). Las escalas de muy alta energía se pueden explorar de esta manera, superando notablemente las alcanzadas através de búsquedas directas de nuevas partículas en el LHC.

Motivación

Es comúmente aceptado el hecho de que el SM no es una teoría final, sino más bien una *teoría efectiva* válida hasta una escala de energía $\Lambda_{\rm NP}$ (de, al menos, varios TeV) donde entran en juego Nueva Física (NP) y grados dinámicos de libertad adicionales. De hecho, el SM está intrínsecamente incompleto porque no incluye la cuarta fuerza, la gravedad y no proporciona la esperada unificación de las interacciones fuertes y electrodébil. También deja abiertas muchas preguntas fundamentales, algunas relacionadas con las observaciones cosmológicas: el origen de la materia oscura y la energía oscura, que juntas llenan el 95 % de nuestro Universo, y asimetría bariónica del Universo (BAU).

El SM (mínimamente extendido para incluir masas de neutrinos) tampoco es satisfactorio como teoría de partículas porque carece de una explicación para el origen de sus estructuras de sabor, masas y mezclas. Aunque su capacidad de predicción depende de ellos, el SM no nos da ninguna pista sobre el valor de ninguno de los parámetros de sabor y, por ello, pueden considerarse como entradas externas necesarias para el modelo. Esto se conoce con el nombre de ***puzzle de sabor*** que, en última instancia, se traduce como nuestra total ignorancia acerca del origen de los acoplamientos Yukawa de los fermiones al Higgs.

La masa de Higgs en sí misma es inexplicablemente ligera considerando que recibe enormes correcciones cuánticas de los efectos virtuales de cada partícula u otros fenómenos que se acoplan al campo de Higgs. ¿Qué protege a la masa del bosón de Higgs de correcciones arbitrariamente grandes de la física a gran escala? Esto se conoce como el *problema de la jerarquía electrodebil* (EW).

De alguna manera es frustrante que, a pesar de haber sido ampliamente probado durante los últimos 50 años, todavía no hay ningún resultado experimental bien establecido que contradiga las predicciones del SM. La única excepción a este éxito es el descubrimiento de oscilaciones de neutrinos que demuestran que los neutrinos son masivos, a la vez que, se mezclan sus sabores. Si FV está bien establecida en el sector de quark, el lagrangiano del SM parece conservar explícitamente el sabor de los leptones cargados para cualquier interacción dada. Esta característica no se basa en ningún principio de gauge, sino que, es una simetría accidental del modelo que surge del minimalismo de la construcción, específicamente de la hipótesis de que los neutrinos no tienen masa, como se creía en ese momento. La observación de las oscilaciones de neutrinos demuestra que hay una violación del sabor leptónico (LFV) en el sector leptónico neutro.

Sorprendentemente, no existe aún ninguna evidencia similar que indique la violación del sabor de los leptones cargados (CLFV), a pesar de su incesante búsqueda a través de diferentes canales, tanto en experimentos especializados como en otros con un propósito más general. La búsqueda de CLFV, como la desintegración radiativa de leptones $\ell \to \ell'\gamma$ o la desintegración a tres cuerpos $\ell \to 3\,\ell'$, son muy prometedoras ya que, en el SM , todos los efectos de violación del sabor en el sector de leptones cargados son proporcionales a las diminutas masas de los neutrinos. Las tasas de desintegración de los leptones pesados con carga en aquellos más ligeros están suprimidos por la relación m_ν^2/M_W^2 y, por lo tanto, son demasiado pequeñas para ser medibles en cualquier experimento imaginable. De hecho, las masas tan absurdamente pequeñas de los neutrinos hacen que la tasa de desintegración del proceso $\mu \to e\gamma$ esté por debajo de 10^{-54} en el SM. Esto a su vez significa que cualquier observación de LFV probaría la existencia de la física BSM. Además, los procesos CLFV tienen la ventaja de ser teóricamente limpios porque son insensibles a los efectos de QCD no perturbacional que, en cambio, sí afectan a los observables en el sector de quark. La situación experimental actual y las perspectivas para la búsqueda de CLFV son ambiciosas : se espera alcanzar una BR $(\mu \to e\gamma) < 6 \times 10^{-14}$ y una tasa de conversión de muones en núcleos CR $(\mu - e)_N < 10^{-17}$ en un futuro cercano. Por ello, es importante estudiar el efecto de los modelos NP en estos observables para restringir su espacio de parámetros y dar predicciones comprobables.

Entre todas las ideas propuestas para abordar el puzzle del sabor, el uso de *simetrías de sabor*, que va desde el mecanismo más simple de Froggatt Nielsen (FN) hasta las simetrías discretas no Abelianas, sigue siendo la herramienta más popular para los creadores de modelos. Esta posibilidad ha sido especialmente explorada en el sector de leptones. Una plétora de opciones posibles para la simetría del sabor y su ruptura son consistentes con los datos de sabor existentes. Desafortunadamente, los modelos de sabor tienen la desventaja de ser poco predictivos.

Mediante asignaciones adecuadas de cargos de sabor a los diferentes campos, el tamaño de los acoplamientos de Yukawa depende sólo del parámetro adimensional $\epsilon = \langle\phi\rangle/M$, donde $\langle\phi\rangle$ es el valor esperado de vacío (VEV) del un campo escalar complejo ϕ, llamado ***flavon***, responsable de la ruptura de la simetría del sabor. Lo que implica que la dinámica del sabor puede ocurrir igualmente en la escala EW y en la escala de Planck. De hecho, según la orientación teórica, las simetrías de sabor a gran escala son más atractivas. El inconveniente de esta perspectiva es que probar teorías de tan alta escala, mediante búsquedas directas de flavones y mediadores FN en colisionadores, sería muy difícil si no imposible.

Un problema bien conocido a nivel de SM es que no podemos reconstruir completamente los parámetros de sabor fundamentales a partir de las matrices Yukawa del SM. En este sentido, los modelos NP, que predicen nuevas interacciones de sabor, son probablemente la única oportunidad que tenemos para poder resolver el puzzle de sabor. La Supersimetría es el ejemplo perfecto de esto.

La Supersimetría (SUSY) ha sido objeto de estudio intenso durante décadas y sigue siendo la opción más justificada y convincente para NP. La encarnación más simple de SUSY, el Modelo Estándar Supersimétrico Mínimo (MSSM), tiene muchas virtudes: un posible candidato a la materia oscura, nuevas fuentes de violación de CP, un mecanismo para estabilizar la masa del Higgs, la posibilidad de unificar las fuerzas fundamentales. Una transformación supersimétrica convierte un estado fermiónico en otro bosónico y viceversa. Un supermultiplete es una representación irreducible del álgebra de SUSY y, por lo tanto, debe contener un número igual de estados fermiónicos y bosónicos, supercompañeros entre sí con masas exactamente iguales. Todos los supercompañeros del SM son partículas nuevas, por lo que SUSY no puede permanecer exacta a la escala electrodébil, pues todos los supercompañeros ya habrían sido descubiertos.

Un modelo realista debe contener la ruptura de SUSY. Sin embargo, el mecanismo preciso a través del cual esta ocurre no es obvio y, por ello, es útil parametrizar nuestra ignorancia introduciendo ***soft terms*** efectivos en el lagrangiano. El espectro de masas de las superpartículas y, en consecuencia, la mayoría de las implicaciones fenomenológicas dependen de los soft terms. En principio, no tenemos información sobre su estructura y, si asumimos entradas genéricas $\mathcal{O}(1)$, los observables FV reciben contribuciones demasiado grandes en contradicción con los valores experimentales. Esto se conoce como el ***problema de sabor supersimétrico***.

La no observación de los supercompañeros predichos durante la fase 1 y 2 de toma de datos del LHC comienza a restringir una formulación tan mínima de supersimetría, apuntando a una escala de masa para las nuevas partículas más pesada de lo que se esperaba inicialmente. En el escenario donde SUSY se da, pero que queda fuera del alcance de los colisionadores actuales, podrian pasar décadas hasta conseguir la energía necesaria para producir los supercompañeros de forma directa. Buscar formas alternativas de sondear o restringir el gran espacio de parámetros disponible en el MSSM es urgente. Estudios a bajas energías con alta precisión, como perturbaciones a los procesos de LFV, pueden ser la clave para encontrar los efectos de esas particulas masivas.

Metodología y principales resultados por artículo

La física del sabor y la origen de las jerarquías de masas podrían dirigirnos hacia el encuetro de nueva física. En esta tesis consideramos que el problema del sabor de SUSY no puede separarse del problema del sabor del SM. De hecho, es natural pensar que el mismo mecanismo que genera las estructuras de sabor en los acoplamientos Yukawa también es responsable de la estructura en los términos de SUSY. En los artículos 1 - 3 mostramos explícitamente que las teorías SUSY complementadas por una simetría de sabor son modelos extremadamente predictivos.

- En **Artículo 1:** Analizamos las estructuras de sabor en teorías supersimétricas donde el MSSM surge como una teoría efectiva a baja energía a partir de una simetría de sabor rota a escalas más altas. Estudié en detalle tres modelos de sabor representativos con grupos de simetría discreta $\mathcal{G}_\ell = \Delta(27)$, A_4, y S_3 y proporcioné una descripción completa en un contexto supersimétrico, que faltaba en la literatura. Esto demostró que los diferentes modelos de sabor se pueden distinguir sistemáticamente a través de las diferentes estructuras de los términos de ruptura suave SUSY, específicamente mediante los acoplamientos trilineales y las matrices de masas supersimétricas. Las matrices deben obtenerse a la escala EW por medio de las ecuaciones del grupo de renormalización del MSSM (RGE), y compararse con los observables de sabor más relevantes. Realicé los cálculos numéricos correspondientes, junto a los asociados al espectro de masas a baja energía, a través del paquete Supersymmetric Phenomenology (SPheno), junto con el paquete SARAH de Mathematica para generar el código fuente, oportunamente automatizado a través de scripts en Bash.
  Los resultados demuestran que la combinación de límites sobre los procesos LFV, especialmente $\mu \to e\gamma$, puede restringir significativamente el espacio de parámetros SUSY mucho más allá del alcance de la actualización a alta luminosidad del LHC. Los procesos de FV limitan los modelos de sabor de diferentes maneras y conducen a diferencias cualitativas e, incluso, cuantitativas que el espacio de parámetros y, en algunos casos, permite distinguir entre los modelos de sabor que, de otro modo, serían difíciles de discriminar al aumentar únicamente la precisión de las masas de fermiones y los parámetros de mezcla.

- En **Artículo 2:** Sobre la base de estos resultados prometedores, apliqué este tipo de análisis a un modelo reciente basado en una simetría de sabor $\Delta(27)$ con una atractiva estructura de las matrices de masa de los fermiones que involucra un *texture zero* universal para todos ellos. Consideramos que este es un modelo

de sabor particularmente interesante, ya que, además, es compatible con una unificación gauge total subyacente basada en el grupo $SO(10)$ y que hace varias postdicciones importantes como, por ejemplo, la relación Gatto-Sartori-Tonin entre el ángulo de Cabibbo y las relaciones de masa de quark. Además, predice el esquema de mezcla tribimaximal (TBM) fenomenológicamente exitoso para los leptones. Los grandes efectos de FV, incluidos los observables de CP en el sector kaon, restringen el espacio de parámetros del modelo, lo que permitirá comprobarlo mediante búsquedas de violación de sabor en la próxima década. El estudio indica que para los valores típicos preferidos por el mecanismo de alineación del vacío del modelo, las limitaciones se vuelven particularmente severas, lo que implica que las suposiciones como las masas de mensajeros universales son demasiado simples y deben abandonarse.

En los últimos años, diferentes experimentos han acumulado una gran cantidad de datos experimentales sobre parámetros de neutrinos que nos han permitido derivar con una precisión razonable la matriz de mezcla Pontecorvo-Maki-Nakagawa-Sakata (PMNS) y las diferencias entre las masas de los neutrinos. Aún así, la determinación de la escala absoluta de masa de los neutrinos y la fase de Dirac CP aún no se ha llevado a cabo. Futuros experimentos arrojarán luz sobre estas cantidades. Probablemente el problema más urgente de la física de los neutrinos esté relacionado con la naturaleza intrínseca de los neutrinos. Como partículas masivas sin carga, pueden ser Dirac (con partículas y antipartículas siendo objetos diferentes) o Majorana (siendo las partículas y antipartículas las mismas).

Si los neutrinos son partículas de Majorana, las masas pequeñas se describen bien a través de un operador de Weinberg en el SM. Pero existen diferentes posibilidades para generar este operador efectivo a partir de una teoría más fundamental a energías más altas, como el seesaw tipo I, tipo II o tipo III, modelos de masa radiativa, etc. El mecanismo del seesaw, en todas sus realizaciones, ofrece una explicación natural de por qué los neutrinos son mucho más ligeros que los otros fermiones y aclara por qué los neutrinos de Majorana han sido tan populares.

Sin embargo, está claro que tan solo la medición de las masas de los neutrinos y sus ángulos de mezcla no será suficiente para discriminar entre los diferentes mecanismos ni inferir los acoplamientos responsables para ellos. Por ejemplo, para un mecanismo de seesaw de tipo I, los acoplamientos Yukawa de neutrinos y la masa Majorana de neutrinos dextrógiros se combinan para generar el operador Weinberg, pero el SM no proporciona información para poder separarlos a partir de los datos experimentales disponibles. Incluso una determinación completa de la matriz de

masa de los neutrinos no será suficiente para reconstruir el mecanismo responsable y descubrir el origen de los patrones de sabor observados.

- En **Artículo 3:** Generalizando los análisis de los Artículo 1 y 2, analizamos las consecuencias fenomenológicas de incluir una simetría de sabor basada en los grupos A_5 y CP en un marco supersimétrico. Nos concentramos en el sector leptónico donde se supone que se conservan dos simetrías residuales diferentes para leptones cargados y neutros, en primera aproximación.
  Investigué todas las realizaciones posibles para generar masas de neutrinos a *tree-level* y calculé el conjunto mínimo de operadores efectivos pertenecientes al potencial Kähler y las masas *soft* para los campos LH y RH. Sin supuestos adicionales sobre la teoría UV, los operadores propuestos están siempre presentes y no pueden evitarse mediante la introducción de simetrías adicionales.
  Para las simetrías residuales consideradas aquí, hemos encontrado que la presencia de mediadores de LH es especialmente relevante y que los flavones asociados con masas de neutrinos también inducen violación del sabor en el sector de leptones cargados. Esto permite un análisis combinado de observables de neutrinos y procesos LFV.
  Escaneé el espacio de parámetros para cada caso e implementé los códigos para una automatización de SPheno que permitió un análisis combinado de algunos observables de neutrinos como las masas efectivas $m_{\beta\beta}$ y m_β, junto con los procesos LFV. De hecho, el origen común de las masas de los neutrinos y la violación del sabor de los leptones cargados induce predicciones comprobables que relacionan el espectro de los neutrinos, la mezcla de leptones y los procesos de LFV. Se encontró una buena complementariedad entre los dos sectores.

Aunque el SM incluye todos los ingredientes necesarios para generar el BAU dinámicamente, la asimetría obtenida en el SM es demasiado pequeña por órdenes de magnitud. Sin embargo, es bien sabido que extender el SM con varios neutrinos dextrógiros (RH) pesados puede producir una BAU a través del mecanismo de ***leptogénesis***. Las desintegraciones que violan el número leptónico de los neutrinos RH, algunas de las cuales se producen fuera de equilibrio, producen una asimetría de leptones. Esto se convierte parcialmente en una asimetría bariónica por las interacciones de esfalerones, que son eficientes por encima de la escala electrodébil. Los neutrinos RH pesados proporcionan simultáneamente una respuesta natural a la pequeñez de las masas de neutrinos levógiros (LH) a través del mecanismo de seesaw.
Es interesante observar que, dado que los neutrinos RH son singletes del SM, leptogénesis vincula la resolución de la BAU a sus acoplamientos Yukawa y, por lo tanto, se

conecta con el rompecabezas del sabor. Si el seesaw es, en efecto, el origen de las masas de los neutrinos ligeros entonces, cualitativamente, leptogénesis es inevitable. Determinar si reproduce con precisión el BAU observado se convierte en una pregunta cuantitativa directamente ligada a un espectro dado de neutrinos RH y sus interacciones con las partículas del SM.
Sorprendentemente, el modelo original (y posiblemente el más simple) de leptogénesis requiere una escala de neutrinos RH $M > 10^9$ GeV, que se corresponde estrechamente con la escala natural del seesaw. Un modelo completo debería dar cuenta de la BAU observada, lo cual proporciona restricciones adicionales para sus parámetros. En particular, como veremos en esta tesis, la coincidencia con la BAU observada nos permite restringir los parámetros, por lo demás desconocidos, del sector de neutrinos RH.

- En **Artículo 4:** Investigamos la posibilidad de una leptogénesis viable en el modelo $\Delta(27)$ introducido en el Artículo 2. Resolví numéricamente las ecuaciones de Boltzmann con sabor para las asimetrías de los leptones, teniendo en cuenta el desacoplamiento gradual de los neutrinos dextrógiros N_1 y N_2.
  El escenario dominado por N_1 resultó ser exitoso y la opción más natural para el modelo, con $M_1 \in [10^9, 10^{12}]$ GeV, que restringe el espacio de parámetros del modelo subyacente y produce límites inferiores en los respectivos acoplamientos Yukawa. Leptogénesis es también posible en el escenario dominado por N_2, con la asimetría en el sabor de los electrones protegida de la dilución generada por N_1 a través del texture zero.
  Sin embargo, esto ocurre en una región de espacio de parámetros que tiene una jerarquía de masa demasiado fuerte , con M_2 relativamente cerca de M_3, lo cual no puede justificarse mediante el modelo $\Delta(27)$.

Los últimos años han sido testigos del surgimiento de varios indicios que apuntan hacia fenómenos no estándar a partir de observables de precisión que involucran sabores de leptones. LHCb y factorías de B han anunciado señales que muestran una desviación en la universalidad de los acoplamientos leptónicos pronosticados por el SM en desintegraciones semileptónicas de estos mesones, tanto en procesos neutros como cargados. Si los datos futuros lo confirman, estas discrepancias ciertamente requerirían un nuevo acoplamiento físico a baja escala de diferente intensidad para diferentes familias de leptones.
Otra discrepancia que apuntaría a una conclusión análoga está relacionada con el momento magnético anómalo del muón, $(g-2)_\mu$. Las mediciones experimentales de $(g-2)_\mu$ han estado en tensión con los cálculos teóricos cada vez más precisos dentro

del SM durante aproximadamente 20 años. La discrepancia actualmente asciende a alrededor de 3.5σ. La situación puede aclararse, con el caso de nueva física posiblemente reforzado, a través de los próximos resultados del nuevo experimento Muon g-2 en FNAL. Curiosamente, otra tensión de 2.4σ entre la teoría y los experimentos también ha aparecido recientemente para el electrón. El $(g-2)_e$ se ha determinado tanto experimental como teóricamente con una precisión tan sobresaliente, que la coincidencia de la predicción SM con la medición se ha utilizado durante muchos años como la forma más precisa de evaluar la constante de estructura fina α. Sin embargo, en presencia de una medida alternativa y suficientemente precisa de α, se puede emplear $(g-2)_e$ como prueba para testear la presencia de nueva física también.
Para un modelo genérico, una contribución considerable del momento magnético anómalo, según lo requerido por las discrepancias observadas, está intrínsecamente relacionada con los procesos LFV y la generación de masa. Cómo suprimir estas contribuciones es un tema que a menudo no se aborda explícitamente en la literatura.

- En **Artículo 5:** Proponemos un mecanismo original en el que la realización de las correcciones al $(g-2)_\ell$ del muón y del electrón se relacionan manifiestamente con la generación de sus masas a través de una simetría de sabor. Calculando los diagramas de Feynman correspondientes y estudiando el espacio de parámetros, analicé si una corrección de flavones radiativos a la masa de fermiones puede dar una contribución considerable al momento magnético anómalo. La respuesta es positiva si introducimos una amplificación quiral a partir de un acoplamiento cuántico no trivial en el potencial escalar.
  La masa radiativa recibe el mismo realce y contribuye significativamente a la generación de masa; esto establece un límite en el tamaño de la contribución $g-2$. Los diagramas FN y radiativo, con signos opuestos, contribuyen a las masas de electrones y muones mediante una cancelación que acomoda la diferencia experimental de signo entre las discrepancias de momento magnético de electrones y muones.
  Demostramos que las anomalías presentes para muones y electrones pueden explicarse simultáneamente en una vasta región del espacio de parámetros con masas para los mediadores vectores tan grandes como $M_\chi \in [0.6, 2.5]$ TeV que podrían conducir a señales observables en el LHC o en futuros colisionadores de leptones. Para mostrar explícitamente esto, construí un modelo sencillo ilustrativo basado en $U(1)_{\rm FN}$. La aplicación a un modelo completo, incluyendo los sectores de los quarks y neutrinos y el estudio de sus consecuencias fenomenológicas en la física del sabor se deja para trabajos futuros.

Introduction

I.1 Overview

Research Context

The *Standard Model* (SM), the model proposed by Glashow, Salam, and Weinberg in the middle sixties, is to present-day the theoretical model describing the electromagnetic, weak and strong interactions of the known elementary particles. The description is mathematically implemented by a gauge theory based on the $SU(3)_C \otimes SU(2)_L \otimes U(1)_Y$ symmetry group under which the Lagrangian is left invariant. This symmetry is spontaneously broken down to $SU(3)_C \otimes U(1)_{\text{em}}$ via the Higgs mechanism. The particle content of the SM can be divided into matter *fermions* (quarks and leptons), force-carrying gauge *bosons* and the *Higgs boson*.

Flavor physics has played a central role in the development of the SM, proven complementary to direct searches for sniffing out new particles. The concept of *flavor* is essentially the existence of three replicas of each elementary fermion.

We can track down the origin of the concept at the beginning of 1947 when the experiment of Conversi, Pancini, and Piccioni showed that the muons μ from cosmic rays were not the mediators of the nuclear force, the pions predicted by Yukawa, but rather electron-like particles although with 200 times its mass. At the time, the opportunity to search for the decay of the muon into an electron plus a photon, $\mu \to e\gamma$, was already put forward.

In 1955 the upper limit on this branching ratio (BR) was set to 2×10^{-5}. This led to the two neutrino hypothesis in which two different neutrinos appear in the decay $\mu \to e\nu_\mu\overline{\nu}_e$ in order to respect the conservation of two additional quantum numbers: the *lepton numbers* L_μ and L_e. Accordingly, the decay $\mu \to e\gamma$ must be forbidden as it violates the lepton numbers L_i.

In 1947 the kaon was also discovered, the first particle containing a strange quark. However, the existence of the strange quark (and that of the up and down quarks)

was only postulated in 1964 by Gell-Mann and Zweig in the *Quark Model*. They suggested that hadrons are not elementary particles, and can be classified as bound states of their valence up u, down d, and strange s quarks and antiquarks.
From the Glashow-Iliopoulos-Maiani (GIM) mechanism to explain the smallness of the $K_L \to 2\mu$ decay rate, the charm quark c was successfully predicted in 1970, before its discovery in 1974 at Stanford Linear Accelerator Center (SLAC) and contemporary at the Brookhaven National Laboratory (BNL). The second generation of each family of particles, μ, ν_μ, s and c, was complete.
The observation of CP violation in neutral kaons decays set forth the hypothesis of a third generation of quarks, which gained strength after the discovery in 1974-77 at SLAC of a third lepton, the τ. It took a few more years to get the full picture, the bottom quark b made its appearance in 1977 at Fermilab and the top quark t in 1995, remarkably the size of CP violation in the neutral kaons and of the neutral B meson oscillations predicted its heaviness.
The gauge bosons W, Z were identified in the early 1980s at the Super Proton Synchrotron (SPS). Finally, the ν_τ appeared in 2000. The last lacking piece of the SM, the Higgs boson H, was discovered in 2012 by the ATLAS and CMS experiments at the Large Hadron Collider (LHC).
Today we are used to including the existence of the three generations in the SM: (e, μ, τ), (u, c, t) and (d, s, b), where the only terms that distinguish between different generations are the *Yukawa interactions* of the fermions with the Higgs. We see that there is much unnecessary redundancy in the SM, three heavy copies of the lighter e, u and d particles made up most of its particle content.
From the discovery of the building blocks of the SM, afterward the role of flavor physics shifted to the measurement of its parameters. Indeed, the majority of the SM parameters are related to the flavor sector and can thus be determined in flavor violating (FV) decays. With increasing experimental and theoretical accuracy, their determination has by now reached an impressive precision, and FV processes are now employed to constrain physics Beyond the Standard Model (BSM). Very high energy scales can be probed in this way, well beyond the reach of direct searches for new particles at LHC.

Motivation

It is commonly accepted that the SM is not a final theory but rather an *effective theory* valid up to an energy scale $\Lambda_{\rm NP}$ (at least of several TeVs) where New Physics (NP) enters, and extra dynamic degrees of freedom come into play. As a matter of fact, the

SM is intrinsically incomplete because it does not include the fourth strength, gravity, and does not provide a unification of the strong and electroweak interactions. It also leaves open many fundamental questions, some related to cosmology observations: the origin of Dark Matter and Dark Energy, which together fill 95% of our Universe, and the Baryon Asymmetry of the Universe (BAU).
The SM (minimally extended to include neutrino masses) is also unsatisfactory as a particle theory because it lacks an explanation for the origin of its flavor structures, masses, and mixings. Although its predicting ability relies on them, the SM gives no clue about the value of any of the flavor parameters, and they can be regarded as necessary external inputs of the model. This goes under the name of *flavor puzzle*, which ultimately is our complete ignorance of the origin or the Yukawa couplings of the fermions to the Higgs.
The Higgs mass itself is inexplicably light, considering that it receives enormous quantum corrections from the virtual effects of every particle or other phenomena that couple to the Higgs field. What protects the Higgs boson mass from arbitrarily large corrections from physics at a high scale? This is known as the electroweak (EW) *hierarchy problem*.
It is somehow frustrating that, despite being extensively tested during the last 50 years, there is yet no established experimental result that contradicts the SM predictions. The only exception to this success was the discovery of neutrino oscillations, which proved that neutrinos are massive as they undergo flavor mixing. While FV in the quark sector is established, the SM Lagrangian explicitly conserves lepton flavor in any given interaction. This feature does not arise from a gauge principle. It is an accidental symmetry of the SM, which arises from the minimality of the construction, specifically from the hypothesis that neutrinos were massless, as observed at that time. The observation of neutrino oscillations demonstrates that there is a lepton flavor violation (LFV) in the leptonic neutral sector.
Although the search for such a violation has been pursued in a host of channels both at dedicated and general-purpose experiments, surprisingly enough, there is yet no evidence of Lepton flavor Violation in processes involving charged leptons (CLFV). The search for CLFV, such as the radiative lepton decays $\ell \to \ell'\gamma$ and the three-body charged lepton decays $\ell \to 3\,\ell'$, is very promising, since in the SM all flavor violating effects in the charged lepton sector are proportional to the tiny neutrino masses. The ratio m_ν^2/M_W^2 suppresses the decay rates of heavy charged leptons into lighter ones, which are by far too small to be measurable in any foreseeable experiment: $\mu \to e\gamma$ is limited to be below 10^{-54} in the SM. This, in turn, implies that any observation of LFV would prove the existence of BSM physics. Besides, LFV processes are theoret-

ically clean because they are not affected by the non-perturbative QCD effects that affect the observables in the quark sector. The current experimental situation and prospects for the search for CLFV are ambitious. We expect $\mathrm{BR}(\mu \to e\gamma) < 6 \times 10^{-14}$ and muon conversion into Nuclei to reach $\mathrm{CR}(\mu - e)_N < 10^{-17}$ in the near future. Therefore, it is necessary to study the effect of NP models on these observables to constrain their parameter space and give testable predictions.

Among the proposed ideas to tackle the flavor puzzle, the use of *flavor symmetries*, from the simplest Froggatt Nielsen (FN) mechanism down to non-Abelian discrete symmetries, remains the most popular tool for model builders. This avenue has been especially explored in the lepton sector. One well-known problem of the SM is that we cannot fully reconstruct the fundamental flavor parameters of the SM Lagrangian, the Yukawa matrices. In this respect, NP models that predict new flavor interactions are probably the only opportunity to sort out the flavor puzzle. Supersymmetry is a perfect example of this.

Supersymmetry (SUSY) has been at the center of extensive research for decades and is still the most motivated and compelling option for NP. The simplest incarnation of SUSY, the Minimal Supersymmetric Standard Model (MSSM), has many virtues: a possible dark matter candidate, new sources of CP violation, a mechanism for stabilizing the mass of the Higgs, the possibility for unification of the fundamental forces. A SUSY transformation turns a fermionic state into a bosonic one and vice versa. A supermultiplet is an irreducible representation of the SUSY algebra and therefore, must contain an equal number of fermionic and bosonic states, superpartners of each other with exact equal masses. All of the superpartners of the SM are new particles. Thus SUSY can not remain unbroken at the electroweak scale, or we would have already discovered all the superpartners.

A realistic model must contain SUSY breaking. However, the precise mechanism through which the breaking occurs is not apparent, and it is useful to parametrize our ignorance introducing effective *soft terms* in the Lagrangian. The mass spectrum of the superparticles and, consequently, most of the phenomenological implications depend on the soft terms. In principle, we have no information on their structure, and if we assume generic $\mathcal{O}(1)$ entries, FV observables would receive too large contributions, this is also known as the *supersymmetric flavor problem*. The non-observance by the LHC in Runs 1 and 2 of any of its predicted superpartners constrains such a minimal realization of supersymmetry, pointing to a mass scale of the new predicted particles heavier than naively expected. In the scenario where SUSY is indeed realized by nature, but out of reach of current colliders, we should look for further ways to (dis)probe or constrain the large parameter space available in the MSSM.

Methodology and main results per article

In this thesis we take the point of view that the SUSY flavor problem can not be detached from the SM flavor problem. Indeed, it is natural to think that the same mechanism generating the flavor structures in the Yukawa couplings is also responsible for the structure in the SUSY soft-breaking terms. In Article 1-3, we explicitly show that SUSY theories supplemented by a flavor symmetry are extremely predictive models.

- In **Article 1:** We analyzed the flavor structures in supersymmetric theories where the MSSM arises as a low energy effective theory from a flavor symmetry broken at higher scales. I studied in detail three exemplifying flavor models with discrete symmetry groups $\mathcal{G}_\ell = \Delta(27)$, A_4, and S_3 and provided a complete description in a supersymmetric context, which was missing in the literature. This showed that different flavor models can be distinguished systematically through the different structures of the SUSY soft-breaking terms, specifically the trilinear couplings and supersymmetric mass matrices.
  The matrices must be evolved to the EW scale by means of the MSSM renormalization group equations (RGE), and compared to the most relevant flavor observables. I performed the numerical calculations for the running, spectrum and low energy processes through the Supersymmetric Phenomenology package (SPheno), together with the SARAH Mathematica package to generate the source code, opportunely automatized through Bash scripts.
  The results prove that the combination of bounds over LFV processes, especially $\mu \to e\gamma$, can significantly restrict the SUSY parameter space far beyond the reach of the LHC high-luminosity upgrade. FV processes constrain flavor models in different ways and lead to qualitative and even quantitative differences that are able to constrain the parameter space of flavor models and even distinguish flavor models that would otherwise be hard to discriminate by solely increasing the precision of fermion masses and mixing parameters.

- In **Article 2:** Building on these promising results, I applied this type of analysis to a recent model based on a $\Delta(27)$ flavor symmetry with a nice unified texture zero structure for the fermion mass matrices. We considered this an appealing flavor model as it is consistent with an underlying $SO(10)$ grand unification and makes several important postdictions, for example the Gatto-Sartori-Tonin relation between the Cabibbo angle and the quark mass ratios. Additionally it predicts the phenomenologically successful tribimaximal (TBM)

mixing scheme for the leptons. The large FV effects, including CP-observables in the kaon sector, constrain the parameter space of the model, allowing it to be (dis)proven by flavor violation searches in the next decade.

In recent years, different experiments have accumulated a wealth of experimental data on neutrino parameters that have allowed us to derive with reasonable precision the Pontecorvo-Maki-Nakagawa-Sakata (PMNS) mixing matrix and the neutrino mass differences. Still, the determination of the absolute neutrino mass scale and the Dirac CP phase remain to be completed. Next to future experiments will shed light on these quantities.
If neutrinos are Majorana particles, the smallness of their masses is well described by adding a Weinberg operator to the Standard Model (SM). There are different possibilities to generate this effective operator from a more fundamental theory at higher energies, like type I, type II, or type III Seesaw, radiative mass models, etc. The measurement of neutrino masses and mixing angles alone will not be enough to discriminate among these alternative mechanisms and to infer the couplings responsible for them. For instance, for a type-I Seesaw mechanism, both the neutrino Yukawa couplings and the right-handed neutrino Majorana mass combine to generate the Weinberg operator. However, the SM does not provide information to disentangle them from the available experimental data. Even a full determination of the neutrino mass matrix will not be enough to fix the mechanism responsible for it and uncover the origin of the observed flavor patterns.

- In **Article 3:** Generalizing the analysis of Article 1 and 2, we analyzed the phenomenological consequences of embedding a flavor symmetry based on the groups A_5 and CP in a supersymmetric framework. We concentrate on the leptonic sector where two different residual symmetries are assumed to be conserved at leading order for charged and neutral leptons.
  I investigated all the possible realizations to generate neutrino masses at tree level and computed the minimal set of effective operators entering the Kähler potential and soft masses for LH and RH fields. I scanned the parameter space for each case and implemented the codes for an automatization of SPheno that allowed for a combined analysis of neutrino observables, like the neutrino effective mass $m_{\beta\beta}$ and m_β, together with LFV processes. In fact, the common origin of neutrino masses and flavor violation for charged leptons, induce testable predictions that relate the neutrino spectrum, lepton mixing and LFV processes. A nice complementarity between the two sectors has been found.

It is well-known that extending the SM by several heavy right-handed (RH) neutrinos can yield a BAU via leptogenesis. Lepton number-violating decays of the RH neutrinos, some portion of which occur out of equilibrium, produce a lepton asymmetry. This is partially converted into a baryon asymmetry by sphaleron interactions, which are efficient above the electroweak scale. Heavy RH neutrinos simultaneously provide a natural answer to the smallness of left-handed (LH) neutrino masses via the Seesaw mechanism.
It is interesting to note that since RH neutrinos are SM singlets, leptogenesis links the resolution of the BAU with their Yukawa couplings, and thus connects with the flavor puzzle. If Seesaw is indeed the origin of light neutrino masses, then qualitatively leptogenesis is unavoidable. Whether it accurately reproduces the observed BAU becomes a quantitative question for a given spectrum of RH neutrinos and their interactions with SM particles.
Remarkably, the original (and arguably simplest) model of leptogenesis requires a RH neutrino scale $M > 10^9$ GeV, which closely corresponds to the natural Seesaw scale. A complete model ought to account for the observed BAU, which provides additional constraints on its parameters. In particular, as we shall see in this analysis, matching to the observed BAU allows us to constrain the otherwise unknown parameters of the RH neutrino sector.

- In **Article 4:** We investigated the possibility of viable leptogenesis in the $\Delta(27)$ model introduced in Article 2. I solved numerically the flavored Boltzmann equations for the lepton asymmetries, taking into account both N_1 and N_2 right handed neutrino decays. The N_1-dominated scenario is successful and the most natural option for the model, with $M_1 \in [10^9, 10^{12}]$ GeV, which constrains the parameter space of the underlying model and yields lower bounds on the respective Yukawa couplings. Viable leptogenesis is also possible in the N_2-dominated scenario, with the asymmetry in the electron flavor protected from N_1 washout by the texture zero. However, this occurs in a region of parameter space which has a stronger mass hierarchy and M_2 relatively close to M_3, which is not a natural expectation of the $\Delta(27)$ model.

Recent years have been witnessing the arising of several hints for non-standard phenomena from precision observables involving lepton flavors. Signs of departure from the universality of leptonic couplings predicted by the SM in semi-leptonic decays of B mesons have been reported by LHCb and B-factories experiments both in neutral and charged current processes. If confirmed by future data, these discrepancies would certainly require low-scale new physics coupling with different strength to

different lepton families.
Another discrepancy that would point to an analogous conclusion is related to the anomalous magnetic moment of the muon, $(g-2)_\mu$. The experimental measurements of $(g-2)_\mu$ have been in tension with the increasingly accurate theoretical calculations within the SM for about 20 years. The discrepancy currently amounts to about 3.5σ. The situation may be clarified, and the case for new physics possibly reinforced, by the upcoming results of the new Muon g-2 experiment at FNAL. Interestingly, a 2.4σ tension between theory and experiments has been recently reported also for the electron. The $(g-2)_e$ has been determined both experimentally and theoretically to such an outstanding precision, that matching the SM prediction to the measurement has been used for many years as the most precise way to evaluate the fine-structure constant α. However, in presence of an alternative and sufficiently precise measurement of α, one can employ $(g-2)_e$ as a test for new physics too.
For a generic model, a sizeable contribution of the anomalous magnetic moment, as required by the observed discrepancies, is intrinsically related to LFV processes a to the mass generation. How to suppress these contributions is an issue that often is not explicitly addressed in literature.

- In **Article 5:** We propose an original mechanism in which the realization of the muon and electron $(g-2)_\ell$ corrections are manifestly related to the mass generation through a flavor symmetry. Computing the corresponding Feynman diagrams and studying the parameter space, I analyzed if a radiative flavon correction to the fermion mass can give a sizable contribution to the anomalous magnetic moment. The answer is positive if we introduce a chiral enhancement from a non-trivial quartic coupling of the scalar potential.
  We showed that the muon and electron anomalies can be simultaneously explained in a vast region of the parameter space with predicted vector-like mediators of masses as large as $M_\chi \in [0.6, 2.5]$ TeV that could lead to signatures observable at the LHC or at future lepton colliders. To explicitly show this I built an explicit $U(1)_{\rm FN}$ toy model.

In the rest of this Introduction I want to address the main topics that the reader will encounter in this dissertation, pointing out the connection between them and summarizing the necessary nomenclature. Every introduced argument has a large associated literature and we will always redirect the curious reader to it for further insights.

I.2 The Flavor puzzle

Not including neutrinos, nineteen is the number of the free parameters of the SM [1]. Of these, only five are flavor blind: the three gauge couplings (g_1, g_2, g_3), the Higgs quartic coupling λ and the Higgs mass μ^2, while fourteen reside in the flavor sector of the SM. Six quark masses $(m_u, m_d, m_s, m_c, m_b, m_t)$, three charged lepton masses (m_e, m_μ, m_τ), three quark mixing angles $(\theta^q_{12}, \theta^q_{23}, \theta^q_{13})$, one weak CP violating phase δ^q and the strong CP violating parameter $\overline{\theta}$. If we include the neutrino sector, nine additional parameters have to be introduced: three neutrino masses (m_1, m_2, m_3), three lepton mixing angles $(\theta^\ell_{12}, \theta^\ell_{23}, \theta^\ell_{13})$ and, in case of Majorana neutrinos, three CP violating phases $(\delta^\ell, \alpha, \beta)$. The experimental value of these parameters is constantly improving in precision and updated values are collected in Tab. I.1. Nonetheless, within the SM these parameters can only be accommodated and not explained. Looking closely at Tab. I.1 several questions might arise

- Why are there three generations of each SM fermion field, in the same representation of the gauge group, differing only by their mass?
- Why do the charged fermion masses exhibit a strong hierarchical structure ranging some six orders of magnitude, from 10^{-4} to 10^2 GeV?
- Why do neutrino masses exhibit a milder hierarchy and are so much smaller than the charged fermion masses, of the order of meV?
- Why are the mixing angles in the quark sector rather small and hierarchical while the lepton mixings are democratically larger?
- What is the origin of CP violation?

The lack of fundamental understanding of such issues is often referred to as the *flavor puzzle*. All the above questions ultimately derive from our lack of understanding of the nature of the Yukawa couplings of Standard Model fermions to the Higgs. Indeed, we have no theoretical guidance to build the Yukawa couplings. If we had to write a SM Lagrangian ignoring the measured quark and lepton masses and mixings, any flavor structure would be possible and we would naturally expect all the different entries in the Yukawa matrices to be $\mathcal{O}(1)$. This would never agree with the observed fermion masses and mixing angles.

	Quark sector		Lepton sector		
	Parameter	**Value**	**Parameter**	**Value**	
				N.O.	**I.O.**
Mixings	$\sin^2\theta_{12}^q\,/10^{-2}$	$5.063^{\pm 0.032}$	$\sin^2\theta_{12}^\ell\,/10^{-1}$	$3.10^{+0.13}_{-0.12}$	$3.10^{+0.13}_{-0.12}$
	$\theta_{12}^q\,/\circ$	$12.91^{\pm 0.04}$	$\theta_{12}^\ell\,/\circ$	$33.82^{+0.78}_{-0.76}$	$33.82^{+0.78}_{-0.76}$
	$\sin^2\theta_{23}^q\,/10^{-3}$	$1.764^{\pm 0.035}$	$\sin^2\theta_{23}^\ell\,/10^{-1}$	$5.63^{+0.18}_{-0.24}$	$5.65^{+0.17}_{-0.22}$
	$\theta_{23}^q\,/\circ$	$2.410^{\pm 0.037}$	$\theta_{23}^\ell\,/\circ$	$48.3^{+1.1}_{-1.9}$	$48.6^{+1.1}_{-1.5}$
	$\sin^2\theta_{13}^q\,/10^{-5}$	$1.351^{\pm 0.049}$	$\sin^2\theta_{13}^\ell\,/10^{-2}$	$2.241^{+0.066}_{-0.065}$	$2.261^{+0.067}_{-0.064}$
	$\theta_{13}^q\,/\circ$	$0.209^{\pm 0.007}$	$\theta_{13}^\ell\,/\circ$	$8.61^{+0.13}_{-0.13}$	$8.65^{+0.13}_{-0.12}$
	$\delta^q\,/\circ$	$66.9^{\pm 2.0}$	$\delta^\ell\,/\circ$	221^{+39}_{-28}	282^{+23}_{-25}
Masses	$m_u\,/10^{-3}\,\mathrm{GeV}$	$2.16^{+0.49}_{-0.26}$	$\Delta m^2_{21}\,/10^{-5}\,\mathrm{eV}^2$	$7.39^{+0.21}_{-0.20}$	$7.39^{+0.21}_{-0.20}$
	$m_c\,/\,\mathrm{GeV}$	$1.27^{\pm 0.02}$	$\Delta m^2_{3j}\,/10^{-3}\,\mathrm{eV}^2$	$+2.528^{+0.029}_{-0.031}$	$+2.510^{+0.030}_{-0.031}$
	$m_t\,/10^{2}\,\mathrm{GeV}$	$1.729^{\pm 0.004}$	$r_j\,/10^{-2}$	$+2.965^{+0.120}_{-0.111}$	$-2.975^{+0.111}_{-0.121}$
	$m_d\,/10^{-3}\,\mathrm{GeV}$	$4.67^{+0.48}_{-0.17}$	$m_e/10^{-4}\,\mathrm{GeV}$	$5.109989461^{\pm 0.000000031}$	
	$m_s\,/10^{-2}\,\mathrm{GeV}$	$9.3^{+0.11}_{-0.05}$	$m_\mu/10^{-1}\,\mathrm{GeV}$	$1.056583745^{\pm 0.000000024}$	
	$m_b\,/\,\mathrm{GeV}$	$4.18^{+0.03}_{-0.02}$	$m_\tau\,/\mathrm{GeV}$	$1.77686^{\pm 0.00012}$	

TABLE I.1: Standard Model flavor parameters last updated on 2018. The CKM mixings are obtained from the global fit of Ref. [2] (available at the website UTfit). The neutrino parameters are the latest results for the global fit of Ref. [3] (website: NuFit). The neutrino parameters are compatible with two mass orderings $m_1 < m_2 < m_3$ (NO) or $m_3 < m_1 < m_2$ (IO). Note that $j = 1$ for NO and $j = 2$ for IO. The analysis prefers a global minimum for NO with respect to the local minimum of IO with $\Delta\chi^2 = \Delta\chi^2_{\mathrm{IO}} - \Delta\chi^2_{\mathrm{NO}} = 0.56$. The charged lepton and quark masses are obtained from Ref.[4] (website: PDGlive). The quark masses correspond to the running mass $m_q(\mu)$ renormalized in the $\overline{\mathrm{MS}}$ scheme with $\mu = 2\mathrm{GeV}$ for $q = u, d, s$ and $\mu = m_q$ for $q = c, b$.

I.2.1 Yukawa sector of the Standard Model

Bare fermion masses $\mathcal{L}_m = -m\overline{\psi}\psi = -m(\overline{\psi}_L\psi_R + \overline{\psi}_R\psi_L)$ are not allowed in the SM because they break gauge symmetry. Fermion masses arise via Yukawa interactions with the Higgs of the type $\overline{\psi}\psi\phi$:

$$\mathcal{L}_Y^{\rm SM} = -Y^u_{ij}\,\overline{Q}_i u_{jR}\widetilde{H} - Y^d_{ij}\,\overline{Q}_i d_{jR}H - Y^e_{ij}\,\overline{L}_i e_{jR}H + \text{h.c.} \tag{I.1}$$

where $i,j = 1,2,3$ are the family indices, Q_i, L_i are left handed $SU(2)_L$ doublets, as the Higgs field H and its conjugate $\widetilde{H} = i\sigma_2 H^*$:

$$Q_i = \begin{pmatrix} u_i \\ d_i \end{pmatrix}_L \quad L_i = \begin{pmatrix} \nu_i \\ e_i \end{pmatrix}_L \quad H = \begin{pmatrix} H^+ \\ H^0 \end{pmatrix} \quad \widetilde{H} = \begin{pmatrix} H^{0*} \\ -H^- \end{pmatrix}, \tag{I.2}$$

and u_{jR}, d_{jR}, e_{jR} are respectively the up, down and charged lepton $SU(2)_L$ singlets. All fermion fields are left-handed, a charge conjugation matrix is understood to be sandwiched between the fermion bilinears. The $Y^{u,d,e}$ are the Yukawa matrices or shortly the *Yukawas*. Expanding the products in Eq.(I.1), fermion mass terms are generated once the H^0 component of the Higgs gets its VEV, $\langle H^0\rangle = v_H/\sqrt{2}$

$$\mathcal{L}_m^{\rm SM} \;=\; -\frac{v_H}{\sqrt{2}}\,Y^u_{ij}\,\overline{u}_{iL}u_{jR} - \frac{v_H}{\sqrt{2}}\,Y^d_{ij}\,\overline{d}_{iL}d_{jR} - \frac{v_H}{\sqrt{2}}\,Y^e_{ij}\,\overline{e}_{iL}e_{jR} + \text{h.c.}\,. \tag{I.3}$$

Thus the Yukawas generate the fermion mass matrices

$$m_{u,d,e} = \frac{v_H}{\sqrt{2}}Y^{u,d,e}\,. \tag{I.4}$$

Mass basis: The *mass basis (or physical basis)* ($'$) is defined where the mass matrices are diagonal with real and positive eigenvalues, this is always possible via a bi-unitary transformation where the two unitary ($V^\dagger V = 1$) rotation matrices are obtained as

$$V_L^\dagger(m\,m^\dagger)V_L = (m\,m^\dagger)' \quad , \quad V_R^\dagger(m^\dagger m)V_R = (m^\dagger m)'\,. \tag{I.5}$$

The change of basis is then given by

$$Q = V_L^{u,d}\,Q' \quad , \quad u_R = V_R^u\,u'_R \quad , \quad d_R = V_R^d\,d'_R\,, \tag{I.6}$$

$$L = V_L^{e,\nu}\,L' \quad , \quad e_R = V_R^e\,e'_R\,, \tag{I.7}$$

where

$$m'_u \equiv \text{diag}(m_u, m_c, m_t) = V_L^{u\dagger} m_u V_R^u \,, \tag{I.8}$$

$$m'_d \equiv \text{diag}(m_d, m_s, m_b) = V_L^{d\dagger} m_d V_R^d \,, \tag{I.9}$$

$$m'_e \equiv \text{diag}(m_e, m_\mu, m_\tau) = V_L^{e\dagger} m_e V_R^e \,. \tag{I.10}$$

The u, d, e are the *flavor (or interaction) eigenstates* and u', d', e' are the *mass eigenstates*. The same transformations should be applied to all the interactions of fermions. The couplings of the photon or the Z boson to fermions maintain the original diagonal form, i.e. there is no tree level flavor changing neutral current in the SM. As there is no right handed neutrino in the SM, one can always choose $V_L^\nu = V_L^e$ so that also the lepton charged current weak interactions remain flavor diagonal. In the basis where both the up and down Yukawa couplings are diagonal, the quark charged current reads

$$\mathcal{L}_{\text{CC}}^q = \frac{g}{\sqrt{2}} \overline{u}_L \gamma^\mu \, d_L W_\mu^+ + \text{h.c.} = \frac{g}{\sqrt{2}} \overline{u}'_L \gamma^\mu V_{\text{CKM}} \, d'_L W_\mu^+ + \text{h.c.} \tag{I.11}$$

where the quark mixing matrix, or the Cabibbo–Kobayashi–Maskawa (CKM) matrix, is defined in terms of the left-handed rotations

$$V_{\text{CKM}} = \begin{pmatrix} V_{ud} & V_{us} & V_{ub} \\ V_{cd} & V_{cs} & V_{cb} \\ V_{td} & V_{ts} & V_{tb} \end{pmatrix} \equiv K_u^* V_L^{u\dagger} V_L^d K_d \,, \tag{I.12}$$

up to two rephasing matrices $K_{u,d} = \text{diag}(e^{i\alpha}, e^{i\beta}, e^{i\gamma})$ that express our freedom to make general phase field redefinitions. Being unitary, the matrix $V_L^{u\dagger} V_L^d$ depends on three angles and six phases, however, we can define $K_{u,d}$ to absorb 5 of these phases.

Parametrizations: A standard parametrization of the physical CKM matrix is given in terms of three Euler angles θ_{ij}^q and a complex phase δ^q that can not be removed by field redefinitions

$$V_{\text{CKM}} = \begin{pmatrix} 1 & 0 & 0 \\ 0 & c_{23}^q & s_{23}^q \\ 0 & -s_{23}^q & c_{23}^q \end{pmatrix} \begin{pmatrix} c_{13}^q & 0 & s_{13}^q e^{-i\delta^q} \\ 0 & c_{13}^q & 0 \\ -s_{13}^q e^{\delta^q} & 0 & c_{13}^q \end{pmatrix} \begin{pmatrix} c_{12}^q & s_{12}^q & 0 \\ -s_{12}^q & c_{12}^q & 0 \\ 0 & 0 & 1 \end{pmatrix} , \tag{I.13}$$

with $s_{ij}^q = \sin\theta_{ij}^q$ and $c_{ij}^q = \cos\theta_{ij}^q$ (for notation economy, we omit the superscript ^{q} when the context is clear). Being the product of three Euler rotations matrices $V_{\text{CKM}} = R_{23}^q U_{13}^q R_{12}^q$ is itself unitary. In the SM, all the flavor and CP violation is contained in the V_{CKM}. The phase δ^q is not a physical parameter, by means of rephasing, it can be shifted to different elements of the CKM matrix. A parametrization-independent and

therefore physical measure of CP violation is instead given by the *Jarlskog invariant*:

$$J^q_{\rm CP} = {\rm Im}\,[V_{us}V_{cb}V^*_{ub}V^*_{cs}] = c_{12}\,c_{23}\,c^2_{13}\,s_{12}\,s_{23}\,s_{13}\,\sin\delta^q\,. \tag{I.14}$$

Experimentally, this is found to be $J^q_{CP} = (3.120 \pm 0.090) \times 10^{-5}$.
The angle θ^q_{12} is known as the Cabibbo angle θ_C and $\lambda_C \equiv \sin\theta_C$ is taken as a natural expansion parameter in the Wolfenstein parametrization of the CKM matrix. This is given in terms of the four parameters λ_C, A, ρ, and η:

$$V_{\rm CKM} = \begin{pmatrix} 1-\frac{\lambda_C^2}{2} & \lambda_C & A\lambda_C^3(\rho-i\eta) \\ -\lambda_C & 1-\frac{\lambda_C^2}{2} & -A\lambda_C^2 \\ A\lambda_C^3(1-\rho-i\eta) & A\lambda_C^2 & 1 \end{pmatrix} + \mathcal{O}(\lambda_C^4)\,, \tag{I.15}$$

$$\text{with} \quad \lambda_C = 0.2250^{\pm 0.0010}\,,\; A = 0.826^{\pm 0.012}\,,\; \rho = 0.152^{\pm 0.014}\,,\; \eta = 0.357^{\pm 0.010}\,.$$

These relates to the standard parametrization as $s^q_{12} \simeq \lambda_C$, $s^q_{23} \simeq A\lambda^2_C$, $s^q_{13} \simeq Ae^{i\delta}\lambda^3_C(\rho - i\eta)$ and $J_{\rm CP} \simeq \lambda^6_C A^2\eta$. Due to the pure left handed nature of charged weak current, in the above discussion, the right handed rotations $V^{u,d,e}_R$ have completely disappeared. Moreover, the left rotations $V^{u,d}_L$ are entangled in the CKM. Unfortunately, there is thus no way to trace it back to the full Yukawa structures in the framework of the SM.

Gatto-Sartori-Tonin relation: Consider only the (12)-block of the mass matrices

$$m_u = \begin{pmatrix} 0 & m^u_{12} \\ m^{u*}_{12} & m^u_{22} \end{pmatrix} \qquad , \qquad m_d = \begin{pmatrix} 0 & m^d_{12} \\ m^{d*}_{12} & m^d_{22} \end{pmatrix}\,. \tag{I.16}$$

The main features of these matrices are at LO the (1,1)-texture zero and their hermicity. Taking $m_{12} = e^{i\delta}\sqrt{-m_1 m_2}$ and $m_{22} = m_2 + m_1$ the above matrices are readily diagonalized with eigenvalues $m' = {\rm diag}(m_1, m_2)$ and the angle of the rotation matrix $R_{12}(\theta)$ satisfies that $\tan\theta_{12} = \sqrt{m_1/m_2}$. This is a result of the pioneering work of Gatto, Sartori and Tonin that gave the GST relation $\tan\theta_{ij} = \sqrt{m_i/m_j}$ [5]. Thus, the rotation angles of Eq.(I.16) are

$$\tan\theta^u_{12} = \sqrt{\frac{m_u}{m_c}} \qquad , \qquad \tan\theta^d_{12} = \sqrt{\frac{m_d}{m_s}}\,. \tag{I.17}$$

Approximating $m_{c,s} + m_{u,d} \simeq m_{c,s}$, this yields a successful prediction for the Cabibbo angle

$$\lambda_C = |\sin\theta_C| \simeq \left|\sqrt{\frac{m_d}{m_s}} - e^{i(\delta^d - \delta^u)}\sqrt{\frac{m_u}{m_c}}\right| \in [0.15, 0.29]\,. \tag{I.18}$$

I.2.2 Neutrino masses and mixings

Neutrinos were massless in the original formulation of the SM, so right-handed neutrinos (RH) do not appear in Eq. (I.1). The first indication that neutrinos have mass and large mixings came from the Homestake experiment [6] during the sixties. Only one-third of the number of neutrinos predicted by the standard solar model was reaching the detector on the Earth. The observation was confirmed in 1998 by Super-Kamiokande [7]. A similar deficit in the ratio of the flux of muon to electron flavor atmospheric neutrinos produced in cosmic rays was also observed.
The odd disappearance of both atmospheric muon neutrinos and solar electron neutrinos can be understood as a phenomenon of *neutrino oscillation*. If neutrinos have mass and their flavor eigenstates $\nu_{\alpha L}$ ($\alpha = e, \mu, \tau$) and mass eigenstates ν_{iL} ($i = 1, 2, 3$) do not coincide, as happens for the quarks, neutrinos can change their flavor. This solves both the atmospheric and solar neutrino anomalies. Muon neutrinos from the atmosphere would be experimentally undetectable when oscillating into tau neutrinos. Likewise, if electron neutrinos from the Sun change into muon or tau neutrinos, they interact at a significantly lower rate. The neutrino oscillation probability, from one flavor eigenstate to another $\nu_\alpha \to \nu_\beta$ is calculated as

$$P(\nu_\alpha \to \nu_\beta) = \left| \sum_{i=1}^{3} V^*_{\alpha i} V_{\beta i} e^{i\, m_i^2 L/2E} \right|^2 \simeq \sin^2(2\theta) \sin^2\left(\frac{\Delta m^2 L}{4E}\right), \tag{I.19}$$

where $E \simeq p$, $L \simeq ct$ is the distance traveled by the neutrino and $V_{\alpha i}$, $V_{\beta i}$ are the entries of the lepton mixing matrix know as the Pontecorvo-Maki-Nakagawa-Sakata (PMNS) matrix. The last expression in (I.19) is valid in the two neutrino approximation. The neutrino oscillation experiments usually give no information about the absolute neutrino mass scale as they are only sensitive to mass-squared differences $\Delta m^2_{ij} = m^2_i - m^2_j$, that is relative signs. The experimental data summarized in Tab. I.1 are compatible with two different neutrino mass orderings: Normal Ordering (NO) with $m_1 < m_2 < m_3$ and Inverted Ordering (IO) with $m_3 < m_1 < m_2$ (with a preference for the NO case). Specifically, the solar neutrino problem can be studied in term of two effective parameters, the solar angle $\theta_\odot \equiv \theta^\ell_{12}$ and the solar mass-squared difference $\Delta m^2_\odot \equiv \Delta m^2_{21}$, while the deficit in the neutrino flux from cosmic rays has been studied using the atmospheric angle $\theta_@ \equiv \theta^\ell_{23}$ and the atmospheric mass-squared difference $\Delta m^2_@ \equiv \Delta m^2_{3j}$ ($j = 1$ for NO and $j = 2$ for IO). However, in the matter, high energy solar neutrino propagation is appreciably affected by interactions with the electrons of the medium, and we can measure a difference between the oscillation in

the vacuum and in a medium. This makes it possible to ascertain the absolute sign of the solar mass difference, so we know that $m_1 < m_2$.
Bounds on the absolute neutrino mass scale from laboratory searches are given by β-decay experiments. The strongest limit comes from the Troitzk and Mainz experiments, that is

$$m_\beta = \sqrt{m_j^2 \sum_j |V_{ej}|^2} \leq 2.05\,\text{eV} \quad \text{at}\,95\%\,\text{CL}[8] \tag{I.20}$$

where m_β is the effective mass that enters the decay. However, the by far strongest constraint on the sum of the neutrino masses $\sum_j m_j$ today comes from cosmological observations. Measurements of the temperature and polarization anisotropy spectrum of the cosmic microwave background (CMB) with the Planck satellite in combination with other cosmological measurements like baryonic acoustic oscillations (BAO) show that

$$\sum_j m_j \leq 0.12\,\text{eV} \quad \text{at}\,90\%\,\text{CL}\,[9]\,. \tag{I.21}$$

Next future data analyses promise even tighter constraints. However, it should be stressed that this bound is model dependent and based on different assumptions, relieving some of them could relax the limit [10]. The bound can be converted into a limit on the smallest neutrino mass m_{min}, in the more conservative case, $m_{\text{min}} \leq \sum_j m_j/3 = 0.04$ eV. For what we know so far of the neutrino mass scale, the neutrino spectrum may or may not be hierarchical:

- Normal Hierarchy (NH): $m_1 \ll m_2 \simeq \sqrt{\Delta m^2_{21}} < m_3 \simeq \sqrt{\Delta m^2_{31}}$.
- Inverted Hierarchy (IH): $m_3 \ll m_1 \simeq \sqrt{|\Delta m^2_{21} + \Delta m^2_{32}|} < m_2 \simeq \sqrt{|\Delta m^2_{32}|}$.
- Quasi Degenerate (QD): $\sqrt{\Delta m^2_{32}} \ll m_1 \simeq m_2 \simeq m_3 < \sum_i m_i$.

The observation of non-zero neutrino masses and mixings is the most established evidence for New Physics Beyond the SM. Therefore additional terms must be added to Eq. (I.1) to accommodate them.
Probably the most pressing problem in neutrino physics is related with the neutrino intrinsic nature. As charge-less and massive they can be either *Dirac* (with particles and antiparticles being different objects: $\nu \neq \nu^c$ like for the other fermions) or *Majorana* (with particles and antiparticles being the same, just as for photons: $\nu = \nu^c$).
In the first case, in analogy with the quarks and charged leptons, a Dirac mass term for the neutrinos requires the existence of three right-handed (RH) neutrinos $N_i \equiv \nu_{iR}$ to be able to write down the Yukawa term $\overline{L}_i Y^\nu_{ij} N_j H$. However, RH neutrinos are

gauge singlets so, they could possess Majorana mass terms that breaks explicitly lepton number. This bare mass term is not constrained by any gauge symmetry and the RH neutrinos can be arbitrarily heavy, so it has to be forbidden by imposing some additional symmetry such as lepton number conservation. The leptonic Lagrangian with Dirac neutrinos reads

$$\mathcal{L}^{D}_{\ell,ij} = -Y^{e}_{ij}\,\overline{L}_i e_{Rj} H - Y^{\nu}_{ij}\,\overline{L}_i N_i \widetilde{H} + \text{h.c.}\,, \tag{I.22}$$

where Y^{ν} is the Yukawa coupling constant. The neutrino mass matrix can be added to Eq.(I.4)

$$m_\nu = \frac{v_H}{\sqrt{2}} Y^{\nu} \quad , \quad m'_\nu = \text{diag}(m_1, m_2, m_3) = V^{\nu\dagger}_L m_\nu V^{\nu}_R \tag{I.23}$$

with $V^{\nu}_{L,R}$ as in Eq.(I.5). The right handed rotation have no physical effect, whereas V^{ν}_L enter in the charged current, which in the mass basis reads

$$\mathcal{L}^{\ell}_{\text{CC}} = \frac{g}{\sqrt{2}} \bar{e}_L \gamma^\mu \nu_L W^-_\mu + \text{h.c.} = \frac{g}{\sqrt{2}} \bar{e}'_L \gamma^\mu V_{\text{PMNS}}\, \nu'_L W^-_\mu + \text{h.c.}\,, \tag{I.24}$$

where, analogously to the quark mixing matrix (I.12), the PMNS matrix is defined in terms of the left handed rotations up to rephasing, which can reabsorb five of the present phases and leave only one physical Dirac phase

$$V_{\text{PMNS}} = \begin{pmatrix} V_{e1} & V_{e2} & V_{e3} \\ V_{\mu 1} & V_{\mu 2} & V_{\mu 3} \\ V_{\tau 1} & V_{\tau 2} & V_{\tau 3} \end{pmatrix} \equiv K^*_e V^{e\dagger}_L V^{\nu}_L K_\nu\,. \tag{I.25}$$

The PMNS, likewise the CKM, can be parametrized in terms of three Euler rotations matrices $V_{\text{PMNS}} = R^{\ell}_{23} U^{\ell}_{13} R^{\ell}_{12}$:

$$V_{\text{PMNS}} = \begin{pmatrix} 1 & 0 & 0 \\ 0 & c^{\ell}_{23} & s^{\ell}_{23} \\ 0 & -s^{\ell}_{23} & c^{\ell}_{23} \end{pmatrix} \begin{pmatrix} c^{\ell}_{13} & 0 & s^{\ell}_{13} e^{-i\delta^{\ell}} \\ 0 & c^{\ell}_{13} & 0 \\ -s^{\ell}_{13} e^{\delta^{\ell}} & 0 & c^{\ell}_{13} \end{pmatrix} \begin{pmatrix} c^{\ell}_{12} & s^{\ell}_{12} & 0 \\ -s^{\ell}_{12} & c^{\ell}_{12} & 0 \\ 0 & 0 & 1 \end{pmatrix}, \tag{I.26}$$

with $s^{\ell}_{ij} = \sin\theta^{\ell}_{ij}$ and $c^{\ell}_{ij} = \cos\theta^{\ell}_{ij}$ (again, we omit the superscript $^{\ell}$ whenever the context is clear). Although the possibility of Dirac neutrinos is allowed on theory grounds, it leaves the smallness of neutrino masses unexplained, implying the need for a tiny Yukawa coupling for neutrinos ($Y^{\nu} \sim \mathcal{O}(10^{-13})$). This is clearly not appealing from a model building point of view.

For the case of Majorana neutrinos, if only Standard Model fields are present, there is a unique lepton number violating dimension-5 operator that gives rise to neutrino masses, the well-known *Weinberg Operator* which couples two lepton doublets and two Higgs. The effective Lagrangian for leptons with Majorana neutrinos reads

$$\mathcal{L}^{M}_{\ell,ij} = -Y^{e}_{ij}\,\overline{L}_i e_{Rj} H - \frac{1}{2}\frac{k^{\nu}_{ij}}{\Lambda}\overline{L}_i L^{c}_j \widetilde{H}\widetilde{H}^{T} + \text{h.c.}\,, \tag{I.27}$$

where the superscript ^{c} stands for charge conjugation $L^{c} = \mathcal{C}\overline{L}^{T}$ ($\mathcal{C} = i\gamma^0\gamma^2$). The Λ can be understood as the cutoff scale where new physics probably sets in. After electroweak symmetry breaking a light Majorana mass term for neutrino is generated

$$m_\nu = \frac{v_H^2}{2}k^{\nu} \quad , \quad m'_\nu = \text{diag}(m_1, m_2, m_3) = V_L^{\nu T} m_\nu V_L^{\nu}\,. \tag{I.28}$$

The charged current reads as (I.24), however, due to the Majorana nature of neutrinos, the matrix K_ν is now physical yielding to a leptonic mixing matrix

$$V_{\text{PMNS}} = \widetilde{V}_{\text{PMNS}}\,\text{diag}(1, e^{i\alpha/2}, e^{i(\beta/2+\delta)}) = K_e^{*} V_L^{e\dagger} V_L^{\nu}\,, \tag{I.29}$$

where $\widetilde{V}_{\text{PMNS}}$ is parametrized as in Eq.(I.26), in terms of three angles θ^{ℓ}_{ij} and the Dirac phase δ^{ℓ}, while the additional Majorana phases are α and β. We used the same parametrization used in Article 4 (more details are given in Appendix D.1).
With the measurements of a non vanishing reactor mixing angle θ^{ℓ}_{13} in 2012 by Double Chooz [11], Daya Bay [12] and RENO [13], we now have complete knowledge of all the three mixing angles θ^{ℓ}_{12}, θ^{ℓ}_{23} and θ^{ℓ}_{13}. From Table I.1 we have large lepton mixing $s^{\ell}_{12} \sim 1/\sqrt{3}$, $s^{\ell}_{23} \sim 1/\sqrt{2}$, $s^{\ell}_{13} \sim \lambda_C/\sqrt{2}$ with λ_C the Wolfenstein parameter. However, we do not have information yet on the Dirac-type CP violating phase δ^{ℓ} nor on the CP violating phases associated with Majorana neutrino masses. Regarding δ^{ℓ}, from combined analyses, we have a hint for maximal CP violation: $\delta^{\ell} \sim 3\pi/2$.
The origin of the Weinberg Operator remains open. Above the cutoff scale the Ultra-Violet (UV) complete theory is at play, involving new *messenger* fields, whose masses lie close to the scale Λ. Since L and H are different fields, there are three different ways of contracting the relevant fields that give an overall $SU(2)_L$ singlet [14]:

$$O_{\text{I}} = (L_i H)_{\mathbf{1}}(L_j H)_{\mathbf{1}} \qquad O_{\text{II}} = (L_i L_j)_{\mathbf{3}}(HH)_{\mathbf{3}} \qquad O_{\text{III}} = (L_i H)_{\mathbf{3}}(L_j H)_{\mathbf{3}}\,. \tag{I.30}$$

The possibility where both $(L_i L_j)_{\mathbf{1}}(HH)_{\mathbf{1}}$ is forbidden, since $(HH)_{\mathbf{1}}$ is symmetric, while the singlet contraction is antisymmetric, and therefore vanishes. In particular,

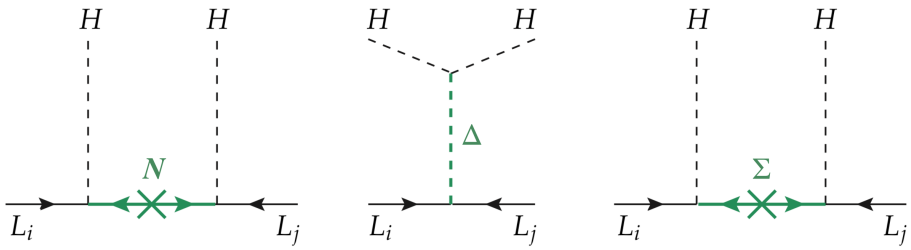

FIGURE I.1: Tree level realizations of the Weinberg operator from the Seesaw type I, II and III mechanism, from left to right. The intermediate states are: singlet fermion N, scalar triplet Δ_L and fermion triplet Σ fields.

the explicit form of the bilinear are as follows:

$$(L_iL_j)_{\mathbf{1}} \sim (\nu_i e_j - e_i \nu_j) \qquad (L_iL_j)_{\mathbf{3}} \sim \begin{pmatrix} \nu_i\nu_j \\ \nu_i e_j + e_i \nu_j \\ e_i e_j \end{pmatrix} \tag{I.31}$$

$$(L_iH)_{\mathbf{1}} \sim (\nu_i H^0 - e_i H^+) \qquad (L_iH)_{\mathbf{3}} \sim \begin{pmatrix} \nu_i H^+ \\ \nu_i H^0 + e_i H^+ \\ e_i H^0 \end{pmatrix} \tag{I.32}$$

$$(HH)_{\mathbf{3}} \sim \begin{pmatrix} H^+H^+ \\ H^+H^0 + H^0H^+ \\ H^0H^0 \end{pmatrix} \tag{I.33}$$

from which we realize that $O_{\rm I}$, $O_{\rm II}$ and $O_{\rm III}$ all contain the combination of fields $\nu_i\nu_j H^{0^2}$ that generate neutrino masses after electroweak spontaneous symmetry breaking. However, giving their different contractions of the $SU(2)_L$ indices, they are associated with the tree-level exchange of various messenger fields. Fig.I.1 illustrates the UV completion of $O_{\rm I,II,III}$. $O_{\rm I}$ has a tree-level realization in terms of the exchange of a heavy SM singlet N: the type-I Seesaw mechanism. Whereas heavy triplets are required to realize $O_{\rm II}$ and $O_{\rm III}$, respectively, by the exchange of a scalar particle Δ: the type-II Seesaw mechanism, or of a fermion field Σ: the type-III mechanism.

Seesaw type I: In the type I mechanism, three heavy RH neutrinos N_i are introduced, that allow for an invariant mass Lagrangian of the form

$$\mathcal{L}_\nu^{\rm I} = -Y_{ij}^\nu \overline{L}_i N_j \widetilde{H} - \frac{1}{2} M_{Nij} \overline{N}_i^c N_j + \text{h.c.}\,. \tag{I.34}$$

Therefore we have the following mass matrix for neutrinos, with a characteristic

(1,1)-texture zero,

$$\mathcal{L}^{\rm I}_{m_\nu} = -\frac{1}{2}\begin{pmatrix}\overline{\nu}_L & \overline{N}^c\end{pmatrix}\begin{pmatrix}0 & \sqrt{2}\,v_H Y^\nu \\ \sqrt{2}\,v_H Y^{\nu T} & M_N\end{pmatrix}\begin{pmatrix}\nu_L^c \\ N\end{pmatrix} + \text{h.c.}\,. \tag{I.35}$$

The Seesaw mechanism is implemented when M_N is much above the electroweak scale and $M_N \gg Y^\nu$, then matrix can be diagonalized yielding to

$$\mathcal{L}^{\rm I}_{m_\nu} = -\begin{pmatrix}\overline{\nu}_L & \overline{N}^c\end{pmatrix}\begin{pmatrix}v_H^2 Y^\nu M_N^{-1} Y^{\nu T} & 0 \\ 0 & M_N/2\end{pmatrix}\begin{pmatrix}\nu_L^c \\ N\end{pmatrix}. \tag{I.36}$$

At low energies, integrating out the RH neutrinos generates an effective Weinberg Operator as in Eq.(I.27). After EW symmetry breaking the light Majorana mass term for the neutrinos reads

$$m_\nu = -v_H^2\, Y^\nu M_N^{-1} Y^{\nu T}\,. \tag{I.37}$$

Compared to the charged lepton masses, the type-I Seesaw mechanism shows that the light neutrino masses depend quadratically on the Dirac masses but are inversely proportional to the large Majorana mass, so that the scale of new physics is $\Lambda_{\rm NP} = M_N$.

Seesaw type II: In the type II mechanism, we need to add at least one scalar $SU(2)_L$ triplet to the field content of the SM. For values of the weak hypercharge equal to +1, the triplet can be arranged in a 2×2 matrix

$$\Delta = \begin{pmatrix}\Delta^+/\sqrt{2} & \Delta^{++} \\ \Delta^0 & -\Delta^+/\sqrt{2}\end{pmatrix}, \tag{I.38}$$

where Δ^0, Δ^+ and Δ^{++} are combinations of the triplet components. The Lagrangian terms that are relevant for neutrino masses are

$$\mathcal{L}^{\rm II}_\nu = (-k^\Delta_{ij}\,\overline{L}^c_i \Delta\, L_j - \mu_\Delta\,\widetilde{H}^\dagger \Delta^\dagger H + \text{h.c.}) + M_\Delta^2\, Tr(\Delta^\dagger\Delta)\,, \tag{I.39}$$

where k^Δ_{ij} are the new Yukawa couplings produced by Δ. Assuming that the scalar potential has a minimum in the component $\langle\Delta^0\rangle = v_\Delta = v_H^2\mu_\Delta/M_\Delta^2$ and the hierarchy $M_\Delta^2 \gg \mu_\Delta v_H$, then the light neutrino mass matrix is

$$m_\nu \simeq -v_H^2\, k^\Delta\, \mu_\Delta M_\Delta^{-2}\,. \tag{I.40}$$

In this case, the scale of new physics is approximately given by $\Lambda_{\rm NP} = M_\Delta^2/\mu_\Delta$.

Observable	Current Bound	Future Bound
$m_{\beta\beta}$ [eV]	0.11 @90% (CUORE[15])	0.005 @90% (nEXO[16])
m_β [eV]	2.05 eV @95% (Troitsk[8])	0.02 @90% (KATRIN[17, 18])
$\sum m_j$ [eV]	0.26 @95% (Planck[9]) 0.12 @95% (Planck+BAO[9])	0.062 @68% (CORE+BAO[19])

TABLE I.2: Current and future bounds on the neutrino observables: $m_{\beta\beta}$, m_β and the total sum of neutrino masses. Note that the latest limits from Planck fall in the quasi-degenerate regime for the neutrino spectrum. In that case, these bounds can be translated into bounds over the lightest mass eigenstate as: $m_{\rm min} \lesssim 0.09$ eV for Planck data and $m_{\rm min} \lesssim 0.04$ eV for Planck+BAO.

Seesaw type III: In the type-III mechanism, as for the case of the type II, the triplet hyperchargeless fermions Σ can be arranged in the following form:

$$\Sigma = \begin{pmatrix} \Sigma^0/\sqrt{2} & \Sigma^+ \\ \Sigma^- & -\Sigma^0/\sqrt{2} \end{pmatrix} . \tag{I.41}$$

where Σ^-, Σ^0 and Σ^+ are combinations of the triplet components. The related Lagrangian reads

$$\mathcal{L}_\nu^{\rm III} = -k_{ij}^\Sigma \overline{L}_i \Sigma_j \widetilde{H} + M_{\Sigma ij} Tr(\overline{\Sigma}_i^c \Sigma_j) + \text{h.c.} , \tag{I.42}$$

where again k_{ij}^Σ is a Yukawa coupling matrix. Under the hypothesis that $M_\Sigma \gg k^\Sigma v_H$, the light mass matrix assumes the form

$$m_\nu \sim -v_H^2 k^\Sigma M_\Sigma^{-1} (k^\Sigma)^T , \tag{I.43}$$

which is very similar to Eq.(I.37) since, regarding neutrino masses, the state Σ^0 acts like a RH neutrino. The Seesaw mechanism, in all its realizations, offers a natural explanation of why the neutrinos are much lighter than the other fermions and clarifies why Majorana neutrinos have been so popular. Note that the light neutrino masses are obtained as the ratio of the Dirac and Majorana parameters $m_\nu = v_H^2 y_\nu^2 / 2M_N$, their absolute scale is therefore not fixed by the Seesaw. To give a reasonable estimate we can assume $m_\nu \sim 2\sqrt{\Delta m_{3j}^2} = 0.1$ eV and $y^\nu = 0.1$, this implies a RH neutrino mass as large as $M_N \sim 4 \times 10^{12}$ GeV. We understand that typically the scale of the RH neutrinos is very large, which makes a direct detection impossible.
However, the characteristic signature [20] of Majorana neutrinos, namely the observation of neutrinoless double beta decay ($0\nu\beta\beta$-decay), has so far remained elusive

[15, 21, 22]. The $0\nu\beta\beta$-decay effective mass is

$$m_{\beta\beta} = \left| \sum_j m_j \, V_{ej}^2 \right| = \left| c_{13}^2 \left(m_1 \, c_{12}^2 + m_2 \, s_{12}^2 e^{i\alpha} \right) + m_3 \, s_{13}^2 e^{i\beta} \right| . \tag{I.44}$$

The neutrinoless double beta decay rate depends significantly on the neutrino mass spectrum. The $0\nu\beta\beta$ experimental search can thus have an enormous impact in constraining the mass hierarchy, the absolute scale of neutrino masses and, together with other sources of information, could provide a unique insight on the value of the CP violating phases appearing in the leptonic mixing matrix. We expect the next generation experiments in Table I.2 to clarify the following questions:

- Are neutrinos Dirac or Majorana particles?
- What is the neutrino mass ordering and the neutrino mass scale?
- What is the value of the Dirac phase δ^ℓ and, possibly, of the Majorana phases?

I.2.3 Sequential Dominance

In a context of small Yukawa mixings, similar to Yukawas of the quark sector, it has been observed that the simultaneous emergence of two large mixing angles and hierarchical neutrino masses are not natural in the Seesaw mechanism, how to account for both of them? An elegant and natural possibility is called *Sequential Dominance* (SD) [23–25]. The idea of SD is that one of the RH neutrinos M_a contributes dominantly to the Seesaw mechanism and determines the atmospheric neutrino mass and mixing. A second RH neutrino contributes sub-dominantly and determines the solar neutrino mass and mixing M_b. The third RH neutrino M_c is effectively decoupled from the Seesaw mechanism, therefore

$$M_a < M_b \ll M_c \, , \tag{I.45}$$

where $M_{a,b,c}$ can then be identified with $M_{1,2,3}$ in all the possible ways. To understand how sequential dominance works, we operate in the basis where the charged lepton and right-handed neutrino mass matrices are diagonal, known as the *flavor basis*, such that all mixing originates in the Dirac sector. So we begin by writing the right-handed neutrino Majorana mass matrix M_N in a diagonal basis as

$$\begin{pmatrix} M_a & 0 & 0 \\ 0 & M_b & 0 \\ 0 & 0 & M_c \end{pmatrix} . \tag{I.46}$$

The neutrino Yukawa matrix in the flavor basis, λ_ν, is explicitly given by

$$\lambda_\nu \equiv V_L^{e\dagger} Y_\nu V_N \,, \tag{I.47}$$

that we can write down in terms of three general column vectors

$$\lambda_\nu = (\phi_a, \phi_b, \phi_c) \,. \tag{I.48}$$

The effective light neutrino mass (after EW symmetry breaking), resulting from integrating out the massive right handed neutrinos, is

$$m_\nu = \frac{v_H^2}{2} \left(\frac{\phi_c \phi_c^T}{M_c} + \frac{\phi_b \phi_b^T}{M_b} + \frac{\phi_a \phi_a^T}{M_a} \right) . \tag{I.49}$$

Sequential dominance $M_a < M_b \ll M_c$ then corresponds to the first term being negligible, the second term subdominant and the third term dominant, so SD immediately predicts a NH neutrino mass $m_1 \ll m_2 < m_3$, because

$$\frac{\phi_c \phi_c^T}{M_c} \ll \frac{\phi_b \phi_b^T}{M_b} < \frac{\phi_a \phi_a^T}{M_a} . \tag{I.50}$$

We write the relevant Yukawa couplings in the most general form

$$\phi_a = \begin{pmatrix} a_1 \\ a_2 \\ a_3 \end{pmatrix} \quad , \quad \phi_b = \begin{pmatrix} b_1 \\ b_2 \\ b_3 \end{pmatrix} \quad \text{with} \quad a_i = |a_i| \, e^{i\delta_{ai}} \, , \, b_i = |b_i| \, e^{i\delta_{bi}} \, . \tag{I.51}$$

The neutrino masses, under the SD condition of Eq.(I.45), are obtained

$$m_3 \sim \frac{v_H^2}{2} \frac{|a_2|^2 + |a_3|^2}{M_a} \quad , \quad m_2 \sim \frac{v_H^2}{2} \frac{|b_1|^2}{s_{12} \, M_b} \quad , \quad m_1 \sim \frac{v_H^2}{2} \frac{\mathcal{O}(|c|^2)}{M_c} \, , \tag{I.52}$$

and for the mixing angles

$$\tan\theta_{23}^\ell \sim \frac{|a_2|}{|a_3|} \qquad , \quad \tan\theta_{12}^\ell \sim \frac{|b_1|}{c_{23} \, |a_2| - s_{23} \, |b_3|} , \tag{I.53}$$

$$\theta_{13}^\ell \sim \frac{e^{-i\delta_{a2}} |b_1|}{\sqrt{|a_2|^2 + |a_3|^2}} \left(e^{i\delta_{b1}} \frac{a_2^* \, b_2 + a_3^* \, b_3}{|b_1|^2} \frac{m_2}{m_3} + e^{i\delta_{a1}} \frac{|a_1|}{|b_1|} \right) . \tag{I.54}$$

We see that small θ_{13} and almost maximal θ_{23} require that

$$|a_1| \ll |a_2| \simeq |a_3| \,. \tag{I.55}$$

In this case an upper bound on the value of the reactor angle is given by $\theta_{13}^{\ell} \leq m_2/m_3 \simeq \sqrt{\Delta m^2_{@}/\Delta m^2_{\odot}} = 0.17$. Quite remarkably this successful prediction was made over a decade before the reactor angle was measured [26]. In order to obtain precise predictions for mixing one can go further and impose constraints on the Dirac Yukawa couplings, using specific vacuum alignments, dubbed Constrained Sequential Dominance (CSD). The TB-mixing corresponds to the choice

$$a_1 = 0 \quad , \quad a_2 = a_3 \quad , \quad b_1 = b_2 = -b_3 \,. \tag{I.56}$$

This is a CSD(1) case, starting from it, general CSD(n) models are built assuming an approximate maximal atmospheric angle, with different proposals for the solar couplings

$$\text{CSD(n)}: \quad \phi_a^T = (0, a, a) \quad , \quad \phi_b^T = (b, n\,b, (n-2)\,b) \,, \tag{I.57}$$

where n is a positive integer. The SD assumption is also especially useful in Leptogenesis to which we dedicate the next section.

I.3 Leptogenesis

The Seesaw mechanism not only renders a natural explanation of the smallness of the neutrino masses, but it also provides a convincing framework, called Leptogenesis, to address the Baryon Asymmetry of the Universe (BAU), that is the difference between the baryon and antibaryon densities, n_B and $\overline{n}_B$. This is measured with respect to the entropy density s to be

$$Y_B = \frac{n_B - \overline{n}_B}{s} = (8.7 \pm 0.1) \times 10^{-11} \quad [27] \,. \tag{I.58}$$

In the SM, the CP violation of the CKM matrix, in the quark sector, is not enough to explain the size of the observed BAU. The physical process generating the baryon asymmetry, called Baryogenesis, is an open issue. Getting information about the CP symmetry in the leptonic sector might allow us to further understand the origin of the observed matter-antimatter asymmetry of the Universe.
The existence in the SM of sphaleron processes violating both baryon B and lepton

number L suggests Baryogenesis through Leptogenesis [28–32]. Leptogenesis is a scenario where New Physics generates a lepton asymmetry through lepton number violating decays of very heavy Majorana neutrino's densities that occur out of equilibrium. RH neutrinos are thermally produced after inflation through scatterings and inverse decays in the thermal plasma. The lepton asymmetry is generated by the out of equilibrium decays of the RH neutrino when the temperature gets below the neutrino mass. The lepton asymmetry is partially converted into the observed baryon asymmetry by the existence of sphaleron interactions. The introduction of singlet heavy neutrinos N_i with Majorana masses and Yukawa couplings to the doublet leptons fulfills the necessary conditions to produce a baryon asymmetry, known as the *Sakharov conditions* :

- B (or L) violation,
- C and CP violation,
- departure from thermal equilibrium.

This means that, if the Seesaw mechanism is indeed the source of the light neutrino masses, then qualitative Leptogenesis is inevitable. The question of whether it solves the mystery of the baryon asymmetry is merely a quantitative one.
We consider classes of neutrino mass models based on the Seesaw mechanism with sequential dominance. Under this assumption, the RH neutrinos do not interfere, and the generation of the asymmetry from each N_i decays proceed independently. Depending on the size of the RH neutrino mass we have to distinguish 3 possible flavor regimes [33]:

- $M_i \gg 10^{12}\,\text{GeV}$: before the charged lepton Yukawa couplings come into equilibrium, the flavor-independent approach is proper.
- $10^9\,\text{GeV} \ll M_i \ll 10^{12}\,\text{GeV}$: only the τ Yukawa coupling is in equilibrium and is arranged separately in the Boltzmann equations. At the same time, the e and μ flavors are indistinguishable and have to be treated with a combined density.
- $10^5\,\text{GeV} \ll M_i \ll 10^{12}\,\text{GeV}$: all flavors in the Boltzmann equations are to be treated separately.

In what follows, we consider the last regime where all flavors in the Boltzmann equations are separately arranged. The generation of a baryon asymmetry is a non-equilibrium process which is generally addressed employing simplified Boltzmann

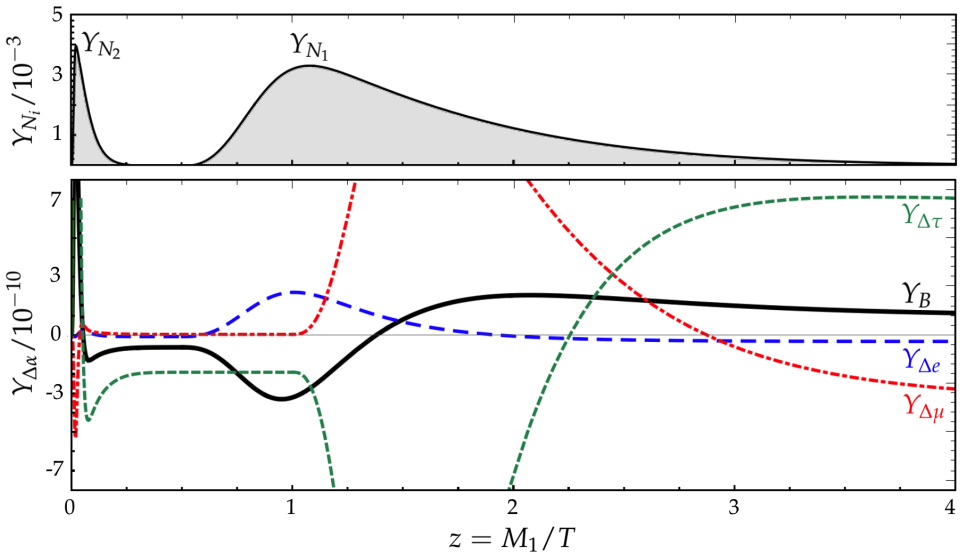

FIGURE I.2: An illustrative example of the solutions of the Boltzmann equations in Eq.(4.20). In Article 4, we employ a two-step procedure in which we solve for the $Y_{\Delta\alpha}$ arising from $N_{i=2}$ decays, and use them as initial conditions for the $N_{i=1}$ calculation. This is justified if the SD framework where $M_1 \ll M_2$. The produced BAU is computed at $z \gg 1$.

equations for the distribution functions, which can be schematically written as

$$\begin{aligned} \frac{dY_{N_i}}{dz} &= -(D+S)\left(Y_{N_i} - Y_{N_i}^{\rm eq}\right) \\ \frac{dY_{\Delta\alpha}}{dz} &= -\varepsilon^{\alpha}_{N_i} D\left(Y_{N_i} - Y_{N_i}^{\rm eq}\right) - K^{\alpha}_{N_i} W Y_{\Delta\alpha} \quad , \quad Y_B = \frac{12}{37}\sum_{\alpha} Y_{\Delta\alpha}, \end{aligned} \tag{I.59}$$

where $\alpha = (e,\mu,\tau)$, $i = (1,2,3)$ and $z = M_i/T$. The Y_{N_i} is the density of neutrino the N_i neutrino and $Y_{N_i}^{\rm eq}$ its equilibrium value. $Y_{\Delta\alpha}$ are defined as $Y_{\Delta\alpha} \equiv Y_B/3 - Y_{L_\alpha}$, where Y_{L_α} are the total lepton number densities for each flavor [1]. Normalization to the entropy density s is understood for all number densities Y. An illustrative example of the solutions of the Boltzmann equations is given in Fig.I.2. There are four types of processes that contribute to the Boltzmann equations through the terms D, S and W: decays and inverse decays ($N \leftrightarrow L_\alpha\, H$), $\Delta L = 1$ scatterings ($NQ \leftrightarrow L_\alpha t$) and $\Delta L = 2$ processes ($L_\alpha\, L_\alpha \leftrightarrow \overline{H}\overline{H}$,$L_e\, H \leftrightarrow \overline{L}_e\, \overline{H}$). Specifically, the factor $D = \Gamma_D/\mathcal{H}z$ accounts for decays and inverse decays, $S = \Gamma_S/\mathcal{H}z$ represents the $\Delta L = 1$ scatterings, while other processes contribute to the washout term $W = \Gamma_W/\mathcal{H}z$ which

[1] It is appropriate to solve the Boltzmann equations for $Y_{\Delta\alpha}$ instead of for the number densities Y_{L_α} of the lepton doublets L_α, since $\Delta_\alpha \equiv B/3 - L_\alpha$ is conserved by sphalerons and by the other SM interactions

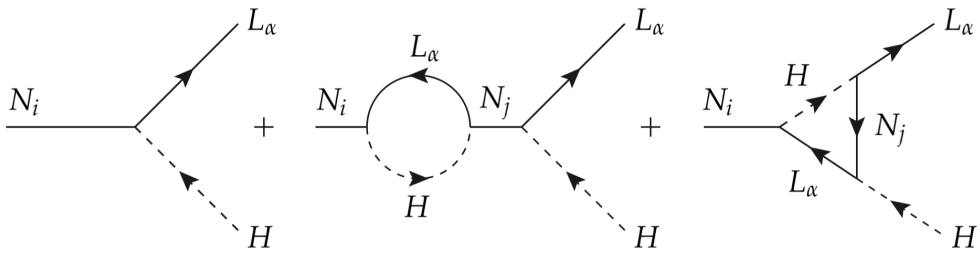

FIGURE I.3: $\Delta L = \pm 1$ neutrino decays.

competes with the decay term.
The final lepton asymmetry in each flavor is entirely determined by neutrino properties, in particular is governed by two sets of parameters which can be computed within a given neutrino model: the *decay factors* $K^{\alpha}_{N_i}$ and the *CP or decay asymmetries* $\varepsilon^{\alpha}_{N_i}$ of the RH-neutrino N_i into Higgs H and lepton doublet L_α (or conjugate final states). In fact, the Majorana nature of the RH-neutrino masses implies the lepton number violating decays $N_i \to L_\alpha\, H$ and $N_i \to \overline{L}_\alpha\, H^*$ with $\Delta L = \pm 1$, the decay factors are defined as

$$K^{\alpha}_{N_i} = \frac{\Gamma(N_i \to L_\alpha\, H) + \Gamma(N_i \to \overline{L}_\alpha\, H^*)}{\mathcal{H}(M_i)}\,, \tag{I.60}$$

where $\mathcal{H}(M_i)$ is the Hubble parameter at the temperature $T = M_i$. The CP-asymmetries are defined as

$$\varepsilon^{\alpha}_{N_i} = \frac{\Gamma(N_i \to L_\alpha\, H) - \Gamma(N_i \to \overline{L}_\alpha\, H^*)}{\Gamma(N_i \to L_\alpha\, H) + \Gamma(N_i \to \overline{L}_\alpha\, H^*)}\,. \tag{I.61}$$

The decay factors are dominated by the single tree level diagram. On the other hand, the CP-asymmetry arises only at a one-loop level from the self-energy plus vertex contributions diagrams displayed in Fig.I.3. In fact, if there is more than a single N_i, then there is a relative CP-violating phase between the tree and the loop diagrams. Considering only N_1 decays (zero initial densities) and the flavor independent regime, an upper bound on the CP asymmetry [30] can be written

$$\varepsilon_{N_1} < \frac{3}{16\pi}\frac{M_1\,\Delta m^2_{31}}{v^2_H}\,. \tag{I.62}$$

It is convenient to parametrize the produced asymmetry in terms of an efficiency

factor $\eta \in [0, 0.2]$, which is a function of only K_{N_1} [33]

$$Y_B = \frac{12}{37} Y_{N_1}^{\rm eq}(z \ll 1)\, \varepsilon_{N_1}\, \eta(K_{N_1}) \simeq 3 \times 10^{-4}\, \varepsilon_{N_1}\,. \tag{I.63}$$

where we used that $Y_{N_1}^{\rm eq}(z \ll 1) \simeq 4 \times 10^{-3}$ and $\eta \simeq 0.2$. From Eq.(I.63), we can deduce $\varepsilon_{N_1} \sim 10^{-7}$, which combined with the limit of Eq.(I.62) provide a lower bound on M_1

$$M_1 \geq 2 \times 10^9\, {\rm GeV}\,. \tag{I.64}$$

Interestingly enough, this is compatible with the typical large scale expected in the Seesaw mechanism. However, this lower bound represents a severe problem to many flavor models, especially those incorporating some grand unification symmetry, where the neutrino Yukawas are strictly related to the up-quark Yukawas. In these kinds of models, the typical values for the lightest right-handed neutrino mass are close to $10^6 - 10^7$ GeV [34]. In general, the requirement of successful leptogenesis yields stringent constraints on the Yukawa couplings and the masses of and heavy neutrinos, which are not constrained by the Seesaw mechanism. An explicit example of this is given in Article 4.

I.4 Flavor Symmetries

An exhaustive solution to the flavor puzzle can come from the interplay of *flavor (or family) symmetries*, Grand Unification Theories (GUT) and the Seesaw mechanism. In this section, we discuss the role of flavor symmetries [35]. Flavor symmetries unify different members within a family, and for this are sometimes called horizontal symmetries, as opposed to GUT symmetries, or vertical symmetries, which unite the same members inside different families. Flavor symmetry models intend to explain the Yukawa structures, which give the masses hierarchies and mixings, in terms of a single expansion parameter with a dynamical motivation. The standard strategy to interpret the large number of seemingly arbitrary parameters in the flavor sector is to assume that, at some high energy scale, the theory is invariant under the action of a flavor symmetry group $\mathcal{G}_f$.

I.4.1 Froggatt-Nielsen mechanism

In the approach of the Froggatt Nielsen (FN) mechanism [36], the SM Yukawa parameters are given a dynamical origin. The hierarchy of masses and mixings of quark and leptons can be understood by assuming an horizontal $\mathcal{G}_f = U(1)_{FN}$ symmetry

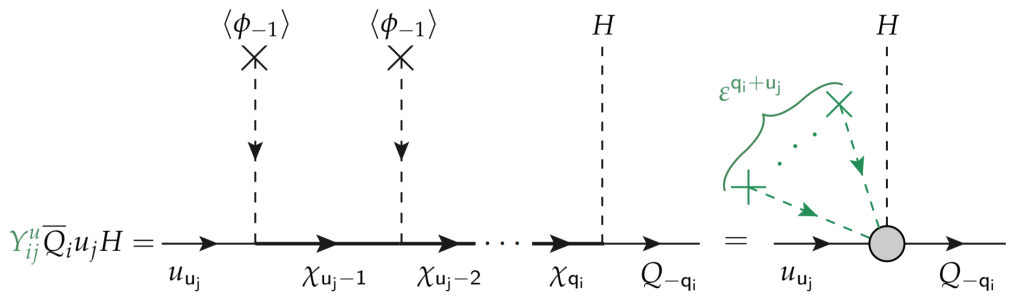

FIGURE I.4: Generation of the effective up-type Yukawa couplings through the typical FN "spaghetti" diagram. The other Yukawa coupling arise from analogous diagrams with different number of flavon insertions.

broken by the vacuum expectation value (VEV) of a complex scalar field $\langle\phi\rangle$ called *flavon*. In the simplest version, the SM fermions carry positive and integer $U(1)_{FN}$ charges: $\{q_i, u_i, d_i, e_i\}$, while the Higgs is neutral and the flavon carries a negative one unit flavor charge. Thus, the Yukawa terms are no longer invariant and the ultraviolet Lagrangian preserving the charge assignment of the underlying $U(1)$ flavor symmetry has the form

$$\mathcal{L}^{\rm UV}_{ij} = -g\left[\overline{Q}_{q_i}\chi_{-q_i}H + \overline{L}_{l_i}\chi_{-l_i}H + \sum_q \overline{\chi}_{(1-q)}\chi_q\phi \right. \tag{I.65}$$

$$\left. + \overline{\chi}_{(1-u_j)}u_{u_j}\phi + \overline{\chi}_{(1-d_j)}d_{d_j}\phi + \overline{\chi}_{(1-e_j)}e_{e_j}\phi + \text{h.c.}\right] , \tag{I.66}$$

where g is a generic $\mathcal{O}(1)$ coupling that, for illustration purposes, we take to be the same for all interactions, and the χs are the *Froggatt Nielsen fields*. These are heavy vector-like mediators with the quantum numbers of RH leptons and quarks. The mass M_χ is the scale of the flavor dynamics. Then the effective Lagrangian, at energies $E \ll M_\chi$, can be written as en expansion in $1/M_\chi$, after integrating out the heavy mediators:

$$\mathcal{L}^{\rm FN}_{ij} = -\overline{Q}_{q_i}u_{u_j}\widetilde{H}\left(\frac{\phi}{M_\chi}\right)^{q_i+u_j} - \overline{Q}_{q_i}d_{d_j}H\left(\frac{\phi}{M_\chi}\right)^{q_i+d_j} - \overline{L}_{l_i}e_{e_j}H\left(\frac{\phi}{M_\chi}\right)^{l_i+e_j} . \tag{I.67}$$

The flavon field acquires a VEV that breaks the flavor symmetry. As long as $\langle\phi\rangle < M_\chi$, the nice feature of this approach is that the Yukawa couplings in Eq.(I.1), and therefore the mass and mixings, are explained as different powers of a common expansion parameter $\epsilon = g\langle\phi\rangle/M_\chi \ll 1$:

$$Y^u_{ij} = \epsilon^{q_i+u_j} \qquad Y^d_{ij} = \epsilon^{q_i+d_j} \qquad Y^e_{ij} = \epsilon^{l_i+e_j} . \tag{I.68}$$

$U(1)_{\rm FN}$ charge assignment												
	$\overline{Q}_1$	$\overline{Q}_2$	$\overline{Q}_3$		u_1	u_2	u_3		d_1	d_2	d_3	
q_i:	3	2	0	u_i:	3	2	0	d_i:	1	0	0	
	$\overline{L}_1$	$\overline{L}_2$	$\overline{L}_3$		e_1	e_2	e_3		H	ϕ	χ	
l_i:	1	0	0	e_i:	3	2	0		0	-1	-3,...,2	

TABLE I.3: A $U(1)_{\rm FN}$ charge assignment for the SM fields, the flavon and the FN mediators involved.

This is depicted in Fig.I.4 via the typical "spaghetti" diagram for the exemplifying case of the up-type Yukawa coupling. The Yukawa couplings become hierarchical if the $U(1)_{\rm FN}$ charges are chosen appropriately. We can take the sine of the Cabibbo angle as a useful expansion parameter $\epsilon = \lambda_C = 0.225$, then in terms of ϵ the mass ratios in the up, down and charged lepton sector read as

$$m_u : m_c : m_t \sim \epsilon^6 : \epsilon^4 : 1\,, \tag{I.69}$$

$$m_d : m_s : m_b \sim \epsilon^4 : \epsilon^2 : 1\,, \tag{I.70}$$

$$m_e : m_\mu : m_\tau \sim \epsilon^4 : \epsilon^2 : 1\,, \tag{I.71}$$

with an identical scaling for the down and charged lepton sectors. To conclude, here we give a three family example, taken from Ref.[37], to show that a $U(1)_{\rm FN}$ flavor symmetry is sufficient to accommodate the SM flavor parameters. Given the charges in Table I.3 we can build the following Yukawa structures that, once order one coefficients are introduced to avoid undesired cancellations, give a good fit of the quark, charged lepton masses and the small CKM mixings

$$Y^u = y_t \begin{pmatrix} \epsilon^6 & \epsilon^5 & \epsilon^3 \\ \epsilon^5 & \epsilon^4 & \epsilon^2 \\ \epsilon^3 & \epsilon^2 & 1 \end{pmatrix}, Y^d = y_b \begin{pmatrix} \epsilon^4 & \epsilon^3 & \epsilon^3 \\ \epsilon^3 & \epsilon^2 & \epsilon^2 \\ \epsilon & 1 & 1 \end{pmatrix}, Y^e = y_\tau \begin{pmatrix} \epsilon^4 & \epsilon^3 & \epsilon \\ \epsilon^3 & \epsilon^2 & 1 \\ \epsilon^3 & \epsilon^2 & 1 \end{pmatrix} \tag{I.72}$$

where the (12)-blocks show an approximate (1,1)-texture zero as in Eq.(I.16). We stress that, in principle, in the physical basis we should also redefine the fields to obtain canonical kinetic terms. In Ref. [38] it is remarked that this can always be achieved by an upper triangular matrix as in Appendix A.1.3. However hierarchical Yukawas usually receive only higher order corrections from the Canonical rotation. Note that in Eq.(I.72), while the $U(1)_{\rm FN}$ flavor charges are used to explain the observed mass hierarchies inside the same family members, the hierarchy between y_t,

y_b, y_τ is left unexplained. Flavor symmetries should be combined with GUT groups to offer a full solution to the flavor puzzle. In this example Q_i, u_i, e_i and d_i, L_i share the same $U(1)_{\rm FN}$ charges, which makes the above structures compatible with an $SU(5)$ unification scenario. Gauge coupling unification suggests that the SM gauge group is generated when a unified larger gauge group is broken at a very high energy scale compared to the electroweak (EW) one. In this picture, SM fermions are accommodated in representations of the unified gauge group $\mathcal{G}_{\rm GUT}$ and an appropriate scalar Higgs sector is introduced both to trigger the spontaneous breaking of $\mathcal{G}_{\rm GUT}$ down to $SU(3)_C \times U(1)_{\rm em}$ and to reproduce the fermion mass matrices. Typically GUTs are quite constrained, and non-trivial relations are obtained among the SM fermion mass matrices. For example, the $SU(5)$ prediction for the Yukawa matrices relates the charged lepton and down quark Yukawas

$$Y^d = Y^{e^T} . \tag{I.73}$$

The relation is not fully rewarding, but it can be improved considering higher Higgs representations, as suggested by Georgi and Jarlskog [39]. This introduces Clebsh-Gordan coefficients (or Georgi and Jarlskog factors) in the relation above that, after the RGE running, turn it nicely consistent with the low energy masses.
The FN approach is successful but mainly useful for explaining hierarchical structures as the order one couplings g remains unspecified. To describe non-hierarchical flavor structures, in the last years, particular attention has been devoted to the study of discrete flavor symmetries, thanks to their simplicity in recovering realistic lepton mixing patterns. The combination of GUT and discrete flavor symmetries has revealed success in various examples [35, 40–43]

I.4.2 Residual symmetries in model building

The two unitary matrices needed to diagonalize the charged lepton and neutrino mass matrices define the PMNS matrix in Eq.(I.25). In the GUT model building, the down type quark mass matrix is related to the charged lepton mass matrix, which is approximately diagonal so that V_e is CKM-like. Therefore it is convenient to work in a basis where the charged leptons are approximately diagonal, and the neutrino mass matrix [35] predominantly defines the entire PMNS matrix. As charged leptons are Dirac particles, one has to consider the square mass matrix $m_e^\dagger m_e$, which, if approximately diagonal, is in general invariant under $U(1)^3$ and thus also under $\mathbb{Z}_m$ for every m. Assuming that the neutrinos are Majorana particles, the maximal

invariance group of the neutrino mass matrix which leaves the neutrino masses unconstrained is the Klein group, the direct product of two copies of the cyclic group of order 2: $\mathbb{Z}_2 \otimes \mathbb{Z}_2$.

This leads to an attractive model-independent approach to get the leptonic mixing matrix $V_{\rm PMNS}$ straight from symmetry considerations [44, 45]. This strategy has already been investigated for several symmetries, for a recent review Ref.[46]. In Article 4 we considered the non-Abelian discrete group A_5 and CP as the leptonic symmetry, as studied in Ref.[47, 48]. At some large energy scale, the theory is invariant under the action of a non-Abelian flavor symmetry group $\mathcal{G}_f = S_4, A_4, A_5, T_7, \Delta(27) \ldots$. Then the scalar sector is built in a suitable way to break $\mathcal{G}_f$ down to two different Abelian subgroups that remain intact: $\mathcal{G}_\nu$ and $\mathcal{G}_e$ in the neutrino and the charged lepton sector respectively. We have to assume

$$\mathcal{G}_e \subset \mathcal{G}_f \quad , \quad \mathcal{G}_\nu \subset \mathcal{G}_f \quad , \quad \mathcal{G}_e \cap \mathcal{G}_\nu = \emptyset \,, \tag{I.74}$$

where $\mathcal{G}_e$ and $\mathcal{G}_\nu$ are often referred to as *residual symmetries*. Here we display that the symmetries $\mathcal{G}_e$ and $\mathcal{G}_\nu$ significantly constrain the form of the neutrino mixing matrix $V_{\rm PMNS}$. For simplicity, we can choose $\mathcal{G}_{e,\nu}$ to be single cyclic groups $\mathcal{G}_e = \mathbb{Z}_m^{g_e}$ and $\mathcal{G}_\nu = \mathbb{Z}_2^{g_\nu}$ with presentation rules

$$\mathbb{Z}_m^{g_e} = \langle 1, g_e \,;\, g_e^m = 1 \rangle \quad , \quad \mathbb{Z}_2^{g_\nu} = \langle 1, g_\nu \,;\, g_\nu^2 = 1 \rangle, \tag{I.75}$$

being $g_{e,\nu}$ elements of $\mathcal{G}_f$ and generators of the $\mathbb{Z}_m^{g_e}$, $\mathbb{Z}_2^{g_\nu}$ subgroups respectively. We can write the action of the elements of the subgroups of $\mathcal{G}_f$ on the lepton mass matrices as

$$\rho(g_e)^\dagger \, m_e m_e^\dagger \, \rho(g_e) = m_e m_e^\dagger \quad , \quad \rho(g_\nu)^T \, m_\nu \, \rho(g_\nu) = m_\nu, \tag{I.76}$$

where in the second equation we used the fact that the neutrinos are Majorana particles [2]. We can diagonalize the group elements $\rho(g_e)$ and $\rho(g_\nu)$ through unitary matrices

$$\rho(g_e)^{\rm d} = \Omega_e^\dagger \rho(g_e) \Omega_e \quad , \quad \rho(g_e)^{\rm d} = \Omega_\nu^\dagger \rho(g_\nu) \Omega_\nu \,, \tag{I.77}$$

where $^{\rm d}$ stands for diagonal. Substituting in Eq.(I.76), it can be checked that the diagonalization of the mass matrices is equivalent to the rotations of the group elements, *i.e.* for diagonal $\rho(g)$, the only matrices that remain invariant are diagonal mass matrices. Therefore, the matrices V_L^e and V_L^ν are determined from $\Omega_{e,\nu}$ up to rephasing

[2] For Dirac neutrinos it will be as for the charged leptons: $\rho(g_\nu)^\dagger m_\nu^\dagger m_\nu \rho(g_\nu) = m_\nu^\dagger m_\nu$.

$K_{e,\nu}$ and permutation $P_{e,\nu}$ matrices:

$$V_L^e = \Omega_e K_e P_e \quad , \quad V_L^\nu = \Omega_\nu K_\nu P_\nu \tag{I.78}$$

Thus, up to Majorana phases and permutations of rows and columns, the lepton mixing matrix $V_{\rm PMNS}$ is given by:

$$V_{\rm PMNS} = V_L^{e\dagger} V_L^\nu = P_e K_e^* \Omega_e^\dagger \Omega_\nu K_\nu P_\nu \, . \tag{I.79}$$

We have seen that the mixing matrix $V_{\rm PMNS}$ is determined through $\mathcal{G}_e$ and $\mathcal{G}_\nu$ and their relative embedding into $\mathcal{G}_f$. However, it is determined only up to exchanges of rows and columns, therefore we do not predict lepton masses in this approach. Hence, the mixing angles are fixed up to a small number of degeneracies, associated with these possible exchanges.
Following the symmetry approach, it is clear that the flavor symmetry must be broken in order to generate the observed non trivial structures. The criteria on the vacuum alignment of the involved flavon VEVs: $\langle\phi^\nu\rangle$,$\langle\phi^e\rangle$ is formulated by the conditions

$$g_e\langle\phi^e\rangle = \langle\phi^e\rangle \quad , \quad g_\nu\langle\phi^\nu\rangle = \langle\phi^\nu\rangle \, . \tag{I.80}$$

where flavons enter linearly in the mass terms

$$\mathcal{L}^\ell = -\frac{\phi^e}{\Lambda}\overline{L}\, e_R H - \frac{\phi^\nu}{\Lambda^2}\overline{L}\, L^c \widetilde{H}\widetilde{H} \, . \tag{I.81}$$

In a consistent model, the alignment must stem from the minimization of the scalar potential without ad-hoc assumptions on its parameters. Popular ingredients for this kind of constructions are:

- the introduction of supplementary scalar degrees of freedom, which are called *driving fields*, singlets under the gauge group.
- additional symmetries, apart from $\mathcal{G}_f$, which are necessary to forbid those Lagrangian operators which would prevent the desired vacuum alignment.

An example with $\mathcal{G}_f = S_4$

We present an explicit example of the above discussion in the case of $\mathcal{G}_f = S_4$, the non Abelian group of permutations of 4 objects. It can be defined in terms of three

generators S, T and U satisfying the presentation rule

$$S_4 = \langle 1, S, T, U \,;\, S^2 = T^3 = U^2 = (ST)^3 = (SU)^2 = (TU)^2 = (STU)^4 = 1 \rangle. \quad \text{(I.82)}$$

It has 5 irreducible representations: two singlets $\mathbf{1}, \mathbf{1}'$, two triplets $\mathbf{3}, \mathbf{3}'$ and a doublet $\mathbf{2}$, such that there are $1^2 + 1^2 + 3^2 + 3^2 + 2^2 = 24 = 4!$ elements in S_4. The Abelian subgroups of S_4 are: four Klein groups $\mathbb{V}$, four $\mathbb{Z}_3$ groups and three different $\mathbb{Z}_4$. For example, from (I.82) it is clear that T is a generator of a cyclic subgroup of order 3 while S, U generate a Klein subgroup. So we choose $\mathcal{G}_e = \mathbb{Z}_3$ and $\mathcal{G}_\nu = \mathbb{V}$ with presentations

$$\mathbb{Z}_3 = \langle 1, T \,;\, T^3 = 1 \rangle \quad , \quad \mathbb{V} = \langle 1, S, U \,;\, S^2 = U^2 = (SU)^2 = 1 \rangle \,. \quad \text{(I.83)}$$

We work in the basis for S_4 in which the irreducible representations of the generators S, T and U are

$$\begin{aligned}
\mathbf{1}, \mathbf{1}' &: && S = 1 \,,\; U = \pm 1 \,,\; T = 1 \,, \\
\mathbf{2} &: && S = \begin{pmatrix} 1 & 0 \\ 0 & 1 \end{pmatrix} \,,\; U = \begin{pmatrix} 0 & 1 \\ 1 & 0 \end{pmatrix} \,,\; T = \begin{pmatrix} \omega & 0 \\ 0 & \omega^2 \end{pmatrix} \,, \\
\mathbf{3}, \mathbf{3}' &: && S = \tfrac{1}{3} \begin{pmatrix} -1 & 2 & 2 \\ 2 & -1 & 2 \\ 2 & 2 & -1 \end{pmatrix} \,,\; U = \mp \begin{pmatrix} 1 & 0 & 0 \\ 0 & 0 & 1 \\ 0 & 1 & 0 \end{pmatrix} \,,\; T = \begin{pmatrix} 1 & 0 & 0 \\ 0 & \omega^2 & 0 \\ 0 & 0 & \omega \end{pmatrix} \,,
\end{aligned} \quad \text{(I.84)}$$

where $\omega = e^{2i\pi/3}$. Note that the T generator is diagonal. We can choose $\rho(g_e) = T_{\mathbf{3}}$ such that $\Omega_e = \mathbb{1}$ and we are directly in a basis where the charged lepton matrix $m_e m_e^\dagger$ is diagonal. We can also choose $\rho(g_\nu) = S_{\mathbf{3}}$, for which the diagonalization matrix Ω_ν is given by

$$\Omega_\nu = V_{\text{TB}} \equiv \begin{pmatrix} \sqrt{\frac{2}{3}} & \frac{1}{\sqrt{3}} & 0 \\ -\frac{1}{\sqrt{6}} & \frac{1}{\sqrt{3}} & -\frac{1}{\sqrt{2}} \\ -\frac{1}{\sqrt{6}} & \frac{1}{\sqrt{3}} & \frac{1}{\sqrt{2}} \end{pmatrix} \,, \quad \text{(I.85)}$$

This leads to a popular simplified form of the neutrino mass matrix called *Tri-Bi-Maximal* (TB) mixing

$$V_{\text{PMNS}} = K_e^* V_{\text{TB}} K_\nu P_\nu \quad \text{(I.86)}$$

which implies $s^2_{12} = 1/3$, $s^2_{23} = 1/2$ and a vanishing reactor angle $s_{13} = 0$. The conditions on the vacuum alignment of Eq.(I.80) correspond to the requirements that

$$T\langle\phi^e\rangle = \langle\phi^e\rangle \quad , \quad S\langle\phi^\nu\rangle = U\langle\phi^\nu\rangle = \langle\phi^\nu\rangle\,. \tag{I.87}$$

The first condition is satisfied from a flavon VEV $\langle\phi^e\rangle$ in either the $\mathbf{1}, \mathbf{1}', \mathbf{3}$ and $\mathbf{3}'$ representations, demanding $T_{\mathbf{3},\mathbf{3}'}(a,b,c)^T = (a,b,c)$ the vacuum alignment is

$$\langle\phi^e_{\mathbf{1},\mathbf{1}'}\rangle = v^e_{\mathbf{1},\mathbf{1}'} \quad , \quad \langle\phi^e_{\mathbf{3},\mathbf{3}'}\rangle = v^e_{\mathbf{3},\mathbf{3}'}\begin{pmatrix}1\\0\\0\end{pmatrix}\,, \tag{I.88}$$

which can only result in a diagonal mass matrix $m_e m_e^\dagger$ for the charged leptons. From Eq.(I.84) we see that U, because of the minus sign in the definition, is always broken by the VEV $\langle\phi^\nu\rangle$ of a flavon transforming in the $\mathbf{1}'$ or $\mathbf{3}$ representations. On the other hand flavon fields in the $\mathbf{1}$, $\mathbf{2}$ and $\mathbf{3}'$ representations can be adopted, demanding $S_{\mathbf{2}}(a,b)^T = (a,b)$ and $S_{\mathbf{3}}(a,b,c)^T = (a,b,c)$, the vacuum alignment is

$$\langle\phi^\nu_{\mathbf{1}}\rangle = v^\nu_{\mathbf{1}} \quad , \quad \langle\phi^\nu_{\mathbf{2}}\rangle = v^\nu_{\mathbf{2}}\begin{pmatrix}1\\1\end{pmatrix} \quad , \quad \langle\phi^\nu_{\mathbf{3}'}\rangle = v^\nu_{\mathbf{3}'}\begin{pmatrix}1\\1\\1\end{pmatrix}\,. \tag{I.89}$$

Substituting in Eq.(I.81) and contracting the fields considering that $L \sim \mathbf{3}, \mathbf{3}'$, the most general neutrino mass matrix looks like

$$m_\nu = \frac{v_H^2}{\Lambda^2}\left[v^\nu_{\mathbf{3}'}\begin{pmatrix}2&-1&-1\\-1&2&-1\\-1&-1&2\end{pmatrix} + v^\nu_{\mathbf{1}}\begin{pmatrix}1&0&0\\0&0&1\\0&1&0\end{pmatrix} + v^\nu_{\mathbf{2}}\begin{pmatrix}0&1&1\\1&1&0\\1&0&1\end{pmatrix}\right]\,. \tag{I.90}$$

Redefining $v^\nu_{\mathbf{3}'} = z/3$, $v^\nu_{\mathbf{1}} = x - 2z/3$, $v^\nu_{\mathbf{2}} = y + z/3$ the neutrino mass matrix is usually displayed in the following form

$$m_\nu = \frac{v_H^2}{\Lambda^2}\begin{pmatrix}x&y&y\\y&y+z&x-z\\y&x-z&y+z\end{pmatrix}\,, \tag{I.91}$$

which is left invariant under the action of S, U and diagonalized by the TB mixing, with eigenvalues $m'_\nu = \mathrm{diag}(x-y, x+y, x+y+2z)$.

I.4.3 Generalized CP symmetry

The measurements of a non vanishing reactor mixing angle θ_{13}^{ℓ} clearly show that many simple patterns like the TB mixing are strongly disfavoured. A variation of the approach adds CP as a residual symmetry in the neutrino sector, such as $\mathcal{G}_\nu \to \mathcal{G}_\nu \times \text{CP}$. This modifies the mixing coming from pure $\mathcal{G}_\nu$ and introduces a continuous variable θ which parametrizes this departure. A non vanishing reactor mixing angle can be easily accommodated by an appropriate choice of θ and, at the same time, testable relations between mixing angles and Dirac as well as Majorana phases are obtained. Under the action of CP, a generic field transforms

$$\psi(x) \to X\,\psi^*(x_{\text{CP}}) \tag{I.92}$$

where X is the representations of the CP operator in field space and $x_{\text{CP}} = (x^0, -\boldsymbol{x})$ is the space-time coordinate transformed under the CP transformation. We choose the framework in which the residual symmetry is $\mathcal{G}_\nu = \mathbb{Z}_2 \times \text{CP}$ as in Article 3. The action of X_ν on the neutrino mass matrices, is given by

$$X_\nu^T m_\nu X_\nu = m_\nu^*\,, \tag{I.93}$$

where the X have to be a symmetric matrix $X^\dagger X = X X^\dagger = 1$, this is a necessary condition, otherwise the neutrino mass spectrum would be partially degenerate [44]. In addition, the consistency condition between $\mathbb{Z}_2^{g_\nu}$ and CP has to be fulfilled

$$X_\nu\,\rho^*(g_\nu) X_\nu^{-1} = \rho(g_\nu)\,. \tag{I.94}$$

To derive the form of the unitary diagonalization matrix V_ν of the Majorana mass matrix m_ν we follow Ref. [44, 49]. Let $\rho(g_\nu)$ be diagonalized by an $\Omega_{\nu 1}$ matrix as in Eq.(I.77), expressing $\rho(g_\nu)$ from this equation and substituting it in the consistency condition in Eq.(I.94), we have

$$\rho(g_\nu)^{\text{d}} \Omega_{\nu 1}^\dagger X_\nu \Omega_{\nu 1}^* \rho(g_\nu)^{\text{d}} = \Omega_{\nu 1}^\dagger X_\nu \Omega_{\nu 1}^* \tag{I.95}$$

this means that $\Omega_{\nu 1}^\dagger X_\nu \Omega_{\nu 1}^*$ is a block diagonal matrix. Being a complex (unitary) symmetric matrix, it is diagonalised by a unitary matrix $\Omega_{\nu 2}$ via the transformation:

$$\Omega_{\nu 2}^\dagger (\Omega_{\nu 1}^\dagger X_\nu \Omega_{\nu 1}^*) \Omega_{\nu 2}^* = (\Omega_{\nu 1}^\dagger X_\nu \Omega_{\nu 1}^*)^{\text{d}}\,. \tag{I.96}$$

We can choose $(\Omega_{\nu 1}^\dagger X_\nu \Omega_{\nu 1}^*)^{\text{d}} = \mathbb{1}$ moving the possible phases to $\Omega_{\nu 2}$. With this choice

the Takagi factorisation of the X_ν (valid for unitary symmetric matrices) gives

$$X_\nu = \Omega_\nu \Omega_\nu^T \tag{I.97}$$

with $\Omega_\nu = \Omega_{\nu 1}\Omega_{\nu 2}$. This implies that the matrix Ω_ν also diagonalizes $\rho(g_\nu)$

$$\Omega_\nu^\dagger \rho(g_\nu)\Omega_\nu = \Omega_{\nu 2}^\dagger \rho(g_\nu)^{\mathrm{d}}\Omega_{\nu 2} = \rho(g_\nu)^{\mathrm{d}} \tag{I.98}$$

Employing the above equation together with Eq.(I.76), we have that

$$\rho(g_\nu)^{\mathrm{d}}\Omega_\nu^T m_\nu \Omega_\nu \rho(g_\nu) = \Omega_\nu^T m_\nu \Omega_\nu \,, \tag{I.99}$$

this implies that the combination $\Omega_\nu^T m_\nu \Omega_\nu$ is constrained to be a real block diagonal matrix. Thus the mass matrix can be fully diagonalized by a rotation $R_{ij}(\theta)$ in the ij-plane of degenerate eigenvalues of $\rho(g_\nu)$. In this way the matrix m_ν can be diagonalized with a unitary matrix defined as

$$V_L^\nu = \Omega_\nu R_{ij}(\theta) K_\nu P_\nu \,. \tag{I.100}$$

The mass spectrum is not fixed and thus permutations of columns are admitted. The inclusion of the charged leptons is as discussed in Sec. I.4.2. The full V_{PMNS} is given by

$$V_{\mathrm{PMNS}} = K_e^* P_e \Omega_e^\dagger \Omega_\nu \, R_{ij}(\theta) K_\nu P_\nu \,. \tag{I.101}$$

Non-Abelian discrete symmetries in conjunction with the CP symmetry have been massively explored in the very recent years, for example, the interplay between S_4 and CP has been studied in Ref.[49, 50]. This class of models are quite predictive and one obtains specific correlations between the values of the three neutrino mixing angles, while the leptonic CP phases are typically predicted to be exactly 0 or π, or else $\pi/2$ or $3\pi/2$.

I.5 The Origin of Flavor

A plethora of possible choices for the flavor symmetry and its breaking are compatible with the existing flavor data: Abelian or non-Abelian, continuous or discrete, and with a variety of gauge groups and representations.
By suitable assignments of flavor charges to the different fields, the size of the Yukawa couplings depends only on the dimensionless parameter $\epsilon = \langle\phi\rangle/M$. Implying that the flavor dynamics can equally occur at the EW scale as well as the Planck

scale. So the flavor symmetry could be broken at any scale above the TeV scale: $M_{\rm EW} \ll \Lambda_f < M_{\rm Pl}$ where $\Lambda_f \simeq \langle\phi\rangle$. Indeed, from theoretical guidance, high scale flavor symmetries are more appealing. The drawback of this perspective is that testing such high scale theories, through direct searches of the flavons and FN mediators at colliders, would be very difficult.

In the framework of the SM, all the information we can extract on flavor is the Yukawa eigenvalues (quark and lepton masses) and the left-handed misalignment between up and down quarks (CKM matrix) or leptons (PMNS matrix). This is not sufficient to settle the full structure of the Yukawa matrices. Therefore, if the Yukawa couplings are the only remnant of flavor symmetry breaking, we may never be able to unravel the *Origin of Flavor*.

The presence of *physics Beyond the Standard Model* (BSM) sensitive to flavor, for instance, Supersymmetry, is not an obstacle for flavor but, on the contrary, an opportunity to advance in our understanding of the flavor puzzle [51]. In supersymmetric extensions of the SM, the new interactions can provide fundamental insights into the physics of flavor. Building on the previous work [52], in Article 1-4, we show that finding a solution to the SM flavor problem will also resolve the so-called supersymmetric flavor problem to a sufficient degree. In this section, we limit ourselves to introduce the Minimal Supersymmetric Standard Model and the supersymmetric flavor problem following the nomenclature or Ref.[53].

I.5.1 Supersymmetry

During the last decades, Supersymmetry (SUSY) has been at the core of extensive research into BSM physics, and it remains yet one of the most compelling possibilities for New Physics (NP).

Supersymmetry is an extension of the Poincaré symmetry of spacetime, establishing a relation between fermions and bosons. A Supersymmetry transformation turns a fermionic state into a bosonic one and vice versa. A *supermultiplet* is an irreducible representation of the Supersymmetry algebra and, therefore, must contain an equal number of fermionic and bosonic states. The combination of a Weyl fermion ψ and a complex scalar field ϕ is referred to as a chiral supermultiplet. While a combination of a Vector boson field A_μ and a Majorana fermion λ is called a gauge supermultiplet. Clearly, the vector bosons of the Standard Model must reside in gauge supermultiplets, their fermionic superpartners are generically referred to as *gauginos*. Meanwhile, a chiral supermultiplet has to accommodate the SM fermions and the Higgs, their superpartners are called *sfermions* and *higgsinos* respectively. None of the su-

	(s) Leptons		**(s) Quarks**			**Higgs (inos)**			**Gaug (inos)**		
Φ_i	L_i	e_i^c	Q_i	u_i^c	d_i^c	H_u	H_d	V_{WZ}	G^a	W^a	B
ϕ_i	$\begin{pmatrix}\widetilde{\nu}_i\\ \widetilde{e}_i\end{pmatrix}_L$	$\widetilde{e}^*_{iR}$	$\begin{pmatrix}\widetilde{u}_i\\ \widetilde{d}_i\end{pmatrix}_L$	$\widetilde{u}^*_{iR}$	$\widetilde{d}^*_{iR}$	$\begin{pmatrix}H_u^+\\ H_u^0\end{pmatrix}$	$\begin{pmatrix}H_d^0\\ H_d^-\end{pmatrix}$	A^a_μ	g^a_μ	W^a_μ	B_μ
ψ_i	$\begin{pmatrix}\nu_i\\ e_i\end{pmatrix}_L$	$e^\dagger_{iR}$	$\begin{pmatrix}u_i\\ d_i\end{pmatrix}_L$	$u^\dagger_{iR}$	$d^\dagger_{iR}$	$\begin{pmatrix}\widetilde{H}_u^+\\ \widetilde{H}_u^0\end{pmatrix}$	$\begin{pmatrix}\widetilde{H}_d^0\\ \widetilde{H}_d^-\end{pmatrix}$	λ^a	$\widetilde{g}^a$	$\widetilde{W}^a$	$\widetilde{B}$
$SU(3)_C$	**1**	**1**	**3**	$\overline{\mathbf{3}}$	$\overline{\mathbf{3}}$	**1**	**1**		**8**	**1**	**1**
$SU(2)_L$	**2**	**1**	**2**	**1**	**1**	**2**	**2**		**1**	**2**	**1**
$U(1)_Y$	$-1/2$	1	$1/6$	$-2/3$	$-1/3$	$1/2$	$-1/2$		0	0	0

TABLE I.4: Supermultiplets in the MSSM. We display the scalar, ϕ, and Weyl fermion, ψ, components of the chiral supermultiplets together with their quantum numbers. For completeness we show also the vector boson A^a_μ and Majorana fermion λ^a components of the gauge supermultiplets.

perpartners of SM particles can be identified with some other Standard Model state. Thus they are new particles that have eluded our searches so far.

In the limit of preserved Supersymmetry, the components of a supermultiplet have equal masses and reside in the same gauge group's representation. As the Supersymmetry generators commute with those of gauge transformations, this implies all fields within a supermultiplet have the same weak hypercharge, weak isospin, and color charge, and consequently equal electric charge. In Table I.4, we display the minimal set of supermultiplets required to house all of the SM particles.

An elegant description of Supersymmetry promotes the supermultiplet to an object known as a superfield. This is defined on a manifold called superspace which is the extension of the ordinary spacetime bosonic coordinates with four fermionic (or Grassmann) coordinates:

$$\left\{x^\mu, \theta^\alpha, \theta^\dagger_{\dot\alpha}\right\}, \tag{I.102}$$

with $\mu = 0,1,2,3$ and $\alpha = 1,2$. As we are interested in the flavor sensitive part of the SUSY Lagrangian, in the following we sketch how a general chiral Lagrangian is built using the superspace formalism. The most general chiral superfield in terms of the coordinates $\left\{x, \theta, \theta^\dagger\right\}$, expanded in the fermionic coordinates, is given by

$$\begin{aligned}\Phi &= \left(1 + i\theta^\dagger\overline{\sigma}^\mu\theta\partial_\mu + \frac{1}{4}\theta\theta\theta^\dagger\theta^\dagger\partial_\mu\partial^\mu\right)\phi(x)\\ &+ \left(\sqrt{2}\theta - \frac{i}{\sqrt{2}}\theta\theta\theta^\dagger\overline{\sigma}^\mu\theta\partial_\mu\right)\psi(x) + \theta\theta\, F(x) \quad \subset \quad (\phi, \psi, F)\,.\end{aligned} \tag{I.103}$$

Hence, a chiral superfield contains as component fields a complex scalar ϕ, a two-component Weyl fermion ψ, together with a non-propagating auxiliary bosonic field F, introduced to define a chiral superfield also off-shell consistently. On-shell, we can use the equation of motion for F to express it in terms of ϕ, ψ, so that, as desired, a chiral supermultiplet contains an equal number of fermionic and bosonic degrees of freedom. From the products of chiral superfields, we can build the most general chiral Lagrangian

$$\mathcal{L}^{\text{SUSY}}_{\text{ch.}} = [\Phi_i^\dagger \Phi_i]_D + [W(\Phi_i) + \text{c.c.}]_F \,, \tag{I.104}$$

$$\text{where} \quad [\cdots]_D = \int d^2\theta d^2\theta^\dagger [\cdots] \,, \tag{I.105}$$

$$[\cdots]_F = \int d^2\theta [\cdots]|_{\theta^\dagger=0} + \int d^2\theta^\dagger [\cdots]|_{\theta=0} \,. \tag{I.106}$$

In Eq.(I.104), the first term gives the kinetic contributions for the component fields while a single holomorphic[3] function of the complex scalar fields determine the non-gauge interactions for chiral supermultiplets, the so-called *Superpotential* W, its most general form is

$$W(\Phi_i) = \frac{1}{2} M^{ij} \Phi_i \Phi_j + \frac{1}{6} y^{ijk} \Phi_i \Phi_j \Phi_k \,. \tag{I.107}$$

Using (I.103) to re-express Eq.(I.104) in terms of its components gives

$$[\Phi_i^\dagger \Phi_i]_D = -\partial^\mu \phi^{*i} \partial_\mu \phi_i + i\psi^{\dagger i} \bar{\sigma}^\mu \partial_\mu \psi_i + F^{*i} F_i + (\text{total deriv.}) \tag{I.108}$$

$$\begin{aligned} [W(\Phi_i)]_F &= \frac{1}{2} M^{ij} \left(\phi_i F_j + \phi_j F_i - \psi_i \psi_j \right) \\ &\quad + \frac{1}{6} y^{ijk} \left(\phi_i \phi_j F_k + \phi_k \phi_i F_j + \phi_i \phi_k F_i + \psi_i \psi_j \phi_k + \psi_k \psi_i \phi_j + \psi_i \psi_k \phi_i \right) \,. \end{aligned} \tag{I.109}$$

No kinematic terms for the auxiliary fields F_i, F_i^* appear in $\mathcal{L}^{\text{ch.}}$, thus they can be integrated out using their equations of motions $\partial \mathcal{L}^c h./\partial F_k = 0$ and $\partial \mathcal{L}^c h./\partial F^{*k} = 0$ that give

$$F_k = -\frac{\partial [W(\Phi_i)]^*_F}{\partial F^{*k}} = -M^*_{ki} \phi^{*i} + \frac{1}{2} y^*_{kij} \phi^{*i} \phi^{*j} \,, \tag{I.110}$$

the same for F_i^*. Once F_i, F_i^* have been removed from (I.108) and (I.109) we can substitute into Eq.(I.104) and the chiral Lagrangian for interactive superfields in terms of

[3] Which means it can not contain vertices involving $\Phi^{\dagger k}$.

the physical components reads

$$\mathcal{L}^{\text{SUSY}}_{\text{ch.}} = -\partial^\mu \phi^{*i} \partial_\mu \phi_i + i\psi^{\dagger i}\bar{\sigma}^\mu \partial_\mu \psi_i + V(\phi, \phi^*) \tag{I.111}$$

$$+ \frac{1}{2} M^{ij}\psi_i\psi_j + \frac{1}{2} y^{ijk}\phi_i\psi_j\psi_k + \text{c.c.}\,, \tag{I.112}$$

$$\text{with} \quad V = F^{*i}F_i = M^*_{ik}M^{kj}\phi^{*i}\phi^j + \frac{1}{2} M^{il} y^*_{jkl}\phi_i\phi^{*j}\phi^{*k} \tag{I.113}$$

$$+ \frac{1}{2} M^*_{il} y^{jkl}\phi^{*i}\phi_j\phi_k + \frac{1}{4} y^{ijl} y^*_{kml}\phi_i\phi_j\phi^{*k}\phi^{*m}\,. \tag{I.114}$$

In the first line, we can see that this lagrangian contains the required kinetic terms and a purely scalar potential V, while, in the second line, we have mass-like contributions and Yukawa interactions for the fermionic components.

Driving fields: In SUSY frameworks, the minimization of the superpotential of the model demands both flavons and driving fields. In the limit of unbroken SUSY, the minimum of the related scalar potential V is given by the derivatives of W with respect to the components of the driving fields ϕ^0, which define a set of equations for the components of the flavon fields ϕ. Suppose that a driving ϕ^0 and a flavon ϕ triplet, with components (ϕ_1, ϕ_2, ϕ_3), comprise the SM singlet, in such a way that terms like $\phi^0\phi$ and $\phi^0\phi^2$ are flavor invariant. Thus, the most general renormalizable superpotential is given by:

$$W = M\,\phi^0\phi + y\,\phi^0\phi\phi\,. \tag{I.115}$$

As we are in unbroken SUSY, the potential is defined positive $V = |F|^2 + D^2$, then the minimum is given by $F = 0$ and $D = 0$. The vacuum conditions for the ϕ field are then

$$\begin{cases} \dfrac{\partial W}{\partial \phi^0_1} = M\phi_1 + y\,\phi_2\phi_3 = 0 \\ \dfrac{\partial W}{\partial \phi^0_2} = M\phi_2 + y\,\phi_3\phi_1 = 0 \\ \dfrac{\partial W}{\partial \phi^0_3} = M\phi_3 + y\,\phi_1\phi_2 = 0 \end{cases} \quad \rightarrow \quad \langle\phi\rangle = v\begin{pmatrix}1\\1\\1\end{pmatrix},\ v = -\frac{M}{y} \tag{I.116}$$

while the vacuum conditions for a driving field always give $\langle\phi^0\rangle = 0$. The presence of driving fields is not a necessary condition for obtaining the correct vacuum alignment. Although this usually implies dealing with longer and more complicated potentials like the one considered in Appendix E.1.

I.5.2 Soft terms and the supersymmetric flavor problem

Supersymmetry cannot remain unbroken at the electroweak scale, or these superpartners would already have been discovered. A realistic phenomenological model must incorporate Supersymmetry breaking.
Theoretically, we presume that Supersymmetry is a spontaneously broken exact symmetry. The specific mechanism through which the breaking occurs is not apparent. What is clear is that it requires to enlarge the MSSM to a hidden sector of particles with not appreciable couplings to the visible sector of chiral supermultiplets of the MSSM. So the breaking should occur in the hidden sector and be communicated to the visible sector either radiatively or through non-renormalizable interactions.
A possibility is to couple the hidden sector to the visible sector through gravitational-strength interactions that is the scenario described in Sec. I.5.3 and the explicit framework of our analysis in Articles 1-4.
Practically, it is useful to parametrize our ignorance of SUSY-breaking by adding explicit terms that break Supersymmetry in the effective Lagrangian. Normally these terms should be *soft* in the sense of positive mass dimension

$$\mathcal{L}_{\text{soft}} = -\left(\frac{1}{2}M_a\lambda^a\lambda^a + \frac{1}{6}a^{ijk}\phi_i\phi_j\phi_k + \frac{1}{2}b^{ij}\phi_i\phi_j + \text{c.c.}\right) - (\widetilde{m}^2)^j_i\phi^{\dagger i}\phi_j\,. \quad \text{(I.117)}$$

They consist of gaugino masses M_a, scalar squared-mass terms $\widetilde{m}^2_{ij}$ and b_{ij} and trilinear couplings a_{ijk}. Clearly these contributions break Supersymmetry since the corresponding terms for the superpartners in (I.111) do not exist. The largest mass scale associated with the soft terms is usually denoted m_{soft}. The total correction to the Higgs scalar squared mass must vanish in the $m_{\text{soft}} \to 0$ limit

$$\Delta m_H^2 = m_{\text{soft}}^2\left[\frac{\lambda}{16\pi^2}\log\left(\frac{\Lambda_{\text{UV}}}{m_{\text{soft}}}\right) + \cdots\right]. \quad \text{(I.118)}$$

The parameters m_{soft}, appearing in $\mathcal{L}_{\text{soft}}$, ascertain the mass splittings between the known SM particles and their superpartners, which tells us that the superpartner masses should not be too large. Otherwise, we would miss the successful remedy for the EW hierarchy problem. Using $\Lambda_{\text{UV}} = M_{\text{Pl}} \sim 10^{19}$ GeV and $\lambda \sim 1$ in, one concludes that m_{soft}, and consequently the masses of at least the lightest few superpartners, should plausibly not be much higher than the TeV scale.

Outlook of the MSSM

A set of minimal assumptions define the *Minimal Supersymmetric version of the Standard Model (MSSM)*:

- Minimal particle content and soft-breaking terms.
- Minimal gauge group $SU(3)_C \times SU(2)_L \times U(1)_Y$ and R-parity conservation.

The R-parity is an additional $\mathbb{Z}_2$ symmetry: the SM particles are assigned $P_R = +1$ while the sfermions, gauginos and higgsinos have $P_R = -1$. This forbids mixing between particles and sparticles. The most intriguing phenomenological consequence of this is that the Lightest Supersymmetric Particle (LSP) is stable and, if electrically neutral, forms an exceptional dark matter candidate, in the category of Weakly Interacting Massive Particles (WIMP).
Against this background, the MSSM Lagrangian can be written as

$$\mathcal{L}^{\text{MSSM}} = \mathcal{L}^{\text{SUSY}}_{\text{ch.}} + \mathcal{L}^{\text{SUSY}}_{\text{gau.}} + \mathcal{L}^{\text{MSSM}}_{\text{soft}}\,, \tag{I.119}$$

where $\mathcal{L}^{\text{SUSY}}$ contains all of the gauge and Yukawa interactions and preserves Supersymmetry invariance, and $\mathcal{L}_{\text{soft}}$ violates Supersymmetry but admits only mass terms and coupling parameters with positive mass dimension. The Superpotential for the MSSM is

$$W^{\text{MSSM}}_{\text{ij}} \;=\; Y^{u}_{\text{ij}}\,\text{Q}_\text{i}\,\text{u}^\text{c}_\text{j}\,\text{H}_\text{u} - Y^{d}_{\text{ij}}\,\text{Q}_\text{i}\,\text{d}^\text{c}_\text{j}\,\text{H}_\text{d} - Y^{e}_{\text{ij}}\,\text{L}_\text{i}\,\text{e}^\text{c}_\text{j}\,\text{H}_\text{d} + \mu\,\text{H}_\text{u}\text{H}_\text{d}\,. \tag{I.120}$$

where $\text{Q}, \text{L}, \text{u}^\text{c}, \text{d}^\text{c}, \text{e}^\text{c}, \text{H}_\text{u}, \text{H}_\text{d}$ are the left-handed chiral superfields corresponding to the chiral supermultiplets in Table I.4 on-shell. The $Y^{u,d,e}$ are the usual Yukawa couplings, and the μ term is the supersymmetric version of the Higgs mass. Note that, due to the Superpotential's holomorphycity, unlike in the SM, the Higgs sector requires two different chiral superfields to be able to write down this term. After EWSB, the W and B bosons mix to generate the $W^\pm$, Z and γ. Meanwhile, the mass eigenstates of their gaugino superpartners are two *charginos* $\chi^\pm_{1,2}$ and four *neutralinos* $\chi^0_{1,2,3,4}$ that come from the mixing among themselves and the higgsinos. Here we are not interested in describing the gauge part of the Lagrangian, for which we refer the reader to Ref.[53].

A complete description of the MSSM needs the soft Supersymmetry breaking terms to be specified. Writing Eq.(I.117) for the MSSM we have

$$\begin{aligned}
\mathcal{L}_{\text{soft}}^{\text{MSSM}} &= \frac{1}{2}\left(M_1\widetilde{B}\widetilde{B} + M_2\widetilde{W}\widetilde{W} + M_3\widetilde{g}\widetilde{g} + \text{c.c.}\right) && \text{(I.121)}\\
&+ m_{H_u}^2 H_u^* H_u + m_{H_d}^2 H_d^* H_d + (b H_u H_d + \text{h.c.}) && \text{(I.122)}\\
&+ \widetilde{m}_Q^2\,\widetilde{Q}^\dagger\widetilde{Q} + \widetilde{m}_u^2\,\widetilde{u}_R^\dagger\widetilde{u}_R + \widetilde{m}_d^2\,\widetilde{d}_R^\dagger\widetilde{d}_R + \widetilde{m}_L^2\,\widetilde{L}^\dagger\widetilde{L} + \widetilde{m}_e^2\,\widetilde{e}_R^\dagger\widetilde{e}_R && \text{(I.123)}\\
&+ \left(a_u\,\widetilde{Q}\,\widetilde{u}_R^* H_u + a_d\,\widetilde{Q}\,\widetilde{d}_R^* H_d + a_e\,\widetilde{L}\,\widetilde{e}_R^* H_d + \text{h.c.}\right). && \text{(I.124)}
\end{aligned}$$

In the second line of we have Supersymmetry-breaking contributions to the Higgs potential: $m_{H_u}^2$ and $m_{H_d}^2$ are mass terms, while b is the only squared-mass term that can occur in the MSSM. Each of the $\widetilde{m}_{Q,L}^2$, $\widetilde{m}_{u,d,e}^2$ is a 3×3 hermitian matrix in family space called *soft mass matrices*. Finally, each of $a_{u,d,e}$ is a complex 3×3 matrix in flavor space known as *trilinear matrices*. A one-to-one correspondence exists between the Yukawa couplings of the Superpotential and the trilinears. We expect

$$M_{1,2,3}\,,\; a_{u,d,e} \sim m_{\text{soft}} \quad , \quad \widetilde{m}_{Q,L}^2\,,\; \widetilde{m}_{u,d,e}^2 \sim m_{\text{soft}}^2 \tag{I.125}$$

with a characteristic mass scale m_{soft}, not much larger than 1 TeV. The expression is the most general soft Supersymmetry-breaking Lagrangian of the form that is compatible with gauge invariance and matter parity conservation in the MSSM. Unlike the Supersymmetry-preserving part of the Lagrangian, the above $\mathcal{L}_{\text{soft}}^{\text{MSSM}}$ introduces many soft new parameters that were not present in the ordinary SM. A careful count reveals 105 additional masses, phases, and mixing angles in the MSSM Lagrangian that cannot be rotated away by field redefinitions for the quark and lepton supermultiplets, and have no counterpart in the ordinary SM. Thus, in principle, Supersymmetry breaking appears to introduce a tremendous arbitrariness in the Lagrangian. We can state the *supersymmetric flavor problem* as follows [51]: the SUSY soft-breaking terms have a completely separate origin from the Yukawa couplings in the Superpotential and we have no knowledge upon their structure. On general grounds, we could expect that all the entries in the soft breaking matrices were $\mathcal{O}(1)$ in any basis and, in particular, in the basis of diagonal Yukawa couplings. In this situation, FCNC and CP violation observables would receive significant contributions from loops involving SUSY particles. This disagrees strongly with the stringent phenomenological bounds on these processes, as discussed in Sec.I.6.

I.5.3 Planck-scale-mediated soft terms

Specific models for the soft terms can predict the masses and the mixing angles for the MSSM in terms of fewer parameters. This is the case of the MSUGRA models in which the spontaneous Supersymmetry breaking sector connects with the MSSM sector mostly through, Planck scale suppressed, gravity interactions. Thus the SUSY mediation scale is the Plank-scale: $\Lambda_{\rm Med} = M_{\rm Pl}$. The most general supersymmetric non-renormalizable Lagrangian involving only chiral superfields is given by

$$\mathcal{L} = \left[K(\Phi_i^\dagger, \Phi_j)\right]_D + \left[\frac{1}{4} f_{ab}(\Phi_i)\widehat{\mathcal{W}}^{a\alpha}\widehat{\mathcal{W}}^b_\alpha + W(\Phi_i) + \text{c.c}\right]_F \tag{I.126}$$

where

- The *Kähler potential* K: it is a function of both chiral and anti-chiral superfields. In renormalizable theories it is just $K = \Phi_i^\dagger \Phi_i$.
- The *Superpotential* W: contrary to the Kähler, it is an arbitrary holomorphic function of the only chiral superfields treated as complex variables.
- The *Gauge kinetic function* f_{ab}: like the superpotential, it a holomorphic function of the chiral superfields treated as complex variables.

Let X be the spurion chiral superfield whose F_X term eventually takes a VEV: $X \to \theta\theta\langle F_X\rangle$, $X^* \to \theta^\dagger\theta^\dagger\langle F_X^*\rangle$ that breaks Supersymmetry. The SUSY breaking scale is given by $\Lambda_{\rm SUSY} = \sqrt{\langle F_X\rangle}$. We assume, for simplicity, that there is a single F-term, that encodes the effects of SUSY-breaking in the hidden sector, and couples, through gravitational interactions, universally to all the visible-sector fields. Then the potentials in Eq.(I.126) expanded in $1/M_{\rm Pl}$ read

$$W = W^{\rm MSSM}_{\rm ren} - \frac{1}{M_{\rm Pl}}\left(\frac{1}{6} y^X_{ijk} X\Phi_i\Phi_j\Phi_k + \frac{1}{2}\mu^X_{ij} X\Phi_i\Phi_j\right) + \dots , \tag{I.127}$$

$$K = \Phi_i^\dagger\Phi_j + \frac{1}{M_{\rm Pl}^2} k_{ij}\Phi_i^\dagger\Phi_j XX^\dagger + \dots , \tag{I.128}$$

$$f_{ab} = \frac{\delta_{ab}}{g_a^2}\left(1 - \frac{2}{M_{\rm Pl}} f_a X + \dots\right) . \tag{I.129}$$

The resulting Supersymmetry-breaking Lagrangian, after integrating out the auxiliary fields in Φ_i is

$$\begin{aligned}\mathcal{L}_{\rm soft} = &- \left(\frac{\langle F_X\rangle}{2M_{\rm Pl}} f_a\lambda_a\lambda_a + \frac{\langle F_X\rangle}{6M_{\rm Pl}} y^X_{ijk}\phi_i\phi_j\phi_k + \frac{\langle F_X\rangle}{2M_{\rm Pl}}\mu^X_{ij}\phi_i\phi_j + \text{c.c.}\right) \\ &- \frac{|\langle F_X\rangle|^2}{M_{\rm Pl}^2} k_{ij}\phi_i^\dagger\phi_j\,.\end{aligned} \tag{I.130}$$

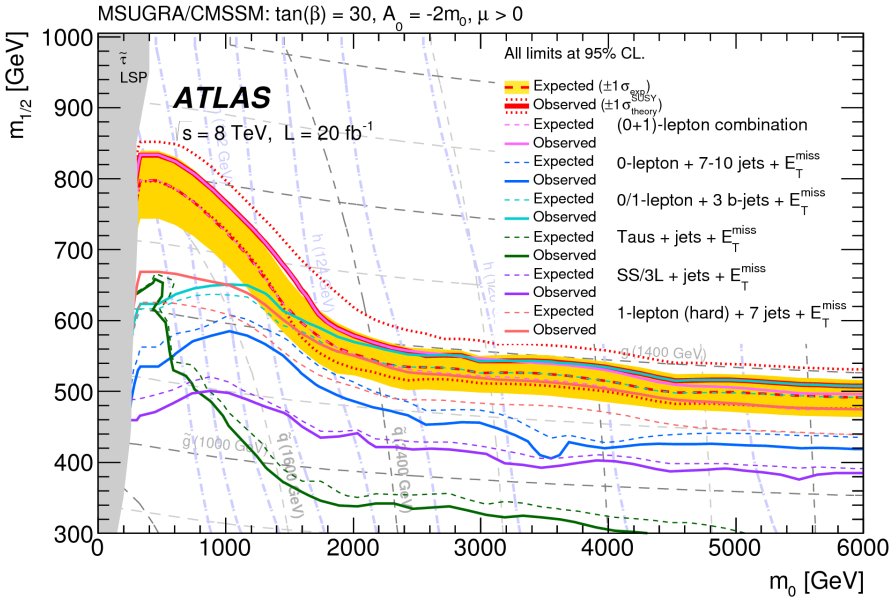

FIGURE I.5: Excluded region of the MSUGRA/CMSSM parameter space in the plane $\{m_0, M_{1/2}\}$ from the ATLAS collaboration with at LHC with luminosity $L = 20\,\text{fb}$ and center of mass energy $\sqrt{s} = 8$ TeV.

This has the same form as Eq.(I.117) with soft terms of order $m_{\text{soft}} \sim \langle F_X \rangle / M_{\text{Pl}}$. If one assumes the scale of SUSY particles to be $m_{\text{soft}} \sim 1$ TeV and $M_{\text{Pl}} \sim 10^{19}$, then $\sqrt{\langle F_X \rangle} \sim 10^{10-11}$ GeV. In principle, the parameters f_a, y^X_{ijk}, μ^X_{ijk} and k_{ji} are determined by the fundamental underlying theory. A very popular simplification is to assume a minimal flavor blind structure in which $f_a = f$, $k_{ij} = k\delta_{ij}$, $y^X_{ijk} = \alpha y_{ijk}$ and $\mu^X_{ij} = \beta\mu_{ij}$, with universal real dimensionless constants, thus four parameters are defined at a renormalization scale $Q = M_{\text{Pl}}$[4]:

$$M_{1/2} = f\frac{\langle F_X \rangle}{2M_{\text{Pl}}} \quad , \quad m_0^2 = k\frac{|\langle F_X \rangle|^2}{M_{\text{Pl}}^2} \quad , \quad A_0 = \alpha\frac{\langle F_X \rangle}{6M_{\text{Pl}}} \quad , \quad B_0 = \beta\frac{\langle F_X \rangle}{2M_{\text{Pl}}}\,. \tag{I.131}$$

In terms of which, the soft terms appearing in Eq.(I.121) are:

$$M_{1,2,3} = M_{1/2} \quad , \quad m^2_{H_u,H_d} = m_0^2 \quad , \quad b = B_0\mu\,, \tag{I.132}$$

$$\widetilde{m}^2_{Q,L} = m_0^2\mathbb{1} \quad , \quad \widetilde{m}^2_{u,d,e} = m_0^2\mathbb{1} \quad , \quad a_{u,d,e} = A_0 Y_{u,d,e}\,. \tag{I.133}$$

After evolving the soft terms down to the EW scale, one can demand that the scalar potential gives correct EWSB. This yields to trade $|\mu|$ and B_0 for one parameter $\tan\beta =$

[4]Although a popular approximation is to start the RG running from the GUT unification scale $M_{\text{GUT}} \sim 10^{15-16}$ GeV instead of M_{Pl}.

v_d/v_u, that is the ratio of VEVs of the two Higgs doublets (thus $v_d = v_H \cos\beta$, $v_u = v_H \sin\beta$). So the entire mass spectrum in MSUGRA models is usually fixed in terms of the following five input parameters

$$M_{1/2}\,,\; m_0^2\,,\; A_0\,,\; \tan\beta\,,\; \mathrm{Arg}(\mu)\,, \tag{I.134}$$

to be added to the usual gauge and Yukawa couplings of the MSSM. This minimal framework has the virtue to be highly predictive and to circumvent the most dangerous types of flavor changing and CP violation. Direct experimental searches have been performed to (dis)prove this simple scenario. The excluded region of the MSUGRA parameter space in the plane $\{m_0, M_{1/2}\}$ ($\tan\beta = 30$, $A_0 = -2m_0$ and $\mu > 0$) is displayed in Fig.I.5.
A more interesting case is represented by models, in which the flavor structure of the matrices is controlled, and to some extent protected, by the same dynamics that generates the hierarchical structure of the SM Yukawa matrices to which we dedicate the next section.

I.5.4 Supersymmetry and Flavor Symmetries

It is natural to think that the same mechanism generating the flavor structures in the Yukawa couplings is also responsible for the structure in the SUSY soft-breaking terms [51]. In this way, finding a solution to the SM's flavor problem can also provide a solution to the SUSY flavor problem. Specifically, it could be the case that an underlying spontaneously-broken flavor symmetry is simultaneously responsible for the fermion masses and mixing angles and the different flavor structures in the soft-breaking terms. Two possible scenarios disclose to us depending on the hierarchy between the SUSY mediation scale Λ_{Med} and the flavor symmetry scale Λ_f:

- $\boldsymbol{\Lambda_f > \Lambda_{\mathrm{Med}}}$ **:** the Soft terms are generated after the breaking of the flavor symmetry $\mathcal{G}_f$, and the only remnants of the flavor symmetry at Λ_{Med} are the Yukawas. At the scale Λ_{Med}, the soft-breaking terms can feel the flavor breaking only through the Yukawa couplings or via non-renormalizable operators proportional to $\Lambda_{\mathrm{Med}}/\Lambda_f$ and therefore are negligible.

- $\boldsymbol{\Lambda_f < \Lambda_{\mathrm{Med}}}$ **:** the Superpotential and Soft terms must respect the flavor symmetry above Λ_f, but, at this scale, they feel the breaking of the flavor symmetry in the same way that the Yukawa couplings. The soft mass matrices and the trilinears offer new flavor observables. Note that this is always the case of Gravity mediation.

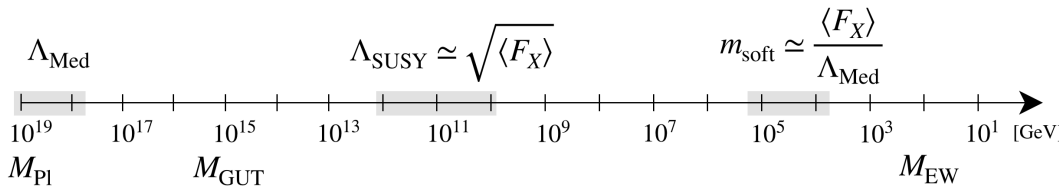

FIGURE I.6: The different scales at play in the breaking of SUSY in the Gravity mediated scenario.

The second is a more appealing situation. In the physical basis, where the Kähler is the identity, i.e. the fields are redefined to obtain canonical kinetic terms, and the Yukawas are diagonal, one might naively expect the soft breaking matrices to be simultaneously diagonalized with the Yukawa structures. This is is not generally the case. Note that the non renormalizable part of Eqs.(I.127, I.128) are written as

$$W - W_{\rm ren} = \frac{X}{M_{\rm Pl}} \times W_{\rm ren} \qquad , \qquad K - K_{\rm ren} = \frac{XX^\dagger}{M_{\rm Pl}^2} \times K_{\rm ren}\,, \tag{I.135}$$

where $(\times)$ stands for all the possible ways in which the spurion field X, or the combination $XX^\dagger$, can be coupled to the visible sector vertices of the Superpotential.

$$(m_0^2)_{ij} = k_{ij} \frac{|\langle F_X \rangle|^2}{M_{\rm Pl}^2} \qquad , \qquad (A_0)_{ij} = \alpha_{ij} \frac{\langle F_X \rangle}{6 M_{\rm Pl}}\,, \tag{I.136}$$

where k_{ij} and α_{ij} are positive integers depending on the number of flavon insertions that generate each supergraph in $W_{\rm ren}$. These coefficients are usually different for each entry of the trilinears and soft masses, thus introducing a mismatch with the corresponding Yukawa and Kähler structures. As a result, even stemming from an ultraviolet flavor-conserving origin, the soft-breaking Lagrangian typically exhibits large tree-level flavor violating effects, better discussed in the next section. However, the flavor symmetry controls the size of flavor violation. Indirect flavor violating measurements provide a new tool to constrain parameters like the gluino mass and the sfermion masses. In Article 1, we show that the constraints, especially in the leptonic sector, are incredibly competitive with direct LHC searches.

To conclude, in the case $\Lambda_f < \Lambda_{\rm Med}$, which is always true when the Supersymmetry breaking is mediated by gravity. Supersymmetric theories supplemented by an underlying flavor symmetry $\mathcal{G}_f$ provide a rich playground for model building aimed at explaining the flavor structure of the Standard Model. Unfortunately, these effects are model dependent.

I.6 Flavor and CP Observables of interest

In this section, we introduce the most relevant observables considered in this dissertation. New physics contributions to flavor changing neutral current (FCNC) processes, which change the flavor of a fermion current without altering its electric charge, tend to be much larger than the SM predictions. In particular, in the analysis of Article 1-3 the most stringent bounds on the parameter space of the considered models are offered by the radiative lepton decays $\ell \to \ell'\gamma$ and the three-body charged lepton decays $\ell \to 3\,\ell'$ as well as from the CP-violating parameter ε in the $(K^0 - \overline{K}^0)$-mixing. In Article 5 we focused on the interplay between LFV, mass generation, and the two discrepancies in the leptonic anomalous magnetic moment.

I.6.1 Anomalous Magnetic Moment

Subatomic particles have a magnetic and an electric dipole moments that are generated by their intrinsic spin $\vec{s}$. The non-relativistic Hamiltonian interaction of a fundamental particle of spin $\vec{s}$ with an electric and magnetic field includes

$$\mathcal{H} = -\vec{d}_s \cdot \vec{E} - \vec{\mu}_s \cdot \vec{B}\,, \tag{I.137}$$

where $\vec{d}_s$ is the *electric dipole moment* (EDM), which measures the separation between positive and negative charge within the particle, and $\vec{\mu}_s$ is the *magnetic dipole moment* (MDM) that measures of how much torque the particle experiences when placed in a magnetic field. The energy terms in Eq.(I.137) are, respectively, odd and even terms under parity (P) and time-reversal (T). Under the assumption of CPT symmetry, T violation implies CP violation so a nonzero value for d is a sign of CP violation. In the SM, the CKM phase is the only source of CP violation and lepton EDMs are strongly suppressed as they arise only at four loop level with three W bosons and one gluon giving $|d_e^{\rm SM}| \sim 10^{-41}$ [54], the muon and tau lepton EDMs arise with the same mechanism, $|d_\mu^{\rm SM}| = m_\mu\, d_e/m_e \sim 10^{-38}$ and $|d_\tau^{\rm SM}| = m_\tau\, d_e/m_e \sim 10^{-37}$. Thus EDMs offer strong constraints over the presence of complex phases in NP scenarios. The MDM can be expressed in terms of the gyromagnetic factor g : $\vec{\mu}_s = g\ (Q/2m)\,\vec{s}$, with $Q = \pm$e the charge of the particle. The Dirac magnetic moment, corresponding to tree-level Feynman diagram, which can be thought of as the classical result, can be calculated from the Dirac equation. The Dirac value of the magnetic dipole moment of a charged lepton is $g = 2$. The *anomalous magnetic moment* (AMM) is defined as the

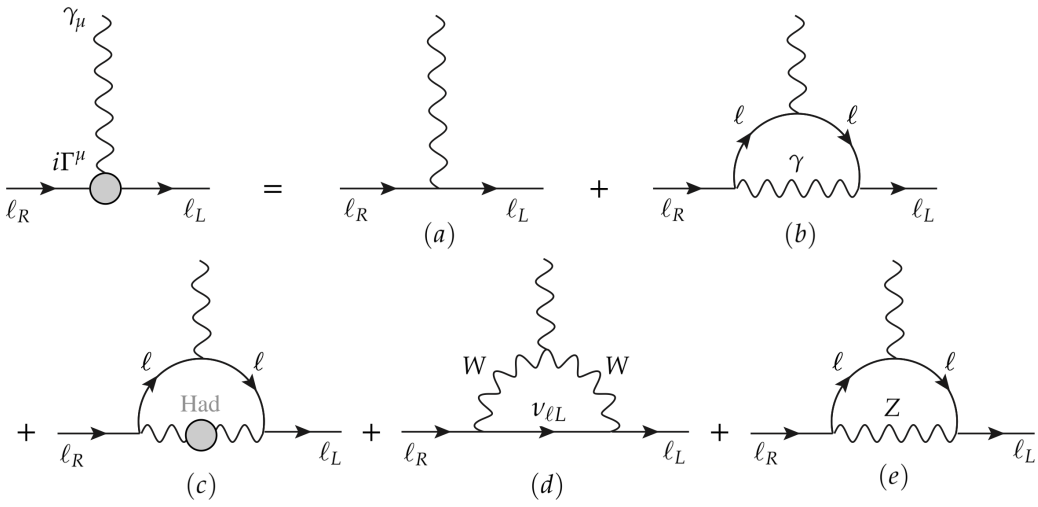

FIGURE I.7: Feynman diagrams contributing to the QED vertex in the SM. (a) Dirac contribution that gives $g = 2$. (b) the first QED correction known as the Schwinger term. (c) the Hadron Vacuum Polarization as the first QCD correction. (d), (e) the first EW contributions of the gauge bosons.

difference with respect to the classical value

$$a = \frac{(g-2)}{2}\,, \tag{I.138}$$

called shortly $(g-2)$. Leptons are elementary particles and have no internal structure, the magnetic moment of a lepton can differ from its Dirac value (the anomaly) through radiative corrections of virtual particles that couple to the lepton. The charged lepton AMMs and EDMs can be extracted from the lepton-photon amplitude with initial and final states of momenta p and p' (the transfer momentum is defined as $q \equiv p' - p$)

$$i\,\mathcal{M} \;=\; -i\,\mathrm{e}\,Q_\ell\,A_\mu(q)\,\overline{u}_\ell(p')\,\Gamma^\mu(q^2)\,u_\ell(p), \tag{I.139}$$

where A_μ is the electromagnetic field and u_ℓ, $\overline{u}_\ell$ are the Dirac spinor fields of the lepton with $\ell = e, \mu, \tau$. The vertex operator, Γ^μ, is restricted by Lorentz invariance to be

$$\Gamma^\mu \;=\; F_1(q^2)\,\gamma^\mu \;+\; F_2(q^2)\,\frac{i\,\sigma^{\mu\nu}q_\nu}{2m_\ell} \;+\; F_3(q^2)\,\gamma_5\,\frac{i\,\sigma^{\mu\nu}q_\nu}{2m_\ell}, \tag{I.140}$$

where γ_μ are the gamma matrices, $\sigma^{\mu\nu} = i[\gamma^\mu, \gamma^\nu]/2$, and $F_{1,2,3}$ are unknown functions of q^2 called *form factors*. In the limit where $q^2 \to 0$, the form factors $F_i(0)$ correspond to classical definitions of the electric charge ($i = 1$), the leptonic anomalous

AMM		Current Value	EDM	Bound
$a_e\ /10^{-3}$	SM	$1.15965218161^{\pm 0.00000000023}$ [55]	$\lvert d_e\rvert$ [e cm]	10^{-29}
	exp	$1.15965218073^{\pm 0.00000000028}$		
$a_\mu\ /10^{-3}$	SM	$1.16591820^{\pm 0.00000006}$ [56]	$\lvert d_\mu\rvert$ [e cm]	10^{-19}
	exp	$1.16592089^{\pm 0.00000063}$		
$a_\tau\ /10^{-3}$	SM	$1.17721^{\pm 0.00005}$ [57]	$\lvert d_\tau\rvert$ [e cm]	10^{-17}
	exp	$[-52, 13]$ at 95% CL		

TABLE I.5: Current experimental and theoretical status of lepton AMMs and EDMs. The experimental values are taken from Ref.[4] (website: PDGlive).

magnetic moment ($i = 2$) and the electric dipole moment ($i = 3$):

$$F_1(0) = 1 \quad , \quad F_2(0) = a_\ell \quad , \quad F_3(0) = \frac{d_\ell}{\mathrm{e}}\,. \tag{I.141}$$

Theoretical value: Within the SM the prediction for the value of the anomalous magnetic moment includes three parts

$$a_\ell^{\mathrm{SM}} = a_\ell^{\mathrm{QED}} + a_\ell^{\mathrm{QCD}} + a_\ell^{\mathrm{EW}} \tag{I.142}$$

where, in order of importance, a^{QED} includes all photonic and leptonic loop contributions up to $\mathcal{O}(\alpha^5)$, a^{QCD} contains contributions from hadronic loops and a^{EW} the loop contributions involving the $W^\pm$, Z. The main diagrams contributing to each term in Eq.(I.142) are displayed in Figure I.7 where the first order QED contribution is the famous Schwinger correction ($\alpha/2\pi \sim 10^{-3}$) and first order QCD contribution to the anomaly results from hadron vacuum polarization (HVP). The HVP contribution can not be calculated perturbatively and the QCD simulations on the lattice represent nowadays the most promising tool for an accurate determination of the hadronic contribution from first principles.

The current experimental and theoretical best estimates for the AMMs of the leptons, together with the limits on EDMs, are displayed in Table I.5. The main sources of the uncertainty for the anomalies are the experiment and the QED calculation for a_e. While for a_μ, they are the experiment and the hadronic contribution. The short lifetime of the tau ($\simeq 2.9 \times 10^{-13} s$) makes yet quite complex a precise experimental determination of a_τ.

To achieve the accuracy of theoretical prediction for $(g-2)_e$ matching the experimental precision, one needs to calculate a vast number of Feynman diagrams, up to

5-loop level for $(g-2)_e$. The QED prediction for the AMM of the electron agrees with the experimentally measured value to 9 significant figures, making it the most accurately verified prediction in the history of physics and the most substantial proof of the SM's predicting capacity. Matching the SM prediction for $(g-2)_e$ to the measurement has been used for many years as the most precise way to evaluate the fine-structure constant α. Recently, a new determination of the fine structure constant α from atomic cesium led to a more precise value of the electron anomaly and highlighted a new discrepancy:

$$\Delta a_e \;=\; a_e^{\rm exp} - a_e^{\rm SM} = -(8.8 \pm 3.6) \times 10^{-13}, \quad [2.4\sigma]\,. \tag{I.143}$$

This is very interesting considering that, as opposed to a_e, the SM result for a_μ is one of the very few of its predictions differing significantly from the experimentally measured value:

$$\Delta a_\mu \;=\; a_\mu^{\rm exp} - a_\mu^{\rm SM} = +(2.7 \pm 0.7) \times 10^{-9} \qquad [3.5\sigma]\,. \tag{I.144}$$

Notice the opposite signs of the electron and muon anomalies. The AMM provides an excellent test for physics beyond the SM. In a large class of models, new-physics contributions to a_ℓ are proportional to m_ℓ^2, a situation that we call naive scaling. In this case, the present value of the $(g-2)_\mu$ anomaly, corresponds to $\Delta a_e = (0.6 \pm 0.2) \times 10^{-13}$. Observing or excluding an anomaly in a_e could become the most convincing way to establish the origin of the a_μ discrepancy.
The Fermilab Muon g-2 experiment (E989) [58] and J-PARC (E34) aim at a fourfold reduction of the experimental uncertainty for the muon a_μ with a relative uncertainty of 140 ppb which has the potential to confirm the discrepancy with a 7σ significance if the central value remains the same. Meanwhile, essential improvements in the precision of the electron a_e are eagerly expected to come from the Harvard group.

I.6.2 Lepton Flavor Violation

In the SM with massless neutrinos, muon can decay only to electron and neutrino pair, $\mu \to e\overline{\nu}_e\nu_\mu$[5], other decays are kinematically forbidden or due to lepton flavor conservation. From neutrino oscillations, we now know that the family lepton numbers, $L_{\rm e}$, L_μ and L_τ, are violated in Nature. This necessarily implies some degree of violation in the charged-lepton sector. Although the search for such a violation has

[5]The decay width for such dominant standard channel is usually used to normalize the branching ratios for more exotic LFV decays

LFV process	Current Bound	Future Bound
$\mathrm{BR}(\mu \to e\gamma)$	4.2×10^{-13} (MEG at PSI[60])	6×10^{-14} (MEG II [61])
$\mathrm{BR}(\mu \to eee)$	1.0×10^{-12} (SINDRUM[62])	10^{-16} (Mu3e[63])
$\mathrm{CR}(\mu - e)_{A_l}$	–	10^{-17} (Mu2e[64], COMET[63])
$\mathrm{BR}(\tau \to e\gamma)$	3.3×10^{-8} (BaBar[65])	5×10^{-9} (Belle II[66])
$\mathrm{BR}(\tau \to \mu\gamma)$	4.4×10^{-8} (BaBar[65])	10^{-9} (Belle II[66])
$\mathrm{BR}(\tau \to eee)$	2.7×10^{-8} (Belle[67])	5×10^{-10} (Belle II[66])
$\mathrm{BR}(\tau \to \mu\mu\mu)$	2.1×10^{-8} (Belle[67])	5×10^{-10} (Belle II[66])

TABLE I.6: Relevant LFV processes considered in this dissertation.

been pursued in a host of channels both at dedicated and general-purpose experiments, the data collected in Table I.6 show that, unlike in the neutrino and quark sector, there is yet no evidence of Lepton Flavor Violation in processes involving charged leptons, see Ref.[59] for a comprehensive review. The branching ratio of $\mu \to e\gamma$ can be computed from the diagram in Figure I.8 and gives

$$\mathrm{BR}(\mu \to e\gamma) = \frac{\Gamma(\mu \to e\gamma)}{\Gamma(\mu \to e\bar{\nu}\nu)} = \frac{3\alpha}{32\pi} \left| \sum_{i=1}^{3} V_{\mu i} V_{ei}^{*} \frac{m_i^2}{M_W^2} \right|^2 \sim 10^{-54}\,, \tag{I.145}$$

where the term inside the modulus is a GIM-like suppression factor

$$\sum_{i=1}^{3} V_{\mu i} V_{ei}^{*}\, m_i^2 = V_{\mu 3} V_{e3}^{*}\, \Delta m_{31}^2 + V_{\mu 2} V_{e2}^{*}\, \Delta m_{21}^2. \tag{I.146}$$

Therefore, adding neutrino mass terms to the SM Lagrangian induces CLFV but forty orders of magnitudes smaller than the sensitivity of present-day experiments, thus at a level of no phenomenological interest. However we stress that LFV process in charged lepton sector are so strongly suppressed not because of the GIM mechanism but rather by the smallness of the neutrino masses compared to the EW scale. If the penguin diagram dominates over the box diagram in Figure I.8, it can be intuitively understood that the rates of $\mu \to 3\,e$ and $\mu N \to eN$ are further suppressed by a factor of order α with respect to $\mu \to e\gamma$:

$$\mathrm{BR}(\mu \to 3\,e) \simeq \frac{\alpha}{3\pi} \left(\log \frac{m_\mu^2}{m_e^2} - 3 \right) \mathrm{BR}(\mu \to e\gamma) \tag{I.147}$$

$$\mathrm{CR}(\mu - e)_N \simeq \alpha\, \mathrm{BR}(\mu \to e\gamma) \tag{I.148}$$

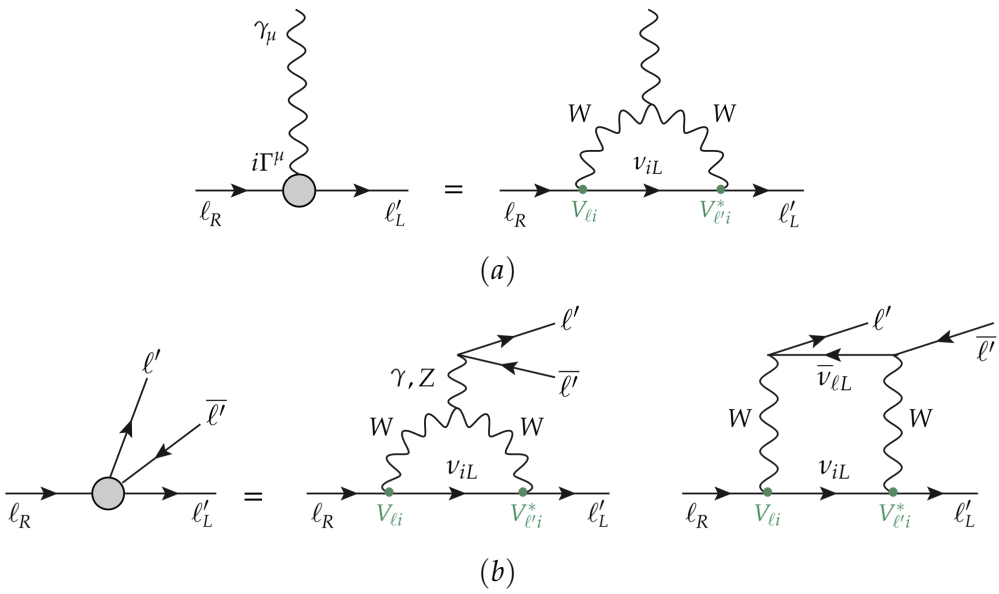

FIGURE I.8: The Feynman diagrams contributing to the LFV processes in Table I.6 at LO: (a) first contribution to the radiative lepton decays $\ell \to \ell'\gamma$, (b) first contribution to the three-body charged lepton decays $\ell \to 3\,\ell'$.

In this way, the MEG bound on BR($\mu \to e\gamma$) translates into a limit on the above observables at the 10^{-15} far from the present bound. Many NP models like the typical supersymmetric frameworks of Article 1-3 maintain this proportionality. Measurement of $\ell \to 3\,\ell'$ above or below the expected scaling would rule out many of these models. The future bounds on the processes in Table I.6, combined, are an ambitious project to identify what kind of NP is eluding us.
The bounds on LFV set already strong limits on NP, especially when considered together with the $(g-2)$-discrepancies. In the following, we quantify this in a model independent approach.

Dipole operator: It is commonly accepted that the SM constitutes only an effective theory which is valid up an energy scale $\Lambda_{\rm NP}$ where NP enters and additional dynamic degrees of freedom become important. In an effective Lagrangian approach, the SM is treated as the Leading Order term of a Standard Model Effective Field Theory (SMEFT) expanded in $1/\Lambda_{\rm NP}$:

$$\mathcal{L}^{\rm SMEFT} = \mathcal{L}^{\rm SM(4)} + \frac{C^{(5)}}{\Lambda_{\rm NP}} O^{(5)} + \sum_n \frac{C_n^{(6)}}{\Lambda_{\rm NP}^2} O_n^{(6)} + \mathcal{O}\left(\frac{1}{\Lambda_{\rm NP}^3}\right). \tag{I.149}$$

where $\mathcal{L}^{\mathrm{SM}(4)}$ is the usual renormalizable part of the SM Lagrangian which contains dimension $\mathrm{d} = 2$ and $\mathrm{d} = 4$ operators only, while O_n are non-renormalizable operators with mass dimension $\mathrm{d} > 4$, suppressed by $\Lambda_{\mathrm{NP}} \gg v_H$, that is the cut-off scale of NP, and the C_n are dimensionless Wilson coefficients. Interestingly, there is only one possible operator that we can write down with $\mathrm{d} = 5$, and this is the Weinberg Operator that was introduced to generate the neutrino Majorana mass term in Eq.(I.27). As we have seen, it induces CLFV effects only at loop level and with negligibly low rates. The first relevant CLFV effects thus arise at the $\mathrm{d} = 6$ level. In this effective Lagrangian approach, non-standard effects to the leptonic observables of interest $(g-2)_\ell$, $\mathrm{BR}(\ell \to \ell'\gamma)$, EDMs may arise via the dipole operators

$$\mathcal{L}^{(6)}_{\ell\gamma} \;=\; \frac{e m_\ell}{8\pi^2}\, C_{\ell\ell'}\, \bar{\ell}\, \sigma_{\mu\nu}\, P_R\, \ell'\, F^{\mu\nu} \;+\; \mathrm{h.c.}, \tag{I.150}$$

where $F^{\mu\nu} = \partial^\mu A^\nu - \partial^\nu A^\mu$ is the field strength tensor and the Wilson coefficient $C_{\ell\ell'}$ is a matrix in flavor space called the dipole matrix. After the rotation to the mass basis, $C \to C' = V_L^\ell\, C\, V_R^{\ell\dagger}$, the anomalous magnetic moment of the leptons and the FV transitions are given, respectively, in terms of the diagonal and off diagonal entries of the dipole matrix

$$(g-2)_\ell = \frac{m_\ell^2}{4\pi^2}\mathrm{Re}(C'_{\ell\ell}) \qquad , \qquad d_\ell = \frac{e m_\ell}{4\pi^2}\mathrm{Im}(C'_{\ell\ell}) \tag{I.151}$$

$$\mathrm{BR}(\ell \to \ell'\gamma) = \frac{3\,\alpha}{\pi\, G_F^2}\left(|C'_{\ell\ell'}|^2 + |C'_{\ell'\ell}|^2\right). \tag{I.152}$$

Therefore, given the values in Table I.5 we can deduce the following constraints on the diagonal entries $C'_{\ell\ell}$ of the dipole matrix in the mass basis

$$\begin{aligned} \mathrm{Re}(C'_{ee}) \;&\simeq\; -7\times 10^{-5}\,\mathrm{GeV}^{-2} \quad , \quad \mathrm{Im}(C'_{ee}) \lesssim 6\times 10^{-7}\,\mathrm{GeV}^{-2}, \\ \mathrm{Re}(C'_{\mu\mu}) \;&\simeq\; +5\times 10^{-6}\,\mathrm{GeV}^{-2} \quad , \quad \mathrm{Im}(C'_{\mu\mu}) \lesssim 10^{-4}\,\mathrm{GeV}^{-2}, \end{aligned} \tag{I.153}$$

and, from Table I.6 the bounds on the off-diagonal entries $C'_{\ell\ell'}$ read

$$\begin{aligned} |C'_{e\mu}|, |C'_{\mu e}| \;&\lesssim\; 10^{-10}\,\mathrm{GeV}^{-2}, \\ |C'_{e\tau}|, |C'_{\tau e}| \;&\lesssim\; 6\times 10^{-8}\,\mathrm{GeV}^{-2}, \\ |C'_{\mu\tau}|, |C'_{\tau\mu}| \;&\lesssim\; 7\times 10^{-8}\,\mathrm{GeV}^{-2}. \end{aligned} \tag{I.154}$$

Eqs.(I.153) and (I.154) quantify the complexity the task. From Eq.(I.153), the diagonal entries of C do not respect the naive mass scaling in m_ℓ^2 because $C'_{ee} > C'_{\mu\mu}$ (although this could be relaxed by considering a larger imaginary part in $C_{\mu\mu}$) and the negative sign of C'_{ee} seem to point to different NP contributions to accommodate the electron and muon discrepancies [68].
Moreover, due to the strong limits on LFV, form Eq.(I.154) we see that the dipole matrix must be diagonal to a very high degree in the mass basis. There are two possibilities, either the lepton Yukawa and the dipole matrix are both generated diagonal to a very good degree, or $C'_{\ell\ell'}$ and $C'_{\ell'\ell}$ are instead non-vanishing and such that they cancel the contributions from C'_{ee} and $C'_{\mu\mu}$ times the mass rotations. Considering the high degree of cancellation, the last case is conceivable only if there is a common origin of C' and Y', which is a possibility that we explore in Article 5.

LFV in Supersymmetry

New sources of LFV can stem from the couplings among the SM leptons, their SUSY partners, and the neutralinos and charginos given in Appendix A.2. These interactions are flavor violating unless the lepton and slepton mass matrices are aligned and can be simultaneously diagonalized, which does not occur in general. The 6×6 slepton mass matrix is given by

$$\left(\widetilde{\ell}_L\, \widetilde{\ell}_R^\dagger\right) \boldsymbol{m}^2_{\widetilde{\boldsymbol{\ell}}} \begin{pmatrix} \widetilde{\ell}_L \\ \widetilde{\ell}_R \end{pmatrix} = \left(\widetilde{\ell}_L^\dagger\, \widetilde{\ell}_R^\dagger\right) \begin{pmatrix} \Delta^{LL} & \Delta^{LR} \\ \Delta^{RL} & \Delta^{RR} \end{pmatrix} \begin{pmatrix} \widetilde{\ell}_L \\ \widetilde{\ell}_R \end{pmatrix}, \tag{I.155}$$

where

$$\begin{aligned} \Delta^{LL}_{ij} &= \widetilde{m}^2_{L,ij} + \frac{v_d^2}{2}(Y^{\ell\dagger}Y^\ell)_{ij} + m_Z^2 \cos 2\beta \left(-\frac{1}{2} + \sin^2\theta_W\right)\delta_{ij}\,, \\ \Delta^{RR}_{ij} &= \widetilde{m}^2_{\ell,ij} + \frac{v_d^2}{2}(Y^{\ell\dagger}Y^\ell)_{ij} - m_Z^2 \cos 2\beta \sin^2\theta_W \delta_{ij}\,, \\ \Delta^{LR}_{ij} &= \Delta^{RL}_{ij} = \frac{v_d}{\sqrt{2}}\left(a_{\ell,ij} - \mu^* Y^\ell_{ij} \tan\beta\right). \end{aligned} \tag{I.156}$$

Usually, these SUSY-breaking matrices can not be simultaneously diagonalized with the Yukawa Y^ℓ and have off-diagonal entries in the mass basis. As a consequence, the physical sleptons are mixtures of different flavors.
In the spirit of the mass insertion approximation (MIA) [69] in Appendix A.3, we can also treat the off-diagonal entries of the slepton mass matrix in Eq.(I.156), normalised

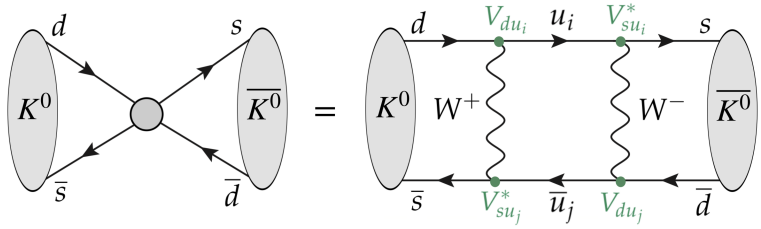

FIGURE I.9: Feynman diagram for meson oscillation : in the SM two different neutral K mesons, carrying different strangeness, can turn from one into another through the weak interactions, where $i, j = 1, 2, 3$.

by the diagonal entries, as mass insertions

$$\delta^{LL}_{ij} = \frac{\Delta^{LL}_{ij}}{\sqrt{\tilde{m}^2_{L,ii}\,\tilde{m}^2_{L,jj}}} \quad , \quad \delta^{RR}_{ij} = \frac{\Delta^{RR}_{ij}}{\sqrt{\tilde{m}^2_{\ell,ii}\,\tilde{m}^2_{\ell,jj}}} \tag{I.157}$$

$$\delta^{LR}_{ij} = \frac{\Delta^{LR}_{ij}}{\sqrt{\tilde{m}^2_{L,ii}\tilde{m}^2_{\ell,jj}}} \quad , \quad \delta^{RL}_{ij} = \frac{\Delta^{RL}_{ij}}{\sqrt{\tilde{m}^2_{\ell,ii}\,\tilde{m}^2_{L,jj}}} \tag{I.158}$$

with $i \neq j$. The above mass insertions can be constrained by the experimental limits on LFV once information on the SUSY spectrum are provided, an example of this is given in Appendix D.2 through the analysis of Article 3.

I.6.3 Neutral Kaon Mixing

Historically, kaon physics has been the main player in the field of flavor physics, being at the source of many of the fundamental ingredients of the SM: the flavor concept of strangeness, the existence of higher-mass scales such as the charm and the top, parity violation, meson-antimeson oscillations, the GIM mechanism, and CP violation.

Two neutral pseudoscalar K mesons exist that are each other's antiparticles: the $K^0(d\bar{s})$ and $\overline{K^0}(s\bar{d})$. In the SM, $(K^0 - \overline{K^0})$-mixing occurs by one loop box diagrams displayed in Figure I.9, the two mass eigenstates are called *K-long* (K_L) and *K-short* (K_S) referring to their lifetimes which are found experimentally to be very different: $\tau(K_S) \sim 90ps$ and $\tau(K_L) \sim 5 \times 10^3 ps$. The explanation of this difference can be found in the CP properties of the two states. The K^0, $\overline{K}^0$ mesons transform into each other under CP conjugation: $\text{CP}|K^0\rangle = -|\overline{K^0}\rangle$ and $\text{CP}|\overline{K^0}\rangle = -|K^0\rangle$. Thus the CP-even and CP-odd eigenstates are respectively given by

$$K_1 = \frac{1}{\sqrt{2}}(K^0 - \overline{K}^0) \quad , \quad K_2 = \frac{1}{\sqrt{2}}(K^0 + \overline{K}^0)\,. \tag{I.159}$$

If CP is conserved in the decay of neutral kaons, then the CP-even state K_1 will decay into two pions $K_1 \to 2\,\pi$, forming a CP-even final state. On the contrary K_2, has to decay into a CP-odd final state, which contains three pions $K_2 \to 3\,\pi$. The three pion final state is phase space suppressed with respect to the two pion final state, the K_1 decay rate is much faster, so that its lifetime is much shorter than the one of K_2. The mass eigenstates $K_{L,S}$ are not pure CP eigenstates but their different lifetimes are explained assuming that $K_S \sim K_1$ is basically the CP-even state, with a small CP-odd admixture, while $K_L \sim K_1$, is approximately the CP-odd state K_2, with a small CP-even admixture.
In 1964, the decay $K_L \to \pi^+\pi^-$ has been observed [70], yielding the first experimental confirmation that CP symmetry is violated. However, this does not tell us where the observed CP violation originates from. CP can either be violated in the neutral kaon mixing, if the mass eigenstates $K_{L,s}$ are not CP eigenstates, CP can be violated in the decay, or also in the interference of mixing and decay amplitudes.

CP-parameters: The key idea to distinguish whether CP is violated in the mixing (*indirect* CP violation) or in the decay process (*direct* CP violation) is that the amount of direct CP violation depends on the decay channel, but indirect CP violation does not. It is possible to disentangle the two types of CP violation studying the set of decays $K_{L,S} \to \pi^0\pi^0$ and $K_{L,S} \to \pi^+\pi^-$ and defining two parameters ε and ε' that parametrize indirect and direct CP violation

$$\varepsilon = \frac{1}{3}\left(\eta_{00} + 2\,\eta_{+-}\right) \quad , \quad \mathrm{Re}\left(\frac{\varepsilon'}{\varepsilon}\right) = \frac{1}{6}\left(1 - \left|\frac{\eta_{00}}{\eta_{+-}}\right|^2\right) , \tag{I.160}$$

where

$$\eta_{00} = \frac{\mathcal{A}(K_L \to \pi^0\pi^0)}{\mathcal{A}(K_S \to \pi^0\pi^0)} = \varepsilon - 2\varepsilon' \quad , \quad \eta_{+-} = \frac{\mathcal{A}(K_L \to \pi^+\pi^-)}{\mathcal{A}(K_S \to \pi^+\pi^-)} = \varepsilon + \varepsilon' . \tag{I.161}$$

Both ε and $\mathrm{Re}(\varepsilon'/\varepsilon)$ have been experimentally and theoretically measured with high precision, with the results

$$\begin{aligned} |\varepsilon|^{\mathrm{exp}} &= (2.228 \pm 0.011) \times 10^{-3}\,[4] \quad , \quad \mathrm{Re}\left(\frac{\varepsilon'}{\varepsilon}\right)^{\mathrm{exp}} = (16.6 \pm 2.3) \times 10^{-4}\,[4]\,, \\ |\varepsilon|^{\mathrm{SM}} &= (1.90 \pm 0.26) \times 10^{-3}\,[71] \quad , \quad \mathrm{Re}\left(\frac{\varepsilon'}{\varepsilon}\right)^{\mathrm{SM}} = (14 \pm 5) \times 10^{-4}\,[72]\,. \end{aligned} \tag{I.162}$$

A value of $\mathrm{Re}(\varepsilon'/\varepsilon)$ different from zero establishes the presence of direct CP violation in the decay amplitudes, confirming that CP violation is associated with a $\Delta S = 1$ transition as predicted by the SM. The SM value of ε is slightly lower, albeit still consistent with the experimental result. More controversial is the theoretical prediction of $\mathrm{Re}(\varepsilon'/\varepsilon)$ because the first next-to-leading order (NLO) calculations claimed SM values one order of magnitude smaller than (I.162). The theoretical prediction is in good agreement with the experimental value, once the long-distance contributions of the final pion dynamics were taken adequately into account [73].
Due to its strong suppression in the SM, ε is sensitive to potential NP contributions. The good agreement of the measured values with its SM predictions results in strong constraints on the NP entering $(K^0 - \overline{K^0})$-mixing.

References

[1] K. S. Babu in Proceedings of Theoretical Advanced Study Institute in Elementary Particle Physics on The dawn of the LHC era (TASI 2008), **2010**, pp. 49–123, arXiv: 0910.2948 [hep-ph].

[2] M. Bona et al., *JHEP* **2006**, *10*, 081, arXiv: hep-ph/0606167 [hep-ph].

[3] I. Esteban et al., *JHEP* **2019**, *01*, 106, arXiv: 1811.05487 [hep-ph].

[4] M. Tanabashi et al., *Phys. Rev.* **2018**, *D98*, 030001.

[5] R. Gatto et al., *Phys. Lett. B* **1968**, *28*, 128–130.

[6] J. Davis, Raymond et al., *Phys. Rev. Lett.* **1968**, *20*, 1205–1209.

[7] Y. Fukuda et al., *Phys. Rev. Lett.* **1998**, *81*, 1562–1567, arXiv: hep-ex/9807003.

[8] V. Aseev et al., *Phys. Rev. D* **2011**, *84*, 112003, arXiv: 1108.5034 [hep-ex].

[9] N. Aghanim et al., **2018**, arXiv: 1807.06209 [astro-ph.CO].

[10] I. M. Oldengott et al., *JCAP* **2019**, *04*, 049, arXiv: 1901.04352 [astro-ph.CO].

[11] Y. Abe et al., *Phys. Rev. D* **2012**, *86*, 052008, arXiv: 1207.6632 [hep-ex].

[12] F. An et al., *Chin. Phys. C* **2013**, *37*, 011001, arXiv: 1210.6327 [hep-ex].

[13] J. Ahn et al., *Phys. Rev. Lett.* **2012**, *108*, 191802, arXiv: 1204.0626 [hep-ex].

[14] D. Meloni, *Front. in Phys.* **2017**, *5*, 43, arXiv: 1709.02662 [hep-ph].

[15] C. Alduino et al., *Phys. Rev. Lett.* **2018**, *120*, 132501, arXiv: 1710.07988 [nucl-ex].

[16] J. B. Albert et al., *Phys. Rev.* **2018**, *C97*, 065503, arXiv: 1710.05075 [nucl-ex].

[17] J. Angrik et al., **2005**.

[18] A. Sejersen Riis et al., *Phys. Rev.* **2011**, *C84*, 045503, arXiv: 1105.6005 [nucl-ex].

[19] E. Di Valentino et al., *JCAP* **2018**, *1804*, 017, arXiv: 1612.00021 [astro-ph.CO].

[20] J. Schechter, J. Valle, *Phys. Rev. D* **1982**, *25*, 2951.

[21] M. Agostini et al., *Nature* **2017**, *544*, 47, arXiv: 1703.00570 [nucl-ex].

[22] J. Albert et al., *Nature* **2014**, *510*, 229–234, arXiv: 1402.6956 [nucl-ex].

[23] S. King, *Phys. Lett. B* **1998**, *439*, 350–356, arXiv: hep-ph/9806440.

[24] S. King, *Nucl. Phys. B* **1999**, *562*, 57–77, arXiv: hep-ph/9904210.

[25] S. King, *Nucl. Phys. B* **2000**, *576*, 85–105, arXiv: hep-ph/9912492.

[26] S. King, *JHEP* **2002**, *09*, 011, arXiv: hep-ph/0204360.

[27] D. Spergel et al., *Astrophys. J. Suppl.* **2007**, *170*, 377, arXiv: astro-ph/0603449.

[28] W. Buchmuller et al., *Annals Phys.* **2005**, *315*, 305–351, arXiv: hep-ph/0401240.

[29] W. Buchmuller et al., *Ann. Rev. Nucl. Part. Sci.* **2005**, *55*, 311–355, arXiv: hep-ph/0502169.

[30] A. Strumia in Les Houches Summer School on Theoretical Physics: Session 84: Particle Physics Beyond the Standard Model, **2006**, pp. 655–680, arXiv: hep-ph/0608347.

[31] Y. Nir in 6th Rencontres du Vietnam: Challenges in Particle Astrophysics, **2007**, arXiv: hep-ph/0702199.

[32] P. Di Bari, *Contemp. Phys.* **2012**, *53*, 315–338, arXiv: 1206.3168 [hep-ph].

[33] S. Antusch et al., *JCAP* **2006**, *11*, 011, arXiv: hep-ph/0609038.

[34] O. Vives, *J. Phys. Conf. Ser.* **2009**, *171*, (Eds.: J. Bernabeu et al.), 012076.

[35] S. F. King, C. Luhn, *Rept. Prog. Phys.* **2013**, *76*, 056201, arXiv: 1301.1340 [hep-ph].

[36] C. D. Froggatt, H. B. Nielsen, *Nucl. Phys.* **1979**, *B147*, 277–298.

[37] D. Das et al., "Work in progress", Work in progress, **2017**.

[38] S. F. King et al., *JHEP* **2005**, *07*, 049, arXiv: hep-ph/0407012 [hep-ph].

[39] H. Georgi, C. Jarlskog, *Phys. Lett. B* **1979**, *86*, 297–300.

[40] C. Hagedorn et al., *Phys. Lett. B* **2012**, *717*, 207–213, arXiv: 1205.3114 [hep-ph].

[41] F. Bjorkeroth et al., *JHEP* **2015**, *06*, 141, arXiv: 1503.03306 [hep-ph].

[42] F. Björkeroth et al., *Phys. Rev. D* **2016**, *94*, 016006, arXiv: 1512.00850 [hep-ph].

[43] F. Bjorkeroth et al., *JHEP* **2017**, *10*, 148, arXiv: 1705.01555 [hep-ph].

[44] F. Feruglio et al., *JHEP* **2013**, *07*, 027, arXiv: 1211.5560 [hep-ph].

[45] M. Holthausen et al., *JHEP* **2013**, *04*, 122, arXiv: 1211.6953 [hep-ph].

[46] S. F. King, *J. Phys. G* **2015**, *42*, 123001, arXiv: 1510.02091 [hep-ph].

[47] A. Di Iura et al., *JHEP* **2015**, *08*, 037, arXiv: 1503.04140 [hep-ph].

[48] A. Di Iura et al., **2018**, arXiv: 1811.09662 [hep-ph].

[49] J. Penedo et al., *JHEP* **2017**, *12*, 022, arXiv: 1705.00309 [hep-ph].

[50] F. Feruglio et al., *Eur. Phys. J. C* **2014**, *74*, 2753, arXiv: 1303.7178 [hep-ph].

[51] O. Vives in 15th International Conference on Supersymmetry and the Unification of Fundamental Interactions (SUSY07), **2007**, arXiv: 0710.3705 [hep-ph].

[52] D. Das et al., *Phys. Rev.* **2017**, *D95*, 035001, arXiv: 1607.06827 [hep-ph].

[53] S. P. Martin in *Perspectives on supersymmetry. Vol.2*, *Vol. 21*, **2010**, pp. 1–153, arXiv: hep-ph/9709356.

[54] M. J. Booth, **1993**, arXiv: hep-ph/9301293.

[55] R. H. Parker et al., *Science* **2018**, *360*, 191–195.

[56] A. Keshavarzi et al., *Phys. Rev.* **2018**, *D97*, 114025, arXiv: 1802.02995 [hep-ph].

[57] S. Eidelman et al., *Nucl. Phys. B Proc. Suppl.* **2007**, *169*, (Eds.: F. Cei et al.), 226–231, arXiv: hep-ph/0702026.

[58] I. Logashenko et al., *J. Phys. Chem. Ref. Data* **2015**, *44*, 031211.

[59] L. Calibbi, G. Signorelli, *Riv. Nuovo Cim.* **2018**, *41*, 71–174, arXiv: 1709.00294 [hep-ph].

[60] A. Baldini et al., *Eur. Phys. J. C* **2016**, *76*, 434, arXiv: 1605.05081 [hep-ex].

[61] A. Baldini et al., *Eur. Phys. J. C* **2018**, *78*, 380, arXiv: 1801.04688 [physics.ins-det].

[62] U. Bellgardt et al., *Nucl. Phys. B* **1988**, *299*, 1–6.

[63] A. Blondel et al., **2013**, arXiv: 1301.6113 [physics.ins-det].

[64] L. Bartoszek et al., **2014**, DOI 10.2172/1172555, arXiv: 1501.05241 [physics.ins-det].

[65] B. Aubert et al., *Phys. Rev. Lett.* **2010**, *104*, 021802, arXiv: 0908.2381 [hep-ex].

[66] T. Aushev et al., **2010**, arXiv: 1002.5012 [hep-ex].

[67] Y. Miyazaki et al., *Phys. Lett. B* **2011**, *699*, 251–257, arXiv: 1101.0755 [hep-ex].

[68] H. Davoudiasl, W. J. Marciano, *Phys. Rev.* **2018**, *D98*, 075011, arXiv: 1806.10252 [hep-ph].

[69] A. Dedes et al., *JHEP* **2015**, *06*, 151, arXiv: 1504.00960 [hep-ph].

[70] J. Christenson et al., *Phys. Rev. Lett.* **1964**, *13*, 138–140.

[71] J. Brod, M. Gorbahn, *Phys. Rev. Lett.* **2012**, *108*, 121801, arXiv: 1108.2036 [hep-ph].

[72] A. Pich in 18th International Conference on B-Physics at Frontier Machines, **2020**, arXiv: 2001.11350 [hep-ph].

[73] H. Gisbert, A. Pich, *Rept. Prog. Phys.* **2018**, *81*, 076201, arXiv: 1712.06147 [hep-ph].

Articles

[1] López-Ibáñez, M. L., Melis, A., Pérez, M. J., and Vives, O. *"Slepton non-universality in the flavor-effective MSSM"*. In: *JHEP 11* **2017**, p.162. arXiv: 1710.02593 [hep-ph].

[2] De Medeiros Varzielas, I., López-Ibáñez, M.L., Melis, A., and Vives, O. *"Controlled flavor violation in the MSSM from a unified $\Delta(27)$ flavor symmetry"*. In: *JHEP 09* **2018**, p.047. arXiv: 1807.00860 [hep-ph].

[3] López-Ibáñez, M.L., Melis, A., Meloni, D., and Vives, O. *"Lepton flavor violation and neutrino masses from A_5 and CP in the non-universal MSSM"*. In: *JHEP 06* **2019**, p.047. arXiv: 1901.04526 [hep-ph].

[4] Björkeroth, F., de Medeiros Varzielas, I., López-Ibáñez, M.L., Melis, A., and Vives, O. *"Leptogenesis in $\Delta(27)$ with a Universal Texture Zero"*. In: *JHEP 09* **2019**, p.050. arXiv: 1904.10545 [hep-ph].

[5] Calibbi, L. , López-Ibáñez, M.L., Melis, A., and Vives, O. *"Muon and electron $g-2$ and lepton masses in flavor models"*. In: *JHEP 06* **2020**, p.087. arXiv: 2003.06633 [hep-ph].

Article 1

Slepton non-universality in the flavor-effective MSSM

JHEP 11 (2017) 162

M. Luisa López-Ibáñez[a], Aurora Melis[a], M. Jay Pérez[a,b] and Oscar Vives[a]

[a] *Departament de Física Tèorica, Universitat de València and IFIC, Universitat de València-CSIC, Dr. Moliner 50, E-46100 Burjassot (València), Spain*

[b] *Valencia State College, Osceola Campus* **1***800 Denn John Ln, Kissimmee, FL, USA*

ABSTRACT: Supersymmetric theories supplemented by an underlying flavor symmetry $\mathcal{G}_f$ provide a rich playground for model building aimed at explaining the flavor structure of the Standard Model. In the case where supersymmetry breaking is mediated by gravity, the soft-breaking Lagrangian typically exhibits large tree-level flavor violating effects, even if it stems from an ultraviolet flavor-conserving origin. Building on previous work, we continue our phenomenological analysis of these models with a particular emphasis on leptonic flavor observables. We consider three representative models which aim to explain the flavor structure of the lepton sector, with symmetry groups $\mathcal{G}_f = \Delta(27)$, A_4, and S_3.

1.1 Introduction

As the LHC marches onward in its search for hints of physics beyond the Standard Model, the community eagerly waits. Unfortunately, despite the overwhelming evidence for its need in order to explain open questions, such as the nature of dark matter, the stability of the Higgs mass with respect to higher scales, the origin of the Baryon asymmetry in the universe, amongst others, New Physics (NP) continues to elude us. We should not despair however, as the LHC, along with a robust set of other dedicated experiments, will continue to probe new corners of parameter space where NP could be hiding. At the same time, as our "first-guess" models come increasingly under pressure, it is worth pausing to consider alternative methods or observables which may help to further constrain them and extend the reach of the LHC.

A class of such models, popular for their ability to shed light on several of the open questions in particle physics, are supersymmetric extensions of the Standard Model. Its simplest incarnation, the Minimal Supersymmetric Standard Model (MSSM) , has many virtues: a possible dark matter candidate; new sources of CP violation; a mechanism for stabilizing the mass of the Higgs; the possibility for unification of the fundamental forces. However the non-observance by the LHC in Runs 1 and 2 of any of its predicted superpartners is beginning to constrain such a minimal realization of supersymmetry, pointing to a mass scale of the new predicted particles which may be heavier than naively expected. In the scenario where supersymmetry is indeed realized by nature, but out of reach of current colliders, we should look for further ways to probe or constrain the large parameter space available in the MSSM.

One curious legacy of the Standard Model (SM) is its rich flavor structure, which has historically [1] proven invaluable and complementary to direct searches for sniffing out new particles. Yet, understanding the peculiar mass and mixing pattern of the fundamental fermions remains one of the biggest puzzles of the SM. Despite a wealth of ideas and models put forth by the theory community, a convincing solution to this puzzle is still missing. Among the proposed ideas, the use of flavor symmetries, both continuous and discrete, remains a popular tool for model builders. This avenue has been especially explored in the lepton sector, where the suggestive form of the Pontecorvo-Maki-Nakagawa-Sakata (PMNS) matrix has led to several ansätze for its decomposition in terms of primitive bare mixing matrices, which give leptonic mixing angles close to their measured values. In most models, the aim is to motivate these special angles through the Clebsch-Gordan (CG) coefficients of a symmetry group, and moreover, to predict the as yet unmeasured parameters of the leptonic

sector: the Dirac CP violating phase, the quadrant of the atmospheric angle, and the neutrino mass ordering.
Unfortunately, a definitive picture has failed to emerge from the large number of present models (for recent reviews, see[2, 3]). One well-known problem at the level of the SM is that we cannot fully reconstruct the fundamental flavor parameters of the SM Lagrangian, the Yukawa matrices. In this regard, NP models which predict new flavor interactions in addition to new particles are particularly interesting, as they are bound to shed additional light (right-handed mixings, etc.) on the flavor puzzle regardless of their original motivations. The MSSM contains a wealth of such new flavor interactions in its soft-breaking sector. Although, in all generality the MSSM contains a host of unknown parameters in the flavor sector, in a previous work [4] we explored a specific class of *predictive* models where the MSSM emerges as an effective theory from an ultraviolet flavor-symmetric theory. These models :

- Arise from a superpotential which is invariant under a given flavor symmetry $\mathcal{G}_f$, spontaneously broken at a scale Λ_f. After the breaking of $\mathcal{G}_f$, new effective operators, à la Froggatt-Nielsen (FN), contribute to the low-energy superpotential. Similar effective operators contribute to the soft-breaking Lagrangian.
- Mediation of Supersymmetry breaking to the visible sector is assumed to occur through interactions at a scale $\Lambda_{\text{Med}} \gg \Lambda_f$, so that the soft-breaking terms, and, more exactly, the visible sector operators giving rise to the soft-breaking terms, respect $\mathcal{G}_f$. An illustrative example of such a mediation scheme, which we will assume for simplicity, is gravity mediation.

Under these conditions, these models contain *tree-level* flavor violating effects, arising from the mismatch between the order one coefficients of their supersymmetric and corresponding supersymmetry-breaking supergraphs after integrating out the mediator fields at Λ_f. In addition, as the flavor parameters [1] are fixed by the structure of the superpotential, these models are minimal, depending only on the traditional supergravity input parameters m_0, $m_{1/2}$, A_0, $\tan\beta$, and μ. This minimality and calculabity of these models makes them interesting in their own right, and especially amenable to constraints from flavor observables; in many cases extending beyond the reach of direct searches at the LHC.
In this work, we continue our investigation of this class of models [4–6], with a particular emphasis on constraints coming from leptonic flavor observables such as $\mu \to e\gamma$, $\mu \to 3\,e$, and $\mu - e$ conversion, although for completeness we scan each

[1] With the exception of the usual unknown order-one parameters.

model over all relevant flavor observables to obtain the strongest constraints. We look at three representative models available in the literature, based on the symmetry groups $\Delta(27)$, A_4 and S_3.

Our paper is organized as follows. We begin in Sec. 1.2 with a short review of the mechanism presented in [4], giving generic formulas applicable for any of the class of models under investigation. In Secs. 1.3-1.5 we apply these general formulae to specific models found in the literature based on the flavor groups $\Delta(27)$, A_4, and S_3. These sections are self-contained, including the relevant phenomenological analyses and results for each group. Finally, we conclude in Sec. 1.6 with brief remarks on our general results and future outlooks for extensions of this work.

1.2 A Review of the Mechanism

In this section we review and update the results of our previous work [4], demonstrating that in SUSY models augmented with a flavor symmetry spontaneously broken at a scale $\Lambda_f \leq \Lambda_{\text{Med}}$, flavor violation in the soft-breaking terms is generically present in the low-energy effective theory. This remains true even starting with completely flavor blind soft-breaking in the full theory and runs contrary to the naive expectation that the soft terms, being controlled by the flavor symmetry, should be diagonalized by the same rotations which diagonalize the Yukawa couplings. This mismatch between the Yukawa or Kinetic mixing matrices and their corresponding soft-term structures stems from the different ways in which SUSY breaking may be inserted in the full theory diagrams, giving rise to a single coupling in the low-energy effective theory.

Supersymmetry breaking can be represented by the insertion of a chiral background superfield, a spurion X, which is assumed to obtain a vacuum value largely along its supersymmetry breaking component $\langle F_X \rangle \gg \langle X \rangle$. Although not necessary, we will make the simplifying assumption in this work that this spurion is the only source of SUSY breaking and couples universally to the visible sector.

This mismatch between the soft-breaking terms and the superpotential or Kähler potential is manifest in terms of the FN fields in the full theory. Corrections to the low-energy superpotential W and Kähler potential K are generated below the flavor scale, Λ_f. These corrections stem from non-renormalizable operators containing an appropriate number of flavon insertions, generated by integrating over the appropriate heavy messengers in the underlying theory, which, in the case of the superpotential,

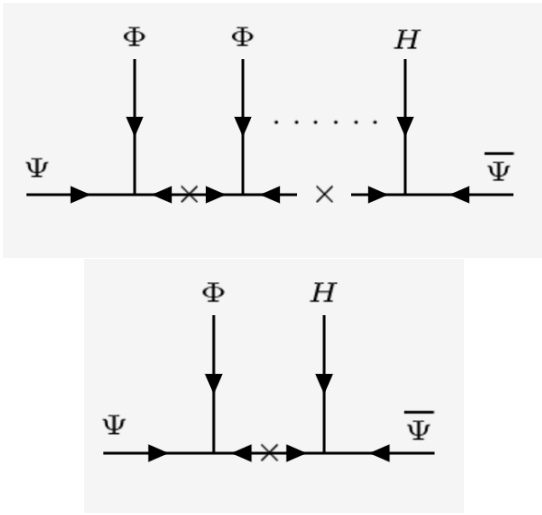

FIGURE 1.1: A supergraph depiction of the corrections to the superpotential represented by Eq. 1.1. An example for $n = 1$ involving a single Flavon insertion is given below. The internal lines are heavy messengers, and the cross denotes a supersymmetric mass insertion M.

may write schematically as,

$$W = W_{\text{ren}} + \Psi\ \Psi^c\ \mathrm{H} \left(\sum_{n=1}^{\infty} x_n \left(\frac{\langle \Phi \rangle}{M} \right)^n \right), \tag{1.1}$$

where Ψ (Ψ^c) denotes any of the left-handed (right-handed conjugate) MSSM superfields, H denotes the SM Higgs field, $\langle \Phi \rangle$ the vacuum expectation values (VEVs) of any of the flavons or heavy Higgses, M the heavy mass scale $\sim \Lambda_f$ of the messengers and x_n is a numerical coefficient depending on the charges of the fields. These corrections may be represented schematically in terms of the supergraphs which generate them, as shown in Fig. 1.1. In addition to correcting to the superpotential, similar supergraphs will generate the so called a-terms in the soft Lagrangian upon inserting a soft-breaking term at any internal point in the diagram, which can be represented by the insertion of a spurion field X with non-vanishing F-term, F_X. Assuming a universal SUSY breaking, these universal corrections in the full theory are of the form

$$\mathcal{L}_{\text{soft}} \sim \frac{F_X}{M_{\text{Pl}}} \times W_{\text{ren}} \equiv m_0 \times W_{\text{ren}}\,.$$

In terms of our supergraph language, this corresponds to attaching an external line involving the spurion X to each of the vertices in a given supergraph.
From here, it is evident that, after integrating out the heavy fields in the Lagrangian to

obtain the low-energy effective theory, the different ways to couple the spurion field produce a mismatch between the a terms and their corresponding Yukawa matrices. For a given supergraph which generates an entry in the Yukawa matrix, we have multiple ways to generate the corresponding a term, one for each insertion of the spurion X at a given vertex. This mismatch may be easily written in terms of the operator dimension which generates the given entry in the Yukawa matrices of the superpotential. Given an operator with n Φ insertions, we have $2n+1$ possible X insertions; 2 for each Φ and mass-insertion vertex, plus one additional for the vertex involving the Higgs. Generically, this implies that for a Yukawa entry Y_{ij} generated by N Flavon insertions,

$$a_{ij} \sim (2n+1)\ A_0\ Y_{ij} \tag{1.2}$$

where $A_0 = k\, m_0$. As in FN models each entry in the Yukawa matrix is generated at a different order, the individual entries in the a matrices will contain different order one coefficients, and not be directly proportional to the Yukawa matrices. Performing a rotation of the superfields and going to the Super-CKM basis, the a terms will not be diagonalized, their off-diagonal terms contributing at tree-level to flavor violating observables.

Similar considerations hold for the Kähler potential. Below Λ_f, corrections to the Kähler potential are generated when integrating over the heavy messengers. In the case of a single flavon, as in the case Abelian models, it can be written schematically as,

$$K_{ij} = \Psi_i\, \Psi_j^\dagger \left(\delta_{ij} + \sum_{n,m} c_{ij}^{(n,m)} \left(\frac{\Phi}{M}\right)^n \left(\frac{\Phi^\dagger}{M}\right)^m \right), \tag{1.3}$$

where, for the leading terms, $c_{ij}^{(n,m)} = \delta_{m,0}\ \delta(q_i + q_j - n)$ if $(q_i + q_j) > 0$ and $c_{ij}^{(n,m)} = \delta_{n,0}\ \delta(q_i + q_j - m)$ if $(q_i + q_j) < 0$. In the case of several flavon fields in complex representations of $\mathcal{G}_f$, as is the case of typical non-Abelian models, the leading contributions appear in the form $\Phi_r \Phi_r^\dagger$[2],

$$K_{ij} = \Psi_i\, \Psi_j^\dagger \left(\delta_{ij} + \sum_{r,n} c_{ij}^{r,n} \left(\frac{\Phi_r \Phi_r^\dagger}{M^2}\right)^n + \dots \right), \tag{1.4}$$

Again, this can be depicted in terms of supergraphs, where now superfields may both enter (undaggered) or leave (daggered) a given vertex. The leading corrections, those that do not contain derivatives or additional suppressions of M, are all of the

[2]Depending on the model, there may exist other contributions, including even non-hermitian combinations of fields, if they are neutral under the different charges. However, they are usually sub-leading with respect to $\Phi_r \Phi_r^\dagger$.

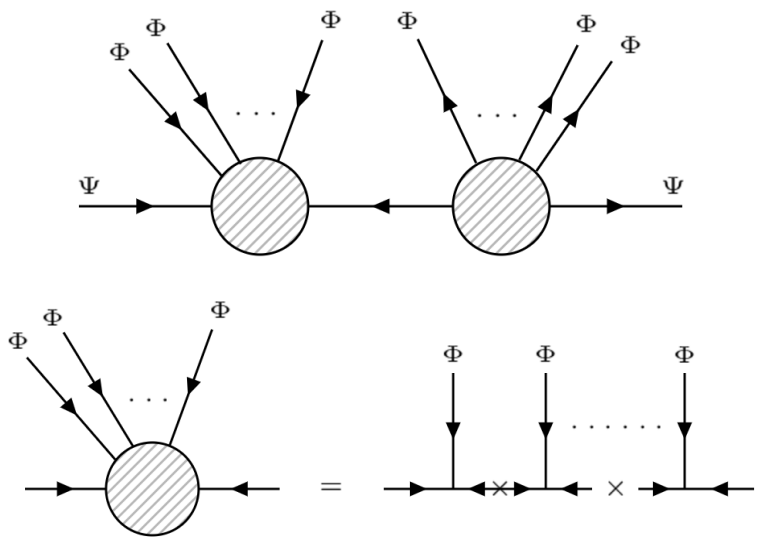

FIGURE 1.2: Supergraphs which correct the Kähler potential.

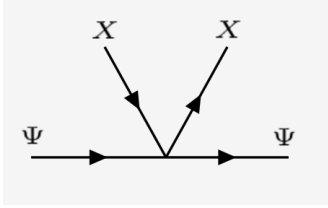

FIGURE 1.3: Diagonal contribution to the soft masses of a given superfield Ψ.

form shown in Fig. 1.2, with one internal line a superpropagator of a given messenger connecting bubbles of Φ's involving only mass insertions in the internal lines. We may therefore organize the corrections generated by a given supergraph by the number of incoming ($n_{\rm in}$) and outgoing ($n_{\rm out}$) Φ's. A given supergraph of this form will generate soft masses for the corresponding scalars $\tilde{\Phi}$ when coupled to the supersymmetry breaking combination $\langle F_X\rangle\langle F_X\rangle^\dagger$, as shown for the diagonal contribution in Fig. 1.3. For a supergraph of the form of Fig. 1.2, we have have two ways to attach the spurion combination $XX^\dagger$, either as in Fig. 1.3 to an internal superpropagator, or with X attached to one of the incoming Φ vertices and $X^\dagger$ attached to one of the outgoing Φ vertices, as shown in Fig. 1.4. As there are $n_{\rm in}$ ways to attach X to a given incoming vertex and $n_{\rm out}$ ways to attach $X^\dagger$ to an outgoing vertex, plus an additional graph involving the correction to the internal superpropagator, we find that the mismatch factor between the soft mass matrices and the Kähler matrices can be written in terms of the total number of Flavon insertions $n = n_{\rm in} + n_{\rm out}$ and the number of

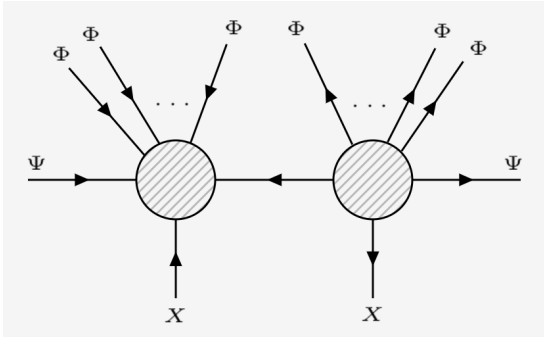

FIGURE 1.4: Schematic contribution to the soft mass of a superfield Ψ.

incoming Flavon insertions n_{in},

$$m_{ij}^2 \sim f\, m_0^2 \cdot K_{ij}, \qquad f \;=\; n_{\text{in}} \cdot n_{\text{out}} + 1 \;=\; n_{\text{in}} \cdot (n - n_{\text{in}}) + 1. \tag{1.5}$$

As a concrete example, we show the case with $n_{\text{in}} = 1$, $N = 3$ in Fig. 1.5, for which Eq. (1.5) gives $f = 3$. Eqs. (1.2) and (1.5) are useful in the sense that without knowing precisely the underlying theory, the mismatch factors can be quickly calculated solely in terms of the number of Flavon insertions, or alternatively, the operator dimension at which a given Yukawa entry is generated. Once these mismatch factors are known and the soft-matrices given, rotations of the superfields, first to canonically normalize [7] and then to diagonalize the Yukawa matrices, may be performed.

It is worth noting that even if the leading non-universal contributions in the soft-mass matrix are proportional to the Kähler matrix, flavor changing entries are generically present in the SCKM basis. In this case, the diagonalization of the Kähler matrix also diagonalizes the soft-mass matrix, but the rescaling of the diagonal Kähler elements does not eliminate the diagonal elements in the soft-mass matrices if $f \neq 1$; off-diagonal elements will always reappear when going to the SCKM basis.

As an illustrative example, consider a simplified non-Abelian model with two flavons. The non-universal corrections to the Kähler potential and soft-mass matrices would be proportional,

$$K_{ij} \;=\; \delta_{ij} + c_1 \left(\frac{\Phi_1 \Phi_1^\dagger}{M^2}\right) + c_2 \left(\frac{\Phi_2 \Phi_2^\dagger}{M^2}\right), \tag{1.6}$$

$$\widetilde{m}_{ij}^2 \;=\; m_0^2 \left(\delta_{ij} + 3c_1 \left(\frac{\Phi_1 \Phi_1^\dagger}{M^2}\right) + 3c_2 \left(\frac{\Phi_2 \Phi_2^\dagger}{M^2}\right)\right). \tag{1.7}$$

Taking $\Phi_1 = (0, 1)$ and $\Phi_2 = (\epsilon, \epsilon)$, it is clear that both matrices are diagonalized with the same rotation U, but the rescaling of the Kähler, $N^{1/2}$, does not reabsorb the

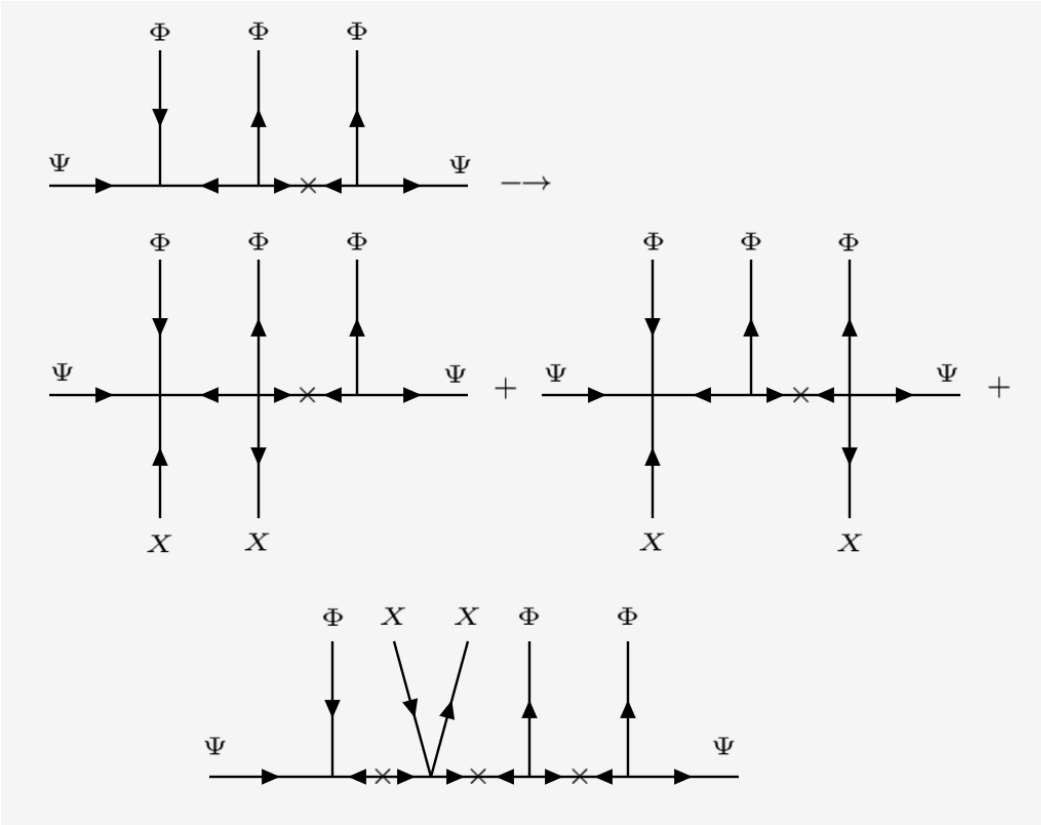

FIGURE 1.5: An example of the mismatch factor in the soft masses for $n_{\text{in}} = 1$, $n = 3$.

non-universal diagonal elements in the soft mass matrix,

$$N^{1/2} V^\dagger K_{ij} V N^{1/2} = \mathbb{1} \tag{1.8}$$

$$N^{1/2} V^\dagger \widetilde{m}^2_{ij} V N^{1/2} \simeq m_0^2 \begin{pmatrix} 1 + 2\, a_2\, \epsilon & 0 \\ 0 & 1 + b_1 + b_2\, \epsilon \end{pmatrix}, \tag{1.9}$$

with $b_1 \simeq 2c_1/(1+c_1)$ and $b_2 \simeq 2c_2/(1+c_1^2)$. Thus, as stated before, when diagonalizing the Yukawa matrix to go to the SCKM basis, the new rotation $V \sim \mathcal{O}(\epsilon)$, will introduce again off-diagonal terms in the soft-mass matrices.

These off-diagonal entries of the a terms and soft masses are very relevant in performing phenomenological analyses of given models. By subjecting them to the appropriate flavor constraints, like those collected in Table I.6 for leptonic processes, complementary bounds to high-energy colliders can be set. Finally, an additional consideration comes from the stability of the vacuum. As shown in [8], the requirement of the absence of charge and color breaking (CCB) minima and unbounded

from below (UFB) directions impose strong limits on the trilinear terms. In our analysis, we establish an upper bound for k (remember that $A_0 = k\, m_0$, Eq. (1.2)) at the GUT scale and, after the running down to the EW scale, only points that satisfy the following relations are considered:

$$| a_{e,ii} |^2 \;\leq\; 3\, Y_{e_i}^2 \left(m_{e_i}^2 + \widetilde{m}_{e_i}^2 + m_{H_d}^2 \right), \tag{1.10}$$

$$| a_{e,ij} |^2 \;\leq\; Y_{e_k}^2 \left(m_{e_i}^2 + \widetilde{m}_{e_j}^2 + m_{H_d}^2 \right), \quad \mathrm{k} = \mathrm{Max(i,j)} \tag{1.11}$$

As an application of these rules, we turn now to a phenomenological analyses using lepton flavor observables for three representative lepton flavor models found in the literature, based on the flavor groups $\mathcal{G}_f = \Delta(27)$, A_4 and S_3.

1.3 A $\Delta(27)$ Model

As a first example, we consider the flavor model of I. de Medeiros Varzielas. G. G. Ross and S. F. King in Ref. [9], where the continuum $SU(3)_f$ family symmetry of Ref. [10], already considered in our previous work to study the quark sector, was replaced by its discrete subgroup $\Delta(27)$. In this way the mechanism for obtaining the desired vacuum structure, which leads to Tri-Bi-maximal (TB) mixing in the lepton sector through a type I see-saw mechanism, is considerably simplified.
$\Delta(27)$ is the simplest non-trivial group in the series $\Delta(3N^2)$, a discrete subgroup of $SU(3)$ that can be defined in terms of the semi-direct product $(\mathbb{Z}_N \times \mathbb{Z}'_N) \times \mathbb{Z}_3$. The elements of the group (g) can be written in terms of the generators of Z_3 (a, a', b) as follows:

$$g \;=\; b^k\, a^m\, a'^n \quad \text{for} \quad k,m,n = 0,1,2\,, \tag{1.12}$$

where the generators must satisfy

$$\begin{aligned} a^3 \;=\; a'^3 \;&=\; b^3 \;=\; e \qquad , \qquad a\, a' \;=\; a'\, a \\ b\, a\, b^{-1} \;&=\; a^{-1} a'^{-1} \qquad , \qquad b\, a'\, b^{-1} \;=\; a\,. \end{aligned} \tag{1.13}$$

These conditions give rise to nine singlets and a triplet/anti-triplet representation. Table 1.1 shows the particle content of the model: left-handed (LH) leptons transform as triplets **3** whereas the right-handed (RH) fields transform as anti-triplets $\bar{\mathbf{3}}$; the Higgs doublets are singlets under the group transformations and flavons, generically denoted as ϕ, transform as triplet or anti-triplets. Unlike the $SU(3)_f$ model, where the VEV of a triplet could be rotated to a single direction, the discrete non-Abelian

Field	L	e^c, ν^c	$H_{u,d}$	Σ	ϕ_{123}	ϕ_1	$\bar{\phi}_3$	$\bar{\phi}_{23}$	$\bar{\phi}_{123}$
$\Delta(27)$	**3**	**3**	**1**	**1**	**3**	**3**	$\bar{\mathbf{3}}$	$\bar{\mathbf{3}}$	$\bar{\mathbf{3}}$
$\mathbb{Z}_2$	1	1	1	1	1	-1	-1	-1	-1
$U(1)_{FN}$	0	0	0	2	-1	-4	0	-1	1
$U(1)_R$	1	1	0	0	0	0	0	0	0

TABLE 1.1: Transformation of the matter superfields under the $\Delta(27)$ family symmetries.

symmetry leads to a finite number of candidate vacuum states. The obtained pattern for the VEVs is then given by [9]:

$$\langle \bar{\phi}_3 \rangle^T = v_3 \begin{pmatrix} 0 \\ 0 \\ 1 \end{pmatrix} \quad , \quad \langle \bar{\phi}_{23} \rangle^T = v_{23} \begin{pmatrix} 0 \\ -1 \\ 1 \end{pmatrix} , \tag{1.14}$$

$$\langle \phi_{123} \rangle \propto \langle \bar{\phi}_{123} \rangle^T = v_{123} \begin{pmatrix} 1 \\ 1 \\ 1 \end{pmatrix} \quad , \quad \langle \phi_1 \rangle \propto v_1 \begin{pmatrix} 1 \\ 0 \\ 0 \end{pmatrix} , \tag{1.15}$$

with $v_{123} \ll v_{23} \ll v_3 \sim v_1$. The leading Yukawa terms responsible for the fermion masses in the $SU(3)_f$ model are still the dominant operators in this example although, beyond the LO, additional contributions enter in the superpotential. Its complete expression is [9]:

$$\begin{aligned} W_e = & \frac{1}{M^2} (L\,\bar{\phi}_3)(e^c\,\bar{\phi}_3)\,H_d + \frac{1}{M^2} (L\,\bar{\phi}_{23})(e^c\,\bar{\phi}_{123})\,H_d + \frac{1}{M^2} (L\,\bar{\phi}_{123})(e^c\bar{\phi}_{23})\,H_d \\ & + \frac{1}{M^3} (L\,\bar{\phi}_{23})\,(e^c\,\bar{\phi}_{23})\,\Sigma\,H_d \\ & + \frac{1}{M^5} (L\,\bar{\phi}_{123})\,(e^c\,\bar{\phi}_3)\,H_d\,\Sigma\,(\phi_1\,\bar{\phi}_{123}) + \frac{1}{M^5} (L\,\bar{\phi}_3)\,(e^c\,\bar{\phi}_{123})\,\Sigma\,H_d\,(\phi_1\,\bar{\phi}_{123}) \\ & + \frac{1}{M^6} (L\,\bar{\phi}_{123})\,(e^c\,\bar{\phi}_{123})\,H_d\,(\phi_{123}\,\bar{\phi}_3)^2 . \end{aligned} \tag{1.16}$$

After the flavor symmetry is broken, the Yukawa and Trilinear structures are given by:

$$Y^e \sim y_\tau \begin{pmatrix} x_1\,\epsilon^8 & -x_2\,\epsilon^3 & x_2\,\epsilon^3 \\ -x_3\,\epsilon^3 & 3\,x_4\,\epsilon^2 & -3\,x_4\epsilon^2 \\ x_3\,\epsilon^3 & -3\,x_4\,\epsilon^2 & x_5\,\alpha \end{pmatrix} , \tag{1.17}$$

$$a_e \;\sim\; y_\tau\, A_0 \begin{pmatrix} 13\, x_1\, \epsilon^8 & -5\, x_2\, \epsilon^3 & 5\, x_2\, \epsilon^3 \\ -5\, x_3\, \epsilon^3 & 21\, x_4\, \epsilon^2 & -21\, x_4\, \epsilon^2 \\ 5\, x_3\, \epsilon^3 & -21\, x_4\, \epsilon^2 & 5\, x_5\, \alpha \end{pmatrix}, \tag{1.18}$$

where $x_i \sim \mathcal{O}(1)$, $\langle\Sigma\rangle/M_e \simeq -3$, $v_3/M_e = \sqrt{y_\tau}$, $v_{23}/M_e \simeq \sqrt{y_\tau}\epsilon$, $v_{123}/M_e \simeq \sqrt{y_\tau}\epsilon^2$ and the expansion parameter is given by $\epsilon \simeq 0.15$. As stated before, Y_e and a_e are not simply proportional due to the mismatch caused by the different ways in which the spurion field can be attached to the Yukawa supergraphs in order to generate the Trilinear terms. Thus, from Eq. (1.2), the multiplicative factors in Eq. (1.17) are simply $2n+1$, with n equal to the number of flavon insertions. For instance, in the case of $Y_{11} \propto \epsilon^8$, $n = 6$ (see last line of the superpotential) and the proportionality factor would be 13. Similarly, for $Y_{22} \propto 3\,\epsilon^2$, $n = 3$ (second line of the superpotential) and $a_{ij} = 7\, A_0\, Y_{ij} \propto 21\,\epsilon^2$.

Regarding the Kähler potential, it is important to stress here that in this model the $SU(2)_L$ doublet-messengers are assumed to be much heavier than their singlet counterpart. Because of that, corrections to the kinetic and soft terms for LH particles will be negligible and, therefore, the associated matrices can be taken as the identity matrix. In contrast, the LO Kähler potential for RH fields is:

$$\begin{aligned} K_R \;&=\; e^c e^{c\dagger} \;+\; \frac{1}{M^2}\left[(e^c\bar{\phi}_3)(\bar{\phi}_3^\dagger e^{c\dagger}) \;+\; (e^c\bar{\phi}_{23})(\bar{\phi}_{23}^\dagger e^{c\dagger}) \;+\; (e^c\bar{\phi}_{123})(\bar{\phi}_{123}^\dagger e^{c\dagger})\right] \\ &+\; \frac{1}{M^3}\left[(e^c\bar{\phi}_{23})(\bar{\phi}_{123}^\dagger e^{c\dagger})\,\Sigma \;+\; \text{h.c.}\right] \\ &+\; \frac{1}{M^5}\left[(e^c\bar{\phi}_{123})\,(\bar{\phi}_{23}^\dagger e^{c\dagger})\,(\bar{\phi}_3\phi_1)\,\Sigma \;+\; \text{h.c.}\right]. \end{aligned} \tag{1.19}$$

Similarly, a mismatch between the soft-mass matrices and the Kähler metric will arise when considering the different ways in which $XX^\dagger$ can be coupled to the diagram, see Fig. 1.5. Once the flavons get their VEV, the Kähler function and soft-mass matrices can be written as:

$$(K_R)_{ij} = \left(\delta_{ij} \;+\; C_{R,ij}\right), \qquad (\widetilde{m}^2_{R,e})_{ij} = m_0^2\left(\delta_{ij} \;+\; B_{R,ij}\right), \tag{1.20}$$

with C_R and B_R given by:

$$C_R \;\sim\; \begin{pmatrix} \epsilon^4 & -3\,(1+\alpha)\,\epsilon^3 & 3\,(1+\alpha)\,\epsilon^3 \\ -3\,(1+\alpha)\,\epsilon^3 & \epsilon^2 & -\epsilon^2 \\ 3(1+\alpha)\,\epsilon^3 & -\epsilon^2 & \alpha^2 \end{pmatrix}, \tag{1.21}$$

$$B_R \sim \alpha \begin{pmatrix} 2\epsilon^4 & -3(4+8\alpha)\epsilon^3 & 3(4+8\alpha)\epsilon^3 \\ -3(4+8\alpha)\epsilon^3 & 2\epsilon^2 & -2\epsilon^2 \\ 3(4+8\alpha)\epsilon^3 & -2\epsilon^2 & 2 \end{pmatrix},$$

where $\alpha = y_\tau$. Again, the multiplicative factors in Eq. (1.22) can be easily computed from Eq. (1.5) just counting the number of flavon fields entering and leaving the diagram, without specifying the complete messenger spectrum of the UV theory.
With the structures of the Kinetic-mixing and Yukawa matrices known, the superfields must now be rotated twice: first, to the basis where canonical kinetic terms are recovered (canonical basis), and again, to the basis where the Yukawa couplings are diagonal (mass basis). Thus, the final matrices are:

$$a_e \rightarrow y_\tau A_0 \begin{pmatrix} \frac{x_2 x_3}{x_4}\epsilon^4 & 2x_2\epsilon^3 & -2\frac{x_2}{x_5}\hat{\alpha}\,\epsilon^3 \\ 2x_2\epsilon^3 & 24x_4\epsilon^2 & -6x_4\hat{\alpha}\,\epsilon^2 \\ -2x_2\epsilon^3 & -6x_4\epsilon^2 & 5x_5\hat{\alpha} \end{pmatrix}, \tag{1.22}$$

$$\widetilde{m}^2_{R,e} \rightarrow m_0^2 \begin{pmatrix} 1 & -3\alpha(3+7\alpha)\epsilon^3 & 3\alpha\left(3+\frac{11}{2}\alpha-\frac{x_2}{3x_4}\right)\epsilon^3 \\ -3\alpha(3+7\alpha)\epsilon^3 & 1+\alpha\epsilon^2 & -\alpha\,(1-3x_4)\,\epsilon^2 \\ 3\alpha\left(3+\frac{11}{2}\alpha-\frac{x_2}{3x_4}\right)\epsilon^3 & -\alpha\,(1-3x_4)\,\epsilon^2 & 1+\alpha \end{pmatrix}, \tag{1.23}$$

where $\hat{\alpha} \equiv 1/\sqrt{1+\alpha^2}$. The net effect of this series of rotations is the following: the canonical normalization makes the multiplicative factors of B_R decrease by one unit, while having no impact on the Yukawa and Trilinear terms; the second rotation to the mass basis results in the reduction from $\epsilon^8 \rightarrow \epsilon^4$ of $A_{\ell,11}$ and gives only additional small corrections to the elements of B_R. The matrix U_ℓ that performs the latter diagonalization gives only $\mathcal{O}(\epsilon^2)$ corrections to $U_{\rm PMNS} = U_\ell^\dagger U_\nu$ so that it mantains the tri-bimaximal LO structure. As a consequence, this model cannot reproduce the experimental value of the reactor angle that would require $\sin\theta_{13}^\ell \propto \epsilon$ [3].
With these matrices, a combined fit to the latest experimental values for $U_{\rm PMNS}$ [12], excluding the 13 entry, and the Yukawas at the GUT scale [13] is performed to fix the values of the x_i coefficients. For $\epsilon = 0.13$ these are reasonably $\mathcal{O}(1)$ coefficients, namely: ($x_1 = 1.0$, $x_2 = 1.2$, $x_3 = 1.$, $x_4 = 1.$, $x_5 = 1.7$). After substituting these

[3] After completion of this work, we came across the preprint [11], where the authors succeed in obtaining a correct $\sin\theta_{13}^\ell$ in the context of a similar $\Delta(27)$ model.

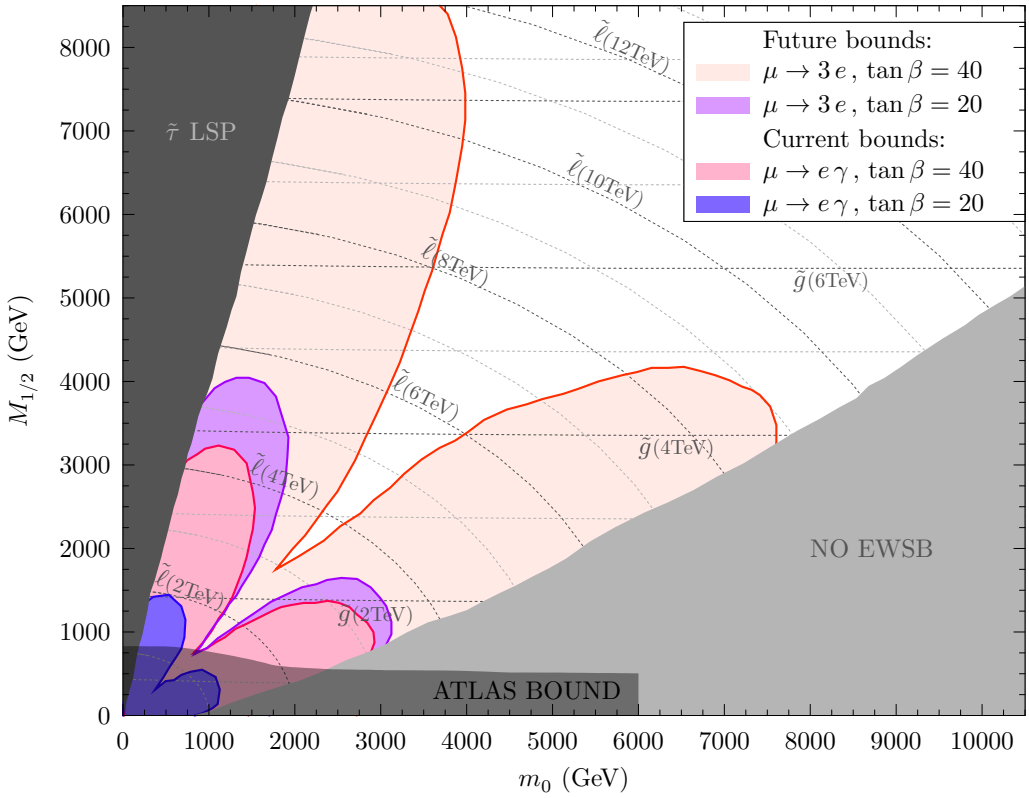

FIGURE 1.6: Excluded regions due to $\mu \to e\gamma$ and $\mu \to eee$ for two reference values: $\tan\beta = 5$ (blue shapes) and $\tan\beta = 20$ (red shapes). In the dark (blue and red) regions, we compare with current $\mu \to e\gamma$ bounds, while in the light (blue and red) regions we compare with the expected $\mu \to eee$ sensitivity in the near future. Interestingly, even for present bounds, these results are competitive with MSUGRA ATLAS limits (gray area).

values, the matrices must be run to the EW scale by means of the MSSM renormalization group equations (RGE), checked to satisfy the charge and color breaking relations, and compared to the most relevant flavor observables. Numerical calculations for the running, spectrum and low energy processes have been done with the Supersymmetric Phenomenology package (SPheno) [14, 15]. The resulting plot is Fig. 1.6. As shown in Fig. 1.6, the most restrictive constraints come from the flavor violating decays $\mu \to e\gamma$ and $\mu \to eee$. In the plot, the colored shapes represent the parameter regions where the analyzed model would dissagree with current and future bounds in Table I.6. As the results strongly depend on $\tan\beta$, two reference values of $\tan\beta$ has been considered that is $\tan\beta = 5$, blue (darker) regions, and $\tan\beta = 20$, red (lighter) regions. It can be observed that, for both values of $\tan\beta$, the obtained bounds are competitive with MSUGRA ATLAS limits, even just considering present $\mu \to e\gamma$

experimental limits. On top of that, if the Mu3e experiment reaches the expected precision finding no sign of the $\mu \to eee$ process, the parameter space of the model will turn out to be significantly constrained.

These results are in good agreement with those obtained with the mass insertion approximation (MIA) [16–20], which provides a simplified description of the phenomenology. As discussed in [20–22], in the absence of off-diagonal δ_{LL} insertions, the main effects come from the RR sector. This sector suffers from a characteristic cancellation among the two $\tan\beta$-enhanced dominant contributions: the one due to the pure bino term (with internal chirality flip and a flavor-conserving δ_{LR} mass insertion) and another from the bino-higgsino exchange. This destructive interference can be easily recognized in Fig. 1.6. Moreover, these contributions require a bino mass insertion, M_1, so, as we see in the figure, the bound practically disappears for small values of $M_{1/2}$.

1.4 An A_4 Model

As a second example, we consider a model belonging to perhaps the most popular class of models based on discrete flavors groups, those with $\mathcal{G}_f = A_4$. This is the discrete group of even permutations of 4 objects; it contains 12 elements and has four inequivalent irreducible representations: three singlets $\{\mathbf{1}, \mathbf{1}', \mathbf{1}''\}$ and a triplet $\mathbf{3}$. It is specially interesting because it is the minimal non-Abelian group containing a triplet representation. We refer to Appendix B.1 for a detailed description of the group, including the associated multiplication rules. Flavor models based on an A_4 symmetry [23–47] have been an attractive option for describing the lepton sector due to their simplicity and economical structure in reproducing the well-known TB-mixing pattern at leading order (LO). Although this scheme predicts a vanishing reactor angle, currently excluded by data [48–50], variations of these models [51–63] may still accommodate an adequate θ_{13}^{ℓ}, once higher order corrections to masses and mixings are taken into account. Here, we analyze the A_4 Altarelli-Meloni model of Ref. [24], which can be seen as a simplest A_4 model in the sense that it is able to generate an appropriate charged-lepton hierarchy between generations without requiring an extra $U(1)_{\rm FN}$ symmetry. The complete flavor symmetry of the model is $\mathcal{G}_f = A_4 \times Z_4$ with an additional $U(1)_R$ symmetry related to R-parity. Table 1.2 shows the symmetry assignments for leptons, electroweak Higgs doublets and flavons. In particular, the three generations of left-handed lepton doublets L and the right-handed neutrino ν^c are ascribed to triplet representations while the right-handed charged leptons e^c,

Field	ν^c	L	e^c	μ^c	τ^c	H_d	H_u	ϕ_S	ϕ_T	ξ	ξ'	$\xi'^\dagger$
A_4	**3**	**3**	**1**	**1**	**1**	**1**	**1**	**3**	**3**	**1**	**1′**	**1″**
Z_4	-1	i	1	i	-1	1	i	1	i	1	i	-i
$U(1)_R$	1	1	1	1	1	0	0	0	0	0	0	0

TABLE 1.2: Transformation of the matter and flavon superfields under the flavor symmetry $\mathcal{G}_f = A_4 \times Z_4$, for non trivial cases the correspondent daggered fields are also specified.

μ^c, τ^c, together with the two Higgs doublets $H_{u,d}$, transform in the trivial singlet representation. Beyond the MSSM fields, the model contains the flavons that transform as singlets or triplets.

The vacuum alignment in this model responsible for the symmetry breaking [24] is given by

$$\begin{aligned} \langle \phi_T \rangle \propto v_T \begin{pmatrix} \delta\hat{v}_{T1} \\ 1+\delta\hat{v}_{T2} \\ \delta\hat{v}_{T3} \end{pmatrix} \quad , \qquad \langle \phi_S \rangle \propto v_S \begin{pmatrix} 1+\delta\hat{v}_S \\ 1+\delta\hat{v}_S \\ 1+\delta\hat{v}_S \end{pmatrix} , \\ \langle \xi \rangle \propto v_\xi \quad , \qquad \langle \xi' \rangle \propto v'_\xi \, (1+\delta\hat{v}'_\xi) \, , \end{aligned} \tag{1.24}$$

where $\delta\hat{v}_i = \delta v_i / M$, $v_T/M \sim v'_\xi/M \sim \epsilon$ and $v_S/M \sim v_\xi/M \sim \delta v_i/M \sim \epsilon'$. The shift in the VEVs, denoted as δv_i, account for NLO corrections arising from higher-order operators in the driving superpotential. A similar order of magnitude is expected for ϵ and ϵ', although a moderate hierarchy can be tolerated among them. The LO effective superpotential contains the following operators

$$\begin{aligned} W_e &= \frac{1}{M} \tau^c (L\phi_T) \, H_d \\ &+ \frac{1}{M^2} \mu^c \left[(L\phi_T^2) \; + \; (L\phi_T)'' \xi' \right] H_d \\ &+ \frac{1}{M^3} e^c \left[(L\phi_T^3) \; + \; (L\phi_T^2)'' \xi' \; + \; (L\phi_T)' \xi'^2 \right] H_d \, , \end{aligned} \tag{1.25}$$

where the brackets stand for each possible product combination of the fields inside. It is easy to see that, replacing Eqs. (1.24) into Eq. (1.25) with $\delta v_i = 0$, the vacuum configuration leads to diagonal and hierarchical Yukawas in the charged-lepton sector. Off-diagonal entries in the Yukawa matrix derive from considering the shifted VEVs ($\delta v_i \neq 0$) in the LO superpotential and higher-order operators obtained by the

insertion of ϕ_S and ξ' [24]. Taking into account the charges of Table 1.2, the correction to the LO superpotential would be:

$$\begin{aligned}\delta W_e &= \frac{1}{M^2}\,\tau^c\left[(L\phi_T\phi_S) + (L\phi_S)''\xi'\right] H_d \\ &+ \frac{1}{M^3}\,\mu^c\left[(L\phi_T^2\phi_S) + (L\phi_T\phi_S)''\xi' + (L\phi_S)'\xi'^2\right] H_d \\ &+ \frac{1}{M^4}\,e^c\left[(L\phi_T^3\phi_S) + (L\phi_T^2\phi_S)''\xi' + (L\phi_T\phi_S)'\xi'^2 + (L\phi_S)\xi'^3\right] H_d\,.\end{aligned} \tag{1.26}$$

As can be seen in Eq. (1.27), these contributions result in non-vanishing off-diagonal entries of the same order of the diagonal term in each row multiplied by ϵ':

$$Y^e \sim \begin{pmatrix} x_1\,\epsilon^3 & x_2\,\epsilon^3\epsilon' & x_3\,\epsilon^3\epsilon' \\ x_4\,\epsilon^2\epsilon' & x_5\,\epsilon^2 & x_6\,\epsilon^2\epsilon' \\ x_7\,\epsilon\,\epsilon' & x_8\,\epsilon\,\epsilon' & x_9\,\epsilon \end{pmatrix} \quad , \quad a_e \sim A_0 \begin{pmatrix} 7\,x_1\,\epsilon^3 & 9\,x_2\,\epsilon^3\epsilon' & 9\,x_3\,\epsilon^3\epsilon' \\ 7\,x_4\,\epsilon^2\epsilon' & 5\,x_5\,\epsilon^2 & 7\,x_6\,\epsilon^2\epsilon' \\ 5\,x_7\,\epsilon\,\epsilon' & 5\,x_8\,\epsilon\,\epsilon' & 3\,x_9\,\epsilon \end{pmatrix} \tag{1.27}$$

with $x_i \sim \mathcal{O}(1)$ generic order one coefficients. Again, Y_ℓ and A_ℓ are not proportional and the multiplicative factors in the Trilinears can be computed with Eq. (1.2) considering N equal to the power associated to ϵ and/or ϵ' in the correspondent Yukawa element. The LO Kähler potential for left-handed (LH) fields is given by:

$$K_L = L\,L^\dagger + \frac{1}{M^2}\left[(L\,L^\dagger\,\phi_S\,\phi_S^\dagger) + (L\,L^\dagger\,\phi_S)\,\xi^\dagger\right] + \text{h.c.}\,, \tag{1.28}$$

whereas the right-handed (RH) Kähler potential would be:

$$\begin{aligned}K_R &= e^c e^{c\dagger} + \mu^c\mu^{c\dagger} + \tau^c\tau^{c\dagger} \\ &+ \frac{1}{M^2}\left[e^c(\phi_T\phi_S^\dagger)\mu^{c\dagger} + \mu^c(\phi_T\phi_S^\dagger)\tau^{c\dagger}\right] \\ &+ \frac{1}{M^3}\,e^c\left[(\phi_S\phi_T^{\dagger 2}) + (\phi_S\phi_T^\dagger)'\xi'^\dagger + \text{h.c.}\right]\tau^{c\dagger} + \text{h.c.}\,,\end{aligned} \tag{1.29}$$

Once the flavons have been integrated out, the Kähler function and soft-mass matrices for both LH- and RH-fields can be written as in Eq. (1.20) with $C_{L(R)}$ and $B_{L(R)}$:

$$C_L \sim \begin{pmatrix} \epsilon^2+\epsilon'^2 & \epsilon'^2 & \epsilon'^2 \\ \epsilon'^2 & \epsilon^2+\epsilon'^2 & \epsilon'^2 \\ \epsilon'^2 & \epsilon'^2 & \epsilon^2+\epsilon'^2 \end{pmatrix}, C_R \sim \begin{pmatrix} \epsilon^2+\epsilon'^2 & \epsilon\,\epsilon' & \epsilon^2\epsilon' \\ \epsilon\,\epsilon' & \epsilon^2+\epsilon'^2 & \epsilon\,\epsilon' \\ \epsilon^2\epsilon' & \epsilon\,\epsilon' & \epsilon^2+\epsilon'^2 \end{pmatrix}, \tag{1.30}$$

$$B_L \sim 2\begin{pmatrix} \epsilon^2+\epsilon'^2 & \epsilon'^2 & \epsilon'^2 \\ \epsilon'^2 & \epsilon^2+\epsilon'^2 & \epsilon'^2 \\ \epsilon'^2 & \epsilon'^2 & \epsilon^2+\epsilon'^2 \end{pmatrix}, B_R \sim 2\begin{pmatrix} \epsilon^2+\epsilon'^2 & \epsilon\,\epsilon' & \frac{3}{2}\epsilon^2\epsilon' \\ \epsilon\,\epsilon' & \epsilon^2+\epsilon'^2 & \epsilon\,\epsilon' \\ \frac{3}{2}\epsilon^2\epsilon' & \epsilon\,\epsilon' & \epsilon^2+\epsilon'^2 \end{pmatrix}. \tag{1.31}$$

Again, the multiplicative factors in Eq. (1.31) can be easily figured out from Eq. (1.5) by just computing the number of flavon fields entering and leaving the diagram. Then, we perform the two rotations to the canonical and the mass basis that result in the following rotated matrices

$$a_e \to A_0 \begin{pmatrix} 7\,x_1\,\epsilon^3 & \left(4\,x_2+2\frac{x_1x_4}{x_5}\right)\epsilon^3\epsilon' & \left(6\,x_3+4\frac{x_1x_7}{x_9}\right)\epsilon^3\epsilon' \\ 2\,x_4\,\epsilon^2\epsilon' & 5\,x_5\,\epsilon^2 & \left(4\,x_6+2\frac{x_5x_8}{x_9}\right)\epsilon^2\epsilon' \\ 2\,x_7\,\epsilon\,\epsilon' & 2\,x_8\,\epsilon\,\epsilon' & 3\,x_9\,\epsilon \end{pmatrix}, \tag{1.32}$$

$$\widetilde{m}_L^2 \to m_0^2 \begin{pmatrix} 1+\epsilon^2+\epsilon'^2 & \epsilon'^2 & \epsilon'^2 \\ \epsilon'^2 & 1+\epsilon^2+\epsilon'^2 & \epsilon'^2 \\ \epsilon'^2 & \epsilon'^2 & 1+\epsilon^2+\epsilon'^2 \end{pmatrix}, \tag{1.33}$$

$$\widetilde{m}_{R,e}^2 \to m_0^2 \begin{pmatrix} 1+\epsilon^2+\epsilon'^2 & \epsilon\,\epsilon' & 2\,\epsilon^2\epsilon'+\left(\frac{x_4}{x_5}-\frac{x_8}{x_9}\right)\epsilon\,\epsilon'^2 \\ \epsilon\,\epsilon' & 1+\epsilon^2+\epsilon'^2 & \epsilon\,\epsilon' \\ 2\,\epsilon^2\epsilon'+\left(\frac{x_4}{x_5}-\frac{x_8}{x_9}\right)\epsilon\,\epsilon'^2 & \epsilon\,\epsilon' & 1+\epsilon^2+\epsilon'^2 \end{pmatrix}. \tag{1.34}$$

We find that the dominant structures of the matrices remain unaltered, the coefficients receiving only small corrections. In this case, the Yukawa rotation matrix U_ℓ gives rise to an $\mathcal{O}(\epsilon')$ correction to the 13 entry of the PMNS matrix, such that the model can reproduce the experimental magnitude of $\sin\theta_{13}^\ell$. This imposes $\epsilon' \sim 0.1$ while the value of ϵ is fixed by the Yukawa hierarchy. Note that the off diagonal entries in the soft mass matrices arise at order ϵ'^2.

The $\mathcal{O}(1)$ coefficients x_i are determined by the combined fit of the experimental values of $U_{\rm PMNS}$ [12] and the Yukawas at the GUT scale [13]. For $\tan\beta = 5$ and $(\epsilon, \epsilon') =$

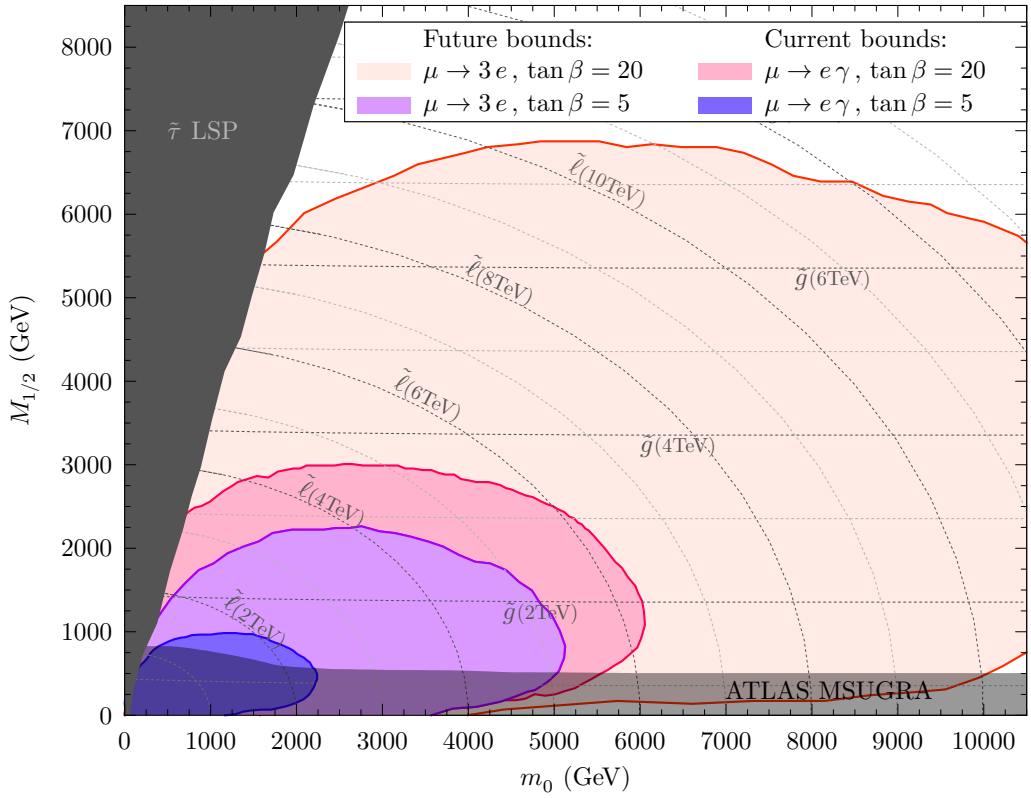

FIGURE 1.7: Excluded regions due to $\mu \to e\gamma$ and $\mu \to eee$ for two reference values: $\tan\beta = 5$ (blue shapes) and $\tan\beta = 20$ (red shapes). In the dark (blue and red) regions, we compare with current $\mu \to e\gamma$ bounds, while in the light (blue and red) regions we compare with the expected $\mu \to eee$ sensitivity in the near future. As before, these results are competitive with MSUGRA ATLAS limits (gray area).

$(0.04\,,\,0.08)$ we obtain: $(x_1 = 0.7,\, x_2 = 1.0,\, x_3 = -1.0,\, x_4 = 1.6,\, x_5 = 5.3,\, x_6 = 0.99,\, x_7 = 4.0,\, x_8 = 5.4,\, x_9 = 3.6)$; whereas for $\tan\beta = 20$ and $(\epsilon, \epsilon') = (0.02\,,\,0.06)$, $(x_1 = 1.3,\, x_2 = 1.0,\, x_3 = 0.99,\, x_4 = 1.8,\, x_5 = 5.3,\, x_6 = 0.99,\, x_7 = 4.4,\, x_8 = 0.81,\, x_9 = 1.8)$.

After RGE evolving the matrices to the SUSY scale with SPheno, checking the charge and color breaking relations, and calculating the low-energy observables, the constraints on the model are shown in Fig. 1.7 for $\tan\beta = 5$, blue (dark) region, and $\tan\beta = 20$, red (light) region. As expected, the most restrictive constraints come from the flavor violating decays $\mu \to e\gamma$ and $\mu \to 3\,e$. Current limits of the first process are competitive with present ATLAS bounds whereas future limits for $\mu \to eee$ will allow us to either discover SUSY or to constraint a considerable part of the parameter space if no signal is measured.

Field	ν_2^c	ν_1^c	e_2^c	e_1^c	L_2	L_1	$H_{u,d}$	ϕ	χ	ξ	χ'	$\chi'^\dagger$
S_3	**2**	$\mathbf{1}'$	**2**	**1**	**2**	**1**	**1**	**2**	**1**	**2**	$\mathbf{1}'$	$\mathbf{1}'$
Z_6	ω	ω	ω^3	ω^3	ω^5	1	1	ω^4	ω^4	ω^4	ω^5	ω^{-5}
Z_3	1	1	ω^2	ω	1	1	1	ω	ω	1	1	1
$U(1)_R$	1	1	1	1	1	1	0	0	0	0	0	0

TABLE 1.3: Transformation of the matter superfields under the S_3 family symmetry.

In contrast with the previous example, no cancellation is observed here. This is because, in this model, the dominant effect comes from the LL mass insertion and, therefore, the two tan β-enhanced terms have the same sign. A detailed discussion of these effects can be found in [20]. We see that present and future LFV constraints are able to explore large values of m_0 and $M_{1/2}$ in these models, well beyond the LHC reach.

1.5 An S_3 Model

Finally, another interesting and minimal group of models are those based on the symmetry group S_3 [64–71] defined as the group of all possible permutations among 3 objects, containing only 6 group elements. The number of irreducible representations is 3, which includes two singlets, $\{\mathbf{1}, \mathbf{1}'\}$, and a doublet, **2**. The detailed description of the group can be found in Appendix B.2. The example that we consider here is the model of D. Meloni in Ref.[72], which generates a PMNS LO-structure compatible with the TB-mixing together with a relatively large reactor angle and a good description of the quark sector. The full flavor symmetry of the model is $\mathcal{G}_f = S_3 \times \mathbb{Z}_6 \times \mathbb{Z}_3$ with and additional $U(1)_R$ continuous symmetry which will eventually break down to R-parity due to small SUSY breaking effects. Table 1.3 shows the complete spectrum for this model. As can be seen, the $SU(2)_L$ doublets and singlets of the second and third generations are arranged in two S_3 doublets, L and e^c:

$$L_2 = \begin{pmatrix} \tau \\ \mu \end{pmatrix} \quad , \quad e_2^c = \begin{pmatrix} \mu^c \\ \tau^c \end{pmatrix} , \tag{1.35}$$

whereas the electron fields are assigned to the real singlets, L_1 and e_1^c. The electron and muon Majorana neutrinos are grouped in a doublet, ν_2^c, while the tau right-handed neutrino transforms as the pseudosinglet representation, ν_1^c.

The minimization of the driving superpotential in the exact SUSY limit generates the desired alignment for the vacuum structure [72]:

$$\langle \phi \rangle \propto v_\phi \begin{pmatrix} 1 \\ 1 \end{pmatrix} \quad , \quad \langle \xi \rangle \propto v_\xi \begin{pmatrix} \delta \hat{v}_\xi \\ 1 \end{pmatrix} ,$$
$$\langle \chi \rangle \propto v_\chi \quad , \quad \langle \chi' \rangle \propto v'_\chi , \tag{1.36}$$

where $\delta \hat{v}_\xi = \delta v_\xi / M$, $v_\phi / M \sim v_\chi / M \sim \epsilon$ and $v_\xi / M \sim v_{\chi'} / M \sim \delta v_\xi / M \sim \epsilon'$.
At LO, only the muon and tau masses are generated by operators involving one and two flavon insertions while the electron remains massless. To obtain its mass, operators with up to 5-flavon insertions must be considered. The dominant terms are given by the following contributions:

$$\begin{aligned} W_e &= \frac{1}{M} \left[(e_2^c L_2 \, \phi) \; + \; (e_2^c L_2) \, \chi \right] H_d \\ &+ \frac{1}{M^2} \, (e_2^c L_2 \phi)' \, \chi' \, H_d \\ &+ \frac{1}{M^4} \, e_1^c \left[(L_2 \, \xi^2) \chi^2 \; + \; (L_2 \, \phi \xi^2) \chi \; + \; (L_2 \, \phi^2 \xi^2) \right] H_d \\ &+ \frac{1}{M^5} \, e_1^c L_1 \left[(\phi \, \xi^2)' \chi' \chi \; + \; (\phi^2 \xi^2)' \chi' \right] H_d \end{aligned} \tag{1.37}$$

In the vacuum alignment configuration, Eqs. (1.36) and (1.36), the resulting effective Yukawa and Trilinear matrices are:

$$Y^e \sim \begin{pmatrix} x_1 \, \epsilon^2 \, \epsilon'^3 & x_2 \, \epsilon \, \epsilon' & -x_2 \, \epsilon \, \epsilon' \\ x_3 \, \epsilon^2 \, \epsilon'^2 & x_4 \, \epsilon & x_5 \, \epsilon \\ x_6 \, \epsilon^2 \, \epsilon'^2 & x_5 \, \epsilon & x_4 \, \epsilon \end{pmatrix} , \; a_e \sim A_0 \begin{pmatrix} 11 \, x_1 \, \epsilon^2 \, \epsilon'^3 & 5 \, x_2 \, \epsilon \, \epsilon' & -5 \, x_2 \, \epsilon \, \epsilon' \\ 9 \, x_3 \, \epsilon^2 \, \epsilon'^2 & 3 \, x_4 \, \epsilon & 3 \, x_5 \, \epsilon \\ 9 \, x_6 \, \epsilon^2 \, \epsilon'^2 & 3 \, x_5 \, \epsilon & 3 \, x_4 \, \epsilon \end{pmatrix} , \tag{1.38}$$

where the proportionality factor between each Yukawa and Trilinear term is given again by Eq. (1.2), with N equal to the total power of ϵ and ϵ'.
The LO contributions in the Kähler potential for LH- and RH-fields are given by:

$$\begin{aligned} K_L &= L_2 L_2^\dagger \; + \; L_1 L_1^\dagger \; + \; \frac{1}{M^2} \left[\left(L_2 L_2^\dagger \phi \phi^\dagger \right) \; + \; \left(L_2 L_2^\dagger \phi \right) \chi^\dagger \; + \; \chi' \left(L_2 \, \xi^\dagger \right)' L_1^\dagger \; + \text{h.c.} \right] , \\ K_R &= e_2^c e_2^{c\dagger} \; + \; e_1^c e_1^{c\dagger} \; + \; \frac{1}{M^2} \left[\left(e_2^c e_2^{c\dagger} \phi \phi^\dagger \right) \; + \; \left(e_2^c e_2^{c\dagger} \phi \right) \chi^\dagger \; + \; \left(e_2^c \xi \phi^\dagger \right) e_1^{c\dagger} \; + \text{h.c.} \right] . \end{aligned} \tag{1.39}$$

Once the flavor symmetry is broken, the Kähler metric and soft-mass matrices can be written in terms of $C_{L(R)}$ and $B_{L(R)}$ as in Eq. (1.20), with:

$$C_L \sim \begin{pmatrix} \epsilon^2+\epsilon'^2 & \epsilon'^2 & \epsilon^2\epsilon' \\ \epsilon'^2 & \epsilon^2+\epsilon'^2 & \epsilon^2 \\ \epsilon^2\epsilon' & \epsilon^2 & \epsilon^2+\epsilon'^2 \end{pmatrix}, \quad C_R \sim \begin{pmatrix} \epsilon^2+\epsilon'^2 & \epsilon\epsilon' & \epsilon\epsilon' \\ \epsilon\epsilon' & \epsilon^2+\epsilon'^2 & \epsilon^2 \\ \epsilon\epsilon' & \epsilon^2 & \epsilon^2+\epsilon'^2 \end{pmatrix}, \tag{1.40}$$

$$B_R \sim 2\begin{pmatrix} \epsilon^2+\epsilon'^2 & \epsilon'^2 & \frac{3}{2}\epsilon^2\epsilon' \\ \epsilon'^2 & \epsilon^2+\epsilon'^2 & \epsilon^2 \\ \frac{3}{2}\epsilon^2\epsilon' & \epsilon^2 & \epsilon^2+\epsilon'^2 \end{pmatrix}, \quad B_R \sim 2\begin{pmatrix} \epsilon^2+\epsilon'^2 & \epsilon\epsilon' & \epsilon\epsilon' \\ \epsilon\epsilon' & \epsilon^2+\epsilon'^2 & \epsilon^2 \\ \epsilon\epsilon' & \epsilon^2 & \epsilon^2+\epsilon'^2 \end{pmatrix}. \tag{1.41}$$

After canonical normalization and diagonalization of the Yukawa matrices, the soft terms in the mass basis are:

$$a_e \;\to\; A_0 \begin{pmatrix} 11\,x_1\,\epsilon^2\epsilon'^3 & \left(-\frac{5}{\sqrt{2}}x_2+\frac{3\sqrt{2}x_2x_5}{x_4+x_5}\right)\epsilon^3\epsilon' & -2\sqrt{2}\,x_2\,\epsilon^3\epsilon' \\ \frac{9}{\sqrt{2}}(x_6+x_3)\,\epsilon^2\epsilon'^2 & 3\,(x_5-x_4)\epsilon & -3\,x_5\,\epsilon^3 \\ \frac{9}{\sqrt{2}}(x_6-x_3)\,\epsilon^2\epsilon'^2 & -3\,x_5\,\epsilon^3 & -3\,(x_5+x_4)\epsilon \end{pmatrix},$$

$$\widetilde{m}_L^2 \;\to\; m_0^2 \begin{pmatrix} 1+\epsilon^2+\epsilon'^2 & \frac{1}{\sqrt{2}}\epsilon'^2 & -\frac{1}{\sqrt{2}}\epsilon'^2 \\ \frac{1}{\sqrt{2}}\epsilon'^2 & 1+2\,\epsilon^2+\epsilon'^2 & 3\,\epsilon^2\epsilon'^2 \\ -\frac{1}{\sqrt{2}}\epsilon'^2 & 3\,\epsilon^2\epsilon'^2 & 1+\epsilon'^2 \end{pmatrix}, \tag{1.42}$$

$$\widetilde{m}_{R,e}^2 \;\to\; m_0^2 \begin{pmatrix} 1+\epsilon^2+\epsilon'^2 & \sqrt{2}\,\epsilon\,\epsilon' & \mathcal{O}(\epsilon^3\epsilon'^3) \\ \sqrt{2}\,\epsilon\,\epsilon' & 1+2\,\epsilon^2+\epsilon'^2 & \mathcal{O}(\epsilon^4\epsilon'^2) \\ \mathcal{O}(\epsilon^3\epsilon'^3) & \mathcal{O}(\epsilon^4\epsilon'^2) & 1+\epsilon'^2 \end{pmatrix}. \tag{1.43}$$

The $\mathcal{O}(1)$ coefficients x_i are set so that the experimental values for $U_{\rm PMNS}$ [12] and the Yukawa couplings at the GUT scale [13] are reproduced. Both for $\tan\beta = 5$ with

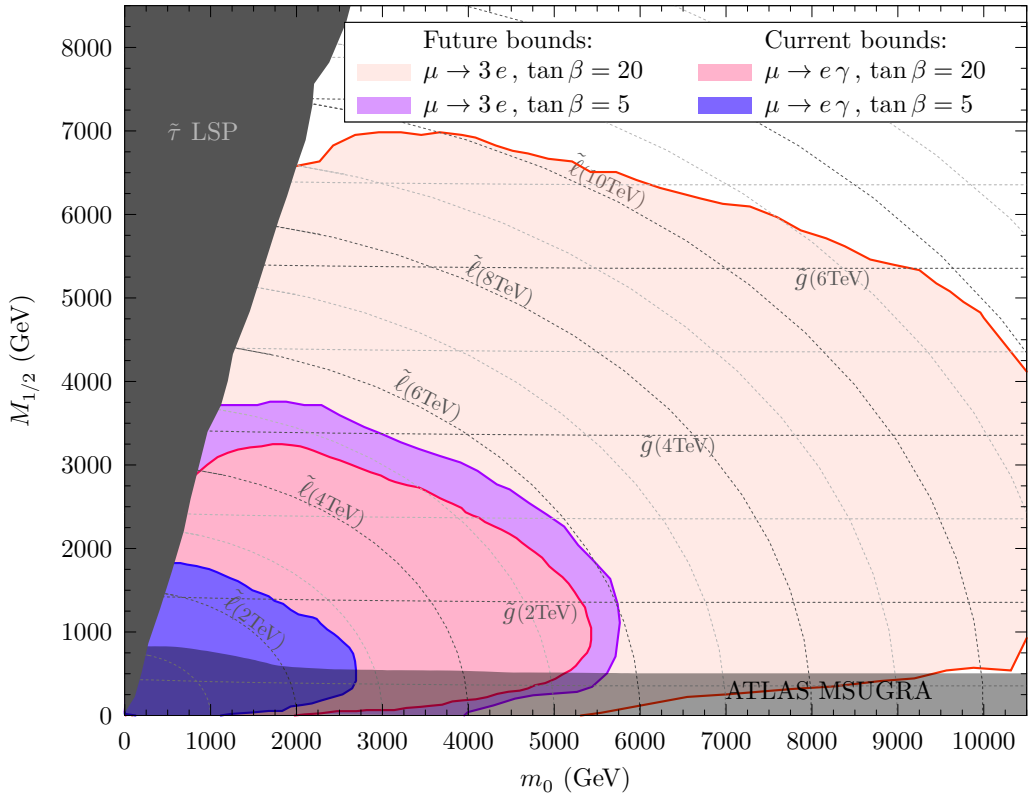

FIGURE 1.8: Excluded regions due to $\mu \to e\gamma$ and $\mu \to eee$ for two reference values: $\tan\beta = 5$ (blue shapes) and $\tan\beta = 20$ (red shapes). In the dark (blue and red) regions, we compare with current $\mu \to e\gamma$ bounds while in the light (blue and red) regions we compare with the expected $\mu \to eee$ sensitivity in the near future.

$(\epsilon\,,\,\epsilon') = (0.08\,,\,0.08)$, and $\tan\beta = 20$ with $(\epsilon\,,\,\epsilon') = (0.1, 0.08)$ we obtain almost the same coefficients, that is ($x_1 = 3.$, $x_2 = 1.6$, $x_3 = 2.3$, $x_4 = 0.6$, $x_6 = 2.2$).

The allowed parameter space for this model is given in Fig. 1.8 for $\tan\beta = 5$, blue (dark) areas, and $\tan\beta = 20$, red (light) areas. Although we check all the low energy observables in Table I.6, we once again find the most constraining processes to be $\mu \to e\gamma$ and $\mu \to 3\,e$. As can be seen in the figure, for low values of $\tan\beta$ this model seems to be slightly more constrained than A_4 whereas, for $\tan\beta = 20$, the limits are practically the same. As in the A_4 case, the dominant contributions to these processes come from the LL sector and therefore an analogous description holds here: the LL leading terms, $\tan\beta$-enhanced, are those corresponding to contributions with an internal chirality flip and no cancellation among these terms occurs, since no relative sign from the hypercharge is present.

1.6 Conclusions

In this work, building on the methods of [4], we continue to analyze the flavor structures in supersymmetric theories where the MSSM arises as a low energy effective theory from a flavor symmetry broken at higher scales. For a specific class of predictive models, if the scale of mediation of Supersymmetry breaking is above the flavor symmetry scale, the resulting flavor structures in the soft-breaking terms are not universal and can give rise to flavor changing effects at low energies.
We have applied these ideas to three representative discrete flavor symmetry models, A_4,S_3, and $\Delta(27)$, able to explain the neutrino and charged lepton structures. In these models, we have been able to obtain the full trilinear couplings and the soft mass matrices and we have applied the constraints from the non-observation of lepton flavor violating processes, like $\mu \to e\gamma$ and $\mu \to 3\,e$. We saw that different models may be distinguished through the different predicted structures in the trilinear terms or soft mass matrices. We have shown that, at present, these constraints are already competitive with direct LHC searches. Future bounds on these observables may discover SUSY with masses far beyond the reach of the LHC high-luminosity upgrade.
In conclusion, flavor symmetries in a supersymmetric context give rise generically to non-universal soft-breaking terms. This non-universality and the resulting flavor-changing effects must be always taken into account when restricting the allowed parameter space in these models. Moreover, the power of flavor changing observables to signal the presence of supersymmetry at higher scales has been explicitly demonstrated in these calculable models. We hope to continue to extend these results to unified models with symmetries that describe both the quark and lepton sectors in a future work.

References

[1] S. L. Glashow et al., *Phys. Rev.* **1970**, *D2*, 1285–1292.

[2] K. S. Babu in Proceedings of Theoretical Advanced Study Institute in Elementary Particle Physics on The dawn of the LHC era (TASI 2008), **2010**, pp. 49–123, arXiv: 0910.2948 [hep-ph].

[3] G. Altarelli, F. Feruglio, *Rev. Mod. Phys.* **2010**, *82*, 2701–2729, arXiv: 1002.0211 [hep-ph].

[4] D. Das et al., *Phys. Rev.* **2017**, *D95*, 035001, arXiv: 1607.06827 [hep-ph].

[5] L. Calibbi et al., *JHEP* **2012**, *06*, 018, arXiv: 1203.1489 [hep-ph].

[6] S. Antusch et al., *Nucl. Phys.* **2011**, *B852*, 108–148, arXiv: 1104.3040 [hep-ph].

[7] S. F. King et al., *JHEP* **2005**, *07*, 049, arXiv: hep-ph/0407012 [hep-ph].

[8] J. A. Casas, S. Dimopoulos, *Phys. Lett.* **1996**, *B387*, 107–112, arXiv: hep-ph/9606237 [hep-ph].

[9] I. de Medeiros Varzielas et al., *Phys. Lett.* **2007**, *B648*, 201–206, arXiv: hep-ph/0607045 [hep-ph].

[10] I. de Medeiros Varzielas, G. G. Ross, *Nucl. Phys.* **2006**, *B733*, 31–47, arXiv: hep-ph/0507176 [hep-ph].

[11] I. de Medeiros Varzielas et al., **2017**, arXiv: 1710.01741 [hep-ph].

[12] C. Patrignani et al., *Chin. Phys.* **2016**, *C40*, 100001.

[13] S. Antusch, V. Maurer, *JHEP* **2013**, *11*, 115, arXiv: 1306.6879 [hep-ph].

[14] W. Porod, F. Staub, *Comput. Phys. Commun.* **2012**, *183*, 2458–2469, arXiv: 1104.1573 [hep-ph].

[15] W. Porod, *Comput. Phys. Commun.* **2003**, *153*, 275–315, arXiv: hep-ph/0301101 [hep-ph].

[16] L. J. Hall et al., *Nucl. Phys.* **1986**, *B267*, 415–432.

[17] F. Gabbiani, A. Masiero, *Nucl. Phys.* **1989**, *B322*, 235–254.

[18] F. Gabbiani et al., *Nucl. Phys.* **1996**, *B477*, 321–352, eprint: hep-ph/9604387.

[19] P. Paradisi, *JHEP* **2005**, *10*, 006, arXiv: hep-ph/0505046 [hep-ph].

[20] M. Ciuchini et al., *Nucl. Phys.* **2007**, *B783*, 112–142, arXiv: hep-ph/0702144 [HEP-PH].

[21] L. Calibbi et al., *Phys. Rev.* **2008**, *D78*, 075007, arXiv: 0804.4620 [hep-ph].

[22] L. Calibbi et al., *Nucl. Phys.* **2010**, *B831*, 26–71, arXiv: 0907.4069 [hep-ph].

[23] G. Altarelli, F. Feruglio, *Nucl. Phys.* **2006**, *B741*, 215–235, arXiv: hep-ph/0512103 [hep-ph].

[24] G. Altarelli, D. Meloni, *J. Phys.* **2009**, *G36*, 085005, arXiv: 0905.0620 [hep-ph].

[25] G. Altarelli, F. Feruglio, *Nucl. Phys.* **2005**, *B720*, 64–88, arXiv: hep-ph/0504165 [hep-ph].

[26] E. Ma, G. Rajasekaran, *Phys. Rev.* **2001**, *D64*, 113012, arXiv: hep-ph/0106291 [hep-ph].

[27] K. S. Babu et al., *Phys. Lett.* **2003**, *B552*, 207–213, arXiv: hep-ph/0206292 [hep-ph].

[28] E. Ma, *Phys. Rev.* **2004**, *D70*, 031901, arXiv: hep-ph/0404199 [hep-ph].

[29] X.-G. He et al., *JHEP* **2006**, *04*, 039, arXiv: hep-ph/0601001 [hep-ph].

[30] K. S. Babu, X.-G. He, **2005**, arXiv: hep-ph/0507217 [hep-ph].

[31] A. Zee, *Phys. Lett.* **2005**, *B630*, 58–67, arXiv: hep-ph/0508278 [hep-ph].

[32] E. Ma, *Phys. Rev.* **2006**, *D73*, 057304, arXiv: hep-ph/0511133 [hep-ph].

[33] S. F. King, M. Malinsky, *Phys. Lett.* **2007**, *B645*, 351–357, arXiv: hep-ph/0610250 [hep-ph].

[34] G. Altarelli et al., *Nucl. Phys.* **2007**, *B775*, 31–44, arXiv: hep-ph/0610165 [hep-ph].

[35] M. Hirsch et al., *Phys. Rev. Lett.* **2007**, *99*, 151802, arXiv: hep-ph/0703046 [HEP-PH].

[36] F. Bazzocchi et al., *JHEP* **2008**, *03*, 063, arXiv: 0707.3032 [hep-ph].

[37] M. Honda, M. Tanimoto, *Prog. Theor. Phys.* **2008**, *119*, 583–598, arXiv: 0801.0181 [hep-ph].

[38] F. Bazzocchi et al., *J. Phys.* **2009**, *G36*, 015002, arXiv: 0802.1693 [hep-ph].

[39] M. Hirsch et al., *Phys. Rev.* **2008**, *D78*, 093007, arXiv: 0804.1521 [hep-ph].

[40] Y. Lin, *Nucl. Phys.* **2009**, *B813*, 91–105, arXiv: 0804.2867 [hep-ph].

[41] C. Csaki et al., *JHEP* **2008**, *10*, 055, arXiv: 0806.0356 [hep-ph].

[42] F. Feruglio et al., *Nucl. Phys.* **2009**, *B809*, 218–243, arXiv: 0807.3160 [hep-ph].

[43] S. Morisi et al., *Phys. Rev.* **2007**, *D75*, 075015, arXiv: hep-ph/0702034 [hep-ph].

[44] M. Hirsch et al., *Phys. Rev.* **2005**, *D72*, [Erratum: Phys. Rev.D72,119904(2005)], 091301, arXiv: hep-ph/0507148 [hep-ph].

[45] M. Hirsch et al., *Phys. Rev.* **2004**, *D69*, 093006, arXiv: hep-ph/0312265 [hep-ph].

[46] M.-C. Chen, S. F. King, *JHEP* **2009**, *06*, 072, arXiv: 0903.0125 [hep-ph].

[47] M. Hirsch et al., **2003**, [PoSAHEP2003,010(2003)], AHEP2003/010, arXiv: hep-ph/0312244 [hep-ph].

[48] Y. Abe et al., *JHEP* **2014**, *10*, [Erratum: JHEP02,074(2015)], 086, arXiv: 1406.7763 [hep-ex].

[49] F. P. An et al., *Phys. Rev. Lett.* **2015**, *115*, 111802, arXiv: 1505.03456 [hep-ex].

[50] J. H. Choi et al., *Phys. Rev. Lett.* **2016**, *116*, 211801, arXiv: 1511.05849 [hep-ex].

[51] Y. Lin, *Nucl. Phys.* **2010**, *B824*, 95–110, arXiv: 0905.3534 [hep-ph].

[52] I. K. Cooper et al., *JHEP* **2012**, *06*, 130, arXiv: 1203.1324 [hep-ph].

[53] D. Hernandez, A. Y. Smirnov, *Phys. Rev.* **2012**, *D86*, 053014, arXiv: 1204.0445 [hep-ph].

[54] S. F. King, C. Luhn, *JHEP* **2011**, *09*, 042, arXiv: 1107.5332 [hep-ph].

[55] Y.-j. Zheng, B.-Q. Ma, *Eur. Phys. J. Plus* **2012**, *127*, 7, arXiv: 1106.4040 [hep-ph].

[56] E. Ma, D. Wegman, *Phys. Rev. Lett.* **2011**, *107*, 061803, arXiv: 1106.4269 [hep-ph].

[57] W. Rodejohann et al., *Nucl. Phys.* **2012**, *B855*, 592–607, arXiv: 1107.3970 [hep-ph].

[58] Y. H. Ahn et al., *Phys. Rev.* **2011**, *D84*, 113007, arXiv: 1107.4549 [hep-ph].

[59] S. Kumar, *Phys. Rev.* **2011**, *D84*, 077301, arXiv: 1108.2137 [hep-ph].

[60] S. Gupta et al., *Phys. Rev.* **2012**, *D85*, 031903, arXiv: 1112.6113 [hep-ph].

[61] G. C. Branco et al., *Phys. Rev.* **2012**, *D86*, 076008, arXiv: 1203.2646 [hep-ph].

[62] Y. H. Ahn, S. K. Kang, *Phys. Rev.* **2012**, *D86*, 093003, arXiv: 1203.4185 [hep-ph].

[63] G. Altarelli et al., *JHEP* **2008**, *03*, 052, arXiv: 0802.0090 [hep-ph].

[64] N. Haba, K. Yoshioka, *Nucl. Phys.* **2006**, *B739*, 254–284, arXiv: hep-ph/0511108 [hep-ph].

[65] S. Morisi, M. Picariello, *Int. J. Theor. Phys.* **2006**, *45*, 1267–1277, arXiv: hep-ph/0505113 [hep-ph].

[66] S.-L. Chen et al., *Phys. Rev.* **2004**, *D70*, [Erratum: Phys. Rev.D70,079905(2004)], 073008, arXiv: hep-ph/0404084 [hep-ph].

[67] Z.-z. Xing et al., *Phys. Lett.* **2010**, *B690*, 304–310, arXiv: 1004.4234 [hep-ph].

[68] W. Grimus, L. Lavoura, *JHEP* **2005**, *08*, 013, arXiv: hep-ph/0504153 [hep-ph].

[69] R. N. Mohapatra et al., *Phys. Lett.* **2006**, *B639*, 318–321, arXiv: hep-ph/0605020 [hep-ph].

[70] F. Feruglio, Y. Lin, *Nucl. Phys.* **2008**, *B800*, 77–93, arXiv: 0712.1528 [hep-ph].

[71] E. Ma, *Phys. Rev.* **1991**, *D44*, 587–589.

[72] D. Meloni, *JHEP* **2012**, *05*, 124, arXiv: 1203.3126 [hep-ph].

Article 2

Controlled flavor violation in the MSSM from a unified $\Delta(27)$ flavor symmetry

JHEP 09 (2018) 047

Ivo de Medeiros Varzielas[a] **, M. Luisa López-Ibáñez**[b,c] **, Aurora Melis**[c] **, Oscar Vives**[c]

[a] *CFTP, Departamento de Física, Instituto Superior Técnico, Universidade de Lisboa Avenida Rovisco Pais 1, 1049 Lisboa, Portugal*

[b] *Departament de Física Tèorica, Universitat de València and IFIC, Universitat de València-CSIC, Dr. Moliner 50, E-46100 Burjassot (València), Spain*

[c] *Dip. di Matematica e Fisica, Università di Roma Tre and INFN, Sezione di Roma III, Via della Vasca Navale 84, 00146 Rome, Italy*

ABSTRACT: We study the phenomenology of a unified supersymmetric theory with a flavor symmetry $\Delta(27)$. The model accommodates quark and lepton masses, mixing angles and CP phases. In this model, the Dirac and Majorana mass matrices have a unified texture zero structure in the $(1,1)$ entry that leads to the Gatto-Sartori-Tonin relation between the Cabibbo angle and ratios of the masses in the quark sectors, and to a natural departure from zero of the θ_{13}^{ℓ} angle in the lepton sector. We derive the flavor structures of the trilinears and soft mass matrices, and show their general non-universality. This causes large flavor violating effects. As a consequence, the parameter space for this model is constrained, allowing it to be (dis)proven by flavor violation searches in the next decade. Although the results are model specific, we compare them to previous studies to show similar flavour effects (and associated constraints) are expected in general in supersymmetric flavor models, and may be used to distinguish them.

2.1 Introduction

Using symmetries to interpret the chaotic picture of flavor parameters in the SM is a well-known and developed strategy. Nevertheless, a univocal picture has not emerged, driving to a plethora of viable choices for the flavor symmetry $\mathcal{G}_f$ and for its breaking, which are consistent with the observed fermionic masses and mixig angles. Likely, the only possibility to disentangle the puzzle of the origin of flavor is to discover flavor-sensitive New Physics (NP). Supersymmetric extensions of the Standard Model (SM) give a good example in this sense, where in addition to the usual Yukawa couplings of the SM we have the soft breaking terms: the trilinears and soft-mass matrices corresponding to the scalar superpartners. Under the requirement that the mediation of Supersymmetry breaking to the visible sector occurs at a higher scale Λ_{Med} than the breaking of the flavor symmetry Λ_f, i.e. $\Lambda_{\text{Med}} \gg \Lambda_f$, these three flavor structures will have to respect the same $\mathcal{G}_f$ and, after the breaking of the symmetry, be similarly non-trivial. In [1, 2] we investigated the case where Supersymmetry breaking is communicated through a spurion field, X, coupling universally to the visible sector, and showed that we can expect a mismatch between the Yukawa, Kinetic matrices, and the soft-breaking terms, that prevents the simultaneous diagonalization of the four structures. The mismatch is simply given by the different ways in which the X-field may be inserted in the full theory diagrams and its calculation is straightforward in terms of the operator dimension of the terms entering in the Superpotential and Kähler potential.

In this work, we have applied this type of analysis to a recent model with a unified texture zero structure in the $(1,1)$ entry [3]. This is an appealing flavor model as it is consistent with an underlying $SO(10)$ grand unification and makes several important postdictions, for example the Gatto-Sartori-Tonin relation in Sec.I.2.1 between the Cabibbo angle and the quark mass ratios. Additionally it predicts the phenomenologically successful trimaximal 1 mixing scheme for the leptons [4, 5]. Nevertheless, it is important to find additional ways to constrain this and other flavor models, in order to better distinguish between models which, by necessity of the experimentally observed values, make similar postdictions for the fermion masses and mixing angles. Flavor violating (FV) effects associated with new particles and interactions provide one of the best options for constraining flavor models, and this applies in particular to supersymmetric flavor models.

The layout of the paper is as follows. In Sec.2.2, we review some relevant details about the model. In Sec.2.3, we present the analysis of FV processes, showing the exclusion regions that constrain the parameter space of the model. We conclude in Sec.2.4.

Field	$\psi_{q,e,\nu}$	$\psi^c_{q,e,\nu}$	H_5	Σ	S	ϕ_3	ϕ_{23}	ϕ_{123}	ϕ	ϕ_X
$\Delta(27)$	**3**	**3**	$\mathbf{1_{00}}$	$\mathbf{1_{00}}$	$\mathbf{1_{00}}$	$\bar{\mathbf{3}}$	$\bar{\mathbf{3}}$	$\bar{\mathbf{3}}$	$\bar{\mathbf{3}}$	**3**
Z_N	0	0	0	2	-1	0	-1	2	0	x

TABLE 2.1: Transformation of the matter superfields under the $\Delta(27)$ flavor symmetry.

2.2 A $\Delta(27)$ model for quarks and leptons

$\Delta(27)$, a finite subgroup of $SU(3)$, has been extensively studied as a flavor symmetry in GUT models, due to it being one of the smallest finite groups with triplet and anti-triplet irreducible representations. In addition to the first work using the group as a flavor symmetry, [6] (considered in [2]), and the model we consider here [3], $\Delta(27)$ has been used in unified models [7–12].

The models in [6, 7] are excluded by the measured value of θ^ℓ_{13}. The main differences between [6, 7, 9, 10] and [3] are most visible in the neutrino sector of the respective models, which do not significantly affect the FV constraints we consider here. Even though the models generically share similar charged fermion mass structures arising from specific VEV directions (in particular, the $(1,1,1)$ direction as a flavor symmetry breaking VEV), the subtle differences in the vacuum alignment of the respective models are relevant, as they can significantly alter the FV constraints.

We now review the relevant details of the model in Ref.[3], where the interested reader can find a more complete description. Although the model is compatible with an underlying $SO(10)$ grand unification, we present the matter superfields as separate Left (LH), ψ, and Right-Handed conjugate (RH), ψ^c, fermions. The flavon fields, ϕ_i, are singlets under the SM group and charged under the flavor symmetry. The model includes a Georgi-Jarlskog field Σ, associated to the breaking of the GUT symmetry, distinguishing down-quark and charged-lepton Yukawas, and a flavor singlet S, needed to preserve the texture zero in the neutrino Majorana matrix [3]. The field content in Table 4.1 give rise to the following superpotential, which leads to the lepton and quarks Yukawas

$$
\begin{aligned}
W &= \frac{1}{M^2}(\psi\,\phi_3)(\psi^c\,\phi_3)\,H_5 + \frac{1}{M^3}(\psi\,\phi_{23})(\psi^c\,\phi_{23})\,\Sigma\,H_5 && (2.1)\\
&+ \frac{1}{M^3}(\psi\,\phi_{23})(\psi^c\,\phi_{123})\,S\,H_5 + \frac{1}{M^3}(\psi\,\phi_{123})(\psi^c\phi_{23})\,S\,H_5 && (2.2)\\
&+ \frac{1}{M^4}(\psi\,\phi_{23})(\psi^c\,\phi_3)\,\Sigma\,S\,H_5 + \frac{1}{M^4}(\psi\,\phi_3)(\psi^c\phi_{23})\,\Sigma\,S\,H_5 && (2.3)\\
&+ \frac{1}{M^4}(\psi\,\phi_3)(\psi^c\,\phi_{123})\,S^2\,H_5 + \frac{1}{M^4}(\psi\,\phi_{123})(\psi^c\phi_3)\,S^2\,H_5\,, && (2.4)
\end{aligned}
$$

and where the last 2 lines, Eqs. (2.3) and (2.4), are comparatively suppressed and do not change the entries (12 and 21) in the matrices that are most relevant for FV bounds, so we have neglected them.
The analysis and minimization of the flavon potential carried out in Appendix A of [3] aligns the VEVs of the flavons in the directions

$$\langle \phi_3 \rangle \propto \begin{pmatrix} 0 \\ 0 \\ 1 \end{pmatrix} \quad , \quad \langle \phi_{23} \rangle \propto \frac{1}{\sqrt{2}} \begin{pmatrix} 0 \\ 1 \\ 1 \end{pmatrix} \quad , \quad \langle \phi_{123} \rangle \propto \frac{1}{\sqrt{3}} \begin{pmatrix} 1 \\ 1 \\ 1 \end{pmatrix} ,$$

written up to relative phases. The VEV of the ϕ_3 flavon is directly related to the third-generation of Dirac-fermions masses $y_3 = \{y_\tau, y_t, y_b\}$ such that $\langle \phi_3 \rangle^2 / M_a^2 \equiv y_{3,a}$ with $a = e, u, d$. The relation between the VEVs and the parameter expansion ϵ_a is determined by requiring a hierarchical Yukawa structure in which the 23 block is dominant with respect to the 12 block

$$\frac{\langle \phi_{23} \rangle^2 \langle \Sigma \rangle}{M^3_{23,a}} \frac{M^2_{3,a}}{\langle \phi_3 \rangle^2} \propto e^{i\,\delta_a}\, r_a\, \epsilon_a^2 \quad , \quad \frac{\langle \phi_{23} \rangle \langle \phi_{123} \rangle \langle S \rangle}{M^3_{123,a}} \frac{M^2_{3,a}}{\langle \phi_3 \rangle^2} \propto e^{i\,\gamma_a} \epsilon_a^3 ,$$

where δ_a, γ_a are phases that appear in the mass matrices and that arise by combining the phases of the various VEVs and coefficients that contribute to the respective entries. The resulting mass matrices are complex and the model is able to reproduce the measured CP-phase in the quark sector and additionally predicts a value for the leptonic CP-phase.
Given that $\langle \Sigma \rangle / M_a = r_a$, with $r_d = r_u = 1/3$ and $r_e = -1$, the first condition tells us that $\langle \phi_{23} \rangle / M_a = \sqrt{y_{3,a}}\, e^{i\,\delta_a/2}\, \epsilon_a$. On the other hand, the second relation only tells us that $\langle \phi_{123} \rangle \langle S \rangle / M_a^2 \sim \epsilon_a^2$ leaving some freedom in the VEV assignment and, to be general, we write $\langle \phi_{123} \rangle / M_a = \sqrt{y_{3,a}}\, e^{i\,(\gamma_a - \delta_a/2)}\, \epsilon_a^\alpha$ and $\langle S \rangle / M_a = \epsilon_a^{2-\alpha}$ with $\alpha \in [0, 1]$.
Given the above considerations, at LO the resulting Yukawa is written as

$$Y^a = y_{3,a} \begin{pmatrix} 0 & x_{1,a}\, e^{i\,\gamma_a}\, \epsilon_a^3 & x_{1,a}\, e^{i\,\gamma_a}\, \epsilon_a^3 \\ x_{1,a}\, e^{i\,\gamma_a}\, \epsilon_a^3 & x_{2,a}\, r_a\, e^{i\delta_a}\, \epsilon_a^2 & x_{2,a}\, r_a\, e^{i\delta_a}\, \epsilon_a^2 \\ x_{1,a}\, e^{i\,\gamma_a}\, \epsilon_a^3 & x_{2,a}\, r_a\, e^{i\delta_a}\, \epsilon_a^2 & 1 \end{pmatrix} , \tag{2.5}$$

independent of the value of α, which on the other hand is important in the soft mass terms. In fact, the present analysis has been carried out considering three reference values for $\alpha = \{0, 1/2, 1\}$. However, the minimization of the flavon potential, which

Param.	$\epsilon_{e,d}$	$(x_1, x_2)_{e,d}$	$(\gamma, \delta)_{e,d}$	ϵ_u	$(x_1, x_2)_u$	$(\gamma, \delta)_u$
L.O.	0.15	(1.24 , 2.42)	(0.13 , 1.83)	0.05	(−1.12 , 3.60)	(0 , 0)
H.O.	0.15	(1.23 , 2.52)	(0 , 2)	0.05	(−1.12 , 3.30)	(0 , 0)

TABLE 2.2: Order-one parameters from the fit of fermionic masses and mixings in [3].

contemplates the case in which the self-coupling terms for the $\phi_{3,123}$ fields are dominant, facilitates large values of ϕ_{123}, and we stress that $\alpha \in [0, 1/2]$ is more consistent with this hypothesis.

It is clear that no operator in Eq.(2.1) can contribute to the (1,1) element, which gives the (1,1) texture zero in all mass matrices that characterizes this model (in contrast, several earlier models had the (1,1) texture zero but only in the mass matrices of the charged fermions [13], [6, 9]). As all fermions and additional flavons are triplets under the finite group, the Dirac masses of both the quarks and leptons share the same universal form, given by Eq.(2.5).

The different hierarchy in the up and down sectors requires two different expansion parameters, namely $\epsilon_u \sim \epsilon_d/3$. This cannot be achieved if the messengers χ are $SU(2)_L$ doublets coupling equally to $(u, d)_L$ so these messengers should be considered much heavier than their singlet counterparts. The singlet messengers in the up-sector can then be taken slightly heavier to accommodate the required difference. Beyond these differences, we consider each type of messenger to have universal masses, denoted M or M_a below, although we note that the messenger masses for each term can in general be different (denoted as $M_{3,a}$, $M_{23,a}$, $M_{123,a}$). In Ref. [3] a detailed numerical fit was performed considering both only leading order (L.O.) terms or including higher order (H.O.) corrections, and it was founf that the present measurements of the fermion masses and mixings in the lepton and quark sectors, can be accommodated. We summarize the results of this analysis in Table 4.2. In order to fit the model, the experimentally allowed ranges for the observables are evolved to the high scale (see [3] for details).

The L.O. fit was done without considering the terms with ΣS and S^2 in the last two lines of W in Eq.(2.1). It is a good fit to the observables, having a $\chi^2_{d.o.f} < 1$ [3], although the values of certain CKM elements are out of the expected ranges and the resulting θ^q_{23} mixing angle is slightly too low, as the L.O. prediction $\theta^q_{23_{L.O.}} = 0.0191$ is just outside of the 3σ range evolved up to the high scale, of $[0.0220, 0.0468]$.

The H.O. fit was done considering all the terms allowed by the symmetry, in particular the ΣS terms whose contribution is larger than the contribution from the S^2 terms. These ΣS terms contribute to the 23 and 32 entries of the Yukawa matrices,

therefore distinguishing these entries from the 13 and 31 entries. This additional freedom significantly improves the fit in the quark sector, particularly as $\theta^q_{23_{H.O.}} = 0.0313$, within the 3σ range.

2.3 Analysis of FV-effects

In this section we construct the structures of the soft-breaking terms under the flavor symmetry and derive the non-proportionality factors as explained in Sec. I.5.4 and 1.2. We show that performing the rotations to go to the standard basis, where the Kähler is the identity and the Yukawas are diagonal, does not diagonalize the obtained structures. Although the analysis has been carried out numerically, we display analytically the resulting matrices to emphasize the order of magnitude of the off-diagonal terms responsible for large Flavor Violating effects. In particular we concentrate on LFV processes, on which we have already very restrictive bounds meant to be significantly improved in the near future as shown in Table I.6 (for an updated review see Ref.[14] and for a recent discussion about experimental limiting factor in the search for $\mu \to e\gamma$ see Ref.[15]). In addition, taking into account the presence of flavor-dependent phases, we must also consider flavor changing CP violating processes in the quark sector, such as ε_K.

2.3.1 Soft breaking terms

The Yukawa and trilinears share the same overall texture but they will not be proportional [1, 2] due to the different numerical factors, in this case of 7, 7 and 5 appearing due to the multiple topologies possible for the respective trilinear terms:

$$a_a \;=\; A_0\, y_{3,a} \begin{pmatrix} 0 & 7\, x_{1,a}\, e^{i\,\gamma_a}\, \epsilon_a^3 & 7\, x_{1,a}\, e^{i\,\gamma_a}\, \epsilon_a^3 \\ 7\, x_{1,a}\, e^{i\,\gamma_a}\, \epsilon_a^3 & 7\, x_{2,a}\, r_a\, e^{i\delta_a}\, \epsilon_a^2 & 7\, x_{2,a}\, r_a\, e^{i\delta_a}\, \epsilon_a^2 \\ 7\, x_{1,a}\, \epsilon_a^3\, e^{i\,\gamma_a} & 7\, x_{2,a}\, r_a\, e^{i\delta_a}\, \epsilon_a^2 & 5 \end{pmatrix} . \tag{2.6}$$

As discussed in Sec. 2.2 we consider the messengers that are $SU(2)_L$ doublets to be much heavier than their singlet counterparts, so that RH messengers dominate the contributions (this is in agreement with the model [3]). Thus, while the off-diagonal corrections to the LH-Kähler potential are negligible, the RH corrections remain relevant:

$$
\begin{aligned}
K_R = \psi^c\psi^{c\dagger} \quad &+ \quad \frac{1}{M^2}\left[(\psi^c\phi_3)(\phi_3^\dagger\psi^{c\dagger}) \;+\; (\psi^c\phi_{23})(\phi_{23}^\dagger\psi^{c\dagger}) \;+\; (\psi^c\phi_{123})(\phi_{123}^\dagger\psi^{c\dagger})\right] \\
&+ \quad \frac{1}{M^3}\left[(\psi^c\phi_3)(\phi_{23}^\dagger\psi^{c\dagger})\, S \;+\; \text{h.c.}\right] \\
&+ \quad \frac{1}{M^3}\left[(\psi^c\phi_3)\,(\phi_{123}^\dagger\psi^{c\dagger})\,\Sigma \;+\; \text{h.c.}\right] \\
&+ \quad \frac{1}{M^4}\left[(\psi^c\phi_{23})\,(\phi_{123}^\dagger\psi^{c\dagger})\,\Sigma\, S^\dagger \;+\; \text{h.c.}\right] .
\end{aligned}
\tag{2.7}
$$

The last term is relatively suppressed and has not been included in the phenomenological analysis. Similar terms apply for the sfermion squared masses, but similar to what happens between the Yukawa couplings and the trilinears above, different prefactors appear due to multiple possible topologies. We have then the following structures

$$
K_{R,a} \;=\; \mathbb{1} + y_{3,a}\begin{pmatrix} \epsilon_a^{2\alpha} & \epsilon_a^{2\alpha} & e^{i(\gamma_a-\frac{\delta_a}{2})}\, r_a\, \epsilon_a^{\alpha} \;+\; \epsilon_a^{2\alpha} \\ \text{c.c.} & \epsilon_a^{2\alpha} & e^{i(\gamma_a-\frac{\delta_a}{2})}\, r_a\, \epsilon_a^{\alpha} \;+\; \epsilon_a^{2\alpha} \\ \text{c.c.} & \text{c.c.} & 1 \end{pmatrix} , \tag{2.8}
$$

$$
\widetilde{m}^2_{R,a} \;=\; m_0^2\,\mathbb{1} + m_0^2\, y_{3,a}\begin{pmatrix} 2\,\epsilon_a^{2\alpha} & 2\,\epsilon_a^{2\alpha} & 4\,e^{i(\gamma_a-\frac{\delta_a}{2})}\, r_a\, \epsilon_a^{\alpha} \,+ 2\,\epsilon_a^{2\alpha} \\ \text{c.c.} & 2\,\epsilon_a^{2\alpha} & 4\,e^{i(\gamma_a-\frac{\delta_a}{2})}\, r_a\, \epsilon_a^{\alpha} \,+ 2\,\epsilon_a^{2\alpha} \\ \text{c.c.} & \text{c.c.} & 1 \end{pmatrix} . \tag{2.9}
$$

Note that even if the 12 block appears to be simultaneously diagonalized here, the rescaling of the Kähler and the rotation to the mass basis, as detailed in Appendix A.1.3, will re-introduce the off-diagonal terms in the soft-mass matrices. After performing the transformations to the diagonal-Yukawa canonical basis, we obtain the following approximate form of the CKM

$$
V_{\text{CKM}} = \begin{pmatrix} 1 - \dfrac{x_{1,d}^2}{2\,r^{2_d}\,x_{2_d}^2}\epsilon_d^2 & \dfrac{x_{1,d}}{r_d\,x_{2,d}}\epsilon_d & x_{1,d}\,\epsilon_d^3 - e^{i\,(\gamma_d-\delta_d)}\dfrac{r_u\,x_{1,d}\,x_{2,u}}{r_d,\,x_{2,d}}\epsilon_d^2\,\epsilon_u \\ -\dfrac{x_{1,d}}{r_d\,x_{2,d}}\epsilon_d & 1 - \dfrac{x_{1,d}^2}{2\,r^{2_d}\,x_{2_d}^2}\epsilon_d^2 & r_d\,x_{2,d}\,\epsilon_d^2 \\ -e^{i\,\delta_d}\dfrac{r_u\,x_{1,d}\,x_{2,u}}{r_d,\,x_{2,d}}\epsilon_d\,\epsilon_u^2 & -r_d\,x_{2,d}\,\epsilon_d^2 & 1 \end{pmatrix} . \tag{2.10}
$$

In can be checked that this matrix reproduces to a good approximation the numerical results obtained in Ref.[3]. The diagonalized Yukawas are

$$Y'^{a} \;=\; y_{3,a} \begin{pmatrix} \pm\dfrac{x_{1,a}^2}{r_a\, x_{2,a}}\,\epsilon_a^4 & 0 & 0 \\ 0 & r_a\, x_{2,a}\,\epsilon_a^2 & 0 \\ 0 & 0 & 1 \end{pmatrix} . \tag{2.11}$$

To obtain the trilinear and sfermion mass matrices in this basis, we perform the following rotations:

$$a_a \to V_L^{a\dagger}\, a_a\, V_R^a \qquad , \qquad \widetilde{m}^2_{R,a} \to V_R^{a\dagger}\, \widetilde{m}^2_{a,R}\, V_R^a \,, \tag{2.12}$$

with the rotation matrices $V^a_{L,R}$ obtained in Appendix A.1.3. Then, in the charged lepton sector at LO we obtain

$$a_e \;\to\; A_0\, y_\tau \begin{pmatrix} -7\,\dfrac{x_{1,e}^2}{r_e\, x_{2,e}}\,\epsilon_e^4 & 0 & 0 \\ 0 & -7\; r_e\, x_{2,e}\,\epsilon_e^2 & 2\, e^{i\,\delta_e}\, r_e\, x_{2,e}\,\epsilon_e^2 \\ 0 & -2\; r_e\, x_{2,e}\,\epsilon_e^2 & 5 \end{pmatrix} , \tag{2.13}$$

$$\widetilde{m}^2_{R,e} \;\to\; m_0^2\,\mathbb{1} + m_0^2\, y_\tau \begin{pmatrix} \epsilon_e^{2\alpha} & -e^{2\,i\,(\gamma_e-\delta_e)}\,\epsilon_e^{2\alpha} & 3\, e^{3\,i(\gamma_e-\frac{\delta_e}{2})}\, r_e\,\epsilon_e^{\alpha} \,+\, \epsilon_e^{2\alpha} \\ \text{c.c.} & \epsilon_e^{2\alpha} & 3\, e^{i(\gamma_e-\frac{\delta_e}{2})}\, r_e\,\epsilon_e^{\alpha} \,+\, \epsilon_e^{2\alpha} \\ \text{c.c.} & \text{c.c.} & 1 \end{pmatrix} . \tag{2.14}$$

Except for the elements 12(21) and 13(31) of the trilinears, it's clear that the final matrices do not get diagonalized. Due to the this block diagonal form of the trilinears, their relevance for FV in the lighter generations is negligible, such as in the process $\mu \to e\gamma$. The same happens in the quark sector. The absence of charge and color breaking (CCB) minima in MSUGRA[1] requires $|a_{ii}|^2 \lesssim 3\, m_0^2\, Y_i^{(\text{diag})}$, as shown in Ref. [16]. Comparing Eqs. (2.13) and (2.11) we see that the element A_{22} gives

[1]We can approximate $m_0^2 \sim (m_{\tilde{\ell}}^2 + m_\ell^2 + m_{H_d}^2)$. A similar condition applies also to off-diagonal elements giving usually less stringent bounds. In the numerical analysis we put a relaxed limit on A_0 and discard the points not respecting the CCB condition after the RGE evolution to the EW scale is performed.

a quite stringent bound on the allowed values of A_0, $A_0 \lesssim \sqrt{3}\, m_0/7$, so that the trilinear contributions are usually subdominant with respect to the soft mass matrix contributions. Looking at Eq.(2.14), and considering that $\alpha \in [0,1]$, we see that large off diagonal entries are obtained (we emphasize that the value of the vacuum expectation value remains perturbative, $v_{123}/M_{23,a} = \sqrt{y_3}\,\epsilon_a^\alpha$). In particular, an $\epsilon_e^{2\alpha} \in [0.02, 1]$ contribution appears in the 12 entry that controls the $\mu \to e$ LFV-decays, and $\epsilon_e^\alpha \in [0.15, 1]$ contributions arise in the 13 and 23 entries, determining the size of the LFV-transitions $\tau \to e$ and $\tau \to \mu$, respectively. Similar results are obtained in the quark sector where the resulting matrices at LO are

$$a_u \;\to\; A_0\, y_t \begin{pmatrix} 7\,\dfrac{x_{1,u}^2}{r_u\, x_{2,u}}\,\epsilon_u^4 & 0 & 0 \\ 0 & 7\; r_u\, x_{2,u}\,\epsilon_u^2 & 2\, e^{-i\,\delta_d}\, r_u\, x_{2,u}\,\epsilon_u^2 \\ 0 & 2\, e^{i\,\delta_d}\; r_u\, x_{2,u}\,\epsilon_u^2 & 5 \end{pmatrix}, \tag{2.15}$$

$$\widetilde{m}_{R,u}^2 \;\to\; m_0^2\,\mathbb{1} + m_0^2\, y_t \begin{pmatrix} \epsilon_u^{2\alpha} & -e^{i\,(\gamma_d-\delta_d)}\,\epsilon_u^{2\alpha} & -e^{-i\gamma_d}\,(3\, r_u\,\epsilon_u^\alpha + \epsilon_u^{2\alpha}) \\ \text{c.c.} & \epsilon_e^{2\alpha} & e^{-i\delta_d}\,(3\, r_u\,\epsilon_u^\alpha + \epsilon_u^{2\alpha}) \\ \text{c.c.} & \text{c.c.} & 1 \end{pmatrix}, \tag{2.16}$$

$$a_d \;\to\; A_0\, y_b \begin{pmatrix} 7\,\dfrac{x_{1,d}^2}{r_d\, x_{2,d}}\,\epsilon_d^4 & 0 & 0 \\ 0 & 7\; r_d\, x_{2,d}\,\epsilon_d^2 & 2\, r_d\, x_{2,d}\,\epsilon_d^2 \\ 0 & 2\, e^{i\,\delta_d}\; r_d\, x_{2,d}\,\epsilon_d^2 & 5 \end{pmatrix}, \tag{2.17}$$

$$\widetilde{m}_{R,d}^2 \;\to\; m_0^2\,\mathbb{1} + m_0^2\, y_b \begin{pmatrix} \epsilon_d^{2\alpha} & -e^{i\,(\gamma_d-\delta_d)}\,\epsilon_d^{2\alpha} & 3\, e^{i(2\,\gamma_d - \frac{3\,\delta_d}{2})}\, r_d\,\epsilon_d^\alpha + \epsilon_d^{2\alpha} \\ \text{c.c.} & \epsilon_d^{2\alpha} & 3\, e^{i(\gamma_d - \frac{\delta_d}{2})}\, r_d\,\epsilon_d^\alpha + \epsilon_d^{2\alpha} \\ \text{c.c.} & \text{c.c.} & 1 \end{pmatrix}. \tag{2.18}$$

In particular, we observe that the series of re-phasings that we have applied result in a dangerous $e^{i\,(\gamma_d-\delta_d)}$ in the 12 entry of the down soft mass matrix, which can be responsible for deviations from the experimental value of ϵ_K.

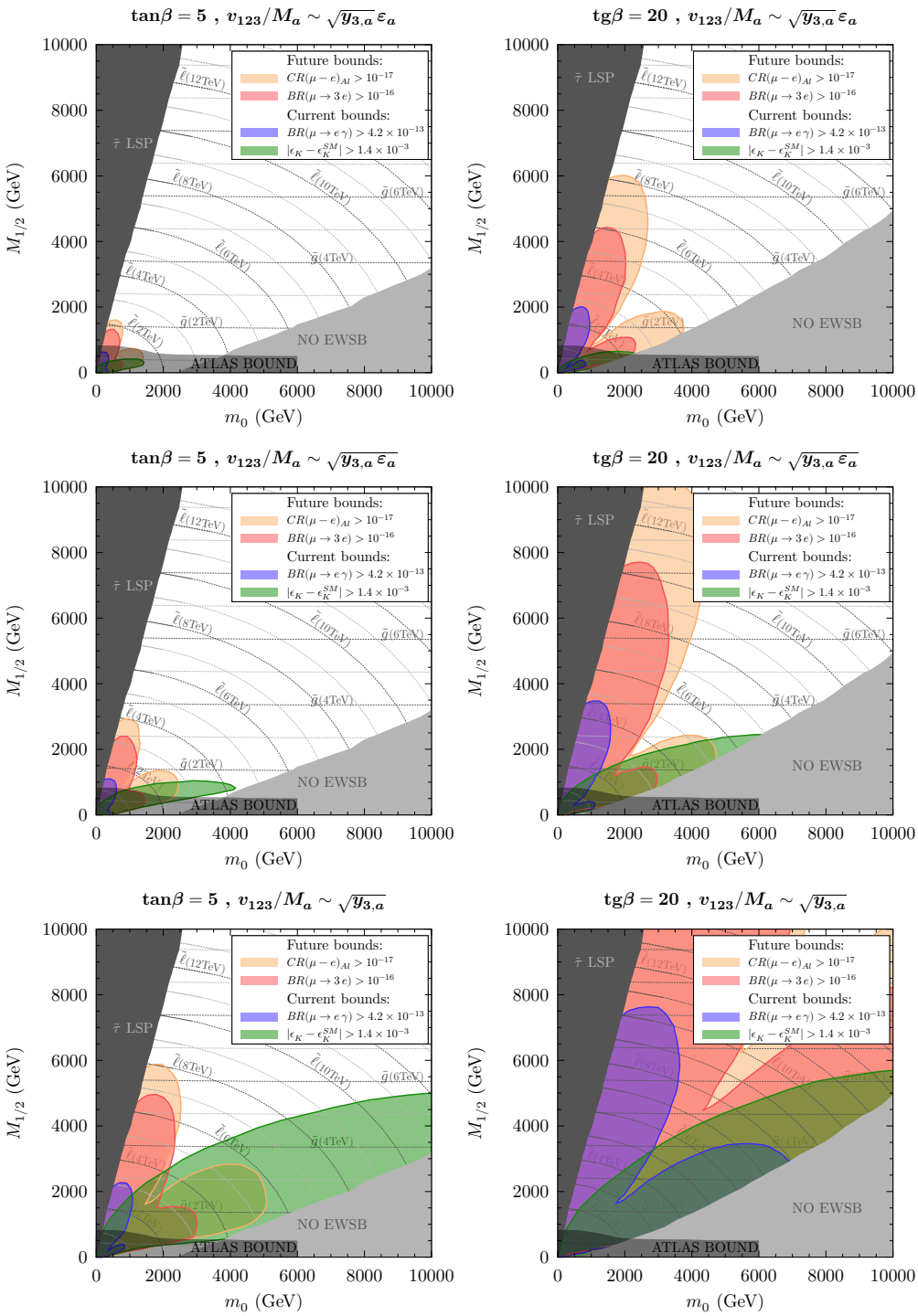

FIGURE 2.1: Excluded regions of the MSSM parameter space due to FV constraints for the cases $\tan\beta = 5, 20$ and 3 different values of the VEV of the ϕ_{123}. Blue and green shapes refer to the current bounds on $BR(\mu \to e\,\gamma)$ and ϵ_K, red and orange shapes are the expected regions to be ruled out if future sensitivity on $BR(\mu \to 3e)$ and $CR(\mu - e)_{Al}$ are reached with no discovery.

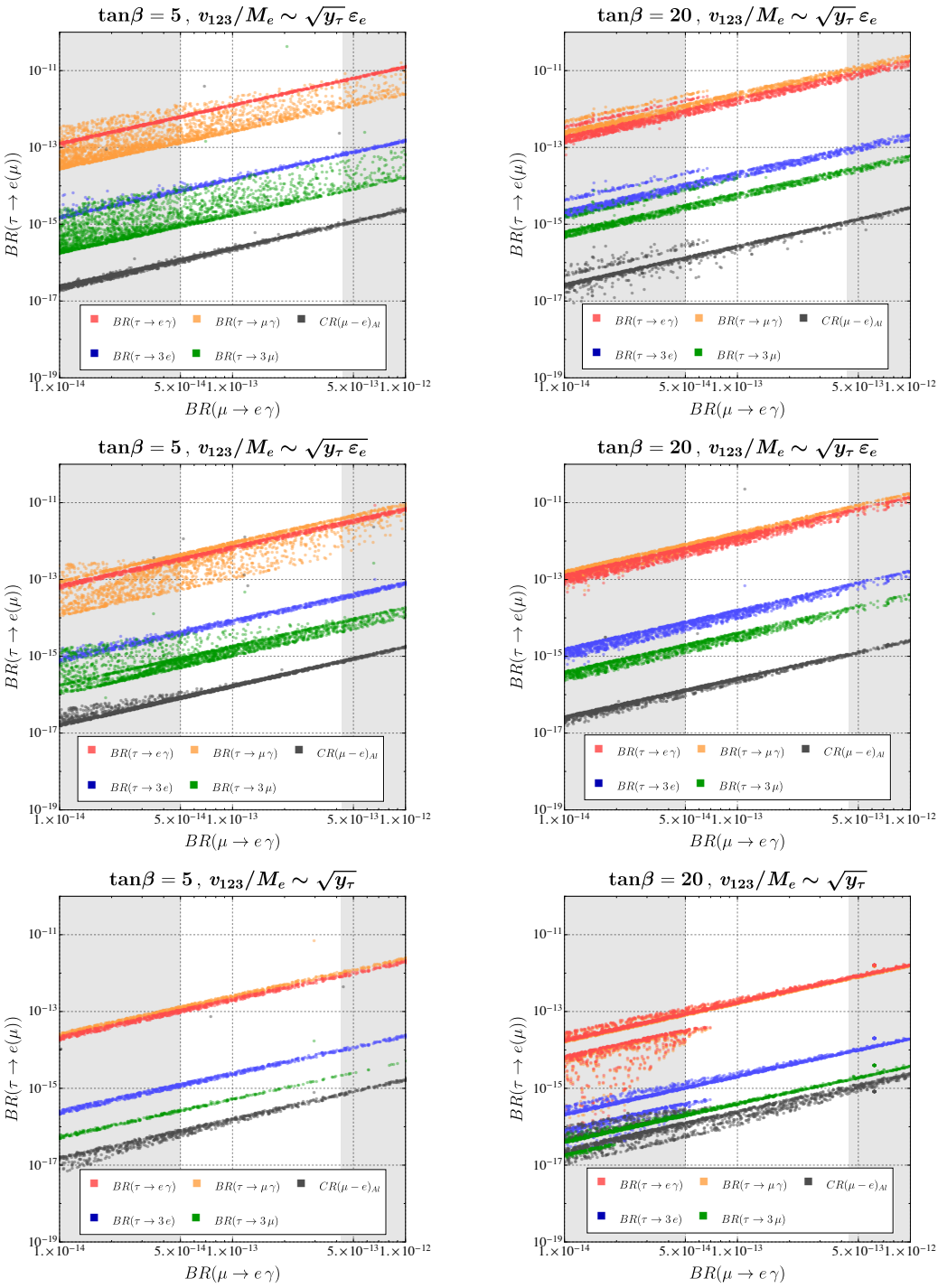

FIGURE 2.2: Lepton flavor violating decays of the τ as a function of $BR(\mu \to e\,\gamma)$ for the same cases considered in Figure 2.1. The white window corresponds to the accessible region between the current bound and the expected future limit for $BR(\mu \to e\,\gamma)$, that is to the region between the blue and red shapes in Figure 2.1. The future limit on the τ-decays is estimated as $\sim 10^{-10}$, so that the given ranges are out of reach for near future experiments.

2.3.2 Phenomenological results

After substituting the numerical values corresponding to the best fit results of Table 4.2, the matrices must be evolved to the EW scale by means of the MSSM renormalization group equations (RGE), and compared to the most relevant flavor observables. Numerical calculations for the running, spectrum and low energy processes have been performed through the Supersymmetric Phenomenology package (SPheno) [17], together with the SARAH Mathematica package [18] to generate the source code. Taking into account that the flavor structures are completely fixed by the $\Delta(27)$ flavor symmetry, the only inputs are the typical supergravity parameters, chosen in the ranges: $\{m_0\,,\, M_{1/2}\} \in [0, 10]$ TeV , $A_0 \in [0\,,\, 0.5]\, m_0$ and $\tan\beta = 5\,,\, 20$ taken as interesting representative cases.
In Fig.2.1, the excluded regions of the MSSM parameter space are shown. In these plots we compare the $\tan\beta = 5$ (left) and $\tan\beta = 20$ (right) results for values of the VEV $v_{123} = \langle\phi_{123}\rangle$ (normalized with respect to the messenger mass) of $\sim \epsilon, \sqrt{\epsilon}$ and 1. The blue and green shapes refer to the present bounds while the red and orange shapes are obtained from expected future limits.
The branching ratio of the $\ell_i \to \ell_j\gamma$ process is given by

$$\frac{BR(\ell_i \to \ell_j\gamma)}{BR(\ell_i \to \ell_j\, \nu_i\, \overline{\nu}_j)} = \frac{48\,\pi^3\,\alpha}{G_F^2}(|\mathcal{A}_L^{ij}|^2 + |\mathcal{A}_R^{ij}|^2) \;\sim\; \frac{\alpha^3}{G_F^2}\,\frac{\delta_{ij}^2}{m_0^4}\,\tan\beta^2\,, \tag{2.19}$$

which holds approximately true for $\ell_i \to 3\,\ell_j$ and μ–e conversion in atoms processes, in which the Z-penguin and box-type diagrams are usually subdominant with respect to the the γ-penguin $\tan\beta$-enhanced contribution. Replacing the value of $\delta_{ij} = y_\tau\epsilon^{2\alpha}$, Eq. (2.14), and taking into account $y_\tau \propto \tan\beta$, we have $\tan\beta/m_0$ constant for a fixed value of the branching ratio, *i.e.* $\tan\beta$ scales linearly with m_0. Thus, in the figures, the m_0–$M_{1/2}$ excluded regions scale almost linearly with $\tan\beta$ (nearly a factor of 4 when going from 5 to 20). Similarly, when the VEV scales by up to a factor of ~ 6.6, the excluded regions growing a factor of around 4, a milder growth in this case. The bounds are relatively mild in the top left corner, with small VEV and $\tan\beta = 5$, allowing m_0 and $M_{1/2}$ of a few TeV, and this remains true when increasing the VEV. On the other hand, even for small values of the VEV, $\tan\beta = 20$ pushes the exclusion such that typical values of m_0 and $M_{1/2}$ need to be larger than 4 to 6 TeV. The strongest exclusions are shown in the bottom right corner, with large VEV and $\tan\beta = 20$ very little parameter space is still allowed within the displayed 10 TeV ranges for m_0 and $M_{1/2}$. Given such severe exclusion limits for $\tan\beta = 20$, one option is to abandon the simplifying assumption of universal messenger masses

(M_a) and consider using the additional freedom of $M_{3,a} \neq M_{23,a}$. Together with the difference between up-type messengers and down-type messengers ($a = (u, d)$), one can accommodate simultaneously the hierarchies between m_b/m_t, m_c/m_t and m_s/m_b without going to large values of $\tan\beta$.

A feature of the model is the heaviness of the Left messengers which results in small off-diagonal δ^{LL}-insertions. Consequently, the shapes that we observe are the typical ones of the δ^{RR} sector which is $\tan\beta$-enhanced and exhibit the usual cancellation between the bino and and bino-higgsino amplitudes in the $0.7\, m_0 \lesssim M_{1/2} \lesssim 1.2\, m_0$ region of the parameter space Ref. [19]. Such cancellations occur in all situations in which the contribution of the off-diagonal trilinear terms δ^{RL} is negligible, which is often the case considering the CCB upper bound on $|A|$ and the texture of the trilinear terms of the model where $\delta_{12(21)} \simeq \delta_{13(31)} \simeq 0$.

Apart from LFV observables, the CP-violating observable ε_K plays also an important role in the restriction of the parameter space of the model. In this case, ε_K is, in principle, independent of $\tan\beta$, but the off-diagonal entries of squark mass matrices are proportional to y_b, which restores the $\tan\beta$ dependence, as we see in Fig.2.1. The exclusion regions in this figure correspond to points out of the 3σ-range $|\varepsilon_K - \varepsilon_K^{SM}| < 3\sqrt{\sigma_{SM}^2 + \sigma_{SUSY}^2} \simeq 1.4 \times 10^{-3}$, where ε_K^{SM} is the SM prediction computed for each point by SPheno with only trivial soft-breaking structures as inputs and congruent with the estimate in Ref.[20]. The σ_{SM}, σ_{SUSY} are the theoretical uncertainties of the SM estimate and the SUSY contribution respectively. In particular $\sigma_{SM} \sim 10\,\% \,\varepsilon_K^{SM}$ [20] while σ_{SUSY} is dominated by the hadronic uncertainties of the f_K decay constant and the B-parameters coming from Lattice QCD computations (see Ref.[21]). To be conservative, we have taken this into account, letting each parameter vary between its minimum and maximum value and taking half of the difference between the respective maximum and minimum values of ε_K. We find that σ_{SUSY} receives the largest contribution from $B_3(\mu) = 1.05\,(12)$ and $B_5(\mu) = 0.73\,(10)$ and can be up to $\sim 20\,\% \,\varepsilon_K^{SM}$ in the region where the SUSY contribution is comparable to the SM one. As we can see in the figure, this observable is very effective in restricting the region of low $M_{1/2}$, which corresponds to realtively light gluino and squark masses, but can reach large m_0 values.

It is interesting to compare the model predictions for LFV processes involving the τ lepton, shown in Fig.2.2, with the benchmark decay $\mu \to e\gamma$. As a reflection of the $m^2_{R,e}$ structure in Eq.(2.14), the τ branching ratios are correlated and increase linearly with the branching ratio of the benchmark decay. For the same value of $BR(\mu \to e\gamma)$, larger $\tan\beta$ (going from a plot in the left to a plot in the right) corresponds to slightly

smaller τ branching ratios, while a larger VEV (going from a plot above to a plot below) corresponds to a more significant reduction of the τ branching ratios (up to one order of magnitude smaller over the the range considered).
It is worth noting that in the cases $\tan\beta = 5$ and $v_{123}/M_e = \sqrt{y_\tau}\,\epsilon_e, \sqrt{y_\tau\,\epsilon_e}$, the observed dispersion for the processes $\tau \to \mu\,\gamma$ and $\tau \to 3\,\mu$ is imputable to a non-negligible effect of the δ^{RL}_{23}-insertion. For larger values of $\tan\beta$ and v_{123} this ceases to be the case.
In some cases, particularly in the $\tan\beta = 20$ panels, for each branching ratio a second line becomes visible, and the two lines correspond to the maximum directions of growth in the $\{m_0, M_{1/2}\}$ planes of Fig.2.1. This is caused by a misalignment of the cancellation region with respect to the one of $\mu \to e\,\gamma$, which results in two distinct directions of growth. The misalignment stems from additional contributions, deriving mainly from the inclusion of the two mass insertions $\delta^{RR}_{ik}\delta^{RR}_{kj}$ [2] (see Ref.[19]), which for these processes is not negligible. Note that, as the exclusion region given by ε_K can reduce or exclude the points in one of the two direction of growth, we are not plotting these points in Fig.2.2.

2.3.3 Comparisons with other models

As explained in Sec. I.5.4, non-universal soft-breaking terms are always expected in supersymmetric models when the flavor symmetry is broken below the SUSY-breaking mediation scale. However, different flavor symmetries give rise to different structures in the soft-breaking terms while reproducing the observed fermion masses and mixing matrices.
This non-universality of soft-terms in supersymmetric flavor models has long been considered in the literature [22–41]. In most of these works, the structure of the soft terms is fixed by the symmetry and it is simply assumed that the unknown O(1) coefficients differ from the ones in the Yukawa matrices. In Refs. [1, 2] this non-proportionality was explicitly demonstrated and the corresponding soft-terms obtained. In [1], two flavor symmetries were considered, $U(1)_f$ and $SU(3)_f$, while in [2], three different models were considered: $\Delta(27)$ (a different model from the one considered here), A_4 and S_3. In this section, we compare their results with the present model in order to extend the validity of our results to a wider class of models.
In Ref. [1], the kaon observables ΔM_K and ε_K were considered, while in [2] only leptonic observables were taken into account. In this work, we consider both kaon and

[2] In principle the misalignment could be also due to the contribution of additional diagrams, however this is not what we observe for the analyzed processes.

leptonic observables and therefore we can compare the exclusion regions with the results presented in these works. In general, the regions for different models have distinct shapes, depending on the respective details of the models. For instance, the shape of the region constrained by ε_K in [1] (shown there in the $m_{\tilde{g}}$–$m_{3/2}$ plane) is very similar to the one we find in this work for the case of the $SU(3)$ symmetry, but distinct from the shape of the $U(1)$ model.
Regions excluded by leptonic observables in [2] are clearly different to the ones found in this work for the A_4 and S_3 models, due to the simultaneous presence of left-handed and right-handed mass insertions. Interestingly, the older $\Delta(27)$ model [6] (now excluded due to θ_{13}^{ℓ}) produces similar exclusion shapes as the unified texture zero model [3] we analyse here. This is not surprising, as the main differences between the two models arise in the neutrino sector and both models use the same flavon VEV directions, in particular the $(1,1,1)$ direction which is most relevant for FV processes as it contributes to the lighter generations (where bounds are more stringent). The particularities of the vacuum alignment mechanisms employed in the two $\Delta(27)$ models would allow them to be distinguished in FV observables. For the cases where FV is enhanced by taking $v_{123}/M \sim \sqrt{y_\tau\,\epsilon}$ or $v_{123}/M \sim \sqrt{y_\tau}$, as preferred by the vacuum alignment mechanism, current FV bounds reach much higher exclusions, up to around 8 TeV in the most sensitive case, as seen in the bottom right panel of Fig. 2.1. In summary, taking into account current leptonic and kaon FV bounds allows us to extend the excluded regions in comparison to previous works.

2.4 Conclusions

We performed an analysis of quark and lepton flavor violating processes in a supersymmetric model enlarged with a $\Delta(27)$ flavor symmetry which is broken below the supersymmetry-breaking mediation scale. We have explicitly shown the non-universality of trilinear terms and supersymmetry soft-breaking masses, with all the SUSY breaking matrices determined in terms of m_0, A_0 and $\tan\beta$.
FV processes allow us to explore this model up to rather heavy sparticle masses, well above the LHC reach. LFV bounds, and specially $\mu \to e\gamma$, are the most restrictive constraints in the parameter space, but thanks to the presence of flavor-dependent phases, ε_K plays an important role in exploring the region of low $M_{1/2}$.
The combination of LFV processes and ε_K can restrict very large values of $M_{1/2}$ and m_0, depending on the $\tan\beta$ value and the model vev, v_{123}. Indeed, if we take the

typical values preferred by the vacuum alignment mechanism of the model, the constraints become particularly severe, reaching values of several TeV for $M_{1/2}$ and m_0. This fact, implies that assumptions such as universal messenger masses are too simple and should be abandoned, in order to relax $\tan\beta$ and still accommodate the hierarchy between the top and bottom mass.

We have compared the results for this flavor model with other models, including a similar flavor model with a $\Delta(27)$ symmetry, and discrete symmetries such as A_4 and S_3. In general, FV processes constrain these models in different ways and lead to qualitative and even quantitative differences.

In conclusion, FV searches are able to constrain the parameter space of flavor models and even distinguish flavor models that would otherwise be hard to discriminate by solely increasing the precision of fermion masses and mixing parameters.

References

[1] D. Das et al., *Phys. Rev.* **2017**, *D95*, 035001, arXiv: 1607.06827 [hep-ph].

[2] M. L. López-Ibáñez et al., *JHEP* **2017**, *11*, [Erratum: JHEP 04, 015 (2018)], 162, arXiv: 1710.02593 [hep-ph].

[3] I. de Medeiros Varzielas et al., **2017**, arXiv: 1710.01741 [hep-ph].

[4] C. H. Albright et al., *Eur. Phys. J. C* **2010**, *70*, 1099–1110, arXiv: 1004.2798 [hep-ph].

[5] I. de Medeiros Varzielas, L. Lavoura, *J. Phys. G* **2013**, *40*, 085002, arXiv: 1212.3247 [hep-ph].

[6] I. de Medeiros Varzielas et al., *Phys. Lett.* **2007**, *B648*, 201–206, arXiv: hep-ph/0607045 [hep-ph].

[7] F. Bazzocchi, I. de Medeiros Varzielas, *Phys. Rev. D* **2009**, *79*, 093001, arXiv: 0902.3250 [hep-ph].

[8] R. Howl, S. King, *Phys. Lett. B* **2010**, *687*, 355–362, arXiv: 0908.2067 [hep-ph].

[9] I. de Medeiros Varzielas, G. G. Ross, *JHEP* **2012**, *12*, 041, arXiv: 1203.6636 [hep-ph].

[10] F. Björkeroth et al., *Phys. Rev. D* **2016**, *94*, 016006, arXiv: 1512.00850 [hep-ph].

[11] F. Björkeroth et al., *JHEP* **2017**, *01*, 077, arXiv: 1609.05837 [hep-ph].

[12] A. E. Cárcamo Hernández et al., *JHEP* **2017**, *07*, 118, arXiv: 1705.06320 [hep-ph].

[13] I. de Medeiros Varzielas, G. G. Ross, *Nucl. Phys.* **2006**, *B733*, 31–47, arXiv: hep-ph/0507176 [hep-ph].

[14] L. Calibbi, G. Signorelli, *Riv. Nuovo Cim.* **2018**, *41*, 71–174, arXiv: 1709.00294 [hep-ph].

[15] G. Cavoto et al., *Eur. Phys. J. C* **2018**, *78*, 37, arXiv: 1707.01805 [hep-ex].

[16] J. A. Casas, S. Dimopoulos, *Phys. Lett.* **1996**, *B387*, 107–112, arXiv: hep-ph/9606237 [hep-ph].

[17] W. Porod, *Comput. Phys. Commun.* **2003**, *153*, 275–315, arXiv: hep-ph/0301101 [hep-ph].

[18] F. Staub, *Comput. Phys. Commun.* **2014**, *185*, 1773–1790, arXiv: 1309.7223 [hep-ph].

[19] P. Paradisi, *JHEP* **2005**, *10*, 006, arXiv: hep-ph/0505046 [hep-ph].

[20] J. Brod, M. Gorbahn, *Phys. Rev. Lett.* **2012**, *108*, 121801, arXiv: 1108.2036 [hep-ph].
[21] M. Ciuchini et al., *JHEP* **1998**, *10*, 008, arXiv: hep-ph/9808328 [hep-ph].
[22] Y. Nir, N. Seiberg, *Phys. Lett.* **1993**, *B309*, 337–343, arXiv: hep-ph/9304307 [hep-ph].
[23] M. Dine et al., *Phys. Rev.* **1993**, *D48*, 4269–4274, arXiv: hep-ph/9304299 [hep-ph].
[24] M. Leurer et al., *Nucl. Phys.* **1994**, *B420*, 468–504, arXiv: hep-ph/9310320 [hep-ph].
[25] A. Pomarol, D. Tommasini, *Nucl. Phys.* **1996**, *B466*, 3–24, arXiv: hep - ph / 9507462 [hep-ph].
[26] R. Barbieri et al., *Phys. Lett.* **1996**, *B377*, 76–82, arXiv: hep-ph/9512388 [hep-ph].
[27] Y. Nir, R. Rattazzi, *Phys. Lett.* **1996**, *B382*, 363–368, arXiv: hep-ph/9603233 [hep-ph].
[28] E. Dudas et al., *Nucl. Phys.* **1996**, *B481*, 85–108, arXiv: hep-ph/9606383 [hep-ph].
[29] R. Barbieri et al., *Nucl. Phys.* **1997**, *B493*, 3–26, arXiv: hep-ph/9610449 [hep-ph].
[30] Y. Nir, G. Raz, *Phys. Rev.* **2002**, *D66*, 035007, arXiv: hep-ph/0206064 [hep-ph].
[31] G. G. Ross et al., *Nucl. Phys.* **2004**, *B692*, 50–82, arXiv: hep-ph/0401064 [hep-ph].
[32] S. Antusch et al., *Phys. Lett. B* **2009**, *670*, 383–389, arXiv: 0807.5047 [hep-ph].
[33] Y. Nomura, D. Stolarski, *Phys. Rev. D* **2008**, *78*, 095011, arXiv: 0808.1380 [hep-ph].
[34] L. Calibbi et al., *Nucl. Phys.* **2010**, *B831*, 26–71, arXiv: 0907.4069 [hep-ph].
[35] L. Calibbi et al., *PoS* **2009**, *EPS-HEP2009*, 167, arXiv: 0909.2501 [hep-ph].
[36] W. Altmannshofer et al., *Nucl. Phys. B* **2010**, *830*, 17–94, arXiv: 0909.1333 [hep-ph].
[37] Z. Lalak et al., *JHEP* **2010**, *08*, 129, arXiv: 1006.2375 [hep-ph].
[38] K. S. Babu et al., *Phys. Rev.* **2011**, *D83*, 095008, arXiv: 1103.1664 [hep-ph].
[39] S. Antusch et al., *Nucl. Phys.* **2011**, *B852*, 108–148, arXiv: 1104.3040 [hep-ph].
[40] L. Calibbi et al., *JHEP* **2012**, *06*, 018, arXiv: 1203.1489 [hep-ph].
[41] K. S. Babu et al., *Phys. Rev.* **2014**, *D90*, 056001, arXiv: 1406.6078 [hep-ph].
[42] J. R. Espinosa, A. Ibarra, *JHEP* **2004**, *08*, 010, arXiv: hep-ph/0405095 [hep-ph].
[43] S. F. King et al., *JHEP* **2005**, *07*, 049, arXiv: hep-ph/0407012 [hep-ph].
[44] R. Roberts et al., *Nucl. Phys. B* **2001**, *615*, 358–384, arXiv: hep-ph/0104088.
[45] A. Dedes et al., *JHEP* **2015**, *06*, 151, arXiv: 1504.00960 [hep-ph].
[46] F. Feruglio, A. Paris, *JHEP* **2011**, *03*, 101, arXiv: 1101.0393 [hep-ph].
[47] S. Antusch et al., *JCAP* **2006**, *11*, 011, arXiv: hep-ph/0609038.
[48] W. Buchmuller et al., *Annals Phys.* **2005**, *315*, 305–351, arXiv: hep-ph/0401240.
[49] P. Di Bari, *Nucl. Phys. B* **2005**, *727*, 318–354, arXiv: hep-ph/0502082.

Article 3

Lepton flavor violation and neutrino masses from A_5 and CP in the non-universal MSSM

JHEP 06 (2019) 047

M.L. López-Ibáñez[a], Aurora Melis[b], Davide Meloni[a] and Oscar Vives[b]

[a] *Dipartimento di Matematica e Fisica, Universitá di Roma Tre and INFN, Sezione Roma Tre, Via della Vasca Navale 84, 00146, Roma (Italy)*

[b] *Departament de Física Tèorica, Universitat de València and IFIC, Universitat de València-CSIC, Dr. Moliner 50, E-46100 Burjassot (València), Spain*

ABSTRACT: We analyze the phenomenological consequences of embedding a flavor symmetry based on the groups A_5 and CP in a supersymmetric framework. We concentrate on the leptonic sector, where two different residual symmetries are assumed to be conserved at leading order for charged and neutral leptons. All possible realizations to generate neutrino masses at tree level are investigated. Sizable flavor violating effects in the charged lepton sector are unavoidable due to the non-universality of soft-breaking terms determined by the symmetry. We derive testable predictions for the neutrino spectrum, lepton mixing and flavor changing processes with non-trivial relations among observables.

3.1 Introduction

In recent years, different experiments have accumulated a wealth of experimental data on neutrino parameters that have allowed us to extract with reasonable precision the Pontecorvo-Maki-Nakagawa-Sakata (PMNS) mixing matrix [1–4] and the neutrino mass differences. Still, the determination of the absolute neutrino mass scale and the Dirac CP phase remain to be completed. Future experiments like DUNE [5–8], T2HK [9], T2HKK [10] and NOνA [11] will shed light on these quantities; however, even a full determination of the neutrino mass matrix m_ν will not be enough to fix the mechanism responsible for it and uncover the origin of the observed flavor patterns. Although this is also true in the case of the quark and charged lepton Yukawa couplings, the smallness of neutrino masses and its favorite explanation through a Seesaw mechanism makes this problem specially critical.

If neutrinos are Majorana particles, their masses are well described through a $d = 5$ Weinberg operator [12] in the Standard Model (SM). But there exist different possibilities to generate this effective operator from a more fundamental theory at higher energies, like type I, type II or type III Seesaw, radiative mass models, etc. It is clear that the measurement of neutrino masses and mixing angles alone will not be enough to discriminate among these alternative mechanisms and to infer the couplings responsible for them. For instance, for a type-I Seesaw mechanism, both the neutrino Yukawa couplings and the right-handed neutrino Majorana mass would combine to generate the Weinberg operator but the SM does not provide information to disentangle them from the available experimental data.

Nevertheless, if flavor dependent new physics is close to the electroweak scale, as naturally expected in most of the extensions of the SM, it will provide additional information on flavor dynamics helping us to inspect the mechanism responsible for neutrino masses and to determine the parameters of the model. One example of this, which has been explored in previous works [13–19] but we do not consider here, supposes that the flavor symmetry is broken around the electroweak scale. In that case, the scalar flavons may mediate lepton flavor violating (LFV) processes in a measurable way while the fields themselves could be produced and detected in future colliders. Another possibility is Supersymmetry (SUSY), which we consider the perfect example for this as it generically contains new flavor interactions in its soft-breaking sector in the presence of a flavor symmetry. As shown in [20–24], non-trivial flavor structures are unavoidable if the scale of mediation of SUSY breaking to the visible sector, $\Lambda_{\rm Med}$, is larger than the scale of breaking of the flavor symmetry, Λ_f.

The group A_5 combined with the so-called generalized CP symmetry has already

been studied in different contexts [25–29]. Here, we aim to extend the work in [29] and analyze the phenomenological implications of considering A_5 and CP in a supersymmetric model. In these conditions, we will show that constraints from lepton flavor violation are very strong and, in many cases, they are able to explore supersymmetric masses well beyond the reach of direct searches at LHC [30, 31]. Besides, if SUSY is found in future experiments, we will obtain additional information on the structure of flavor matrices that will help us to distinguish between the different mechanisms responsible for neutrino masses.
The paper is organized as follows: in Sec.3.2 and 3.3, we revisit the implications of introducing a flavor symmetry in SUSY and the main features of A_5 and CP as a flavor group; Sec.3.4 is dedicated to derive the minimal set of flavor-conserving operators entering the Kähler potential and the soft-mass terms; in Sec.3.5, the phenomenology of the model is analyzed; finally, we conclude in Sec.3.6 summarizing the most important results.

3.2 Flavor symmetries in supersymmetric theories

The embedding of a flavor symmetry in a supersymmetric theory implies that the different superfields have definite transformation properties under the flavor symmetry and, then, the whole Lagrangian in terms of component fields is necessarily invariant under this symmetry. Initially, the SM Yukawa couplings are forbidden and they are only generated after spontaneous breaking of the symmetry [32]. Similarly, the flavor structures of the soft-breaking terms will be determined in terms of the flavon vevs [20–24].
Sizable non-universal contributions to the soft-terms appear in the low-energy effective theory if the scale of mediation of SUSY breaking, $\Lambda_{\rm Med}$, is above the scale of flavor symmetry beaking Λ_f, $\Lambda_{\rm Med} \gg \Lambda_f$. Supergravity serves as illustrative example to show this, although the results outlined here are more general [20]. In the following, we consider MSUGRA, which depends only on five input parameters and gives rise to the Minimal Supersymmetric Standard Model (MSSM) at low energies.
In Supergravity, SUSY breaking is propagated to the visible sector through gravitational interactions, suppressed by the Planck scale $M_{\rm Pl}$. MSUGRA is the simplest and most conservative scenario that parametrizes the breaking of supersymmetry by a single field, universally coupled to the visible sector, with a non-vanishing F-term, $\langle X \rangle = F_X \neq 0$. In the full theory, before the breaking of the flavor symmetry, the soft-breaking operators are generated from those associated with the Yukawa couplings

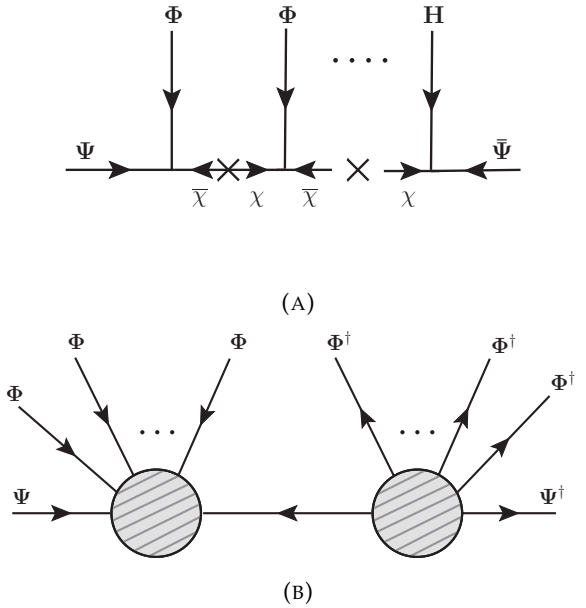

FIGURE 3.1: (A) A supergraph representation of the processes that generate the corrections to the Superpotential in the second term of Eq.(3.1). It involves n_{in} flavon insertions. Internal lines represent the heavy mediators χ while the crosses stand for SUSY mass insertions M_χ.
(B) A supergraph depiction of the processes that generate the correction to the Kähler potential in the second term of Eq.(3.2). Each bubble with entering (leaving) lines represent a set of n_{in} (n_{out}) fields (dagger fields) in the same fashion than the upper diagram, mediated by χ heavy superfields.

in the superpotential (W) and kinetic terms in the Kähler potential (K) through the insertion of the spurion field and, in these conditions, they are completely universal. However, after the breaking of the flavor symmetry, the superpotential and Kähler potential receive corrections from non-renormalizable operators coming from diagrams like those depicted in Figure 3.1. Integrating over the heavy mediators χ, the Superpotential and Kähler potential can be schematically written as:

$$W = W_{\text{ren}} + \Psi\,\Psi^c\,\mathrm{H}\sum_{\Phi}\sum_{n_{\text{in}}=1}^{\infty} x_{\mathrm{n_{in}}}\left(\frac{\langle\Phi\rangle}{M_\chi}\right)^{n_{\text{in}}}, \tag{3.1}$$

$$K = \Psi\,\Psi^\dagger\left[\mathbb{1} + \sum_{\Phi,\Phi^\dagger}\sum_{\substack{n_{\text{in}},\\ n_{\text{out}}=1}}^{\infty} c_{(n_{\text{in}},n_{\text{out}})}\left(\frac{\langle\Phi\rangle}{M_\chi}\right)^{n_{\text{in}}}\left(\frac{\langle\Phi^\dagger\rangle}{M_\chi}\right)^{n_{\text{out}}}\right], \tag{3.2}$$

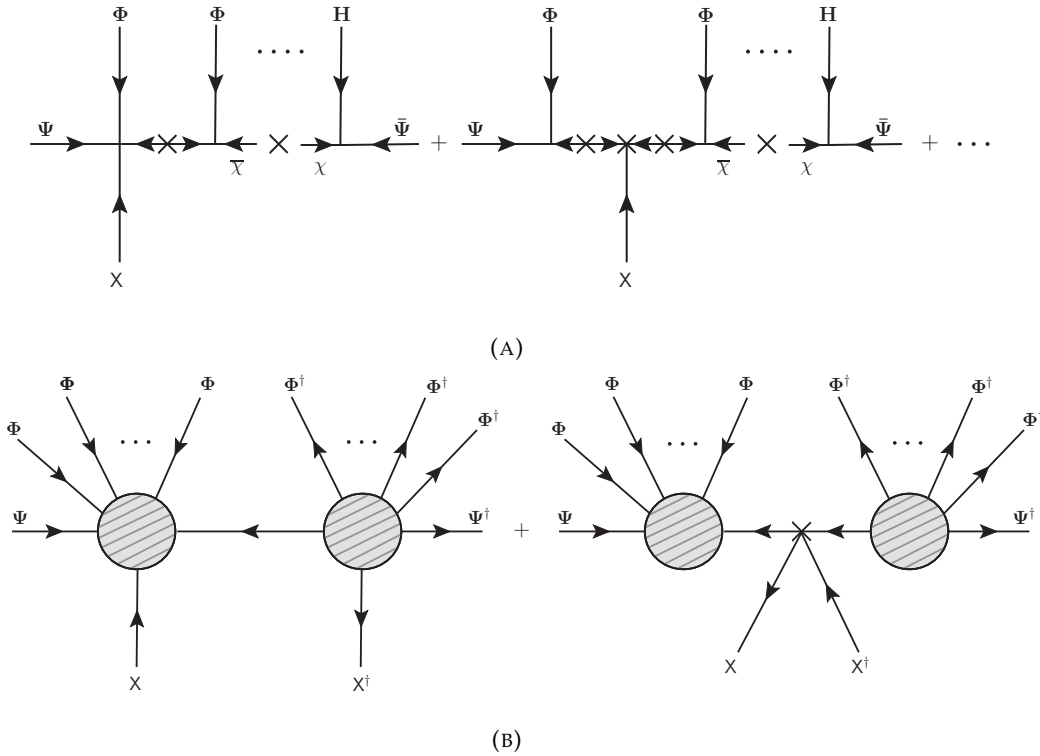

FIGURE 3.2: (A) A supergraph representation of two processes contributing to the same trilinear coupling. In the first diagram, the spurion field is attached to the vertex Ψ-Φ-χ while, in the second diagram, it is inserted in the χ mass insertion. The same can be done for each flavon and Higgs insertion. Therefore, for a Yukawa diagram involving n_{in} flavons, there will be $(2\,n_{\text{in}}+1)$ possibilities to generate the associated trilinear coupling. All of them have to be taken into account.
(B) A schematic supergraph depiction of the two types of processes that contribute to the same soft mass due to the insertion of the spurion $XX^\dagger$ combination in different positions. The bubbles with n_{in} (n_{out}) flavons and a X ($X^\dagger$) insertion symbolize the $(2\,n_{\text{in(out)}}-1)$ possible diagrams resulting from attaching X as in the upper diagram. The second diagram accounts for the insertion of $XX^\dagger$ in the internal heavy mediator. Combining all of them, $\left[(2\,n_{\text{in}}-1)\,(2\,n_{\text{out}}-1)+1\right]$ possibilities contribute to the soft mass.

where Ψ stands for any field belonging to the visible sector[1] and W_{ren} consists of renormalizable operators such as the Higgs μ-term or a possible top Yukawa coupling. Therefore, the standard Yukawa couplings are only generated by these operators as powers of the expansion parameter $\epsilon = \langle\Phi\rangle / M_\chi$, where $\langle\Phi\rangle$ is the vev of the scalar flavon and M_χ the mass of the heavy mediators. The bubbles of fields entering

[1]We follow the usual superfield notation throughout the article. Thus, all the fields in Eqs.(3.1) and (3.2) must be read as superfields. In Table 3.1, the relevant particle content for our analysis is specified.

and leaving in Figure 3.1-(b) are the sets of n_{in}- and n_{out}-flavon insertions in Eq.(3.2) which enclose similar structures to those in Figure 3.1-(a).
Adding the spurion field to these non-renormalizable Yukawa couplings or to the Kähler potential generates the trilinear terms and soft mass matrices. From Figure 3.2 one may see that, for each operator with n-flavon insertions, the number of effective operators contributing to the trilinear couplings and soft masses at the same order is equal to the number of different ways in which the spurion field can be inserted in the diagram. Thus, the proportionality factor between trilinears (soft masses) and the corresponding Yukawa coupling (Kähler term) is given by:

$$a_{ij} = (2\,n_{\text{in}} + 1)\,A_0\,Y_{ij}, \tag{3.3}$$

$$\widetilde{m}^2_{ij} = m_0^2\,f_{ij}\,(K)_{ij} \quad \text{with} \quad f_{ij} = [\,(2\,n_{\text{in}} - 1)(2\,n_{\text{out}} - 1) + 1\,], \tag{3.4}$$

where $m_0 \equiv \langle F_X \rangle / M_{\text{Pl}}$ and $A_0 \equiv k\,m_0$ with $k \sim \mathcal{O}(1)$. The main consequence of Eqs. (3.3) and (3.4) is that, although term by term the trilinears and the soft masses are proportional to Yukawas and Kähler elements, the full matrices are not proportional to them. Therefore, going to the canonical basis, where the Kähler metric is the identity, and to the mass basis, where the Yukawas are diagonal, does not ensure that the soft terms are diagonalized. Actually, as we will see below in the case of A_5, off-diagonal contributions will generally survive the rotations and they will have an impact on the low-energy phenomenology.

3.3 Lepton masses and mixing from A_5 and CP

A_5 is the non Abelian discrete group composed of the even permutations of five objects. It has 60 elements and five irreducible representations (irrep): one singlet **1**, two triplets **3** and **3′**, one tetraplet **4** and one pentaplet **5**. It can be generated by two elements, s and t, satisfying[2]:

$$s^2 = (s\,t)^3 = t^5 = e. \tag{3.5}$$

The specific form of these generators for each irrep of the group in our basis convention is shown in Appendix B.3. The A_5 group contains several subgroups: fifteen associated with a $\mathbb{Z}_2$ symmetry, five Klein subgroups $\mathbb{Z}_2 \times \mathbb{Z}_2$, ten related to $\mathbb{Z}_3$ transformations and six $\mathbb{Z}_5$ subgroups. Combinations of them may play the role of

[2]Lowercase letters are for the abstract elements of the group. Capital letters refer to specific representations in terms of $n \times n$ matrices.

residual symmetries for charged leptons and neutrinos. Here we are interested in the combination of A_5 and CP as proposed in [33] (see also [34–36]), where the CP transformation generally acts non trivially on the flavor space [37–39]. The action of a generalized CP transformation, X, over a field $\psi(x)$ is given by[3]:

$$\psi(x) \longrightarrow \psi'(x) = X\psi^\star(x_{\rm CP}), \tag{3.6}$$

with X a matrix representation of the CP transformation and $x_{\rm CP} = (x^0, -\overrightarrow{x})$. The transformation X can be chosen as a constant, unitary and symmetric matrix:

$$XX^\dagger = XX^\star = \mathbb{1} \tag{3.7}$$

To ensure a consistent definition of the CP symmetry with the flavor group, the following condition must be verified:

$$(X^{-1}\, A\, X)^\star = A' \tag{3.8}$$

where A, $A' \in A_5$. In particular for A_5, Eq.(3.8) is fulfilled with $A = A'$.
A_5 as a family symmetry for leptons leads to the Golden Ratio (GR) mixing, which predicts a vanishing reactor angle θ_{13}. A consequence of introducing CP as a symmetry is that the pure GR mixing is modified and a continuous parameter, θ , that quantifies this departure is introduced. In fact, the small value of the reactor angle can be reproduced in terms of this variable that, at the same time, determines the amount of observable CP violation in the leptonic mixings.
The set of combinations of residual symmetries for A_5 and CP that accommodates well the observed mixing in the leptonic sector has been discussed in previous works [25–27]. Assuming that the lepton $SU(2)_L$-doublet, L, transforms like a triplet representation of A_5, the authors in [26] conclude that only four possibilities are allowed: two for $\mathcal{G}_e = \mathbb{Z}_5$, one for $\mathcal{G}_e = \mathbb{Z}_3$ and another for $\mathcal{G}_e = \mathbb{Z}_2 \times \mathbb{Z}_2$; for neutrinos, $\mathcal{G}_\nu = \mathbb{Z}_2 \times$CP has been always considered. Here we are interested in the phenomenology of Case II of [26], corresponding with $\mathcal{G}_e = \mathbb{Z}_5$. The neutrino spectrum for this scenario has been fully analyzed in [29]. A tuple of generators, Q of $\mathcal{G}_e = \mathbb{Z}_5$ and $(Z,\, X)$ of $\mathcal{G}_\nu = \mathbb{Z}_2 \times$CP, characterizing this realization is:

$$(Q,\, Z,\, X) = (T,\, T^2ST^3ST^2, X_0), \tag{3.9}$$

[3]Do not mistake the spurion chiral field responsible for the breaking of SUSY, X, for the matrix representation of the generalized CP transformation X.

Mechanism	L	ν^c	H_u	$\phi_{\mathbf{1}}^{\nu}$	$\phi_{\mathbf{3}}^{\nu}$	$\phi_{\mathbf{3'}}^{\nu}$	$\phi_{\mathbf{4}}^{\nu}$	$\phi_{\mathbf{5}}^{\nu}$
I	**3**	–	**1**	**1**	–	–	–	**5**
II a-2	**3**	**3**	**1**	**1**	**3**	–	–	**5**
II c-2	**3**	**3'**	**1**	–	–	–	**4**	**5**

TABLE 3.1: Particle content for the different mechanisms examined here and its representation under the flavor group A_5 and CP. Note that all these fields should be understood as chiral superfields that contains a spin-0 and a spin-1/2 component.

where X_0 expressed in the **3** representation is

$$X_0 \;=\; P_{23} \;\equiv\; \begin{pmatrix} 1 & 0 & 0 \\ 0 & 0 & 1 \\ 0 & 1 & 0 \end{pmatrix}. \tag{3.10}$$

Its form in the rest of irreps of A_5 can be found in Appendix B.3.

3.3.1 Charged-lepton masses

Residual symmetries constrain the form of the flavon vevs that break the invariance under the family symmetry $\mathcal{G}_\ell$. Assuming that charged leptons are symmetric under the subgroup $\mathcal{G}_e = \mathbb{Z}_5$,

$$Q_{\mathbf{r}} \langle \phi_{\mathbf{r}}^{e} \rangle = \langle \phi_{\mathbf{r}}^{e} \rangle, \tag{3.11}$$

with the generators $Q_{\mathbf{r}}$ and the flavon fields $\phi_{\mathbf{r}}^{e}$ in the $\mathbf{r}$ representation, must be satisfied. The condition in Eq.(3.11) implies that non-zero vevs are possible only for the triplet and pentaplet representations and their form is forced to be[4]

$$\langle \phi_{\mathbf{3}}^{e} \rangle = \begin{pmatrix} \omega_3 \\ 0 \\ 0 \end{pmatrix}, \qquad \langle \phi_{\mathbf{3'}}^{e} \rangle = \begin{pmatrix} \omega_{3'} \\ 0 \\ 0 \end{pmatrix}, \qquad \langle \phi_{\mathbf{5}}^{e} \rangle = \begin{pmatrix} \omega_5 \\ 0 \\ 0 \\ 0 \\ 0 \end{pmatrix}, \tag{3.12}$$

[4]Here we just provide the form of the flavon vevs symmetric under the residual symmetry. In general, the scalar potential responsible for them, which we do not specify here, will require the presence of additional superfields.

where ω_3, $\omega_{3'}$ and ω_5 are real parameters. The flavons in Eq.(3.12) generate non-renormalizable operators that enter the superpotential and give rise to the charged lepton masses as discussed in Eq.(3.1),

$$W_\ell \supseteq W_e \;=\; W_e^{\rm ren} \;+\; L\, e^c\, H_d \sum_{n=1}^{\infty} x_n \left(\frac{\langle \phi^e \rangle}{M_\chi}\right)^n , \tag{3.13}$$

where we have not assumed any specific representation for the right-handed fields. The residual symmetry also imposes an invariance requisite under the (3×3) effective mass matrix:

$$Q_{\mathbf{3}}^\dagger\, m_e^\dagger\, m_e\, Q_{\mathbf{3}} = m_e^\dagger\, m_e, \tag{3.14}$$

where the generators are given in the triplet representation. A straightforward consequence of Eq.(3.14) is that $m_e^\dagger m_e$ must be diagonal in the basis where the set of generators of the group $\{Q_{\mathbf{r}}\}$ are diagonal. In our case, the generator of $G_e = \mathbb{Z}_5$ in the tuple of Eq.(3.9) is $Q = T$, which is diagonal according to Eq.(B.15). Therefore, the operators in Eq.(3.13) must produce a diagonal mass matrix at leading order (LO) (higher order corrections are discussed in Sec.3.3.4). Its elements should exhibit the correct hierarchy between generations:

$$m_e \;\propto\; \begin{pmatrix} \lambda_C^4 & 0 & 0 \\ 0 & \lambda_C^2 & 0 \\ 0 & 0 & 1 \end{pmatrix}, \tag{3.15}$$

where $\lambda_C = 0.2257$ stands for the Cabibbo angle. In order to keep our discussion as model-independent as possible, we do not suppose any specific mechanism responsible for this pattern. However, for completeness, we mention some possibilities that have been already proposed in the literature.

One way to generate the observed structure of masses for charged leptons is through processes like those depicted in Figure 3.3, where the effective mass of each generation involves a different number of flavon insertions. Each of them is proportional to the expansion parameter $\epsilon \equiv \langle \phi^e \rangle / M_\chi \ll 1$ that, in this specific case, might be $\epsilon \propto \lambda_C^2$. This type of diagrams can be easily arranged with an Abelian symmetry (continuous or discrete) assigning adequate quantum numbers to the lepton and flavon fields. Another strategy could be having a symmetry that is broken at separated scales. In this scenario, a natural hierarchy between the flavon vevs is expected. Notice that the χ heavy mediators involved in all these constructions may be generally left-handed (LH) or right-handed (RH) under $SU(2)_L$. In the absence of further hypothesis, we naturally expect all of them to be present and have masses of the same order.

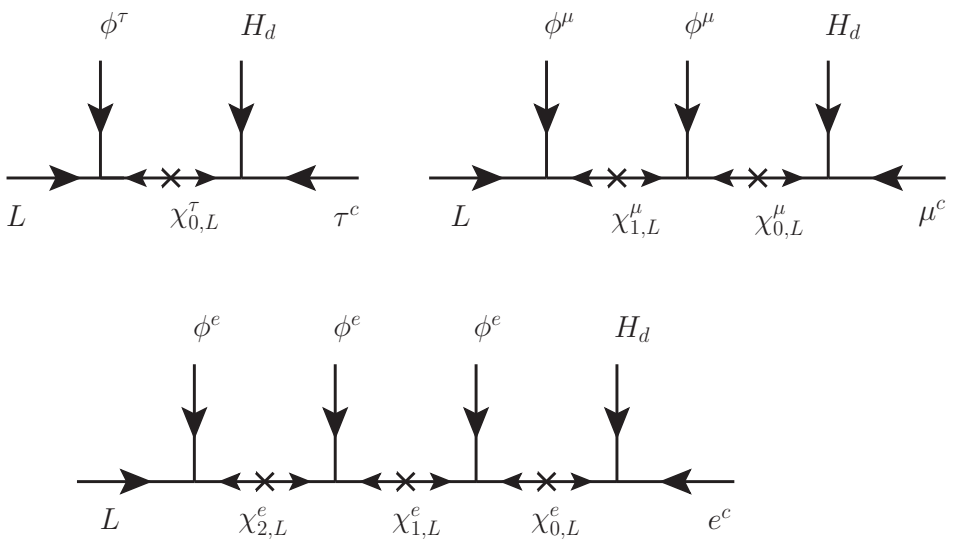

FIGURE 3.3: Example where the hierarchy in the charged-lepton sector is due to the number of flavon insertions: tau, muon and electron masses are generated by diagrams involving one, two and three flavons, respectively. In this specific example the heavy mediators are doublets under $SU(2)_L$.

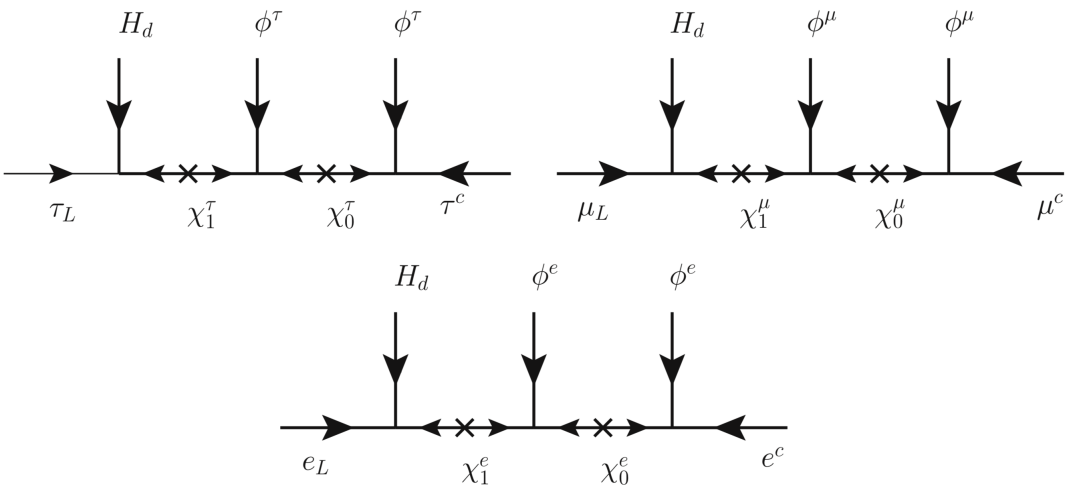

FIGURE 3.4: Example where the hierarchy for the charged-lepton masses comes from the flavon vevs that break the family symmetry at different scales. Then, $\langle\phi^e\rangle \ll \langle\phi^\mu\rangle \ll \langle\phi^\tau\rangle$ is expected. In this specific example the heavy mediators are singlets under $SU(2)_L$.

3.3.2 Neutrino masses

The residual symmetry in the neutrino sector, $\mathcal{G}_\nu = \mathbb{Z}_2 \times \text{CP}$, delimits the form of the light neutrino mass matrix m_ν through the following invariance conditions:

$$Z_{\mathbf{3}}^T \, m_\nu \, Z_{\mathbf{3}} \, = \, m_\nu \qquad \text{and} \qquad X_{\mathbf{3}} \, m_\nu \, X_{\mathbf{3}} \, = \, m_\nu^*, \tag{3.16}$$

where $Z_{\mathbf{3}}$ and $X_{\mathbf{3}}$ are the generators of $\mathbb{Z}_2$ and CP in the triplet representation. The texture of the matrix that satisfies Eq.(3.16) is

$$m_\nu = m_0^\nu \begin{pmatrix} s+x+z & \frac{3}{2\sqrt{2}}(z+i\varphi y) & \frac{3}{2\sqrt{2}}(z-i\varphi y) \\ \frac{3}{2\sqrt{2}}(z+i\varphi y) & \frac{3}{2}(x+iy) & s-\frac{x+z}{2} \\ \frac{3}{2\sqrt{2}}(z-i\varphi y) & s-\frac{x+z}{2} & \frac{3}{2}(x-iy) \end{pmatrix}, \tag{3.17}$$

where $\{s,\, x,\, y,\, z\}$ are dimensionless and real numbers, $\varphi = (1+\sqrt{5})/2$ is the GR and m_0^ν is the absolute mass scale for neutrinos. Similarly, the flavon vevs breaking the family symmetry in this sector must satisfy

$$Z_{\mathbf{r}} \, \langle \phi_{\mathbf{r}}^\nu \rangle \, = \, \langle \phi_{\mathbf{r}}^\nu \rangle \qquad \text{and} \qquad X_{\mathbf{r}} \, \langle \phi_{\mathbf{r}}^\nu \rangle^* \, = \, \langle \phi_{\mathbf{r}}^\nu \rangle, \tag{3.18}$$

where $\langle \phi_{\mathbf{r}}^\nu \rangle$ and the generators of $\mathbb{Z}_2$ and CP, $Z_{\mathbf{r}}$ and $X_{\mathbf{r}}$, are expressed in the $\mathbf{r}$ representation. The vacuum alignment is then subject to verify the general structure[5]:

$$\langle \phi_{\mathbf{1}}^\nu \rangle \, = \, v_1, \qquad \langle \phi_{\mathbf{3}}^\nu \rangle \, = \, v_3 \begin{pmatrix} -\sqrt{2}\varphi^{-1} \\ 1 \\ 1 \end{pmatrix}, \qquad \langle \phi_{\mathbf{3'}}^\nu \rangle = v_{3'} \begin{pmatrix} \sqrt{2}\varphi \\ 1 \\ 1 \end{pmatrix}, \tag{3.19}$$

$$\langle \phi_{\mathbf{4}}^\nu \rangle \, = \, \begin{pmatrix} y_r - iy_i \\ (1+2\varphi)y_r - iy_i \\ (1+2\varphi)y_r + iy_i \\ yr + iy_i \end{pmatrix}, \qquad \langle \phi_{\mathbf{5}}^\nu \rangle = \begin{pmatrix} -\sqrt{\frac{2}{3}}(x_r + x_{r,2}) \\ -x_r + i\varphi x_i \\ x_{r,2} - ix_i \\ x_{r,2} + ix_i \\ x_r + i\varphi x_i \end{pmatrix}, \tag{3.20}$$

[5] As for the charged leptons, we simply present the structure of the flavon vevs compatible with the residual symmetry in the neutrino sector. The scalar potential originating them, which we do not compute here, will generally involve additional superfields to those detailed in Table 3.1.

where all the coefficients are real.
Majorana neutrino masses can be generated through the so-called dimension 5 Weinberg operator, which is produced at tree level by type I, II or III see-saw mechanisms. Each case is related to the addition of one extra particle to the SM spectrum: RH neutrinos, a scalar triplet or a fermion triplet, respectively. In the effective low-energy theory some of these constructions are equivalent to others (a detailed discussion about this can be found in Appendix C of [29]) so that we can reduce the discussion to just two cases: Mechanism I, consisting of the Weinberg operator and type II see-saw, and Mechanism II, which includes type I and III see-saw realizations. In the following, we specify the operators generating the neutrino masses for each mechanism. The quantum numbers of the fields for each scenario are displayed in Table 3.1, where the nomenclature of [29] has been conserved.

Mechanism I

Here we consider neutrino masses generated by the Weinberg operator. In this case, a lepton doublet ℓ transforming as the **3** or the **3′** representation produces the same phenomenological results under a redefinition of the parameters as indicated in [29]. Therefore, without loss of generality, one may simply consider $L \sim \mathbf{3}$. The LO contributions to the effective superpotential responsible for the neutrino masses are:

$$W_\ell \supset W_\nu^{\mathrm{I}} \;=\; y_1^\nu \frac{\left[L^2 H_u^2 \phi_{\mathbf{1}}^\nu\right]_{\mathbf{1}}}{M_\chi^2} \;+\; y_5^\nu \frac{\left[L^2 H_u^2 \phi_{\mathbf{5}}^\nu\right]_{\mathbf{1}}}{M_\chi^2}, \tag{3.21}$$

where y_i^ν are dimensionless parameters and brackets mean that different contractions are possible. In the low-energy theory all of them are equivalent, since they give rise to the same predictions. However, as can be seen in Figure 3.5, the mediator sector involved in each process is very different and thereby their ultraviolet (UV) origin: while in the first diagram the heavy messengers are both LH and RH, the second process considers RH fields and the last one scalar triplets. In the absence of additional hypothesis about the high-energy theory, all these mediators are present and have similar masses, M_χ.
Once the flavor symmetry is broken, the mass matrix in Eq.(3.17) is generated with

$$s \propto y_1^\nu \frac{v_1}{M_\chi} \qquad x \propto -y_5^\nu \frac{x_{r,2}}{M_\chi} \qquad y \propto -y_5^\nu \frac{x_i}{M_\chi} \qquad z \propto -y_5^\nu \frac{x_r}{M_\chi}, \tag{3.22}$$

where v_1 and $\{x_i,\, x_r,\, x_{r,2}\}$ are the vevs of the singlet and pentaplet flavons respectively, see Eqs.(3.19) and (3.20).

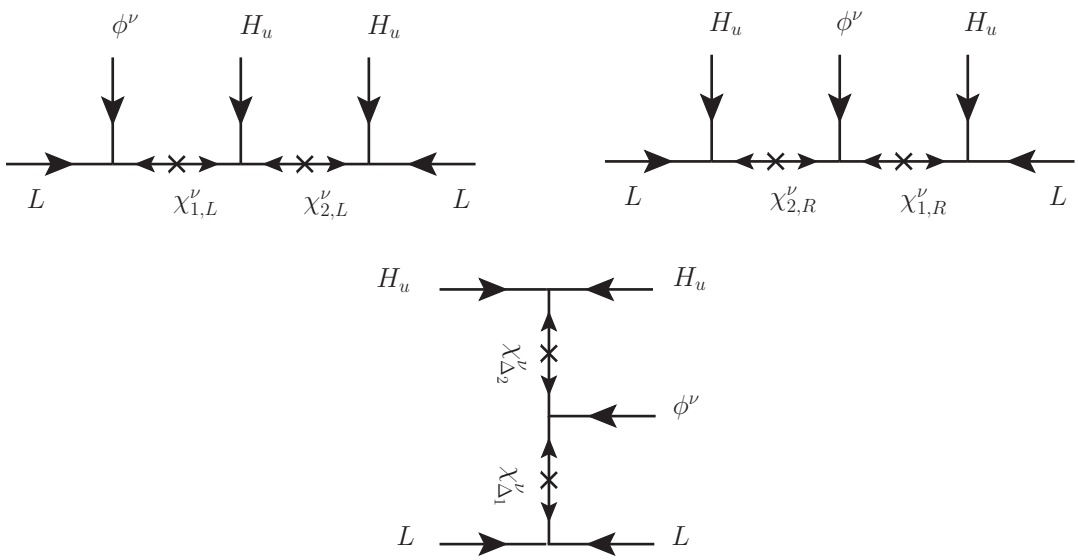

FIGURE 3.5: Different contractions generating the Weinberg Operator of Mechanism I in Sec.3.3.2. The first diagram involves $SU(2)_L$ doublets and singlets as mediators whereas the second and third only require singlets or triplets. The phenomenological implications in each case are different.

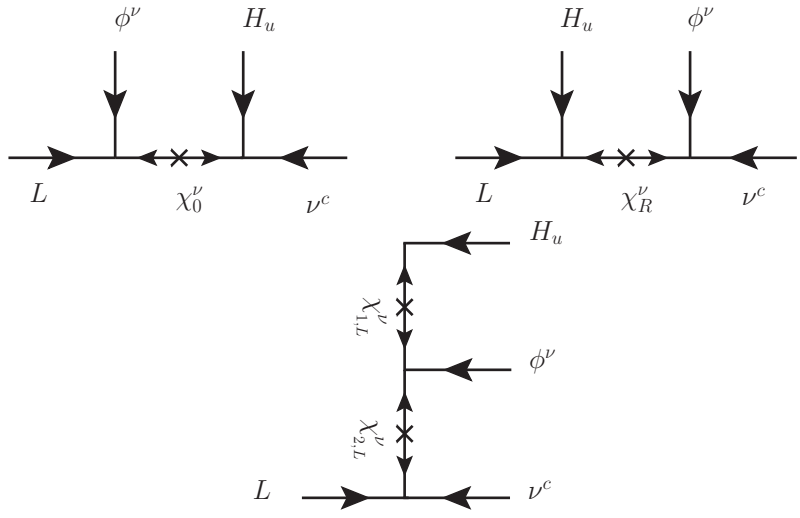

FIGURE 3.6: Different contractions generating the Dirac mass matrix of Mechanism II *a*-2 and *c*-2 in Sec.3.3.2. The first and third diagrams involve $SU(2)_L$ doublets as mediators whereas the second requires singlets. The phenomenological implications in each case are different.

Mechanism II

The type I see-saw formulation is investigated in Mechanism II. Two different situations are analyzed in this framework: both L and ν^c transform in the same triplet representation (II *a*-2) or in opposite ones (II *c*-2). The specific choice, $L \sim \mathbf{3}$ or $L \sim \mathbf{3'}$, does not affect the resulting phenomenology. Therefore, $L \sim \mathbf{3}$ is always assumed. Here we consider a trivial Majorana matrix, namely $M_N = MP_{23}$, with P_{23} defined in Eq.(3.10), while the Dirac mass matrix, Y_ν, is more complicated. The opposite option, non-trivial Majorana mass and trivial Dirac matrix, does not introduce observable effects in the LFV observables examined in the following section, hence we do not discuss this possibility further.
The effective operators entering the superpotential that produces the Dirac mass are:

$$\begin{aligned} W_\ell \supset W_\nu^{\mathrm{II}a2} &= Y_1^\nu \left[\nu^c L\right]_{\mathbf{1}} H_u + y_1^\nu \frac{\left[\nu^c L\, \phi_{\mathbf{1}}^\nu\right]_{\mathbf{1}} H_u}{\Lambda} \\ &+ y_3^\nu \frac{\left[\nu^c L\, \phi_{\mathbf{3}}^\nu\right]_{\mathbf{1}} H_u}{\Lambda} + y_5^\nu \frac{\left[\nu^c L\, \phi_{\mathbf{5}}^\nu\right]_{\mathbf{1}} H_u}{\Lambda} + \text{c.c.} \end{aligned} \tag{3.23}$$

for Mechanism II *a*-2, and

$$W_\ell \supset W_\nu^{\mathrm{II}c2} = y_4^\nu \frac{\left[\nu^c L\, \phi_{\mathbf{4}}^\nu\right]_{\mathbf{1}} H_u}{\Lambda} + y_5^\nu \frac{\left[\nu^c L\, \phi_{\mathbf{5}}^\nu\right]_{\mathbf{1}} H_u}{\Lambda} + \text{c.c.} \tag{3.24}$$

for Mechanism II *c*-2. Again the brackets indicate that different contractions are possible. Figure 3.6 shows the UV origin of each of them involving LH mediators, RH mediators and triplets under $SU(2)_L$. Once the flavor symmetry is broken, the neutrino mass matrix is generated through the usual type I see-saw process,

$$m_\nu = -Y^\nu M_N^{-1} Y^{\nu T} = -\frac{1}{M} Y^\nu P_{23}^{-1} Y^{\nu T}. \tag{3.25}$$

The coefficients $\{s, x, y, z\}$ entering m_ν as in Eq.(3.17) are intricate linear combinations of the dimensionless parameters:

$$f \propto Y_1 + y_1^\nu \frac{v_1}{M_\chi} \quad g \propto y_3^\nu \frac{v}{M_\chi} \quad h_r \propto y_5^\nu \frac{x_r}{M_\chi} \quad h_i \propto y_5^\nu \frac{x_i}{M_\chi} \quad h_{r,2} \propto y_5^\nu \frac{x_{r,2}}{M_\chi} \tag{3.26}$$

for Mechanism II *a*-2, and

$$f_r \propto y_4^\nu \frac{y_r}{M_\chi} \quad f_i \propto y_4^\nu \frac{y_i}{M_\chi} \quad h_r \propto y_5^\nu \frac{x_r}{M_\chi} \quad h_i \propto y_5^\nu \frac{x_i}{M_\chi} \quad h_{r,2} \propto y_5^\nu \frac{x_{r,2}}{M_\chi} \tag{3.27}$$

for Mechanism II *c*-2.

3.3.3 Lepton Mixing

The $V_{\rm PMNS}$ is the matrix that measures the misalignment between the rotations of LH charged-leptons and neutrinos to the mass basis. It is defined as

$$V_{\rm PMNS} \;=\; V_L^{e\dagger}\, V_L^{\nu}\,. \tag{3.28}$$

The conservation of CP and residual transformations determine the form of this matrix up to permutations of rows and columns. In our case, the residual symmetry in the charged sector indicates that for $\mathcal{G}_e = \mathbb{Z}_5$ generated by $Q = T$ diagonal, the unitary rotation to the mass basis for LH charged leptons V_L^e is the identity. Therefore the $V_{\rm PMNS}$ will be determined only by the neutrino mixing at LO. The unitary transformation that diagonalizes the neutrino mass matrix in Eq.(3.17) is [33]

$$V_{\rm PMNS} = \Omega_\nu\, R_{13}(\theta)\, K_\nu\,, \tag{3.29}$$

where Ω_ν defines a change of basis that block-diagonalizes the initial matrix in Eq.(3.17) and it is directly related to the GR mixing, $R_{13}(\theta)$ is a rotation of an angle θ in the $1-3$ plane and K_ν is a diagonal matrix with entries $\{\pm 1, \pm i\}$ needed to have positive eigenvalues. The explicit form of the matrix Ω_ν is

$$\Omega_\nu = \frac{1}{\sqrt{2}} \begin{pmatrix} \sqrt{2}\cos\phi & \sqrt{2}\sin\phi & 0 \\ \sin\phi & -\cos\phi & i \\ \sin\phi & -\cos\phi & -i \end{pmatrix}, \tag{3.30}$$

with $\sin\phi \equiv 1/\sqrt{1+\varphi^2}$ and $\cos\phi \equiv \varphi\sqrt{/(1+\varphi^2)}$. The rotation is given by

$$R_{13}(\theta) \;=\; \begin{pmatrix} \cos\theta & 0 & \sin\theta \\ 0 & 1 & 0 \\ -\sin\theta & 0 & \cos\theta \end{pmatrix}, \tag{3.31}$$

where the size of the angle θ is totally fixed by the entries of the block-diagonalized mass matrix. In our case:

$$\tan 2\theta \;=\; \frac{2\sqrt{2+\varphi}\, y}{2\,x+z}. \tag{3.32}$$

Mixing angles and complex phases can be directly extracted from Eqs.(3.29)$-$(3.32) using the standard $V_{\rm PMNS}$ parametrization that we detail in Appendix D.1. The

reactor angle is proportional to the angle θ as:

$$\sin^2\theta_{13} \;=\; \frac{2+\varphi}{5}\,\sin^2\theta. \tag{3.33}$$

Eq.(3.33) implies that a small value of θ is required in order to reproduce $\theta_{13}\sim 9^\circ$. Indeed, $\theta_{\rm bf}=0.175$ has been found as the best fit value for this realization in [26]. Inspecting Eq.(3.32), one may see that such a tiny value for θ can only be obtained considering the following hierarchy among vevs[6]: $y \ll x, z, s$.
The atmospheric angle is predicted to be maximal, $\sin^2\theta_{23}=1/2$, and the solar angle is related to the reactor angle through the sum rule:

$$\sin^2\theta_{12} \;=\; \frac{3-\varphi}{5\cos^2\theta_{13}} \;\simeq\; \frac{0.276}{\cos^2\theta_{13}} \tag{3.34}$$

CP invariants and complex phases are also predicted in this framework. The Jarlskog invariant [40] is

$$J_{\rm CP} \;=\; \frac{1}{8}\sin 2\theta_{12}\sin\theta_{23}\sin 2\theta_{13}\cos\theta_{13}\sin\delta \;=\; -\frac{\sqrt{2+\varphi}}{20}\,\sin 2\theta. \tag{3.35}$$

The Dirac phase δ can be inferred from Eq.(3.35) and it is maximal, $|\sin\delta|=1$. The other CP invariants, defined as

$$I_1 \;\equiv\; {\rm Im}\left[V_{12}V_{12}V_{11}^*V_{11}^*\right] = \sin^2\theta_{12}\cos^2\theta_{12}\cos^4\theta_{13}\sin\alpha \tag{3.36}$$

$$I_2 \;\equiv\; {\rm Im}\left[V_{13}V_{13}V_{11}^*V_{11}^*\right] = \sin^2\theta_{13}\cos^2\theta_{12}\cos^2\theta_{13}\sin\beta, \tag{3.37}$$

vanish exactly. Hence Majorana phases, α and β, must be 0 or π.

3.3.4 Next-to-Leading Order Corrections

Notice that Eqs.(3.12) and (3.19)-(3.20) indicate that the LO masses of the neutral and charged leptons must be induced by two separate set of flavons. In practice, this division can be always ensured introducing an additional $\mathbb{Z}_N$ symmetry that

[6] A natural way of obtaining this hierarchy is through the two step symmetry breaking $\mathcal{G}_\ell \to \mathcal{G}_\nu = \mathbb{Z}_2\times\mathbb{Z}_2\times{\rm CP} \to \mathbb{Z}_2\times{\rm CP}$ as explained in [29].

distinguishes among them at LO[7]. However, at higher orders, flavons belonging to the opposite sector (the *wrong* flavons) are allowed to enter the LO diagrams and may introduce sizable corrections. In this section we comment how these effects can be adequately taken into account.

The NLO corrections to the leading predictions of masses and mixing usually come from higher-order operators that enter the scalar potential and the superpotential. The former induce a shift in the flavon vevs while the latter is usually generated by extra flavon insertions to the LO operators. As commented before, some of these insertions may be due to the *wrong*-flavons. For neutrinos, one may check that these contributions are usually subleading. Assuming that the heavy fields χ mediating the diagrams in both sectors have masses of the same order, corrections to the neutrino mass matrix are of the form

$$\delta m_\nu \sim \lambda_C^2\, m'_\nu, \tag{3.38}$$

where m'_ν is a 3×3 matrix with elements given in terms of the $\{s,\, x,\, y,\, z\}$ parameters defined in Eq.(3.17). Therefore, barring accidental cancellations in the LO elements which may make the NLO terms dominant, we expect these corrections to be mostly subleading.

Similarly, a suitable choice of charge assignments under a $\mathbb{Z}_N$ symmetry can guarantee that insertions of the neutrino flavons to the charged sector are also subleading. For instance, if the following set of charges are considered

$$N_{\phi^\tau} = N_{\phi^\mu} = N_{\phi^e} = k \quad \text{and} \quad N_{\phi^\nu} = 1, \tag{3.39}$$

such that $\mathcal{Q}_{\mathbb{Z}_N}(\phi) = e^{i\,2\pi N_\phi/N}$, it is easy to see that one charged-lepton flavon could only be substituted by k neutrino-flavon insertions[8]. Then, in its most general form,

[7] For instance, considering the diagrams in Figure 3.4 and the first diagram in Figure 3.6 as the responsible mechanisms for lepton masses, one may see that the charges discriminating both sectors would be:

$$\begin{aligned} N_{\chi^l_n} &= N_{H_l} + N_{\ell^c} + nN_{\phi_l} - (n+1)N\,, \\ N_{\phi^e} &= (3N - N_\ell - N_{H_d} - N^c_e)/2\,, \\ N_{\phi^\nu} &= 2N - N_\ell - N_{H_u} - N^c_\nu\,, \end{aligned}$$

with $\ell \equiv \{e,\mu,\tau,\nu\}$. For the remaining cases, similar assignments can be done.

[8] For the diagrams in Figures 3.4 and 3.5 (Mechanism I), the charges of the flavons in Eq.(3.39) can be easily obtained solving the equation system:

$$\begin{aligned} N_{\phi^\nu} &= N - 2\,N_\ell - 2\,N_{H_u} &&= 1\,, \\ N_{\phi^\tau} &= N_{\rm CL} - N_{\tau^c} &&= k\,, \\ N_{\phi^\mu} &= (N_{\rm CL} - N_{\mu^c})/2 &&= k\,, \\ N_{\phi^e} &= (N_{\rm CL} - N_{e^c})/3 &&= k, \end{aligned}$$

corrections to the charged-lepton mass matrix will be given by

$$\delta m_e \sim \left(\frac{\langle \phi^{\nu} \rangle}{M_{\chi}}\right)^k \begin{pmatrix} 1 & 1 & 1 \\ 1 & 1 & 1 \\ 1 & 1 & 1 \end{pmatrix} . \tag{3.40}$$

Adjusting the value of k, the required suppression can always be obtained.

3.4 Kähler Potential and Soft Terms

In Sec.3.2, the main consequences of embedding a flavor symmetry in supersymmetric theories where $\Lambda_{\rm Med} \gg \Lambda_f$ have been discussed, see also [20–24]. Even in the most conservative case where SUSY breaking is parametrized by a single universal spurion field, *tree-level* flavor violating effects generally arise from the mismatch between the order one coefficients in the soft-breaking structures and the Yukawa and kinetic terms due to the different equivalent options of inserting this spurion field [20]. Moreover, we observe that, in the absence of further hypothesis over the UV spectrum, the common origin of the flavor structures for charged leptons and neutrinos may induce testable relations between observables belonging to these two sectors. Finally, we notice that, for some configurations, significant corrections from the Kähler potential emerge that break the residual symmetries and could modify the LO predictions. This fact is independent of SUSY and it actually corresponds to the usual wave-function renormalization that should always be taken into account [24, 41–44].

3.4.1 Kähler corrections

The effective Kähler potential for a multiplet ψ of A_5 and CP can be schematically written as

$$K \;=\; \psi_i^{\dagger}\psi_j \left[\, \delta_{ij} + \sum_{n,a,b} c^{n}_{ij\,ab} \left(\frac{\langle \phi^{\ell\,\dagger}_{\mathbf{r}_a} \rangle \, \langle \phi^{\ell}_{\mathbf{r}_b} \rangle}{M_{\chi}}\right)^n \right] , \tag{3.41}$$

with $\ell = e, \nu$ and M_{χ} the generic mass of the χ heavy mediators. The specific terms entering the sum depend on the symmetries of the model. We are interested in the Kähler potential for lepton doublets and singlets. Under no further assumptions, we

with $N_{\rm CL} = N - N_{H_d} - N_{\ell}$. For other cases, one may proceed in a similar way.

can at least write the following terms for the former:

$$K_L = \left[1+\frac{1}{M_\chi^2}\sum_{\mathbf{r}}\left(\phi_{\mathbf{r}}^{e\dagger}\,\phi_{\mathbf{r}}^{e}+\phi_{\mathbf{r}}^{\nu\dagger}\,\phi_{\mathbf{r}}^{\nu}\right)+\dots\right]\times \left[L^\dagger L+\frac{1}{M_\chi^2}\sum_{\mathbf{r}}\left(\left[L^\dagger\phi_{\mathbf{r}}^{e\dagger}\right]_{\mathbf{1}}\left[L\phi_{\mathbf{r}}^{e}\right]_{\mathbf{1}}+\left[L^\dagger\phi_{\mathbf{r}}^{\nu\dagger}\right]_{\mathbf{1}}\left[L\phi_{\mathbf{r}}^{\nu}\right]_{\mathbf{1}}\right)+\dots\right], \tag{3.42}$$

where dots stand for higher order terms in the same fashion and the sum in $\mathbf{r}$ accounts for the flavons at work depending on the mechanism, see Table 3.1. The first line is associated with singlet contractions that contribute to every element of the Kähler metric, so they can be factorized as a global constant. The second line corresponds to non-trivial contractions and generates off-diagonal entries in the Kähler metric. Note that, being $\phi\phi^\dagger$ combinations, all terms in Eq.(3.42) are neutral under any possible charge. Hence, they cannot be avoided and must be adequately taken into account. The Kähler function for RH charged-leptons can be written as:

$$K_{R,e} = \left[1+\frac{1}{M_\chi^2}\sum_{\forall\mathbf{r}}\phi_{\mathbf{r}}^{e\dagger}\,\phi_{\mathbf{r}}^{e}+\cdots\right]\times \left[e^{c\,\dagger}e^{c}+\frac{1}{M_\chi^2}\sum_{\forall\mathbf{r}}\left[e^{c\,\dagger}\phi_{\mathbf{r}}^{e\dagger}\right]_{\mathbf{1}}\left[e^{c}\phi_{\mathbf{r}}^{e}\right]_{\mathbf{1}}+\cdots\right]. \tag{3.43}$$

In contrast to the previous case, here only the flavons associated with charged leptons contribute. An analogous expression can be written for RH neutrinos replacing $\phi^e \to \phi^\nu$ and $e^c \to \nu^c$.

The Kähler structures in Eqs.(3.42) and (3.43) can be explicitly computed simply by inserting the flavon vevs in Eqs.(3.12) and (3.19)-(3.20). The results are rather intricate, so we omit them here. We find that the charged-lepton flavons only contribute to the diagonal of the Kähler metric, while neutrino flavons also induce off-diagonal entries. Because of that, a redefinition of the fields is required in order to go to the physical basis where the kinetic terms are canonical, that is $\widehat{K}=\mathbb{1}$. This can be always achieved making use of an upper triangular matrix that decomposes the Hermitian Kähler metric as $K = T^\dagger T$ [42] (see Appendix A.1.3):

$$\widehat{\psi} \quad\longrightarrow\quad \widehat{\psi} = T\,\psi \;/\quad \psi^\dagger K\,\psi = \widehat{\psi}^\dagger\,\widehat{\psi} \tag{3.44}$$

The upper triangular matrix T defined by Eq.(3.44) has the schematic form

$$T \simeq \begin{pmatrix} 1+\epsilon_{11}^2 & \epsilon_{12}^2 & \epsilon_{13}^2 \\ 0 & 1+\epsilon_{22}^2 & \epsilon_{23}^2 \\ 0 & 0 & 1+\epsilon_{33}^2 \end{pmatrix}, \tag{3.45}$$

where ϵ_{ij}^2 are complex entries linearly dependent on the flavon vevs squared. In our case, the size of these entries may vary from 10^{-7} up to 10^{-2}, depending on the mechanism[9]. The field redefinition to the canonical basis affects the lepton masses in Eqs.(3.15) and (3.17), which should be rotated as:

$$m_e \longrightarrow \widehat{m}_e = \left(T^{-1}\right)^\dagger m_e\, T^{-1}, \tag{3.46}$$

$$m_\nu \longrightarrow \widehat{m}_\nu = \left(T^{-1}\right)^T m_\nu\, T^{-1}. \tag{3.47}$$

Initially, the charged leptons in the non-canonically normalized flavor basis satisfy that $m_e^\dagger\, m_e$ is diagonal and hierarchical. The canonical rotation introduces corrections to the product in Eq.(3.15) as:

$$m_e^\dagger\, m_e \longrightarrow \widehat{m}_e^\dagger \widehat{m}_e \simeq \begin{pmatrix} \lambda_C^8 & \epsilon_{12}^2\,\lambda_C^8 & \epsilon_{13}^2\,\lambda_C^8 \\ . & \lambda_C^4 & \epsilon_{23}^2\,\lambda_C^4 \\ . & . & 1 \end{pmatrix}. \tag{3.48}$$

The corrected diagonalizing matrix at LO is then

$$V_L^e \longrightarrow \widehat{V}_L^e = V_L^e + \delta V_L^e \simeq \begin{pmatrix} 1 & \epsilon_{12}^{2^\star}\,\lambda_C^4 & \epsilon_{13}^{2^\star}\,\lambda_C^8 \\ -\epsilon_{12}^2\,\lambda_C^4 & 1 & \lambda_C^8 \\ -\epsilon_{13}^2\,\lambda_C^8 & -\lambda_C^8 & 1 \end{pmatrix}. \tag{3.49}$$

It enters the new $V_{\rm PMNS}$ but does not introduce sizable modifications to the initial angles. This is in agreement with [42], where the authors analyzed the effects of the canonical rotation for hierarchical Yukawa matrices.

The situation for neutrinos is slightly more involved because their mass matrix is not completely hierarchical and analytical expressions accounting for these effects are

[9] Notice that this upper-triangular form ensures that the corrections of canonical normalization are always subleading for hierarchical matrices.

difficult to obtain. We expect that corrections from the canonical rotation are important when affecting small quantities, such as the reactor angle or the lightest mass for a very hierarchical spectrum, and in those cases where the neutrino spectrum has two or more quasi-degenerated masses, since small contributions can modify the ordering. Numerically, this has been confirmed: while the correlations among vevs obtained in [29] approximately remain after the canonical rotation, the range of possible values for the free parameters is significantly reduced because of these effects[10].

3.4.2 Soft-breaking Masses

Once we have the Kähler potential, the soft-breaking masses before canonical normalization can be obtained just examining the effective operators in K_Ψ, as detailed in Sec.3.2. At LO, the soft-mass matrices are proportional, element by element, to the Kähler metric, see Eq.(3.4), and the proportionality factor, f_{ij}, accounts for the different ways in which the spurion F-term F_X can be inserted in the representative Kähler diagram [20, 21]. In our case:

$$\begin{aligned}
\widetilde{m}^2_L &= m_0^2 \left[L^\dagger L + \frac{2}{M_\chi^2} \sum_{\mathbf{r}} \left(\left[L^\dagger \phi^{e\dagger}_{\mathbf{r}} \right]_{\mathbf{1}} \left[L \, \phi^e_{\mathbf{r}} \right]_{\mathbf{1}} + \left[L^\dagger \phi^{\nu\dagger}_{\mathbf{r}} \right]_{\mathbf{1}} \left[L \, \phi^\nu_{\mathbf{r}} \right]_{\mathbf{1}} \right) + \cdots \right], \\
\widetilde{m}^2_{R,e} &= m_0^2 \left[e^{c\,\dagger} e^c + \frac{2}{M_\chi^2} \sum_{\forall \mathbf{r}} \left[e^{c\,\dagger} \phi^{e\dagger}_{\mathbf{r}} \right]_{\mathbf{1}} \left[e^c \phi^e_{\mathbf{r}} \right]_{\mathbf{1}} + \cdots \right].
\end{aligned} \tag{3.50}$$

Going to the canonical basis,

$$\widetilde{m}^2 \longrightarrow \widehat{\widetilde{m}}^2 = \left(T^{-1} \right)^\dagger \widetilde{m}^2 \, T^{-1}, \tag{3.51}$$

and then to the mass basis,

$$\widehat{\widetilde{m}}^2 \longrightarrow \widehat{V}_e^\dagger \, \widehat{\widetilde{m}}^2 \, \widehat{V}_e \,, \tag{3.52}$$

one observes that some off-diagonal terms in the LH soft mass matrix of Eq.(3.52) survive the rotations. They can manifest in LFV processes such as $\ell_i \to \ell_j \, \gamma$, $\ell_i \to 3 \, \ell_j$ or $\mu - e$ conversion. Moreover, since the LFV contributions for LH charged-sleptons and the neutrino flavor structure arise from the same flavons, testable relations between observables from each sector can be inferred. On the other hand, RH charged

[10] Notice, however, that these corrections will affect only the determination of the parameters of a given model from the experimental results. Almost always these variations lead to no measurable effects on the observable predictions.

leptons do not receive observable corrections to their soft masses since they are generated by the flavons in Eq.(3.12), which only contribute to the diagonal. As previously discussed for the Kähler potential, they can simply be reabsorbed through a redefinition of the fields.

3.5 Predictions on flavor observables

Here we perform a combined analysis of the phenomenology of charged leptons and neutrinos for the two mechanisms exposed in Sec.3.3.2. Following the strategy of [29], each case is divided in several subcases, where one (Mechanism I) of two (Mechanism II) vevs of the active neutrino flavons are set to zero[11]. This allows to reduce the number of independent parameters and to inspect relations among the vevs that correctly reproduce the neutrino properties showed in Table I.1. We make predictions for the total sum of the light neutrino masses, the effective mass $m_{\beta\beta}$ and the flavor changing processes collected in Table I.6. Our numerical scan is realized as follows:

- First, we randomly generate the independent parameters corresponding to each mechanism in a range $[-1,+1]$, Eqs.(3.22, 3.26, 3.27). Then, we compute the light neutrino mass matrix m_ν in Eq.(3.17), the Kähler metric in Eq.(3.42) and the soft masses in Eq.(3.50). The mass matrix for charged leptons is assumed to be like in Eq.(3.15).

- The structures obtained before have to be rotated to the canonical basis as indicated in Eqs.(3.46, 3.47, 3.51). After that, the lepton mass matrices are diagonalized and re-phased to obtain real and positive eigenvalues.

$$\widehat{V}_L^{\nu\dagger}\,\widehat{m}_\nu^\dagger \widehat{m}_\nu\,\widehat{V}_L^{\nu} = \mathrm{diag}(m_1^2, m_2^2, m_3^2)\,, \tag{3.53}$$

$$\widehat{V}_L^{e\dagger}\,\widehat{m}_e^\dagger \widehat{m}_e\,\widehat{V}_L^{e} = \mathrm{diag}(m_e^2, m_\mu^2, m_\tau^2)\,. \tag{3.54}$$

  At this stage, the $V_{\rm PMNS}$ defined as in Eq.(3.28), with $V^\ell \to \widehat{V}^\ell$, and the mass splittings[12], $\Delta m^2_{21} = m_2^2 - m_1^2$ and $\Delta m^2_{3j} = m_3^2 - m_j^2$ with $j = 1$ for Normal

[11] In many situations, that is equivalent to leave out some of the flavons in a model; if not, it could be arranged working out the correspondent vacuum alignment that produces it.

[12] We assume that RGEs effects for the neutrino parameters are negligible so that our observables computed at high scales, $\Lambda \simeq 10^{14} - 10^{16}$ GeV, can be directly compared with the data in Table I.1. Although this is the case for a hierarchical neutrino spectrum, it is not necessarily true for degenerate masses [45]. However, in our case, the degenerate scenarios correspond to those subcases that are already disfavored by cosmological bounds.

Hierarchy (NH) and $j = 2$ for Inverted Hierarchy (IH), are checked to be in the 3σ-allowed region for both hierarchies, see Table I.2.

- For those points which correctly reproduce lepton masses and mixing in the 3σ region, we fix the value of m_0^ν comparing with the best fit result for Δm^2_{21}. The value of m_0^ν is expected to be some eV at most, so we discard points that correspond to $m_0^\nu > 5$ eV.
- The soft mass matrices are evolved from the GUT to the EW scale by means of the MSSM renormalization group equations and the branching ratios for the lepton flavor violating observables in Table I.2 are computed[13]. We also provide estimations for the total sum of light neutrino masses and the effective mass $m_{\beta\beta}$.

3.5.1 Neutrinos

For the neutrino sector, we follow the analysis performed in [29]. The results are displayed in Figure 3.7, where the effective neutrino mass $m_{\beta\beta}$ is plotted against the minimum neutrino eigenvalue, that is $m_{\text{min}} \equiv m_1$ for NH and $m_{\text{min}} \equiv m_3$ for IH. The upper panel reproduces the estimations presented in [29] whilst the lower panel shows the effect of rotating to the canonical basis where the Kähler is the identity. Blue points are related to Mechanism I, where neutrino masses are produced by the Weinberg operator or type II see-saw. Red points to Mechanism II *a*-2, corresponding to type I and III see-saw with trivial Majorana matrix and left- and right-handed neutrinos transforming in the same triplet representation. Green points are associated with Mechanism II *c*-2, which considers the same framework as Mechanism II *a*-2 but with the lepton doublet and the neutrino singlet transforming in different triplet representations. According to [29], each case is divided in several subcases where one (Mechanism I) or two (Mechanism II) flavon vevs are set to zero. Each subcase allows for NH, IH or both of them. For Mechanism I, we have three subcases corresponding to $z = 0$, $x = 0$ and $s = 0$. For Mechanism II *a*-2, a total of six subcases are studied: $f = 0$, $h_r = 0$ and $h_{r,2} = 0$ with either $h_i = 0$ or $g = 0$. Finally, Mechanism II *c*-2 consists of six more cases: $f_i = 0$, $h_r = 0$ and $h_{r,2} = 0$ with either $h_i = 0$ or $f_r = 0$. For conciseness we identify the different cases with the first vev and specify the second vev only when necessary. In addition, we use the subscripts "N" and "I" as shorthand notation for NH and IH.

[13] Numerical calculations for the running, spectrum and low-energy processes have been performed through the Supersymmetric Phenomenology package (SPheno) [46], together with the SARAH Mathematica package [47] for the generation of the source code.

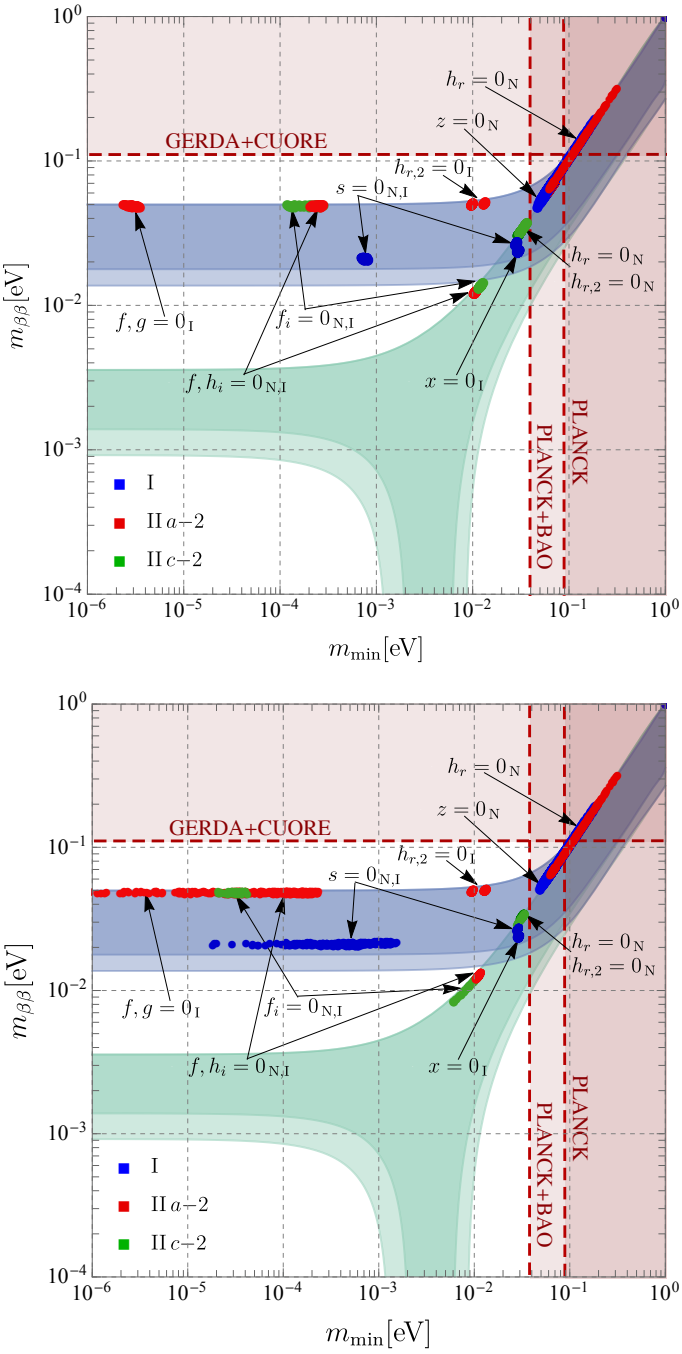

FIGURE 3.7: The observable $m_{\beta\beta}$ against $m_{\rm min}$. The (bottom) top panel corresponds to the assumption of UV LH-mediators originating (non-)negligible corrections to the Kähler metric. Blue points correspond to Mech. I, red points to Mech. II *a*-2 and green points are due to Mech. II *c*-2. The green and blue shadows are the ones allowed for NO and IO respectively. Red shaded regions are already excluded by experimental observations.

From Figure 3.7 we conclude that the scenarios $z = 0_{\rm N}$ of Mechanism I and $h_r = 0_{\rm N}$ of Mechanism II a-2 are incompatible with the latest data from `Planck` + BAO, while other cases like Mechanism I with $s = 0_{\rm N}$ and $x = 0_{\rm I}$ or Mechanism II with $h_r = 0_{\rm N}$ and $h_{r,2} = 0_{\rm N}$ could be tested in the future with further cosmological data. As shown in Table I.2, future sensitivity in neutrinoless double beta decay experiments could probe those realizations that predict IH and the region for quasi-degenerate masses with a sensitivity $m_{\beta\beta} = (0.01 \div 0.05)$ eV (for reviews see [48, 49]).
Comparing upper and lower panels of Figure 3.7, it is evident that the predictions on $m_{\rm min}$ for some subcases change significantly and result in being extended by one or two orders of magnitude. That happens for those hierarchical subcases where the smallness of $m_{\rm min}$ make it more susceptible to higher order corrections from the canonical rotation. Significant cancellations between leading and higher order terms happen in Mechanism I with $s = 0_{\rm I}$, Mechanism II a-2 with $f = 0_{\rm I}$, and Mechanism II c-2 with $f_i = 0_{\rm N}$, see the second plot of Figure 3.7. However, note that a direct measurement of $m_{\rm min}$ is of no feasible pursue in the near future. From this point of view, $m_{\rm min}$ can be considered as much as an additional model parameter so we may conclude that the canonical rotation has no substantial consequences on the testable predictions of the model in [29]. The two exceptions to this are the subcases Mechanism II a-2 with $\{f, h_i\} = 0_{\rm N}$ and Mechanism II c-2 $f_i = 0_{\rm N}$ where, with enough resolution, a small discrepancy with the predictions in [29] for $m_{\beta\beta}$ may be experimentally found.

3.5.2 Charged Leptons

It has been pointed out in previous works the importance of correctly account for the flavor effects that emerge from the inclusion of a flavor symmetry in SUSY [20–22]. On the one hand, it allows for a characterization of the flavor models of interest through their contributions to flavor-changing (FC) observables while, on the other hand, the search for experimental signals on those processes will help us to explore the SUSY spectrum at energies that go far beyond the LHC high-luminosity upgrade. In this section we follow the strategy in [21] and we study the flavor contributions arising from the breaking of A_5 and CP in the LFV observables collected in Table I.6. The structure of the soft mass matrix for LH fields is given in Eq.(3.50). We compute its numerical value for each of the points that reproduce the neutrino experimental parameters in the 3σ region, Table I.2, plus the `Planck` bound on the total sum of light neutrino masses, Table I.2. The range of possible values for the off-diagonal entries

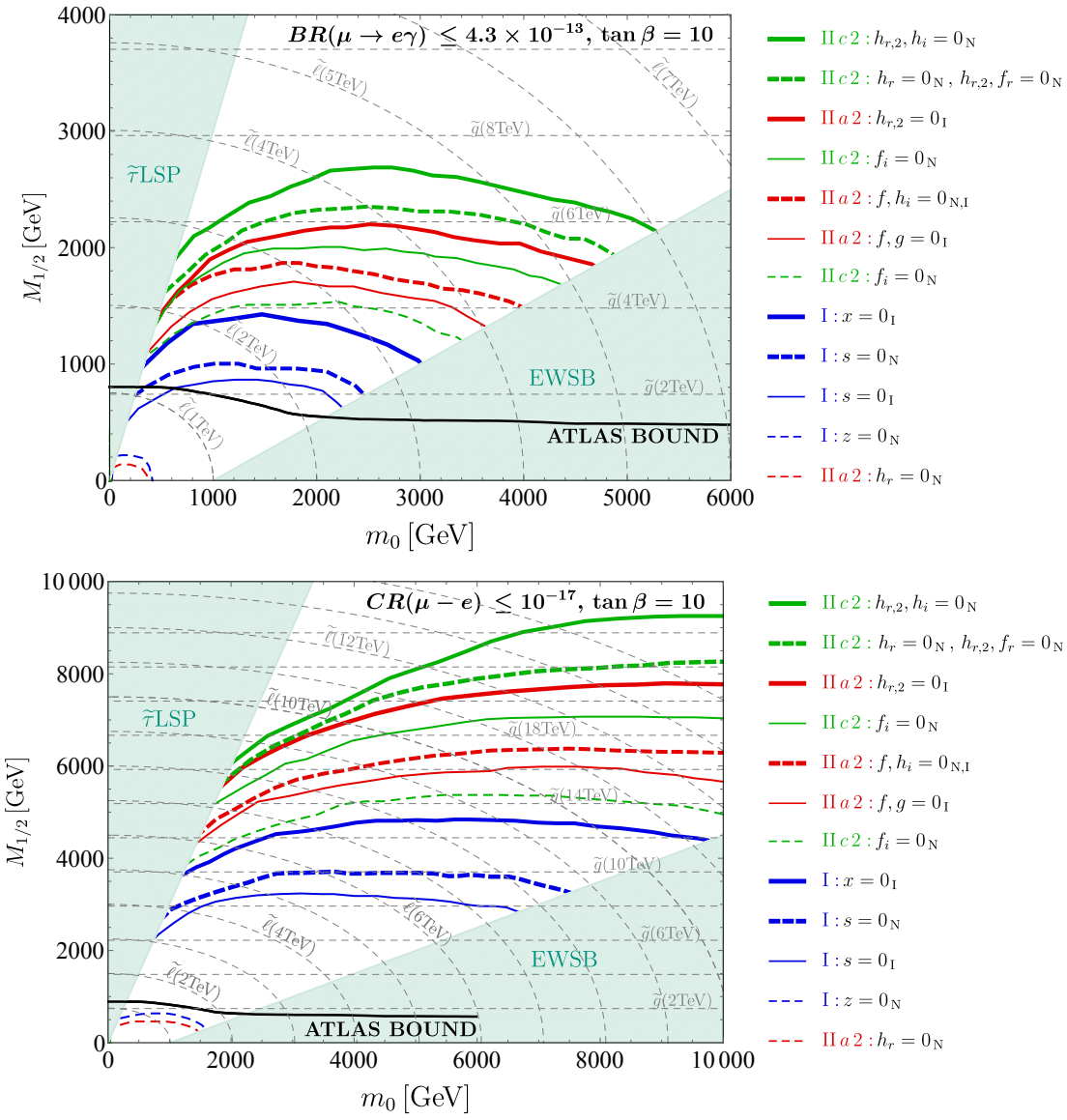

FIGURE 3.8: Excluded regions of the MSSM parameter space due to LFV constraints for $\tan\beta = 10$. The upper panel is obtained imposing the current bound for $\mathrm{BR}(\mu \to e\gamma)$, the bottom panel show the regions expected to be ruled out if the future sensitivity for $\mathrm{CR}(\mu - e)_{\mathrm{Al}}$ is reached with no discovery. The different mechanisms are distinguished through different colors: I (blue), II a-2 (red) and II c-2 (green). The black line is the ATLAS bound for mSUGRA models.

results in being constrained by the phenomenology (upper bound) and by the absolute mass scale $m_0^\nu \sim 5$ eV (lower bound). The interval corresponding to each case is reported in Table D.1.

The minimum value of the off-diagonal elements in Table D.1 can be used to constrain the MSSM parameter space as it has been done in [20–22]. Concretely, we compute the branching ratio (BR) for the LFV processes displayed in Table I.6 considering an hypothetical soft mass matrix for LH sleptons whose off-diagonal elements correspond to those minimum values. We choose a representative value of $\tan\beta = 10$ and calculate our predictions for different values of $\{m_0,\, M_{1/2}\}$. Comparing with current and future experimental bounds in Table I.6, we are able to set excluded regions in the $\{m_0, M_{1/2}\}$ plane. Barring accidental cancellations, we expect that bounds for specific models based on the realizations studied throughout this work will be like those presented in Figure 3.8 in the most optimistic scenario.

The most interesting results are shown in Figure 3.8, where the upper panel has been obtained from the most restrictive process nowadays, $\mathrm{BR}(\mu \to e\gamma) \leq 4.3 \times 10^{-13}$, and the lower panel corresponds to the expected future sensitivity on $\mathrm{CR}(\mu - e)_{\mathrm{Al}} \leq 10^{-17}$. Shaded green areas correspond to the stau as the lightest supersymmetric particle ($m_0 \ll M_{1/2}$) and no correct electroweak symmetric breaking ($M_{1/2} \ll m_0$). The ATLAS MSUGRA limit covers up to $M_{1/2} = (500 \div 800)$ GeV for $m_0 \leq 6$ TeV. We note that the excluded regions, the remaining areas below the corresponding lines, have the typical shape due to LH insertions, see [21].

Current bounds are already competitive with the experimental limit in Mechanism I, for which the excluded slepton and gluino masses in the less constrained case reach $\widetilde{\ell} \lesssim 800$ GeV and $\widetilde{g} \lesssim 1.5$ TeV[14]. These bounds could be increased up to $\widetilde{\ell} \lesssim 3$ TeV and $\widetilde{g} \lesssim 5$ TeV with future sensitivity from $\mu - e$ conversion, (see lower panel in Figure 3.8). More severe are the constraints imposed by Mechanism II. In particular, for current bounds, we can infer the following global lower limits: $\widetilde{\ell} \lesssim 1.5\,\mathrm{TeV}$ and $\widetilde{g} \geq 2.8\,\mathrm{TeV}$. They become much stronger considering the future reach of $\mu - e$ conversion which translates into $\widetilde{\ell} \geq 5\,\mathrm{TeV}$ and $\widetilde{g} \geq 8\,\mathrm{TeV}$.

It means that precision experiments will allow us to put constraints over the supersymmetric spectrum for masses that are beyond the LHC sensitivity in a factor of $3 \div 5$. Conversely, the discovery of SUSY partners in the TeV range will put significant constraints on these simple realizations with LH mediators, which will have to be reformulated in more elaborated scenarios: for instance, suppressing the LH contributions in the Kähler function or increasing the degrees of freedom in the neutrino sector by considering non-trivial Majorana and Dirac structures simultaneously.

[14] Hereafter, we omit the cases $z = 0$ in Mechanism I and $h_r = 0$ in Mechanism II a-2 from the discussion since they are already disfavored by the `Planck` + BAO limit on the total sum of light neutrino masses.

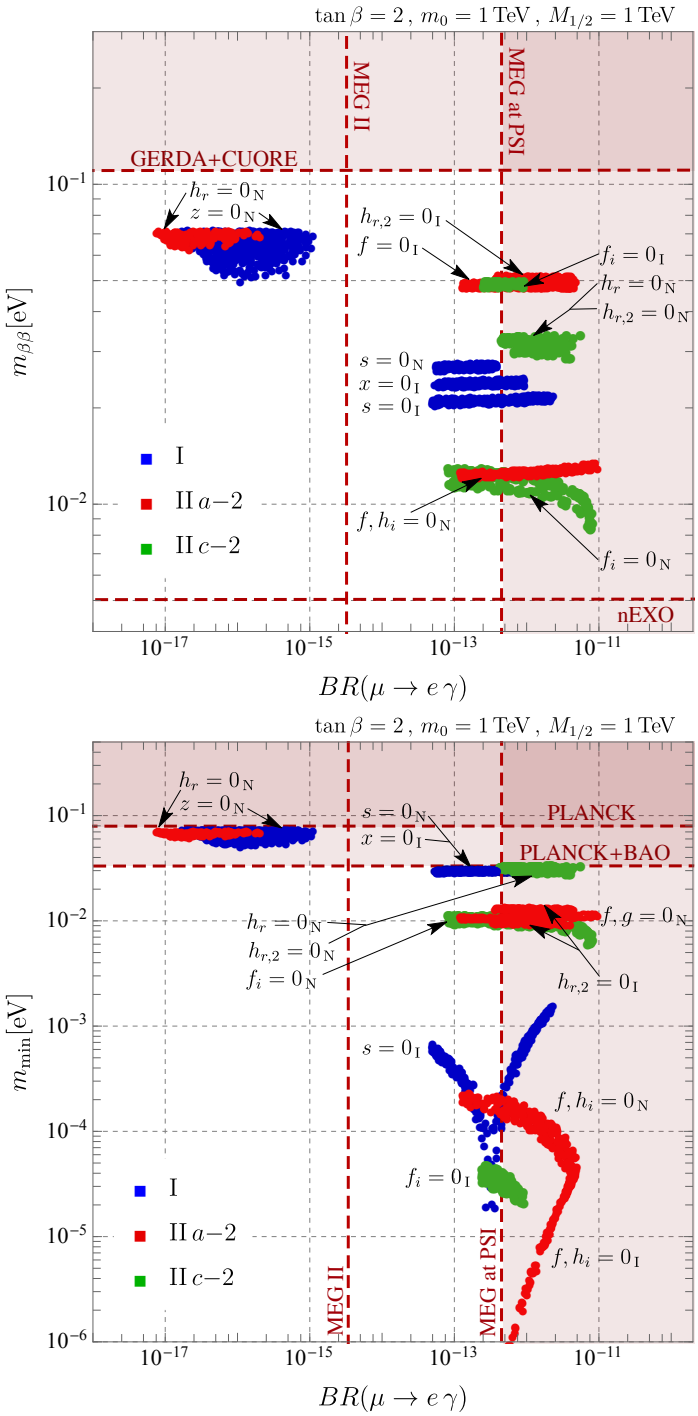

FIGURE 3.9: The quantities $m_{\beta\beta}$ and $m_{\rm min}$ versus the muon flavor violating decay $BR(\mu \to e\gamma)$. The MSUGRA input parameters are fixed to the conservative values $m_0 = M_{1/2} = 1\,\text{TeV}, \tan\beta = 2$. The shaded regions are already excluded by current bounds.

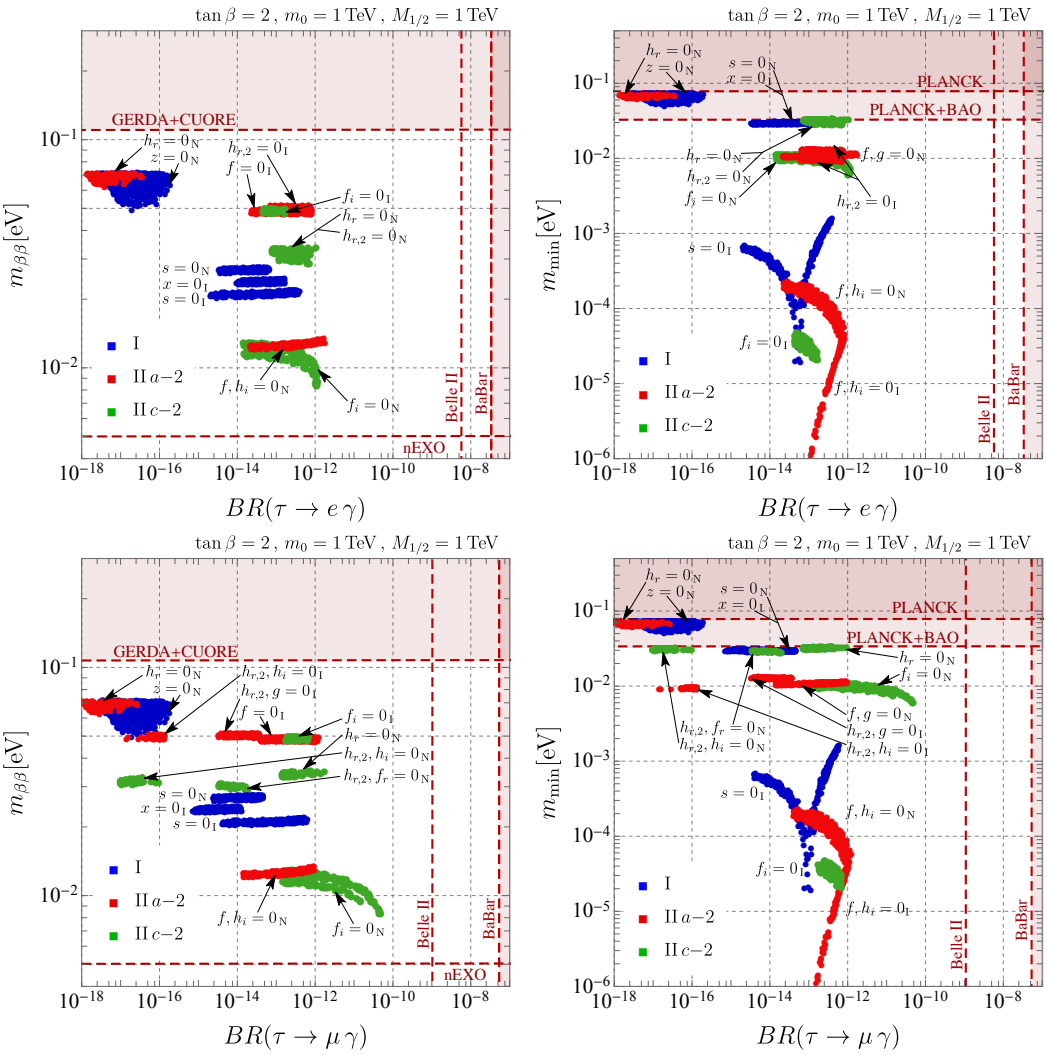

FIGURE 3.10: The quantities $m_{\beta\beta}$ and $m_{\rm min}$ versus the flavor violating decays of the τ: $BR(\tau \to e\gamma)$ (top panels) and $BR(\tau \to \mu\gamma)$ (bottom panels). The mSUGRA input parameters are fixed to the conservative values $m_0 = M_{1/2} = 1\,\text{TeV}, \tan\beta = 2$. The shaded regions are already excluded by current bounds.

3.5.3 Relations among observables

In this framework it is possible to predict testable relations among the LFV observables in the charged sector, Table I.6, and the neutrino mass observables $m_{\beta\beta}$ and $m_{\rm min}$ discussed in Sec.3.5.1. This allows to disentangle cases that are not distinguishable only through the analysis in [26]. To this end we fix the mSUGRA parameters to $m_0 = M_{1/2} = 1$ TeV, which would correspond to sleptons and gluinos masses

around 1.5 TeV and 2.5 TeV respectively, and a very conservative value $\tan\beta = 2$, which ensures that the $\tan\beta$-enhanced contributions to the FC processes are minimized. Then, we study the dependence of both $m_{\beta\beta}$ and $m_{\rm min}$ on $\mathrm{BR}(\mu \to e\,\gamma)$ and $\mathrm{BR}(\tau \to e\,(\mu)\,\gamma)$. Our results for each process are shown in Figures 3.9 and 3.10. It is worth emphasizing the interplay of the experimental bounds coming from the two sectors, which acts in a complementary way in constraining the different realizations of the neutrino masses.

In fact, current bounds on LFV observables allow to constrain some regions that otherwise were not testable with present neutrino data, since they predict too low values for $m_{\beta\beta}$ and $m_{\rm min}$ (bottom-right). In particular, the cases $h_r = 0$ and $h_{r,2} = 0$ of Mechanism II (both a-2 and c-2) are severely constrained, while the cases $s = 0$ and $x = 0$ for Mechanism I, $f = 0$ for Mechanism II a-2 and $f_i = 0$ for Mechanism II c-2 result partially excluded. Moreover, with the expected sensitivity of `MEG II` [50] in $\mathrm{BR}(\mu \to e\gamma)$ all the scenarios detailed before will be completely (dis)proved. And vice versa, those realizations out of the scope of `MEG II`, namely $z = 0$ in Mechanism I and $h_r = 0$ in Mechanism II a-2, happen to be incompatible with the recent cosmological data presented by the `Planck` collaboration for the neutrino masses [51].

3.6 Conclusions

In this work we have analyzed the phenomenological consequences of combining A_5 and CP as a flavor symmetry in SUSY. We have focused on the leptonic sector where two residual symmetries, $\mathbb{Z}_5$ and $\mathbb{Z}_2\times$CP, remain conserved at LO for charged leptons and neutrinos. In Sec.3.2, the main effects of introducing a flavor symmetry into SUSY theories have been summarized. It can been shown that, even in the most conservative scenario, tree-level FC soft couplings arise when $\Lambda_{\rm Med} \gg \Lambda_f$, producing sizable effects in LFV observables.

The main features of A_5 and CP as a group have been reviewed in Sec.3.3, where the structure for the lepton mass matrices, the vev of the flavon fields and the leptonic mixing have been derived. The mass matrix for charged leptons results in being diagonal at LO while, for neutrinos, all possible realizations to generate their masses at tree level have been investigated. We noticed that two different set of flavons are required to generate the neutrino and charged lepton masses at LO. Each of them can induce corrections in the opposite sector at NLO, as discussed in Sec.3.3.4.

Sec.3.4 has been devoted to compute the minimal set of effective operators entering the Kähler potential and soft masses for LH and RH fields. Under no additional assumptions about the UV theory, the proposed operators are always present and

cannot be avoided through the introduction of additional symmetries. For the residual symmetries considered here, we have found that the presence of LH mediators is specially relevant and that the flavons associated with neutrino masses also induce flavor violation in the charged-lepton sector. This allows for a combined analysis of neutrino observables and LFV processes.

In Sec.3.5.1, we have computed our predictions for the neutrino effective mass $m_{\beta\beta}$ versus m_{min}. We observed that the canonical rotation may have some effect over the model parameter m_{min}. Although these variations seem to be difficult to measure, we think that this information could be useful when (re)constructing theoretical models from experimental data. Regarding charged leptons, in Sec.3.5.2, we have interpreted our predictions for the LFV processes $\mu \to e\gamma$ and $\mu - e$ conv. in terms of exclusion limits on the plane $\{m_0, M_{1/2}\}$. The results depend on the mechanism responsible for the neutrino masses; however, even in the less restricted realizations, we obtain limits that are competitive with those coming from direct searches of ATLAS on MSUGRA scenarios. This type of analysis is very useful to indirectly explore the supersymmetric spectrum in concrete models: in the absence of experimental signals of new physics, stringent limits can be set over the superpartner masses for each specific setup; if SUSY is discovered at the TeV scale, the simplified constructions analyzed throughout this article will have difficulties to accommodate it so that more refined scenarios must be considered.

Finally, the common origin of neutrino masses and flavor violation for charged leptons induce testable relations between neutrino and charged-lepton observables. This has been expounded in Sec.3.5.3, where a nice complementarity between both sectors has been found: those realizations difficult to test with neutrino data will be totally probed with the expected sensitivity of `MEGII` on $\mu \to e\gamma$; conversely, the two scenarios that remain out of the scope of this experiment should be already discarded if the latest limits from `Planck`+BAO on the total sum of the neutrino masses are imposed.

References

[1] B. Pontecorvo, *Sov. Phys. JETP* **1957**, *6*, [Zh. Eksp. Teor. Fiz.33,549(1957)], 429.

[2] B. Pontecorvo, *Sov. Phys. JETP* **1958**, *7*, [Zh. Eksp. Teor. Fiz.34,247(1957)], 172–173.

[3] Z. Maki et al., *Prog. Theor. Phys.* **1962**, *28*, [,34(1962)], 870–880.

[4] B. Pontecorvo, *Sov. Phys. JETP* **1968**, *26*, [Zh. Eksp. Teor. Fiz.53,1717(1967)], 984–988.

[5] R. Acciarri et al., **2015**, arXiv: `1512.06148 [physics.ins-det]`.

[6] R. Acciarri et al., **2016**, arXiv: `1601.02984 [physics.ins-det]`.

[7] R. Acciarri et al., **2016**, arXiv: `1601.05471 [physics.ins-det]`.

[8] J. Strait et al., **2016**, arXiv: 1601.05823 [physics.ins-det].

[9] K. Abe et al., *PTEP* **2015**, *2015*, 053C02, arXiv: 1502.05199 [hep-ex].

[10] K. Abe et al., *PTEP* **2018**, *2018*, 063C01, arXiv: 1611.06118 [hep-ex].

[11] A. Himmel in, Nova Collaboration.

[12] S. Weinberg, *Phys. Rev. Lett.* **1979**, *43*, 1566–1570.

[13] K. Tsumura, L. Velasco-Sevilla, *Phys. Rev.* **2010**, *D81*, 036012, arXiv: 0911.2149 [hep-ph].

[14] A. J. Buras et al., *JHEP* **2012**, *03*, 088, arXiv: 1112.4477 [hep-ph].

[15] L. Calibbi et al., *JHEP* **2012**, *07*, 004, arXiv: 1204.1275 [hep-ph].

[16] Y. Koide, *Phys. Rev.* **2013**, *D87*, 016016, arXiv: 1209.1694 [hep-ph].

[17] S.-S. Bao et al., *Nucl. Phys.* **2016**, *B904*, 1–17, arXiv: 1505.03583 [hep-ph].

[18] S. Pascoli, Y.-L. Zhou, *JHEP* **2016**, *10*, 145, arXiv: 1607.05599 [hep-ph].

[19] L. Heinrich et al., **2018**, arXiv: 1810.05648 [hep-ph].

[20] D. Das et al., *Phys. Rev.* **2017**, *D95*, 035001, arXiv: 1607.06827 [hep-ph].

[21] M. L. López-Ibáñez et al., *JHEP* **2017**, *11*, [Erratum: JHEP 04, 015 (2018)], 162, arXiv: 1710.02593 [hep-ph].

[22] I. De Medeiros Varzielas et al., *JHEP* **2018**, *09*, 047, arXiv: 1807.00860 [hep-ph].

[23] L. Calibbi et al., *JHEP* **2012**, *06*, 018, arXiv: 1203.1489 [hep-ph].

[24] S. Antusch et al., *Nucl. Phys.* **2011**, *B852*, 108–148, arXiv: 1104.3040 [hep-ph].

[25] C.-C. Li, G.-J. Ding, *JHEP* **2015**, *05*, 100, arXiv: 1503.03711 [hep-ph].

[26] A. Di Iura et al., *JHEP* **2015**, *08*, 037, arXiv: 1503.04140 [hep-ph].

[27] P. Ballett et al., *Phys. Rev.* **2015**, *D92*, 093008, arXiv: 1503.07543 [hep-ph].

[28] J. Turner, *Phys. Rev.* **2015**, *D92*, 116007, arXiv: 1507.06224 [hep-ph].

[29] A. Di Iura et al., **2018**, arXiv: 1811.09662 [hep-ph].

[30] CMS, Supersymmetry Physics Results, http://cms-results.web.cern.ch/cms-results/public-results/publications/SUS/index.html.

[31] ATLAS, Supersymmetry Physics Results, https://twiki.cern.ch/twiki/bin/view/AtlasPublic/SupersymmetryPublicResults.

[32] C. D. Froggatt, H. B. Nielsen, *Nucl. Phys.* **1979**, *B147*, 277–298.

[33] F. Feruglio et al., *JHEP* **2013**, *07*, 027, arXiv: 1211.5560 [hep-ph].

[34] M. Holthausen et al., *JHEP* **2013**, *04*, 122, arXiv: 1211.6953 [hep-ph].

[35] M.-C. Chen et al., *Nucl. Phys.* **2014**, *B883*, 267–305, arXiv: 1402.0507 [hep-ph].

[36] W. Grimus, M. N. Rebelo, *Phys. Rept.* **1997**, *281*, 239–308, arXiv: hep-ph/9506272 [hep-ph].

[37] G. Ecker et al., *Nucl. Phys.* **1984**, *B247*, 70–82.

[38] G. Ecker et al., *J. Phys.* **1987**, *A20*, L807.

[39] H. Neufeld et al., *Int. J. Mod. Phys.* **1988**, *A3*, 603–616.

[40] C. Jarlskog, *Phys. Rev. Lett.* **1985**, *55*, 1039–1042.

[41] S. F. King, I. N. R. Peddie, *Phys. Lett.* **2004**, *B586*, 83–94, arXiv: hep-ph/0312237 [hep-ph].

[42] S. F. King et al., *JHEP* **2005**, *07*, 049, arXiv: hep-ph/0407012 [hep-ph].

[43] J. R. Espinosa, A. Ibarra, *JHEP* **2004**, *08*, 010, arXiv: hep-ph/0405095 [hep-ph].

[44] M.-C. Chen et al., *Nucl. Phys.* **2013**, *B873*, 343–371, arXiv: 1302.5576 [hep-ph].
[45] S. Antusch et al., *Nucl. Phys. B* **2003**, *674*, 401–433, arXiv: hep-ph/0305273.
[46] W. Porod, *Comput. Phys. Commun.* **2003**, *153*, 275–315, arXiv: hep-ph/0301101 [hep-ph].
[47] F. Staub, *Comput. Phys. Commun.* **2014**, *185*, 1773–1790, arXiv: 1309.7223 [hep-ph].
[48] S. Dell'Oro et al., *Adv. High Energy Phys.* **2016**, *2016*, 2162659, arXiv: 1601.07512 [hep-ph].
[49] P. F. De Salas et al., *Front. Astron. Space Sci.* **2018**, *5*, 36, arXiv: 1806.11051 [hep-ph].
[50] A. Baldini et al., *Eur. Phys. J. C* **2016**, *76*, 434, arXiv: 1605.05081 [hep-ex].
[51] N. Aghanim et al., **2018**, arXiv: 1807.06209 [astro-ph.CO].

Article 4

Leptogenesis in $\Delta(27)$ with a universal texture zero

JHEP 09 (2019) 050

Fredrik Björkeroth[⋆], Ivo de Medeiros Varzielas[†], M.L. López-Ibáñez[‡], Aurora Melis[‡] and Oscar Vives[‡]

[⋆] *INFN, Laboratori Nazionali di Frascati, C.P. 13, 100044 Frascati, Italy.*

[†] *CFTP, Departamento de Física, Instituto Superior Técnico, Universidade de Lisboa, Avenida Rovisco Pais 1, 1049 Lisboa, Portugal*

[‡] *Departament de Física Tèorica, Universitat de València & IFIC, Universitat de València & CSIC, Dr. Moliner 50, E-46100 Burjassot (València), Spain.*

ABSTRACT: We investigate the possibility of viable leptogenesis in an appealing $\Delta(27)$ model with a universal texture zero in the (1,1) entry. The model accommodates the mass spectrum, mixing and CP phases for both quarks and leptons and allows for grand unification. Flavoured Boltzmann equations for the lepton asymmetries are solved numerically, taking into account both N_1 and N_2 right-handed neutrino decays. The N_1-dominated scenario is successful and the most natural option for the model, with $M_1 \in [10^9, 10^{12}]$ GeV, and $M_1/M_2 \in [0.002, 0.1]$, which constrains the parameter space of the underlying model and yields lower bounds on the respective Yukawa couplings. Viable leptogenesis is also possible in the N_2-dominated scenario, with the asymmetry in the electron flavour protected from N_1 washout by the texture zero. However, this occurs in a region of parameter space which has a stronger mass hierarchy $M_1/M_2 < 0.002$, and M_2 relatively close to M_3, which is not a natural expectation of the $\Delta(27)$ model.

4.1 Introduction

The Standard Model (SM) has been experimentally confirmed as the correct description of Nature, with excellent precision, up to scales of $\mathcal{O}$(TeV). Nevertheless we know that the SM is not a complete theory. It includes a host of free parameters, the majority of which relate to the Yukawa sector, into whose origin and nature the SM offers no insight. This is despite obvious indications of internal structure, such as large mass hierarchies between generations of fermions, and small CKM mixing. It is also unclear as to how the SM should be extended to account for massive neutrinos and lepton mixing. The combined questions of charged fermion hierarchies and the CKM and PMNS mixing patterns is typically referred to as the flavour puzzle. Moreover, the SM fails to accommodate several observational facts in cosmology. It lacks dark matter and inflaton candidates, has no explanation for dark energy, and does not account for the baryon asymmetry of the Universe (BAU).

Among these cosmological issues, perhaps the BAU is the most distressing one. The SM is (nearly) symmetric in particles and anti-particles; despite this, no evidence of the presence of primordial anti-matter in our observable universe has been found so far. The BAU, that is, the difference between the baryon n_B and antibaryon $\bar{n}_B$ number densities, is measured with respect to the entropy density s to be

$$Y_B = \frac{n_B - \bar{n}_B}{s} = (0.87 \pm 0.01) \times 10^{-10}. \tag{4.1}$$

Although the SM includes all the necessary ingredients to generate this BAU dynamically [1], namely, CP violation in the CKM matrix, B violation through sphaleron interactions, and out-of-equilibrium processes in the electroweak phase transition, the asymmetry obtained in the SM is too small by orders of magnitude [2].

It is well-known that extending the SM by several heavy right-handed (RH) neutrinos can yield a BAU via leptogenesis [3]. Lepton number-violating decays of the RH neutrinos, some portion of which occur out of equilibrium, produce a lepton asymmetry. This is partially converted into a baryon asymmetry by sphaleron interactions, which are efficient above the electroweak scale. Heavy RH neutrinos simultaneously provide a natural answer to the smallness of left-handed (LH) neutrino masses via the seesaw mechanism.

It is interesting to note that since RH neutrinos are SM singlets, leptogenesis links the resolution of the BAU with their Yukawa couplings, and thus connects with the flavour puzzle. If seesaw is indeed the origin of light neutrino masses, then qualitatively leptogenesis is unavoidable. Whether it accurately reproduces the observed

BAU becomes a quantitative question for a given spectrum of RH neutrinos and their interactions with SM particles. Remarkably, the original (and arguably simplest) model of leptogenesis requires a RH neutrino scale $M \gtrsim 10^9$ GeV, which closely corresponds to the "natural" seesaw scale.

The flavour sector of the SM, including lepton mixing, comprises 22 (20) physical parameters, assuming neutrinos are Majorana (Dirac) particles. A popular approach to relate these parameters, and reduce the effective number of degrees of freedom in the SM, is that of spontaneously broken flavour (or family) symmetries. Non-Abelian discrete symmetries have been especially successful, able to simultaneously describe charged lepton and neutrino parameters, and in several cases, also the quark sector [4–12]. A very appealing $\Delta(27)$ model was introduced in [13], consistent with an underlying $SO(10)$ grand unified theory (GUT). The family symmetry leads to a predictive structure with a universal texture zero (UTZ) for all fermion mass structures, including the effective neutrinos after seesaw. The family symmetry is also responsible for controlling flavour-violating processes, which are sufficiently suppressed for certain regions of the model parameter space, as shown in [14]. A complete model ought to account for the observed BAU, which provides an additional constraints on its parameters. In particular, as we shall see in this analysis, matching to the observed BAU allows us to constrain the otherwise unknown parameters of the RH neutrino sector.

The paper is organized as follows. Section 4.2 summarizes the main features of the model, originally presented in [13]. The seesaw implementation is described in Section 4.3, explaining the existing UTZ result in an elegant new way based on rank-one matrices (described in more detail in Appendix C.2). In Section 4.4 we write down the Boltzmann equations describing the evolution of the neutrino and asymmetry densities; this is supplemented by Appendix C.1. Section 4.5 presents the results and our analysis. We conclude in Section 5.5. Appendices C.2 and C.3 provide additional insight into the model and leptogenesis within it.

4.2 Overview of the $\Delta(27)$ Model

In this section we review the model introduced in [13]. Given that we are interested in leptogenesis, we focus on the lepton sector, where SM fermions are contained in superfields L (lepton $SU(2)$ doublets) and e^c, N^c (following conventional notation, conjugates of the RH charged leptons and neutrinos, respectively). The field content and their transformation properties under the $\mathcal{G}_f = \Delta(27) \times \mathbb{Z}_N$ flavour group are

given in Table 4.1. The superpotential that generates the Yukawa structures at leading

Field	L	e^c	N^c	$H_{u,d}$	Σ	S	ϕ_c	ϕ_b	ϕ_a	ϕ	ϕ_X
$\Delta(27)$	**3**	**3**	**3**	**1**	**1**	**1**	$\bar{\mathbf{3}}$	$\bar{\mathbf{3}}$	$\bar{\mathbf{3}}$	$\bar{\mathbf{3}}$	**3**
$\mathbb{Z}_N$	0	0	0	0	2	-1	0	-1	2	0	x

TABLE 4.1: Representations of superfields under the flavour symmetry $\mathcal{G}_f = \Delta(27) \times \mathbb{Z}_N$.

order for Dirac fermions is

$$\begin{aligned} W_Y = L_i e^c_j H_d \left[\frac{g^e_c}{\Lambda^2}\phi^i_c\phi^j_c + \frac{g^e_b}{\Lambda^3}\phi^i_b\phi^j_b\Sigma + \frac{g^e_a}{\Lambda^3}(\phi^i_a\phi^j_b + \phi^i_b\phi^j_a)S \right] \\ + L_i N^c_j H_u \left[\frac{g^\nu_c}{\Lambda^2}\phi^i_c\phi^j_c + \frac{g^\nu_b}{\Lambda^3}\phi^i_b\phi^j_b\Sigma + \frac{g^\nu_a}{\Lambda^3}(\phi^i_a\phi^j_b + \phi^i_b\phi^j_a)S \right]. \end{aligned} \tag{4.2}$$

where $i, j = (1,2,3)$ lower (upper) indices denote the $\Delta(27)$ triplets (anti-triplets). Non-renormalizable terms are suppressed by messenger masses, which are in general different [13]; they are denoted here by a common scale Λ, with variations in messenger masses contained in an arbitrary coupling g for each term. The superpotential responsible for RH neutrino Majorana masses is

$$W_N = N^c_i N^c_j \left[\frac{g^N_c}{\Lambda}\phi^i\phi^j + \frac{g^N_b}{\Lambda^4}\phi^i_b\phi^j_b(\phi^k\phi^k\phi^k_a) + \frac{g^N_a}{\Lambda^4}(\phi^i_a\phi^j_b + \phi^i_b\phi^j_a)(\phi^k\phi^k\phi^k_b) \right]. \tag{4.3}$$

The ϕ fields are flavons that break $\Delta(27)$ and provide the structure of the mass matrices, with the vacuum alignment

$$\langle\phi_c\rangle = v_c \begin{pmatrix} 0 \\ 0 \\ 1 \end{pmatrix} \propto \langle\phi\rangle\,, \qquad \langle\phi_b\rangle = \frac{v_b}{\sqrt{2}} \begin{pmatrix} 0 \\ 1 \\ 1 \end{pmatrix}, \qquad \langle\phi_a\rangle = \frac{v_a}{\sqrt{3}} \begin{pmatrix} 1 \\ 1 \\ -1 \end{pmatrix}. \tag{4.4}$$

The core prediction of the model is universal complex-symmetric mass matrices with the UTZ in the (1,1) entry, of the form

$$M = \begin{pmatrix} 0 & a & a \\ a & b+2a & b \\ a & b & c+b-2a \end{pmatrix}, \tag{4.5}$$

for some complex a, b, c. Assuming a strong hierarchy $a < b < c$, the eigenvalues are approximately given by $|a^2/b|$, $|b|$ and $|c|$. This applies in particular to the Dirac and Majorana mass matrices. Up to $\mathcal{O}(1)$ coefficients, they yield the following hierarchies between families:

$$Y^{e,\nu} \sim y_c^{e,\nu} \begin{pmatrix} 0 & \epsilon_{e,\nu}^3 & \epsilon_{e,\nu}^3 \\ \epsilon_{e,\nu}^3 & \epsilon_{e,\nu}^2 & \epsilon_{e,\nu}^2 \\ \epsilon_{e,\nu}^3 & \epsilon_{e,\nu}^2 & 1 \end{pmatrix}, \qquad M_N \sim M_c \begin{pmatrix} 0 & \epsilon_N^2 & \epsilon_N^2 \\ \epsilon_N^2 & \epsilon_N^2 & \epsilon_N^2 \\ \epsilon_N^2 & \epsilon_N^2 & 1 \end{pmatrix}, \tag{4.6}$$

with $y_c^{e,\nu}$ and M_c the dominant contributions to the third and heaviest generation. Masses and mixing are compatible with the expansion parameters $\epsilon_e \simeq 0.15$ and $\epsilon_N \sim \epsilon_\nu^3$. In addition to y_c^ν, Y_ν depends on effective parameters $y_{a,b}^\nu$, sourced from the subleading operators in Eq. (4.2) and defined explicitly in Eqs. (4.9)–(4.10) below. Due to the flavon VEVs, they correspond to a hierarchy $y_a^\nu : y_b^\nu : y_c^\nu \approx \epsilon_\nu^3 : \epsilon_\nu^2 : 1$. The expansion parameter for Dirac neutrinos, ϵ_ν, is not constrained by phenomenology, but internal consistency of the model requires that it remains perturbative, i.e. $\epsilon_\nu \lesssim 0.5$. We shall see that numerically viable regions in parameter space correspond to $\epsilon_\nu \in [0.05, 0.5]$. Note that the large hierarchy between the first two RH neutrinos $N_{1,2}$ and the heaviest one N_3 is characteristic of this kind of model [15–19], where rather different mixing patterns in the quark and lepton sectors are obtained from the same universal Yukawa structures, on the condition that $\langle \phi_c \rangle$ is dominant in the quark and charged lepton sectors and irrelevant for the neutrino mass matrix. The structure in Eq. (4.5) can written precisely as

$$\begin{aligned} Y^{e,\nu} &= y_a^{e,\nu}(\square_{ab} + \square_{ba}) + y_b^{e,\nu}\square_b + y_c^{e,\nu}\square_c, \\ M_N &= M_a(\square_{ab} + \square_{ba}) + M_b\square_b + M_c\square_c, \end{aligned} \tag{4.7}$$

where $\square_i = \phi_i \phi_i^T$ and $\square_{ij} = \phi_i \phi_j^T$ are rank-one matrices,

$$\square_{ab} = (\square_{ba})^T = \begin{pmatrix} 0 & 0 & 0 \\ 1 & 1 & -1 \\ 1 & 1 & -1 \end{pmatrix}, \quad \square_b = \begin{pmatrix} 0 & 0 & 0 \\ 0 & 1 & 1 \\ 0 & 1 & 1 \end{pmatrix}, \quad \square_c = \begin{pmatrix} 0 & 0 & 0 \\ 0 & 0 & 0 \\ 0 & 0 & 1 \end{pmatrix}. \tag{4.8}$$

The set of parameters $(y_a^{e,\nu}, y_b^{e,\nu}, y_c^{e,\nu})$ and (M_a, M_b, M_c) in Eq. (4.7) are generally complex[1] with phases coming either from the VEVs or the coefficients,

[1] The presence of a CP symmetry can constrain them to be real, with CP being broken spontaneously e.g. through the flavon VEVs as in [20]. We don't consider this possibility here.

$$\begin{aligned} y_a^{e,\nu} &\equiv |y_a^{e,\nu}| e^{i\gamma_{e,\nu}}, & y_b^{e,\nu} &\equiv |y_b^{e,\nu}| e^{i\delta_{e,\nu}}, & y_c^{e,\nu} &\equiv |y_c^{e,\nu}|, \\ M_a &\equiv |M_a| e^{i\gamma_N}, & M_b &\equiv |M_b| e^{i\delta_N}, & M_c &\equiv |M_c|. \end{aligned} \tag{4.9}$$

Given that phenomenology depends only on two independent combinations of the phases, we follow [13] in taking just δ and γ as independent phases (see also Table 4.2). In terms of the fundamental parameters of the superpotential in Eqs. (4.2)–(4.3), they are

$$\begin{aligned} |y_a^{e,\nu}| &= \frac{g_a^{e,\nu} v_a v_b \langle S \rangle}{\sqrt{6}\Lambda^3}, & |y_b^{e,\nu}| &= \frac{g_b^{e,\nu} v_b^2 \langle \Sigma \rangle}{2\Lambda^3}, & |y_c^{e,\nu}| &= \frac{g_c^{e,\nu} v_c^2}{\Lambda^2}, \\ |M_a| &= \frac{g_a^N v_a v_b^2 v_\phi^2}{2\sqrt{3}\Lambda^4}, & |M_b| &= \frac{g_b^N v_a v_b^2 v_\phi^2}{2\sqrt{3}\Lambda^4}, & |M_c| &= \frac{g_c^N v_\phi^2}{\Lambda}. \end{aligned} \tag{4.10}$$

The superfield S is a gauge singlet, while Σ is not [13] and introduces Clebsch-Gordan (CG) coefficients, although for our purposes here it is sufficient to consider their respective VEVs $\langle S \rangle$ and $\langle \Sigma \rangle$ as real numbers, and absorb the different CG contributions to charged leptons and neutrino into $g_b^{e,\nu}$. The expansion parameters of the model in Eq. (4.6) are recovered from the parameters in Eq. (4.7) as

$$\begin{aligned} \epsilon_{e,\nu} &\sim \left| y_a^{e,\nu} / y_b^{e,\nu} \right| \sim \left| y_b^{e,\nu} / y_c^{e,\nu} \right|^{1/2} \sim \left| y_a^{e,\nu} / y_c^{e,\nu} \right|^{1/3}, \\ \epsilon_N &\sim \left| M_a / M_c \right|^{1/2} \sim \left| M_b / M_c \right|^{1/2}. \end{aligned} \tag{4.11}$$

The lepton asymmetries are obtained in the flavour basis, wherein the charged lepton Yukawa matrix Y_e and RH neutrino mass matrix M_N are diagonal. They are diagonalized by unitary matrices, such that

$$\begin{aligned} \hat{Y}^e &= V_L^{e\dagger} Y^e V_R^e, \\ \hat{M}_N &= V_N^T M_N V_N, \end{aligned} \tag{4.12}$$

where hats ($\hat{}$) denote diagonal matrices of positive eigenvalues and, Y^e being complex symmetric, we have $V_R^{e\dagger} = V_L^{eT}$. In the flavour basis, in the LR phase convention (where the Yukawa couplings are given by $\mathcal{L} \sim \bar{L} H_d e_R + \bar{L} H_u \nu_R + \text{h.c.}$), the neutrino Yukawa matrix is given by λ_ν, where

$$\lambda_\nu^* \equiv V_L^{e\dagger} Y_\nu V_N, \tag{4.13}$$

where the additional conjugation on λ_ν appears due to the change from the supersymmetry basis to the seesaw basis [21].

4.3 The UTZ seesaw mechanism

In this section we review the results from [13] for how the seesaw mechanism operates in the UTZ model, understanding them through a new formulation based on rank-one matrices. As the Dirac and Majorana matrices are expressed in terms of the same rank-one matrices, the application of the usual seesaw formula,

$$m_\nu = -v_u^2 Y_\nu M_N^{-1} Y_\nu^T, \tag{4.14}$$

provides a light neutrino mass matrix m_ν which can be expanded in the same fashion, i.e.

$$m_\nu = m_a(\square_{ab} + \square_{ba}) + m_b\square_b + m_c\square_c, \tag{4.15}$$

with the $\square$ matrices defined in Eq. (4.8). Notably, the UTZ is preserved. A detailed discussion of this elegant property can be found in Appendix C.2. The parameters $m_{a,b,c}$ entangle the combinations of Dirac and Majorana neutrino couplings as

$$m_a = -\frac{v_u^2 y_a^{\nu 2}}{M_a}, \qquad m_b = m_a\left(2\frac{y_b^\nu}{y_a^\nu} - \frac{M_b}{M_a}\right), \qquad m_c = -\frac{v_u^2 y_c^{\nu 2}}{M_c}. \tag{4.16}$$

Obtaining the correct neutrino mixing requires $m_c < m_a < m_b$. In fact, if $m_c < m_a, m_b$, the light neutrino mass matrix in Eq. (4.15) is semi-diagonalized by a tri-bimaximal (TB) rotation (see e.g. [22]). Moreover if $m_a < m_b$, the resulting pattern has a Gatto-Sartori-Tonin [23] structure which can be fully diagonalized by a rotation of an angle θ in the 23 block. Consequently Eq. (4.15) is compatible with a normal-ordered neutrino spectrum, with

$$\hat{m}_\nu \equiv \text{diag}\,(m_1, m_2, m_3) \simeq \text{diag}\left(\frac{|m_c|}{6}, 3\left|\frac{m_a^2}{m_b}\right|, 2|m_b|\right). \tag{4.17}$$

At leading order the full PMNS matrix is given by

$$V_{\text{PMNS}} = \frac{1}{\sqrt{6}}\begin{pmatrix} 2 & \sqrt{2}c_\theta & \sqrt{2}s_\theta \\ -1 & \sqrt{2}c_\theta - \sqrt{3}s_\theta & \sqrt{3}c_\theta + \sqrt{2}s_\theta \\ 1 & -\sqrt{3}c_\theta - \sqrt{2}s_\theta & \sqrt{2}c_\theta - \sqrt{3}s_\theta \end{pmatrix}, \; s_\theta = \sqrt{\frac{m_2}{m_3}} \simeq \sqrt{\frac{3}{2}}\left|\frac{m_a}{m_b}\right|. \tag{4.18}$$

In this class of model [15–19] the different mixing patterns in the quark and lepton sectors require a large hierarchy between the first two RH neutrinos and the third, i.e. $M_{1,2} \ll M_3$. Indeed, given the relations in Eq. (4.16) and the hierarchy in the Dirac

sector (see Eq. (4.6)), i.e. $y_a^\nu \sim \epsilon_\nu^3 y_c^\nu$ and $y_b^\nu \sim \epsilon_\nu^2 y_c^\nu$, the requirement that $m_c < m_a < m_b$, implies the following relations for the RH neutrino parameters: $M_a/M_b < \epsilon_\nu$ and $M_a/M_c < \epsilon_\nu^6$. Therefore, N_3 with $M_3 \sim M_c$ effectively decouples after seesaw. The parameters $M_{a,b}$ are given by the same operator and a moderate hierarchy between them is obtained by the relative size of the coefficients g_a^N, g_b^N. For those values of the Dirac neutrino expansion parameter ϵ_ν preferred by the model, we thus expect a hierarchical spectrum for the Majorana neutrino masses in which $M_1 < M_2 \ll M_3$.[2]

4.4 Leptogenesis

4.4.1 Boltzmann equations

The generation of a BAU through N_i-leptogenesis is a non-equilibrium process which is generally treated by means of Boltzmann equations for the number densities of RH (s)neutrinos, Y_{N_i} and $Y_{\widetilde{N}_i}$ (for an N_i neutrino with mass M_i), and leptons, Y_{L_α}. It is useful to consider the quantities $Y_{\Delta\alpha} = Y_B/3 - Y_{L_\alpha}$ rather than Y_{L_α}, since $\Delta_\alpha = B/3 - L_\alpha$ is conserved by sphalerons and other SM interactions. L_α and Δ_α asymmetries are related by a flavour coupling matrix A, i.e. $Y_{L_\alpha} = \sum_{\alpha'} A_{\alpha\alpha'} Y_{\Delta\alpha}$. The form of A depends on which interactions are in thermal equilibrium during leptogenesis; it is defined explicitly in Appendix C.1. The produced lepton asymmetries are partially converted into a baryon asymmetry Y_B by the sphalerons, given in the MSSM by

$$Y_B = \frac{10}{31} \sum_\alpha Y_{\Delta\alpha} \quad , \tag{4.19}$$

with Y_{Δ_α} computed at a temperature $T \ll M_i$, where the densities Y_{N_i}, $Y_{\widetilde{N}_i}$ are effectively zero. In the fully flavoured regime, $M_i \ll 10^9(1+\tan^2\beta)$ GeV, all lepton flavours are to be treated separately, i.e. $\alpha = e, \mu, \tau$. In the two-flavour regime, $10^9(1+\tan^2\beta)$ GeV $\ll M_i \ll 10^{12}(1+\tan^2\beta)$ GeV, only the interaction mediated by the τ Yukawa coupling is in equilibrium and the asymmetries in the e and μ flavours can be treated with a combined density $Y_{\Delta e\mu} = Y_{\Delta e + \Delta\mu}$.

In the MSSM, with hierarchical RH neutrinos only N_1 and N_2 participate in the leptogenesis process and we can neglect the contribution from N_3. We have three different scenarios, depending on M_1 and M_2. Assuming first that both $M_1, M_2 \ll 10^9(1+\tan^2\beta)$ GeV, the three charged-lepton states are active in the plasma during

[2] This different hierarchy in the neutrino Dirac and Majorana matrices can be accommodated in the model through different mediator masses for the Dirac, and RH Majorana mediators, respectively Λ_D, Λ_N. From Eqs. (4.2) and (4.3), if $v_b/\Lambda_D \simeq v_a/\Lambda_D \simeq \epsilon_\nu$, requiring $\Lambda_D/\Lambda_N \simeq \epsilon_\nu$ leads to $M_a/M_c < \epsilon_\nu^6$.

leptogenesis and the Boltzmann equations take the form [24]

$$\begin{aligned}
\frac{dY_{N_i}}{dz} &= -2D\left(Y_{N_i} - Y_{N_i}^{\mathrm{eq}}\right), \\
\frac{dY_{\widetilde{N}_i}}{dz} &= -2D\left(Y_{\widetilde{N}_i} - Y_{\widetilde{N}_i}^{\mathrm{eq}}\right), \\
\frac{dY_{\Delta\alpha}}{dz} &= 2\varepsilon^{\alpha}_{N_i} D\left(Y_{N_i} - Y_{N_i}^{\mathrm{eq}}\right) + 2\varepsilon^{\alpha}_{\widetilde{N}_i} D\left(Y_{\widetilde{N}_i} - Y_{\widetilde{N}_i}^{\mathrm{eq}}\right) + \frac{K^{\alpha}_{N_i}}{K_{N_i}} W \sum_{\alpha} A_{\alpha\alpha'} Y_{\Delta\alpha'} \quad ,
\end{aligned} \tag{4.20}$$

where $z = M_i/T$ and $Y_{N_i}^{\mathrm{eq}}$, $Y_{\widetilde{N}_i}^{\mathrm{eq}}$ are the equilibrium densities of (s)neutrinos N_i, $\widetilde{N}_i$, respectively. In this case, the flavour index α runs over the three lepton flavours, $\alpha = e, \mu, \tau$, and the asymmetries $Y_{\Delta\alpha}$ are stored separately in the different flavours. The factors D and W govern the decay and washout behaviour, respectively, and contain information about decays, inverse decays, and scattering processes. [25–28]. The expressions used in our calculation are collected in Appendix C.1, where we follow in particular the notation and method of [24]. The decay factors $K^{\alpha}_{N_i}$ and CP asymmetries $\varepsilon^{\alpha}_{N_i}$, arising from the interference between tree-level and loop diagrams of the RH neutrino decay, are determined by the flavour parameters of the model, and are explored in the next subsection.

In the case $M_1 < 10^9(1+\tan^2\beta)$ GeV $< M_2$, only the tau Yukawa coupling is in equilibrium during N_2 decays. We thus have two lepton flavours in the process, $\alpha = \tau, (e+\mu)$. In this first step, two asymmetries are generated, Y_{Δ_τ} and $Y_{\Delta_{e\mu}}$, following Eq. (4.20). However, before the decay of N_1, the muon Yukawa coupling reaches equilibrium and $Y_{\Delta_{e\mu}}$ is projected on the e and μ flavours, proportionally to $K^{e}_{N_2}$ and $K^{\mu}_{N_2}$, respectively. We then use these values as initial conditions in N_1 decays, using again Eq. (4.20) with $\alpha = e, \mu\tau$.

Finally, we can have both N_1 and N_2 in the two-flavour regime, $10^9(1+\tan^2\beta)$ GeV $\ll M_1, M_2$. An asymmetry is generated from N_2 decays in the $(e+\mu)_2$ flavour, i.e. in the combination of e and μ that couples to N_2. This combination maintains the coherence in the plasma between a decay and a subsequent inverse decay. Then, when $T \sim M_1$, the couplings of N_1 select a different combination of of e and μ in the direction of the N_1 Yukawa coupling, $(e+\mu)_1$. This implies that only the component of the $(e+\mu)_2$ asymmetry in the $(e+\mu)_1$ direction can be washed-out by N_1 inverse decays, while the rest, orthogonal to $(e+\mu)_1$, remains untouched by N_1.

Note that in all numerical calculations below, we use the instantaneous approximation to describe the transition between the two-flavour and three-flavour regime. A more rigorous description of the transition between two different flavoured scenarios would require the use of density matrix equations, as noted in [28, 29] and described in detail in [30].

4.4.2 Decay factors and CP asymmetries

The lepton asymmetry in each flavour is governed by two sets of parameters which can be computed within a given neutrino model: the decay factors $K^{\alpha}_{N_i}$ and CP asymmetries $\varepsilon^{\alpha}_{N_i}$, for a neutrino N_i decaying into a Higgs H_u and lepton doublet L_α (or their conjugates). The Majorana nature of the RH neutrino masses implies the decays $N_i \to L_\alpha H_u$ and $N_i \to \bar{L}_\alpha H_u^*$ violate lepton number by one unit ($\Delta L = 1$). The decay factors are defined as

$$K^{\alpha}_{N_i} = \frac{\Gamma(N_i \to L_\alpha H_u) + \Gamma(N_i \to \bar{L}_\alpha H_u^*)}{\mathcal{H}(M_i)}, \qquad K_{N_i} = \sum_\alpha K^{\alpha}_{N_i}, \tag{4.21}$$

where $\mathcal{H}(T)$ is the Hubble parameter at the temperature T, and $\mathcal{H}(M_i) \simeq 1.66\sqrt{g_*}M_i^2/M_{\rm Pl}$. The CP asymmetries are defined as

$$\varepsilon^{\alpha}_{N_i} = \frac{\Gamma(N_i \to L_\alpha H_u) - \Gamma(N_i \to \bar{L}_\alpha H_u^*)}{\Gamma(N_i \to L_\alpha H_u) + \Gamma(N_i \to \bar{L}_\alpha H_u^*)}. \tag{4.22}$$

The decay factors are dominated by the single tree-level diagram, while the CP asymmetries arise only at one-loop level from the self-energy plus vertex diagrams. In the two-flavour regime, $K^{e\mu}_{N_i} = K^{e}_{N_i} + K^{\mu}_{N_i}$, with the corresponding decay asymmetry $\varepsilon^{e\mu}_{N_i} = \varepsilon^{e}_{N_i} + \varepsilon^{\mu}_{N_i}$.
Explicitly in terms of the neutrino Yukawa matrix in the flavour basis, λ_ν, the decay factors are given by

$$K^{\alpha}_{N_i} = \frac{v_u^2}{m_* M_i}(\lambda_\nu^\dagger)_{i\alpha}(\lambda_\nu)_{\alpha i}, \tag{4.23}$$

where $m_* \simeq (1.58 \times 10^{-3}\ \text{eV})\sin^2\beta$. For N_i decay, the relative phase between the tree diagram and the loop diagram with an intermediate N_j will be the phase of $(\lambda_\nu^\dagger\lambda_\nu)_{ij}$. Then the CP-asymmetries for the two lightest RH-neutrinos is expressed as

$$\varepsilon^{\alpha}_{N_i} = \frac{1}{8\pi}\sum_{j\neq i}\frac{\text{Im}[(\lambda_\nu^\dagger)_{i\alpha}(\lambda_\nu^\dagger\lambda_\nu)_{ij}(\lambda_\nu)_{\alpha j}]}{(\lambda_\nu^\dagger\lambda_\nu)_{ii}} g\left(\frac{M_j^2}{M_i^2}\right). \tag{4.24}$$

where $g(x)$ is a loop function given by the sum of the vertex and the self energy contributions [24, 31]; in the MSSM,

$$g(x) = \sqrt{x}\left[\frac{2}{1-x} - \log\left(\frac{1+x}{x}\right)\right]. \tag{4.25}$$

An exploration of the CP asymmetries and decay factors – responsible for the production and washout of a lepton asymmetry, respectively – provides some insight into how leptogenesis proceeds in this model. The decay factors appear in the arguments of exponential damping terms, and a large $K^{\alpha}_{N_i}$ is associated with strong washout. As it is inversely proportional to the RH neutrino mass, in the "vanilla" picture of flavour-independent N_1 leptogenesis, this yields a lower bound on the N_1 mass, $M_1 \gtrsim 10^9$ GeV [25]. When considering asymmetry generation from next-to-lightest RH neutrinos (N_2 leptogenesis), typically a crucial requirement is that $K^{\alpha}_{N_1} \lesssim 1$ in some lepton flavour, to not completely wash out a previously generated asymmetry from N_2 decays [27]. This depends in particular on the Yukawa structures that give λ_ν; N_2 leptogenesis and its compatibility with low-scale neutrino phenomenology has been studied in [32–35].

As we are considering the case in which $M_1 \ll M_3$ then we can also neglect the $i = 3$ contribution to $\varepsilon^{\alpha}_{N_1}$. In Appendix C.3 we show that λ_ν (in the flavour basis) maintains the hierarchical structure suggested by the model, and a rough estimate for the leptogenesis parameters gives

$$
\begin{aligned}
K^{\alpha}_{N_1} &\sim \left|\frac{M_b M_c}{M_a^2}\right| \epsilon_\nu^6 \begin{pmatrix} \epsilon_\nu^2 \\ 1 \\ 1 \end{pmatrix}, \qquad \varepsilon^{\alpha}_{N_1} \sim \frac{3}{8\pi}\left|\frac{M_a}{M_b}\right|^2 \epsilon_\nu^4 \begin{pmatrix} \epsilon_\nu^2 \\ 1 \\ 1 \end{pmatrix}, \\
K^{\alpha}_{N_2} &\sim \left|\frac{M_c}{M_b}\right| \epsilon_\nu^4 \begin{pmatrix} \epsilon_\nu^2 \\ 1 \\ 1 \end{pmatrix}, \qquad \varepsilon^{\alpha}_{N_2} \sim \frac{3}{8\pi}\left|\frac{M_b}{M_c}\right| \begin{pmatrix} \epsilon_\nu^4 \\ \epsilon_\nu^2 \\ 1 \end{pmatrix} + \frac{1}{4\pi}\left|\frac{M_a}{M_b}\right|^2 \epsilon_\nu^6 \begin{pmatrix} \epsilon_\nu^2 \\ 1 \\ 1 \end{pmatrix}.
\end{aligned}
\tag{4.26}
$$

From this we can make some *a priori* considerations: (i) due to the UTZ in the electron coupling to N_1, lepton asymmetries from N_1 decays are dominated by the μ and τ flavours, while $\varepsilon^{e}_{N_1}$ is generally too small to contribute significantly to asymmetry production, (ii) we similarly expect a strong washout in the μ and τ flavours for both N_1 and N_2 leptogenesis, and comparatively weak washout for the electron, and (iii) despite the large hierarchy between M_b and M_c, the $\varepsilon^{\alpha}_{N_2}$ are typically dominated by the first term, which generates non-negligible asymmetry only if M_b and M_c are not too separated.

Neutrinos		Charged leptons	
m_a/meV	8.95	y_a^e	3.01×10^{-4}
m_b/meV	24.6	y_b^e	3.90×10^{-3}
m_c/meV	2.26	y_c^e	7.16×10^{-2}
γ_m	2.51	γ_e	0.13
δ_m	1.26	δ_e	-1.31

TABLE 4.2: Fitted values for the low-scale model parameters, extracted from the computation in [13].

4.5 Analysis and results

4.5.1 Numerical results

In this section we present the numerical solutions to the fully flavoured Boltzmann equations in the MSSM as given in Section 4.4, following a similar procedure to the one already adopted in [36]. The analysis has been performed under the assumption that the spectrum of the heavy neutrinos in the model is hierarchical, $M_1 < M_2 \ll M_3$. Within this framework,

- a possible asymmetry generated by the heaviest RH neutrino N_3 is always washed out and assumed to be negligible,
- the generation of the asymmetry and the washout from decays and inverse decays of the N_1 neutrinos starts only after the end of the analogous processes from the N_2. The two lightest RH neutrinos do not interfere with each other, such that the generation of the asymmetry from N_1 decays and from N_2 decays proceed independently.

Consequently, the Boltzmann equations in Eq. (4.20) are solved twice for each point in the model parameter space. In the first step, we solve for Y_{Δ_α} arising from $N_{i=2}$ decays, assuming thermal initial conditions (zero neutrino and asymmetry densities). The solutions for Y_{Δ_α} are then used as initial conditions for the $N_{i=1}$ calculation. The final asymmetry is obtained from the sum over Y_{Δ_α} after N_1 leptogenesis.
The input parameters are comprised of those not already fixed by the fit to low-scale neutrino phenomenology. In particular, we use the fit to quark and lepton masses and mixing for our flavour model performed in [13], with relevant best fit values for the lepton sector given in Table 4.2. We fix $\tan\beta = 10$ in this analysis. Note also that, as the model does not determine the absolute mass scale for fermions, the fit only provides estimates for the parameters in Eq. (4.9) up to an overall scale, which is set

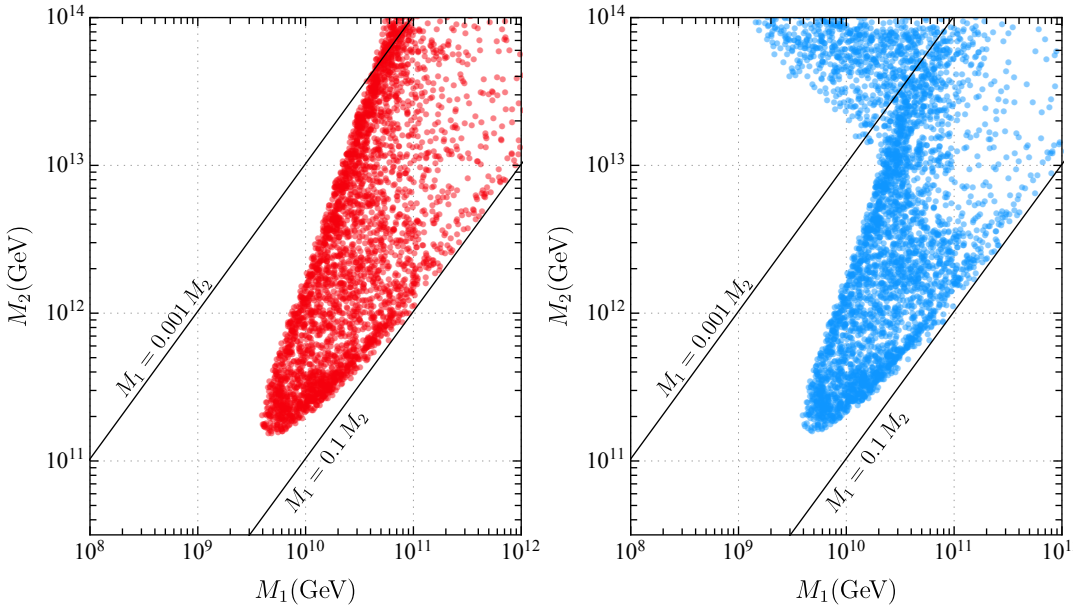

FIGURE 4.1: Allowed values of RH neutrino eigenvalues $M_{1,2}$ giving Y_B within 20% of the observed value. The N_3 mass is fixed to be $M_3 = 5 \times 10^{14}$ GeV. Red points assume the only contributions are from N_1 decays, while blue points take into account both N_1 and N_2 decays.

by the third generation, i.e. by M_c and $y_c^{e,\nu}$. With $\tan\beta$ fixed, we can infer the charged lepton scale y_c^e, while the neutrino scales y_c^ν and M_c remain unfixed. The fit fixes the values of the neutrino mass parameters $m_{a,b,c}$ and charged lepton parameters $y^e_{a,b,c}$. The seesaw relation in Eq. (4.16) entangles the three Dirac and three Majorana neutrino couplings ($y^\nu_{a,b,c}$ and $M_{a,b,c}$, respectively), constrained only by the three fitted values of $m_{a,b,c}$, leaving three (real) free parameters which enter into the leptogenesis analysis. The phases of the couplings are similarly related: Y_ν and M_N each contain two independent phases (γ_ν, δ_ν and γ_N, δ_N, respectively); combinations of these yield the two fitted independent phases of m_ν.

For this analysis, we choose the sets $M_{a,b,c}$ and γ_N, δ_N as the inputs, scanning over the ranges $|M_{a,b}| \in [10^7, 10^{14}]$ GeV with fixed $|M_c| = 5 \times 10^{14}$ GeV, and $\gamma_N, \delta_N \in [-\pi, \pi]$. For each point, we solve the N_1 and N_2 Boltzmann equations for $z \in [0, \infty]$. We stress that, as the parameters of Y^e and m_ν are fixed by the fit, each point automatically satisfies current experimental bounds on lepton masses and mixing. The results are shown in Figures 4.1 and 4.2. Figure 4.1 shows the regions that reproduce the experimental value of Y_B to within 20%, in terms of the RH neutrino mass eigenvalues $M_{1,2}$,

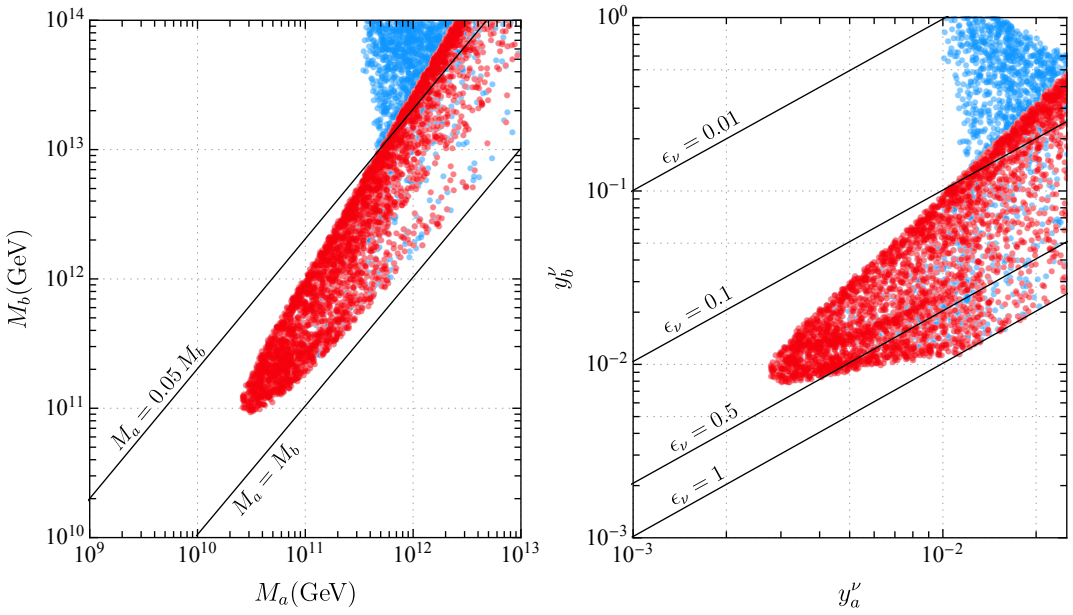

FIGURE 4.2: Allowed values of RH input mass parameters $M_{a,b}$, Dirac neutrino couplings $y^\nu_{a,b}$, and RH neutrino masses $M_{1,2}$ giving Y_B within 20% of the observed value. The colours correspond to those Figure 4.1.

with $M_3 \simeq 5 \times 10^{14}$ GeV. In Figure 4.1a we see the successful leptogenesis regions taking into account only N_1 decays, while in Figure 4.1b we consider both N_1 and N_2 decays. The comparison between plots allows us to conclude that, over most of the parameter space of the model, the BAU is consistent with leptogenesis proceeding entirely from N_1 decays, assuming thermal initial conditions. In other words, the asymmetries generated by N_2 decays are efficiently washed out in all flavours. In the N_1 case, the dominant contributions to the viable regions are from the μ and τ asymmetries, while the electron asymmetry is completely negligible. This agrees well with the expectations from the analytical approximations in Section 4.4. Nevertheless, in Figure 4.1b we find a small region where the N_2 contribution to the BAU dominates. We can see that this scenario requires a small splitting between the heavy RH neutrinos, $M_2/M_3 \gtrsim 0.1$. The N_2 case is discussed further in Section 4.5.2, where we show that this region of parameter space is not natural in the UTZ model.

Figure 4.2a displays the regions corresponding to Y_B within 20% of the observed value, in terms of the RH neutrino mass parameters $M_{a,b}$, with $M_c = 5 \times 10^{14}$ GeV. Most of the points correspond to N_1 leptogenesis (red points) with $M_a/M_b \in [0.05, 1]$. Figure 4.2b shows the corresponding regions in terms of the neutrino Dirac couplings $y^\nu_{a,b}$, and the expansion parameter $\epsilon_\nu = y^\nu_a/y^\nu_b$. In N_1-dominated leptogenesis, we

have $y_a^\nu \in [0.003, 0.03]$, $y_b^\nu \in [0.008, 0.5]$ and $\epsilon_\nu \in [0.05, 1]$.
Recalling that $M_1 \sim M_a^2/M_b$ and $M_2 \sim M_b$, the eigenvalues $M_{1,2}$ display a bigger hierarchy when compared to $M_{a,b}$ and these points satisfy $M_1/M_2 \in [0.002, 0.1]$. Therefore, we conclude that the correct BAU is found for RH neutrino masses above $M_1 \gtrsim 4 \times 10^9$ GeV and $M_2 \gtrsim 2 \times 10^{11}$ GeV. In this regime it is relevant to discuss the issues related to the potential overproduction of gravitinos [37]. There are several ways around it [38, 39], one of which is to keep the reheating temperature low and to produce the RH neutrinos non-thermally (e.g. produced in decays of the inflaton). Nonetheless, even for thermal production scenarios, if the gravitino is unstable with mass $m_{3/2} \gtrsim 10$ TeV, these relatively high reheating temperatures around 10^9 or 10^{10} GeV remain borderline viable.
Finally, it is interesting to analyse the restrictions that a requirement of successful leptogenesis set on the flavour model. As we have seen in Figures 4.1 and 4.2, the best possibility, if we demand a relatively low reheating temperature, would correspond to RH eigenvalues $M_1 \simeq 4 \times 10^9$ GeV and $M_2 \simeq 2 \times 10^{11}$ GeV, with $M_3 \geq 10^{14}$ GeV. In terms of the model parameters these points correspond roughly to $M_a \simeq 3 \times 10^{10}$ GeV, $M_b \simeq 10^{11}$ GeV, $y_a^\nu \simeq 0.003$ and $y_b^\nu \simeq 0.009$. We emphasize again that independent information on the neutrino Yukawa couplings and RH neutrino masses is not available from oscillation experiments, but when the BAU is accounted for we can obtain several unknown parameters. With the above values we obtain the expansion parameter $\epsilon_\nu \simeq 0.3$. The heaviest RH neutrino is then $M_c \times g_b^\nu / g_c^\nu \simeq 2\sqrt{3} M_b / \epsilon_\nu^6 \simeq 5 \times 10^{14}$ GeV. However, these restrictions depend strongly on the details of the flavour model and may change with small variations [14]. If supersymmetry is found in the neighbourhood of the electroweak scale, we would obtain additional information on the flavour symmetry that could help restrict these possibilities [14, 40–42].

4.5.2 N_2 leptogenesis and comparison with other models

As we have seen in the comparison of Figures 4.1a and 4.1b, there is a small region where the BAU is generated mainly by N_2 leptogenesis. This region corresponds to $M_1 \leq 0.002 M_2$, with $M_2 \geq 10^{13}$ GeV and $M_3 = 5 \times 10^{14}$ GeV. These points correspond to relationships between model parameters, $M_a < 0.002 M_b$ and $0.01 < \epsilon_\nu < 0.1$.
Here, the mechanism of asymmetry generation and washout is slightly more involved [28, 29, 43, 44]. At temperatures $T \sim M_2 \sim 10^{13}$ GeV, a comparatively large asymmetry is generated in each of the two active lepton flavours $\alpha = (e\mu), \tau$ from

N_2 decays. These serve as initial conditions of the subsequent N_1 system, which occurs at much lower temperatures $T \sim M_1 \sim 10^9$ GeV. This lies in the fully flavoured regime, wherein the active flavours are $\alpha = e, \mu, \tau$. The asymmetry $Y_{\Delta_{e\mu}}$, initially generated in the combined $e\mu$ flavour, is split into the e and μ flavours proportionally to $K^e_{N_2} \propto |\lambda_{e2}|^2$ and $K^\mu_{N_2} \propto |\lambda_{\mu 2}|^2$, respectively [28, 43, 44].[3] Assuming the number density of e and μ asymmetries are equal at the moment where μ couplings reach equilibrium, the initial conditions for the N_1 decays are thus $Y_{\Delta_e} \simeq x^2 Y_{\Delta_{e\mu}}$ and $Y_{\Delta_\mu} \simeq (1 - x^2) Y_{\Delta_{e\mu}}$, where $x = |y^\nu_a / y^\nu_b - M_a / M_b|$.

As the CP asymmetries $\varepsilon^\alpha_{N_1}$ are sensitive to the ratio $M_1/M_2 \ll 1$, no significant additional contribution to the BAU is generated by N_1 decays in this regime. However, if a large asymmetry is generated by N_2 decays, even a small portion stored in the electron flavour can survive washout and reproduce the observed asymmetry. To understand this, we make two observations: 1) the decay factors $K^\alpha_{N_1}$ are approximately proportional to $1/M_1$, and 2) in each lepton flavour, they go like $(K^e_{N_1}, K^\mu_{N_1}, K^\tau_{N_1}) \sim (\epsilon_\nu^2, 1, 1)$. In other words, the flavour structure of the model implies the washout in the electron flavour is generally weaker than other flavours. Indeed, we observe that the Y_{Δ_μ} and Y_{Δ_τ} asymmetries are efficiently washed out, while some portion of Y_{Δ_e} remains.

So, as we can see, N_2 leptogenesis is possible (in part) due to the texture zero, which is enforced by symmetry. However, from the perspective of the UTZ model based on $\Delta(27)$, described above, this N_2-dominated scenario is not "natural", while N_1 leptogenesis is still viable and natural in large parts of the parameter space. This unnaturalness is a direct consequence of the structure of the neutrino matrices (see Eq. (4.7)) and can be understood by looking at Eqs. (4.16)–(4.18). Using Eq. (4.18) with the measured value for $\sin\theta_{13} \simeq 0.15$, we obtain

$$2\frac{y^\nu_b}{y^\nu_a} - \frac{M_b}{M_a} \simeq 8.2 \tag{4.27}$$

Barring accidental cancellations, this expression fixes $|M_2/M_1| = |M_b^2/M_a^2| \approx 8$. As a consequence, the structure of Yukawa matrices enhances the leptogenesis effects from N_1, proportional to M_1/M_2, and suppresses N_2 effects, proportional to M_2/M_3 (see Eq. (4.26)).

[3] In principle, we should also include the so-called phantom terms [44]. However, for $\delta = e, \mu$ and using $p_\delta = (\varepsilon^\delta_{N_2} - \varepsilon^{(e+\mu)}_{N_2} K^\delta_{N_2} / K^{(e+\mu)}_{N_2}) N^{\rm in}_{N_2}$, it is straightforward to check from Eq. (4.26) that, even assuming an initial N_2 abundance $N^{\rm in}_{N_2}$, these terms are always subdominant in our scenario, at least by ϵ_ν^2, with respect to $\varepsilon^{(e+\mu)}_{N_2} K^\delta_{N_2} / K^{(e+\mu)}_{N_2}$. They can therefore be safely neglected in the model considered.

N_2 leptogenesis can be important in situations where $M_2/M_1 \gg 1$, as seen in Figure 4.1, but this requires a strong cancellation of several orders of magnitude in Eq. (4.27). Moreover, the structure of the neutrino Yukawa matrices in the UTZ model is not hierarchical in this region, as we have $0.1 \leq y_b^\nu \lesssim 1$ while $y_c^\nu \simeq 0.1$. These values are not natural to the UTZ model, where most of the flavon VEVs are required to be much smaller than 1. In conclusion, N_2 leptogenesis is possible, but disfavoured. This can be compared with the situation in typical $SO(10)$ models [34, 45, 46] and, in general, in models of sequential dominance (SD) [36]. In these models, the three LH neutrino mass scales are each determined independently by a single RH neutrino. Schematically, SD in the limit of $M_1 < M_2 \ll M_3$ gives

$$m_1 \propto \frac{y_3^{\nu 2} v_u^2}{M_3}, \qquad m_2 \propto \frac{y_1^{\nu 2} v_u^2}{M_1}, \qquad m_3 \propto \frac{y_2^{\nu 2} v_u^2}{M_2}, \tag{4.28}$$

with a strong hierarchy of $m_1 < m_2 < m_3$, and where $y_3^\nu \propto m_t$, $y_2^\nu \propto m_c$ and $y_1^\nu \propto m_u$ (and thus $y_a^\nu < y_b^\nu < y_c^\nu$). Models with special flavon directions like the so-called Constrained Sequential Dominance 3 alignment [36] have simply $\sin\theta_{13} \simeq m_1/(m_1 + m_2)$, which does not constrain the ratio M_2/M_1. The only constraint on RH neutrino masses comes from Eq. (4.28). Setting $m_1 = m_{\text{sol}}$ and $m_2 = m_{\text{atm}}$ implies $M_2 \simeq 10^{11}$ GeV and $M_2/M_1 \simeq m_c^2/(6m_u^2) \simeq 5 \times 10^4$. Under these conditions N_1 contributions to the BAU are far too small, but N_2 can still successfully contribute, as shown explicitly in [30, 47, 48]. Unlike this traditional case for N_2 leptogenesis, which is typically aimed at resolving the problem of having a lightest neutrino with too small a mass ($M_1 \ll 10^9$ GeV), in our case even the N_2 region requires $M_1 \gtrsim 10^9$ GeV, to avoid too-large washout. In some sense, separate to the above discussion on naturalness, some balancing is also required to ensure the initial N_2 asymmetry, which may be one or two orders of magnitude larger than anticipated by the observed BAU, is washed out just the right amount by N_1 interactions to yield the correct value of Y_B.

In the UTZ model we can also compare ratios between the $y_{a,b,c}^\nu$ presented here and ratios of their respective counterparts from the up quark sector, which have $y_a^u/y_b^u \sim 0.05$, $y_b^u/y_c^u \sim 0.05^2$ [13], in accordance with an expansion parameter $\varepsilon_u \sim 0.05$. By contrast, the hierarchy between y_a^ν and y_b^ν is only up to one order of magnitude.

In the numerical analysis above, the parameters $\tan\beta$ and $M_c \sim M_3$ are kept fixed. The main impact of $\tan\beta$ is only to define the boundary between the two- and three-flavor regimes. Given that the model favours large $\tan\beta$ values, we have taken a moderately large value of $\tan\beta = 10$, for which N_2 leptogenesis takes place in the two-flavour regime, N_1 leptogenesis takes place in the three-flavour regime, and a

sizable asymmetry in the electron flavour survives. Although the results would be qualitatively similar for larger $\tan\beta$ values, for $\tan\beta < 10$ the entire asymmetry production occurs in the two-flavoured regime and, due to the alignment of N_1 and N_2 Yukawa couplings in the $e-\mu$ plane, it is more difficult to obtain a sufficient asymmetry. Ideally, a more natural realization of N_2 leptogenesis would be achieved in the fully three flavoured regime $M_1, M_2 \leq 10^9(1+\tan\beta^2)$ GeV, but this situation can not be realized while simultaneously maintaining the required hierarchy $M_1 < M_2$. Regarding M_c, the scenario in which the N_2 production dominates is where the ratio M_2/M_3 is large, $M_2/M_3 \gtrsim 0.1$. We have considered a value for M_c consistent with the model and which illustrates the relevant leptogenesis features. Another choice will see the viable N_2-leptogenesis region shifted up- or downwards in the mass M_2 in order to maintain this large ratio.

4.6 Conclusions

We have studied the generation of the baryon asymmetry of the Universe through leptogenesis in the Universal Texture Zero $SO(10) \times \Delta(27) \times \mathbb{Z}_N$ flavoured GUT model [13]. Here, leptogenesis yields the observed BAU for a considerable region of the parameter space. When expressed in terms of the RH neutrino masses M_1 and M_2, which are functions of the model parameters M_a and M_b. The viable ranges for the mass of the lightest RH neutrino eigenstate have a lower bound of $M_1 \gtrsim 4 \times 10^9$ GeV, which is still barely compatible with a gravitino mass $m_{3/2} \gtrsim 10$ TeV, provided the gravitino is unstable [37].

We specifically considered the effect of N_2 leptogenesis, which we conclude to be disfavored: although there exists a egion of parameter space where N_2 leptogenesis provides the dominant contribution to the final asymmetry, this corresponds to a scenario with both a very strong hierarchy between the two lightest RH neutrinos, i.e. $M_1 \ll M_2$, and comparatively small hierarchy between M_2 and M_3. This is not a natural expectation in the model, which predicts a strong hierarchy between the heaviest neutrino and the two lighter ones, i.e. $M_1 < M_2 \ll M_3$. Lepton asymmetries generated by decays of the heaviest neutrino N_3 are therefore also negligible.

The preferred mechanism is thus N_1 leptogenesis. The requirement that it accounts for the entire baryon asymmetry allows us to restrict the parameters governing the neutrino Yukawa matrix and RH neutrino mass matrix. These are otherwise only partially constrained by the observed neutrino masses and mixing, namely those combinations of parameters which appear in the neutrino matrix after seesaw. We

find that viable N_1 leptogenesis requires $M_1 \gtrsim 4 \times 10^9$ GeV, with $M_2 \gtrsim 2 \times 10^{11}$ GeV, while $0.002 \lesssim M_1/M_2 \lesssim 0.1$. By consistency with low energy observables, we can similarly constrain the neutrino Yukawa couplings, which are bounded from below, $y_a^\nu \gtrsim 0.003$, $y_b^\nu \gtrsim 0.008$.

In conclusion, flavoured leptogenesis is viable for the UTZ model in the standard N_1 regime. Through this we are able to place further constraints on the parameter space of the UTZ model, leading to direct constraints on the scale of the parameters M_a, M_b governing the RH neutrino masses. Given that in the model the active neutrino masses originate from type-I seesaw leading to normal ordering with a strong hierarchy, the leptogenesis constraint on M_a, M_b can then be combined with the observed mass-squared differences to indirectly constrain the Dirac neutrino couplings y_a^ν, y_b^ν. These constraints are complementary to those provided by the study of flavour-changing processes [14] in the UTZ model.

References

[1] A. Sakharov, *Sov. Phys. Usp.* **1991**, *34*, 392–393.

[2] V. Kuzmin et al., *Phys. Lett. B* **1985**, *155*, 36.

[3] M. Fukugita, T. Yanagida, *Phys. Lett. B* **1986**, *174*, 45–47.

[4] A. Blum et al., *Phys. Rev. D* **2008**, *77*, 076004, arXiv: 0709.3450 [hep-ph].

[5] C. Hagedorn, D. Meloni, *Nucl. Phys. B* **2012**, *862*, 691–709, arXiv: 1204.0715 [hep-ph].

[6] M. Holthausen, K. S. Lim, *Phys. Rev. D* **2013**, *88*, 033018, arXiv: 1306.4356 [hep-ph].

[7] H. Ishimori et al., *Phys. Lett. B* **2015**, *743*, 172–179, arXiv: 1411.5845 [hep-ph].

[8] C.-Y. Yao, G.-J. Ding, *Phys. Rev. D* **2015**, *92*, 096010, arXiv: 1505.03798 [hep-ph].

[9] I. de Medeiros Varzielas et al., *Int. J. Mod. Phys. A* **2017**, *32*, 1750047, arXiv: 1605.03581 [hep-ph].

[10] J.-N. Lu, G.-J. Ding, *Phys. Rev. D* **2018**, *98*, 055011, arXiv: 1806.02301 [hep-ph].

[11] C. Hagedorn, J. König, *Phys. Rev. D* **2019**, *100*, 075036, arXiv: 1811.07750 [hep-ph].

[12] J.-N. Lu, G.-J. Ding, *JHEP* **2019**, *03*, 056, arXiv: 1901.07414 [hep-ph].

[13] I. de Medeiros Varzielas et al., **2017**, arXiv: 1710.01741 [hep-ph].

[14] I. De Medeiros Varzielas et al., *JHEP* **2018**, *09*, 047, arXiv: 1807.00860 [hep-ph].

[15] S. F. King, G. G. Ross, *Phys. Lett.* **2003**, *B574*, 239–252, arXiv: hep-ph/0307190 [hep-ph].

[16] G. G. Ross et al., *Nucl. Phys.* **2004**, *B692*, 50–82, arXiv: hep-ph/0401064 [hep-ph].

[17] I. de Medeiros Varzielas, G. G. Ross, *Nucl. Phys.* **2006**, *B733*, 31–47, arXiv: hep-ph/0507176 [hep-ph].

[18] I. de Medeiros Varzielas, *JHEP* **2012**, *01*, 097, arXiv: 1111.3952 [hep-ph].

[19] I. de Medeiros Varzielas, G. G. Ross, *JHEP* **2012**, *12*, 041, arXiv: 1203.6636 [hep-ph].

[20] F. Björkeroth et al., *Phys. Rev. D* **2016**, *94*, 016006, arXiv: 1512.00850 [hep-ph].

[21] F. Björkeroth et al., *JHEP* **2015**, *10*, 104, arXiv: 1505.05504 [hep-ph].
[22] I. de Medeiros Varzielas, *JHEP* **2015**, *08*, 157, arXiv: 1507.00338 [hep-ph].
[23] R. Gatto et al., *Phys. Lett. B* **1968**, *28*, 128–130.
[24] S. Antusch et al., *JCAP* **2006**, *11*, 011, arXiv: hep-ph/0609038.
[25] S. Davidson, A. Ibarra, *Phys. Lett. B* **2002**, *535*, 25–32, arXiv: hep-ph/0202239.
[26] G. Giudice et al., *Nucl. Phys. B* **2004**, *685*, 89–149, arXiv: hep-ph/0310123.
[27] W. Buchmuller et al., *Annals Phys.* **2005**, *315*, 305–351, arXiv: hep-ph/0401240.
[28] A. Abada et al., *JCAP* **2006**, *04*, 004, arXiv: hep-ph/0601083.
[29] R. Barbieri et al., *Nucl. Phys. B* **2000**, *575*, 61–77, arXiv: hep-ph/9911315.
[30] S. Blanchet et al., *JCAP* **2013**, *01*, 041, arXiv: 1112.4528 [hep-ph].
[31] P. Di Bari, *Nucl. Phys. B* **2005**, *727*, 318–354, arXiv: hep-ph/0502082.
[32] P. Di Bari, A. Riotto, *JCAP* **2011**, *04*, 037, arXiv: 1012.2343 [hep-ph].
[33] P. Di Bari, L. Marzola, *Nucl. Phys. B* **2013**, *877*, 719–751, arXiv: 1308.1107 [hep-ph].
[34] P. Di Bari et al., *Nucl. Phys. B* **2015**, *893*, 122–157, arXiv: 1411.5478 [hep-ph].
[35] P. Di Bari et al., *JCAP* **2014**, *03*, 050, arXiv: 1401.6185 [hep-ph].
[36] F. Björkeroth et al., *JHEP* **2017**, *01*, 077, arXiv: 1609.05837 [hep-ph].
[37] M. Kawasaki et al., *Phys. Rev. D* **2008**, *78*, 065011, arXiv: 0804.3745 [hep-ph].
[38] K. Jedamzik, *Phys. Rev. D* **2006**, *74*, 103509, arXiv: hep-ph/0604251.
[39] J. Pradler, F. D. Steffen, *Phys. Rev. D* **2007**, *75*, 023509, arXiv: hep-ph/0608344.
[40] D. Das et al., *Phys. Rev.* **2017**, *D95*, 035001, arXiv: 1607.06827 [hep-ph].
[41] M. L. López-Ibáñez et al., *JHEP* **2017**, *11*, [Erratum: JHEP 04, 015 (2018)], 162, arXiv: 1710.02593 [hep-ph].
[42] M. López-Ibáñez et al., *JHEP* **2019**, *06*, 047, arXiv: 1901.04526 [hep-ph].
[43] E. Nardi et al., *JHEP* **2006**, *01*, 164, arXiv: hep-ph/0601084.
[44] S. Antusch et al., *Nucl. Phys. B* **2012**, *856*, 180–209, arXiv: 1003.5132 [hep-ph].
[45] O. Vives, *Phys. Rev. D* **2006**, *73*, 073006, arXiv: hep-ph/0512160.
[46] P. Di Bari, S. F. King, *JCAP* **2015**, *10*, 008, arXiv: 1507.06431 [hep-ph].
[47] E. Bertuzzo et al., *Nucl. Phys. B* **2011**, *849*, 521–548, arXiv: 1007.1641 [hep-ph].
[48] F. J. de Anda et al., *JHEP* **2017**, *12*, [Erratum: JHEP 04, 069 (2019)], 075, arXiv: 1710.03229 [hep-ph].

Article 5

Muon and electron $g-2$ and lepton masses in flavor models

JHEP 06 (2020) 087

Lorenzo Calibbi[a], M.L. López-Ibáñez[b], A. Melis[c] and O. Vives[d]

[a] *School of Physics, Nankai University, Tianjin 300071, China*

[b] *CAS Key Laboratory of Theoretical Physics, Institute of Theoretical Physics, Chinese Academy of Sciences, Beijing 100190, China*

[c] *Departament de Física Tèorica, Universitat de València & IFIC, Universitat de València & CSIC, Dr. Moliner 50, E-46100 Burjassot (València), Spain.*

ABSTRACT: The stringent experimental bound on $\mu \to e\gamma$ is compatible with a simultaneous and sizable new physics contribution to the electron and muon anomalous magnetic moments $(g-2)_\ell$ ($\ell = e,\ \mu$), only if we assume a non-trivial flavor structure of the dipole operator coefficients. We propose a mechanism in which the realization of the $(g-2)_\ell$ correction is manifestly related to the mass generation through a flavor symmetry. A radiative flavon correction to the fermion mass gives a contribution to the anomalous magnetic moment. In this framework, we introduce a chiral enhancement from a non-trivial $\mathcal{O}(1)$ quartic coupling of the scalar potential. We show that the muon and electron anomalies can be simultaneously explained in a vast region of the parameter space with predicted vector-like mediators of masses as large as $M_\chi \in [0.6, 2.5]$ TeV.

5.1 Introduction

Despite the lack of direct signals for new physics from the high-energy collision data collected by the LHC experiments, we have a number of solid arguments, both theoretical and observational, that call for extensions of the Standard Model (SM). The most convincing of those — related to the origin of neutrino masses, dark matter, baryon asymmetry etc. — do not necessarily point to new particles at scales accessible at colliders in the foreseeable future. However, recent years have been also witnessing the arising of several hints for non-standard phenomena from precision observables involving lepton flavors. Signs of departure from the universality of leptonic couplings predicted by the SM in semi-leptonic decays of B mesons have been reported by LHCb and B-factories experiments both in neutral- and charged-current processes — for recent reviews see [1–3]. If confirmed by future data, these discrepancies would certainly require low-scale new physics coupling with different strength to different lepton families.

Another discrepancy that would point to an analogous conclusion is related to the anomalous magnetic moment of the muon, $(g-2)_\mu$. The experimental measurements of $(g-2)_\mu$ have been in tension with the increasingly accurate theoretical calculations within the SM for about 20 years. The discrepancy currently amounts to about $3.5\,\sigma$ [4–10].[1] The situation may be clarified — and the case for new physics possibly reinforced — by the upcoming results of the new Muon g-2 experiment at FNAL [14]. It is well known that new particles coupling to muons can easily account for the $(g-2)_\mu$ provided that their mass are few TeV at most — for a recent review see [15]. This makes the new physics possibly required by the $(g-2)_\mu$ anomaly an ideal target for direct searches at LHC experiments, which in fact have already reached the sensitivity so to exclude substantial portions of the parameter space of typical models [15–20].

Interestingly, a 2σ tension between theory and experiments has been recently reported also for the electron $g-2$. The $(g-2)_e$ has been determined both experimentally and theoretically to such an outstanding precision, that matching the SM prediction to the measurement has been used for many years as the most precise way to evaluate the fine-structure constant α. However, in presence of an alternative and sufficiently precise measurement of α, one can employ $(g-2)_e$ as a test for new physics too [21]. This has become possible in recent years and the most precise

[1] See, however, the very recent lattice result of the leading order hadronic vacuum polarization [11], which, contrary to previous results, could reduce this discrepancy. On the other hand, even if the anomaly is accounted for by the hadronic vacuum polarization, this would reflect in a deterioration of the EW fit and the arising of tensions of comparable significance in other observables [12, 13].

result, obtained by employing matter-wave interferometry with cesium-133 atoms [22], highlighted the discrepancy for $(g-2)_e$ mentioned above. Expressed in terms of $a_\ell \equiv (g-2)_\ell/2$, the present situation can be summarized as follows:

$$\Delta a_e^{\rm exp} \equiv a_e^{\rm exp} - a_e^{\rm SM} = -(8.8 \pm 3.6) \times 10^{-13}, \tag{5.1}$$

$$\Delta a_\mu^{\rm exp} \equiv a_\mu^{\rm exp} - a_\mu^{\rm SM} = (2.7 \pm 0.7) \times 10^{-9}. \tag{5.2}$$

It is very tempting to speculate about a simultaneous new-physics origin of the results above, outlining the same mechanism or, at least, a single model able to explain both discrepancies. In fact, this has been recently attempted in a number of works [23–35]. Although a common explanation has been shown to be possible, the model building task has proved non-trivial. First, as Eqs.(5.1, 5.2) show, the new-physics contributions need to be positive for Δa_μ and negative for Δa_e. Secondly, the absolute magnitude of Δa_μ and Δa_e do not match the naive scaling $\Delta a_\mu / \Delta a_e \sim m_\mu^2/m_e^2$ [21] expected in models where the chirality flip of the lepton field in the dipole operator is provided by the lepton Yukawa coupling itself — see discussion below. In fact, such a scaling would result in an absolute value for Δa_e way too suppressed compared to the experimental range in Eq.(5.1). New physics giving a chirally-enhanced contribution — i.e. featuring the chirality flip inside the loop — at least to Δa_e is thus required in order to account for Eqs.(5.1, 5.2) simultaneously. The third and perhaps most important challenge model building has to face concerns the tight experimental limits on lepton-flavor-violating (LFV) processes — see e.g. [36] for a recent review — in particular $\mu \to e\gamma$. It is clear that any new physics contributing to both the electron and the muon dipole moment will in general induce the corresponding $\mu - e$ dipole transition.

We can quantify the above difficulties as follows. In an effective Lagrangian approach, non-standard effects to the leptonic observables of interest (Δa_ℓ, $\mu \to e\gamma$, EDMs, etc.) arise via the dipole operators:

$$\mathcal{L} \supset \frac{e\, m_\ell^{\rm exp}}{8\,\pi^2}\, C_{\ell\ell'} \left(\bar{\ell}\sigma_{\mu\nu} P_R \ell'\right) F^{\mu\nu} + \text{h.c.} \qquad \ell, \ell' = e, \mu, \tau. \tag{5.3}$$

This effective Lagrangian constitutes a model-independent description of the new-physics effects we are interested in, so long as the new-physics scale is much larger than the energy scale associated to our observables, i.e. the lepton masses. In terms of

the above Wilson coefficients — that in our convention have mass dimension GeV^{-2} — the new-physics contribution to the Δa_ℓ reads:

$$\Delta a_\ell = \frac{m_\ell^{\exp\,2}}{(2\pi)^2}\,\text{Re}(C_{\ell\ell}). \tag{5.4}$$

In order to fit the experimental results — for illustration we focus here on the central values in Eqs.(5.1, 5.2) — the dipole coefficients need to attain the following numerical values:

$$\text{Re}(C_{ee}) \;\approx\; -7\times 10^{-5}\ \text{GeV}^{-2}, \tag{5.5}$$

$$\text{Re}(C_{\mu\mu}) \;\approx\; 5\times 10^{-6}\ \text{GeV}^{-2}. \tag{5.6}$$

The flavor-changing couplings instead contribute to LFV processes, in particular to the radiative decays:

$$\frac{\text{BR}(\ell\to\ell'\gamma)}{\text{BR}(\ell\to\ell'\nu\bar{\nu}')} = \frac{3\alpha}{\pi G_F^2}\left(|C_{\ell\ell'}|^2+|C_{\ell'\ell}|^2\right), \tag{5.7}$$

where the coefficients $C_{\ell\ell'}$ are defined in the basis where the lepton Yukawa matrix Y_ℓ is diagonal. The experimental bound $\text{BR}(\mu\to e\gamma) < 4.2\times 10^{-13}$ [37] then translates into the following constraint:

$$|C_{e\mu}|,\ |C_{\mu e}| \lesssim 10^{-10}\ \text{GeV}^{-2}. \tag{5.8}$$

Notice that defining the coefficients in Eq.(5.3) we have factored out the dependence on the lepton masses. Hence, in models where the chirality flip of the lepton fields required by gauge invariance in Eq.(5.3) is due to a lepton mass insertion, the coefficients C_{ee} and $C_{\mu\mu}$ should be of the same order $1/\Lambda^2$, where Λ is the scale of new physics, with no further chirality suppression. Nevertheless, Eqs.(5.5, 5.6) tell us that this would result in a contribution to the electron magnetic moment a factor of 15 too small. If, on the other hand, the chirality flip in Eq.(5.3) is due to the insertion of a Higgs vev inside the loop, one expects an enhancement of the order $C_{\ell\ell}\sim y_\chi/y_\ell$ where y_χ is the coupling of the new fields to the Higgs and y_ℓ is the lepton Yukawa — see e.g. the discussion in [38]. If the same coupling y_χ enters the diagrams for the electron and the muon dipole moment, one would then obtain $\Delta a_\mu/\Delta a_e \sim m_\mu/m_e$. Again this is not compatible with the observed ranges of Eqs.(5.1, 5.2): besides the sign, in this case the contribution to the electron $g-2$ would result about a factor 15 too large.

From this discussion, it is clear that suitable new physics contributions should be flavor-dependent and rather sizable without disturbing the small values of the electron and muon masses — any loop contributing to dipole operators would generate a radiative contribution to lepton masses as well — and without being in conflict with LFV constraints. In fact, Eqs.(5.5, 5.6) and Eq.(5.8) show that a simultaneous explanation of the two anomalies requires a relative suppression of the LFV coefficients by more than five orders of magnitude. In other words, the matrix $C_{\ell\ell'}$ and the lepton Yukawa matrix have to be almost aligned in flavor space, to such extent that the relative misalignment angle can not exceed $\mathcal{O}(10^{-6})$. A priori there is no reason why generic new physics responsible of non-standard $g-2$ of leptons should have a flavor structure so perfectly aligned to the SM lepton mass matrix, unless of course the two sectors share a common origin. Hence we find it natural to investigate the possibility of a combined explanation of the electron and muon $g-2$ within a model of flavor, i.e. directly arising from the same dynamics behind the observed lepton masses. Our idea is to focus on flavor models *à la* Froggatt-Nielsen [39–41] and calculate the contribution to the lepton $g-2$ of the flavons and the mediator fields that generate the charged-lepton masses.
The rest of the paper is organized as follows. In Section 5.2 we highlight the general idea and the fundamental ingredients to obtain successful lepton masses and $g-2$ from a flavor model. Section 5.3 shows how this is realized in a toy model example. In Section 5.4 we discuss the phenomenology of flavons and mediators and we conclude in Section 5.5.

5.2 General Idea

As discussed in the introduction, the new contributions to the anomalous magnetic moment must be flavor dependent, but with a different flavor dependence from the SM Yukawa couplings.[2] Although, in principle, it would be possible to assign an *ad hoc* flavor structure, both to the magnetic moments and to the Yukawas, it is more satisfactory to try to explain these observables in terms of a new symmetry in flavor space. Indeed, flavor symmetries *à la* Froggatt-Nielsen (FN) have been used for a long time to understand the complex structure of Yukawa couplings. In this framework, it looks completely natural to use the same mechanism to explain the new structures

[2] However, for an exception see Ref. [32]

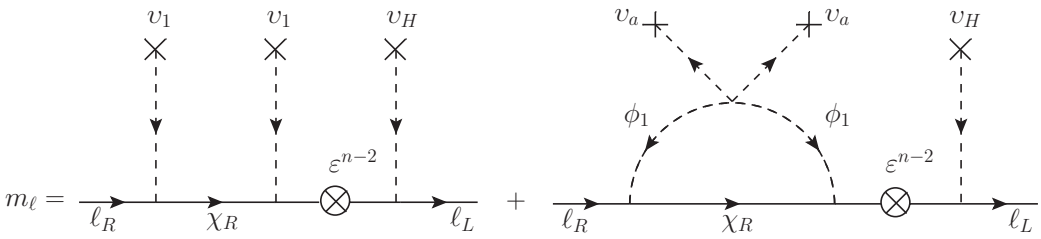

FIGURE 5.1: Froggatt Nielsen (Left) and Radiative (Right) lepton mass.

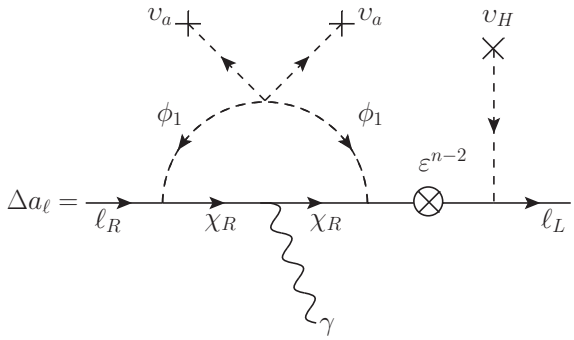

FIGURE 5.2: Flavon contribution to $(g-2)_\ell$

of dipole operators.[3] Fermion masses and anomalous magnetic moments, both chirality changing operators, are intimately connected. Any radiative correction to the fermion masses gives a contribution to the anomalous magnetic moment if we attach a photon to one of the internal lines. However, the FN contributions to the Yukawas usually considered are tree-level diagrams while we necessarily need a loop to generate the dipole operators. In any case, loop corrections to the tree-level diagrams are always present and, as we will see below, under certain conditions they can be sizeable with respect to the tree-level diagrams. Yukawa couplings are accounted for as powers of a dimensionless ratio $v/M \leq 1$, with v a scalar vacuum expectation value, singlet under the SM symmetries, and M the mass of a heavy vector-like mediator with the SM quantum numbers. These contributions are obtained from tree-level diagrams as shown in Figure 5.1. Nevertheless, the radiative corrections to this diagram can be large. In particular, we could consider loops involving the flavons with small vevs, so that we could "replace" two small vevs by an $\mathcal{O}(1)$ loop function. Obviously, this is not so easy, as the flavons carry a flavor charge and they must break

[3] During the completion of this work, an article appeared [42], that also proposes a possible connection between anomalous magnetic moments and a $U(1)$ flavor symmetry, although in the context of a multi-Higgs doublet model rather than FN models.

the symmetry to connect the low energy fermionic fields and thus the loop must also break the symmetry by the same amount. This could be done through the flavon vev itself. However, as we will see in the following, the above mentioned enhancement can be achieved only if a larger vev of a different flavon field is inserted, being the size of this vev not fixed if this field does not couple directly to the fermions. In this way, it is possible to partially compensate the loop suppression and make this loop contribution, with the correct symmetry-breaking properties, comparable to the tree-level FN diagram.

Now, it is clear that this loop diagram generating a loop correction to the Yukawa would be the same as the diagram generating the dipole coefficients simply adding a photon, see Figure 5.2. In general, we expect that the anomalous magnetic moment $a_\ell = C m_\ell^2/M^2$ [43] with C a loop factor if the fermion mass is present at tree-level or $C \sim \mathcal{O}(1)$ if the mass is generated at loop level [44]. In our flavor symmetry models, we could have radiative corrections to the mass similar to the tree-level contribution which implies that a large contribution to a_ℓ, with $C \sim \mathcal{O}(1)$, can be expected. Moreover, the measured discrepancies in the muon and electron magnetic moments, which do not follow this quadratic scaling with the fermion mass, can also be explained with flavor models where additional flavor dependence can enter naturally the magnetic moment. The main problem of this construction, as discussed in the introduction, is to suppress off-diagonal LFV dipole operators which requires some non-trivial model building.

On the other hand, in flavor symmetry models, the dimensionless Yukawa couplings depend only on ratios v/M and therefore can not fix the scale of symmetry breaking or the mediator masses. Anomalous magnetic moments are dimension 6 operators, and then the contributions to a_ℓ are suppressed, compared to the radiative contribution to the mass, by the heaviest mass in the loop, i.e. in our flavor models, the mediator mass, M_χ^2, or the flavon mass, M_ϕ^2. Therefore, this implies that anomalous magnetic moments could provide a hint on the scale of flavor symmetry breaking if the measured discrepancies are due to these flavon contributions.

At this point, we would like to emphasize that the relation between anomalous magnetic moments and radiative corrections to the masses is true for a generic model. In particular, models with a chiral enhancement in the lepton anomalous magnetic moments can also have large corrections to the tree-level lepton masses. This is what happens, for instance, in the MSSM with large $\tan\beta$ or in models with leptoquarks (LQs) where the chirality flip can be given by a quark mass, e.g. m_t, instead of m_μ or m_e. In fact, the required contributions to the anomalous magnetic moments generically imply a large correction to the mass, which is usually not taken into account

in the literature. For instance, models with multi-TeV chirality-flipping vector-like leptons or LQs that can explain $(g-2)_\mu$, as is the case in Refs. [38, 45–52], could give a sizable correction to the mass. Assuming the loop functions in the radiative mass and anomalous magnetic moments to be of the same order, we can estimate $m_\mu^{\rm RAD} \sim \Delta a_\mu \, M_\chi^2/2m_\mu \sim 0.05 \, (M_\chi/2\,{\rm TeV})^2$ GeV, with M_χ the leptoquark mass. This large contribution could cancel against a tree level mass contribution with some degree of tuning, but radiative corrections to the mass should be taken into account in these analysis.

Notice that, in this work, we concentrate on the charged-lepton sector and we do not discuss neutrino mixings. The observed neutrino mixings can always be accommodated with the help of the right-handed neutrino mass matrices in a type-I seesaw mechanism, possibly with additional breaking of the flavor symmetry. In the following, we apply these general ideas to explain the measured discrepancies Δa_e and Δa_μ in models of flavor symmetries. For this, we will construct an explicit example of this mechanism.

5.2.1 Lepton masses and $g-2$ contribution

Assuming a minimal set of fields and couplings, the Yukawa-like interactions responsible for the masses in a FN framework can be schematically written as:

$$\mathcal{L}_Y \;=\; g_\ell \left(\overline{\chi}_R \, \ell_R \, \phi_1 \;+\; \ldots \;+\; \overline{L} \, \chi_R \, H \right) \;+\; \text{h.c.}, \tag{5.9}$$

with χ_R a heavy vector-like mediator with the quantum number of a right-handed lepton ℓ_R,[4] ϕ_1 a flavon field carrying non-zero flavor charge, and g_ℓ a generic $\mathcal{O}(1)$ coupling that, for illustration purposes, we took to be the same for all interactions. As we will see below, our results not depending on this choice. Then, the minimal potential should contain the following couplings:

$$V(\phi) \;=\; \sum_i \, -\mu_i^2 \, (\phi_i^\dagger \phi_i) + \lambda_i (\phi_i^\dagger \phi_i)^2 \;+\; \frac{1}{2} \sum_{i \neq j} \lambda_{ij} \, (\phi_i^\dagger \phi_i)(\phi_j^\dagger \phi_j) \;+\; \left[\lambda \, (\phi_a^\dagger \phi_1)^2 \;+\; \text{h.c.} \right], \tag{5.10}$$

where the indices $i, j = 1, a, \ldots$ go through all the flavons present in the model. We have introduced ϕ_a as a general complex scalar field that does not couple directly to leptons. Other quartic terms of the kind $(\phi_i^\dagger \phi_j)^2$ could also be present in Eq.(5.10)

[4] Obviously one could also consider mediators carrying the quantum numbers of left-handed leptons, or a combination of right-handed and left-handed mediators with the Higgs not coupling directly to the light chiral fields. For a detailed discussion of the messenger sector of FN models see [53–56].

provided they respect the flavor symmetry. The interactions in Eq.(5.9) induce a mass term for the charged leptons through the processes depicted in Figure 5.1. For a diagram with n flavon insertions, the effective mass is:

$$m_\ell^{\rm FN} \;=\; g_\ell^{n+1}\,\frac{v_H}{\sqrt{2}}\,\epsilon^{n-2}\,\left(\frac{v_1}{M_\chi}\right)^2\,, \tag{5.11}$$

where $v_1 \equiv \langle\phi_1\rangle$, M_χ is the heavy mediator mass and $\epsilon \equiv v/M_\chi$ stands for possible additional insertions of the same ϕ_1 as well as of other flavons generally present in a complete flavor model. Depending on the number of different flavons and vertices in the lagrangian, we have to take into account possible degeneracy coefficients, which count for the possible ways of inserting each flavon. However, they can always be absorbed into the g_ℓ coupling. In Figure 5.1, we show that, together with the FN-diagram, the last vertex of Eq.(5.10) also induces a radiative mass term $m_\ell^{\rm RAD}$. The computation of the diagram gives:

$$m_\ell^{\rm RAD} \;=\; g_\ell^{n+1}\,\frac{v_H}{\sqrt{2}}\,\epsilon^{n-2}\,\left(\frac{v_a}{M_\chi}\right)^2\,\frac{\lambda}{16\pi^2}\,I_m^{\times}(x_\phi), \tag{5.12}$$

and the following loop function

$$I_m^{\times}(x_\phi) \;=\; \frac{1+2\log x_\phi - x_\phi^2}{(1-x_\phi^2)^2} < 0\,, \tag{5.13}$$

with $x_\phi = \mu_{\phi_1}/M_\chi$, being $\mu_{\phi_1}^2$ the bilinear coupling in the scalar potential before symmetry breaking. We must remark here that ϕ_1 is a complex scalar and the FN-operator involves ϕ_1^2, therefore a bilinear coupling, μ_i^2, can not close the loop in Figure 5.1 and we must take a quartic couplings with two vevs breaking the flavor symmetry. Comparing Eqs. (5.11) and (5.12), they differ for the loop factor $\lambda\, I_m^{\times}/(16\,\pi^2)$ and the replacement $v_1 \to v_a$. The contribution $m_\ell^{\rm RAD}$ is comparable with $m_\ell^{\rm FN}$ if $(v_a/v_1)^2$ is big enough to compensate for the suppression of the loop factor. Note that, if more than two insertions of ϕ_1 are present, we have to take into account the alternative ways of closing the loop. As a consequence, typically there is a mismatch between the degeneracy coefficients of the FN and RAD diagrams that can not be reabsorbed. The function in Eq.(5.13) is defined negative; this means that as long as $\lambda > 0$, the two diagrams in Figure 5.1 interfere destructively among each other.

What we want to emphasize is that the same processes which generates the radiative contribution to the lepton masses induces a correction to the anomalous magnetic moment coupling a photon to the loop. It contributes to the anomalous magnetic

moment as:

$$\Delta a_\ell \;=\; g_\ell^{n+1}\frac{v_H}{\sqrt{2}}\frac{m_\ell}{M_\chi^2}\,\epsilon^{n-2}\left(\frac{v_a}{M_\chi}\right)^2\frac{\lambda}{8\,\pi^2}\,I^{\times}_{\Delta a}(x_\phi). \tag{5.14}$$

where the loop function is given by

$$I^{\times}_{\Delta a}(x_\phi) \;=\; -\frac{1+4x_\phi^2(1+2\log x_\phi)\;-\;x_\phi^4(5-4\log x_\phi)}{2(1-x_\phi^2)^4} < 0\,. \tag{5.15}$$

In the mechanism described so far, the realization of the $(g-2)$ correction is directly related to the mass generation through a flavor symmetry. This implies that $\text{Sign}(\Delta a_\ell) = \text{Sign}(m_\ell^{\text{RAD}})$ as they come from the same diagram. In this framework, the obstacle of obtaining the experimental sign difference, between Δa_μ and Δa_e, can be nicely overcome. We can achieve it by requiring $\text{Sign}(\Delta a_\mu) = \text{Sign}(m_\mu)$ while $\text{Sign}(\Delta a_e) = -\text{Sign}(m_e)$. The rotation to the physical basis where $m_e, m_\mu > 0$ automatically gives $\Delta a_e < 0$ and $\Delta a_\mu > 0$. In particular, the SM contribution to a_e will get the chirality change through the electron mass itself, including both tree and radiative contributions to the mass, while our new contribution gets the chirality change through the radiative contribution only, with negative sign after rephasing. As the electron and muon masses are generated through a destructive interference between the FN and the radiative processes in Figure 5.1, basically what we need is an opposite cancellation in the muon and electron sectors, i.e. $m_\mu^{\text{RAD}} > m_\mu^{\text{FN}}$ while $m_{\text{e}}^{\text{RAD}} < m_{\text{e}}^{\text{FN}}$. Now, taking g_ℓ, v_1 and ϵ positive in Eq.(5.11), this means that the radiative masses and anomalous moments, as the muon mass before rephasing, are negative while the electron mass is positive. Altogether, this implies that the radiative and the tree level contributions must be of the same order. We let m_ℓ^{RAD}, and consequently m_ℓ^{FN}, to be up to one order of magnitude larger than m_ℓ^{exp}, i.e.

$$|m_\ell^{\text{RAD}}| \;=\; c_\ell\, m_\ell^{\text{exp}} \quad \text{with} \quad c_\ell \in [1,10]\,. \tag{5.16}$$

Notice that in the following ratios the dependence on the variables of our mechanism is to great extent simplified [44],

$$\frac{\Delta a_\ell}{m_\ell^{\text{RAD}}} \;=\; \frac{|\Delta a_\ell|}{c_\ell\, m_\ell^{\text{exp}}} = \frac{2\,m_\ell^{\text{exp}}}{M_\chi^2}\,\frac{I^{\times}_{\Delta a}(x_\phi)}{I^{\times}_{m}(x_\phi)}\,, \tag{5.17}$$

$$\left|\frac{\lambda\, m_\ell^{\text{FN}}}{m_\ell^{\text{RAD}}}\right| \;=\; \lambda\frac{c_\ell \pm 1}{c_\ell} = \frac{16\pi^2}{I^{\times}_{m}(x_\phi)}\left(\frac{v_1}{v_a}\right)^2, \tag{5.18}$$

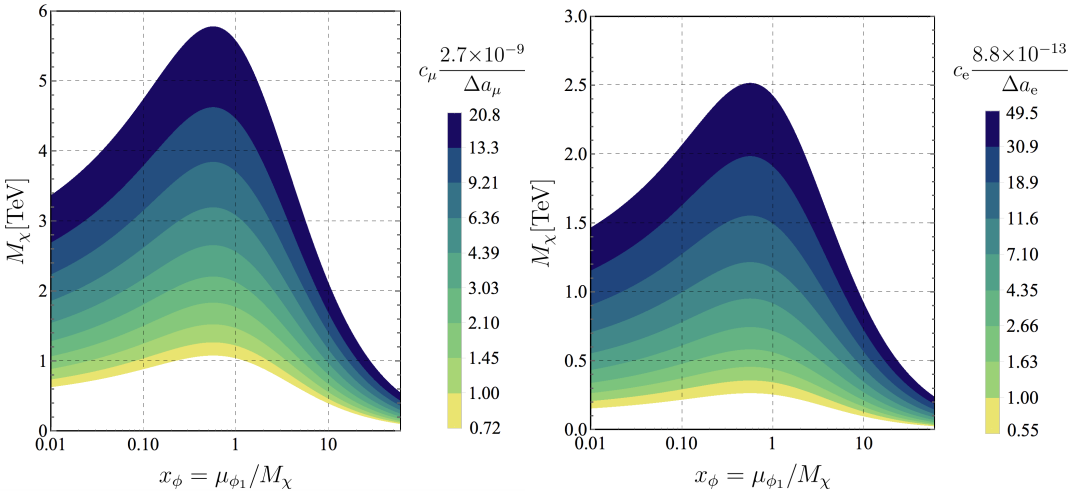

FIGURE 5.3: Mediator mass M_χ as function of x_ϕ for the muon case (Left panel) and the electron case (Right panel). We have used Eq.(5.17) imposing $\Delta a_\ell^{\rm exp} - 2\sigma_\ell < \Delta a_\ell < \Delta a_\ell^{\rm exp} + 2\sigma_\ell$ and $c_\ell \in [1, 10]$. For a given value of Δa_ℓ, we can read the required loop factor, c_ℓ, from the bar legend.

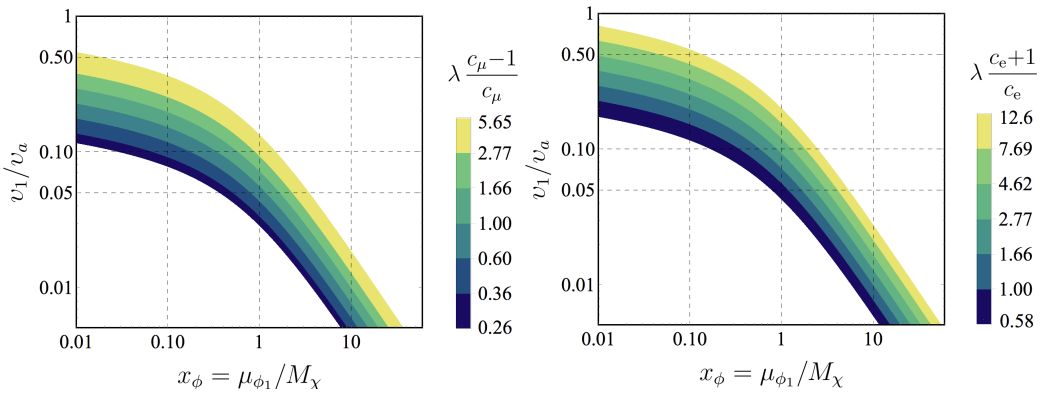

FIGURE 5.4: Ratio v_1/v_a as function of x_ϕ for the muon case (Left panel) and the electron case (Right panel). We have used Eq.(5.18) with $1/2 < m_\mu^{\rm FN}/m_\mu^{\rm RAD} < 9/10$ and $10/9 < m_e^{\rm FN}/m_e^{\rm RAD} < 2$ and $\lambda \in [\pi/6, 2\pi]$. For a given c_ℓ, we can read the required value of λ from the bar legend.

with $(+)$ for the electron and $(-)$ for the muon, where, as before, we take $\lambda > 0$. As we announced before, the ratios $m^{\rm FN}/m^{\rm RAD}$ and $\Delta a/m^{\rm RAD}$ do not depend on the choice of g_ℓ, as the same couplings necessarily enter the three observables. From Eq.(5.17) we can directly deduce the dependence of $M_\chi(x_\phi)$ once we impose the experimental bounds on $\Delta a_\ell^{\rm exp}$ together with $c_\ell = [1, 10]$, as shown in Figure 5.3. On the other hand, in Figure 5.4, we can see that Eq.(5.18) gives the relation of $v_1/v_a(x_\phi)$.

Field	μ_L	μ_R	$\mathbf{e}_L$	$\mathbf{e}_R$	χ_R	ϕ_1	ϕ_3	ϕ_a	ϕ_b	H
$U(1)_f$	-2	0	8	3	$1,2\ldots6,7,8$	1	3	2/5	8/5	0
Z_2	$+$	$+$	$-$	$+$	$\pm$	$-$	$-$	$+$	$+$	$+$

TABLE 5.1: Fields and their flavor symmetry assignments.

From Figure 5.4 we see that it is always true that $v_a > v_1$, as expected from the previous discussion. Notice that, although a quartic coupling $(\phi_1^\dagger\phi_1)^2$, present in Eq.(5.10), also closes the loop in Figure 5.1, these results demonstrate the need of the non-trivial quartic coupling $(\phi_a^\dagger\phi_1)^2$ in the scalar potential. The results shown in Figure 5.3 and 5.4 rely exclusively on the level of cancellation between the FN and radiative diagrams, therefore they can be considered to some extent independent of the model details. Nonetheless, their validity can only be established within a specific flavor model. For instance, the required relation between μ_{ϕ_1} and $v_{(1,a)}$ will be allowed only for certain regions of the viable parameter space. Our results show superposition over the muon and electron parameter space for $M_\chi \in [0.6, 2.5]$ TeV. Consequently, we use the mechanism described in this section to build a toy model based on a $U(1)_f$ flavor symmetry that accommodates both the muon and electron $(g-2)$ anomalies.

5.3 A $U(1)_f$ toy model

To give an illustrative realization of the mechanism described in the previous section, let us consider an Abelian flavor symmetry $U(1)_f$ generating the flavor structures. The field charges, supplemented by the appropriate mediator sector, are specified in Table 5.1. Here we do not consider the flavor structures involving the τ, as it goes beyond our exemplifying purposes. Apart from flavor charges, all flavons are SM singlets and mediators have the quantum numbers of lepton singlets, while the SM Higgs boson does not transform under the flavor symmetry.

We do not contemplate the presence of mediators of fractional charge. This is a crucial assumption, as it forbids the possibility for $\phi_{(a,b)}$ to participate to the mass generation at tree-level through the FN mechanism. Besides, two distinct fields ϕ_a and ϕ_b are required if they must have fractional charges. A term $(\phi_a^\dagger\phi_1)^2$, as in Eq. (5.10), would require $(2q_1 - 2q_a = 0)$ and hence the same charge as ϕ_1. Furthermore, in this model we introduce other two different flavons, ϕ_1 and ϕ_3, to obtain different cancellations between m^{FN} and m^{RAD} for the electron and the muon. If we have a single

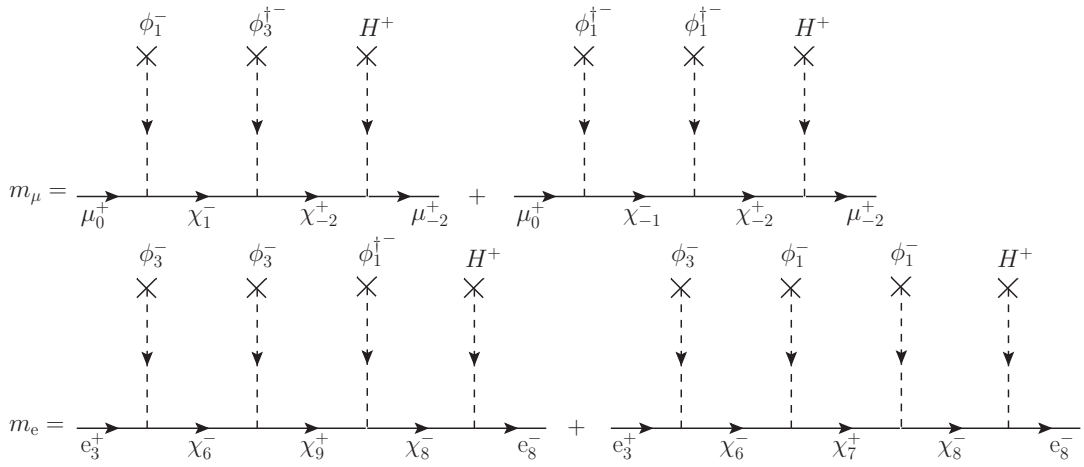

FIGURE 5.5: FN diagrams entering in the generation of the electron and muon masses. The field subscripts indicate the $U(1)_f$ charge while the superscripts specify the Z_2 assignments.

flavon, ϕ_1, it is easy to see that $m^{\rm FN}/m^{\rm RAD}$ is the same for both electrons and muons. Moreover, we need this ratio to be negative to obtain a cancellation. As we will see below, both conditions are met with the introduction of ϕ_3.

The Z_2 symmetry plays a fundamental role. Any diagram that couples $\ell^+ \to \ell^{+(-)}$, where superscripts refer to Z_2 charges, requires an even (odd) number of insertions. As we consider only flavons with odd charges, our choice of $U(1)$ charges could allow $e_R^+ \to \mu_L^+$ only at the level of $(2n+1)$-insertions and $\mu_R^+ \to e_L^-$ with $(2n)$-insertions. However the Z_2 symmetry prevents any of these flavor-changing couplings that would give rise to $\mu \to e\gamma$. For the same reason, it also eliminates any effective vertex $\mu_R^\dagger e_R$ and $\mu_L^\dagger \mathrm{e}_L$. Thus the charge assignments in Table 5.1 conserves leptonic flavors.

The effective Lagrangian preserving the charge assignment of the underlying $U(1)_f$ flavor symmetry has the form

$$\mathcal{L}_\ell = g_\mu \left[\mu_R^{(0)} \overline{\chi}_R^{(1)} \phi_1^\dagger + \overline{\mu}_L^{(2)} \chi_R^{(-2)} H^{(0)}\right] + g_e \left[\mathrm{e}_R^{(3)} \overline{\chi}_R^{(-6)} \phi_3 + \overline{e}_L^{(8)} \chi_R^{(-8)} H^{(0)}\right] \quad (5.19)$$

$$+ \; g \sum_q \left[\overline{\chi}_R^{(q)} \chi_R^{(q+1)} \phi_1 + \overline{\chi}_R^{(q)} \chi_R^{(q+3)} \phi_3\right] + \text{h.c.} \quad . \quad (5.20)$$

Given the charge assignment in Table 5.1, the most general scalar potential can be

written as

$$\begin{aligned} V &= \mu_1^2\,\phi_1^\dagger\phi_1 + \mu_3^2\,\phi_3^\dagger\phi_3 + \mu_a^2\,\phi_a^\dagger\phi_a + \mu_b^2\,\phi_b^\dagger\phi_b \\ &+ \lambda_1\left(\phi_1^\dagger\phi_1\right)^2 + \lambda_3\left(\phi_3^\dagger\phi_3\right)^2 + \lambda_a\left(\phi_a^\dagger\phi_a\right)^2 + \lambda_b\left(\phi_b^\dagger\phi_b\right)^2 \\ &+ \lambda_{13}\left(\phi_1^\dagger\phi_1\right)\left(\phi_3^\dagger\phi_3\right) + \lambda_{1a}\left(\phi_1^\dagger\phi_1\right)\left(\phi_a^\dagger\phi_a\right) + \lambda_{1b}\left(\phi_1^\dagger\phi_1\right)\left(\phi_b^\dagger\phi_b\right) \\ &+ \lambda_{3a}\left(\phi_3^\dagger\phi_3\right)\left(\phi_a^\dagger\phi_a\right) + \lambda_{3b}\left(\phi_3^\dagger\phi_3\right)\left(\phi_b^\dagger\phi_b\right) + \lambda_{ab}\left(\phi_a^\dagger\phi_a\right)\left(\phi_b^\dagger\phi_b\right) \\ &+ \left(\lambda_{1ab}\,\phi_a^\dagger\phi_b^\dagger\phi_1^2 + \lambda'_{13}\,\phi_3^\dagger\phi_1^3 + {\mu'_a}^2\phi_a^2 + {\mu'_b}^2\phi_b^2 + \text{h.c.}\right), \end{aligned} \tag{5.21}$$

where the last two terms are introduced to break explicitly the $U(1)_f$ symmetry and allow to give a small mass to the two Goldstone bosons [5] present in the model, while the Z_2 is preserved.[6] For simplicity we consider the λs to be real. The flavor symmetry is spontaneously broken when the flavons get a nonzero vev at the minimum of the scalar potential. As detailed in Appendix E.1, the potential in Eq.(5.21) allows for a non trivial minimum with $v_3 \sim -2v_1$ and $v_b \sim v_a$, $v_{(1,a)} \neq 0$ and $v_1 < v_a$. The mass matrices of the CP-even (S_i) and -odd bosons (P_i) can be diagonalized by two orthogonal matrices as detailed in Appendix E.1. The relevant (pseudo) scalar masses are

$$\begin{aligned} m_{S_1}^2 &\simeq 2v_1^2\left(2\lambda_1 - \lambda_{13} - \frac{9}{4}\lambda'_{13}\right),\; m_{P_1}^2 \simeq -2\,v_a^2\left(\lambda_{1ab} + \frac{v_1^2}{2v_a^2}(\lambda_{1ab} - 18\lambda'_{13})\right), \\ m_{S_2}^2 &\simeq 2\,v_1^2\left(2\lambda_1 + 4\lambda_{13} - 6\lambda'_{13} - \frac{5}{4}\frac{(2\lambda_{1a} + \lambda_{1ab})^2}{2\lambda_a + \lambda_{ab}}\right). \end{aligned} \tag{5.22}$$

These physical masses are related to the $\mu_{\phi_1}^2 \equiv \mu_1^2$ in Figure 5.3 as $m_{S_{1,2}}^2 \sim (2\lambda_{1a} + \lambda_{1ab})v_a^2 + 6\lambda_1 v_1^2 - \mu_{\phi_1}^2$ and $m_{P_1}^2 \sim (2\lambda_{1a} - \lambda_{1ab})v_a^2 + 6\lambda_1 v_1^2 - \mu_{\phi_1}^2$, relations that are valid up to $\mathcal{O}(v_1^2/v_a^2)$ corrections. Looking at $m_{P_1}^2$, it is clear that the necessary condition for a minimum is $\lambda_{1ab} < 0$.

[5] It is easy to check that taking $\mu'_a = \mu'_b = 0$, the potential has two unconstrained charges and therefore two global symmetries. Initially, we have four charges q_1, q_3, q_a and q_b, *i.e.* 4 symmetries. Then, only the last row in Eq. (5.21) constrains these charges, $(2q_1 - q_a - q_b = 0)$ and $(3q_1 - q_3 = 0)$. So, there remain two global symmetries that are explicitly broken by μ'_a and μ'_b. As can be seen in the Appendix, we have two pseudoscalar masses directly proportional to ${\mu'}^2_{(a,b)}$.

[6] As mentioned in Section 5.2, neutrino masses can be accommodated through the right-handed neutrino Majorana masses. The breaking of Z_2 would be produced by the same flavons breaking lepton number, coupling only to ν_R. This allows $\mu - e$ mixing in the ν_R and, hence, in the ν_L mass matrices. In this way, the charged-lepton sector would be practically unaffected, with flavor changes in charged-leptons always proportional to neutrino masses.

5.3.1 Mass generation and $(g-2)_\ell$

Using the vertices in Eq.(5.19), we can write down the FN diagrams entering in the mass generation of m_μ and m_e. They are displayed in Figure 5.5, where it is important to notice that due to the presence of ϕ_3 we have different tree-level diagrams contributing to m_μ and m_e with different weights for $v_3 \sim -2v_1$. From the potential in Eq.(5.21) we see that different quartic couplings can act closing the loop in one of these diagrams for m_μ and m_e. In our toy model, the λ introduced in Eqs.(5.12,5.14) is given by the sum of different terms

$$\lambda \to \lambda_{1ab}\frac{v_b}{v_a} + \lambda_1\frac{v_1^2}{v_a^2} + \lambda'_{13}\frac{v_3 v_1}{v_a^2}. \tag{5.23}$$

Nevertheless, the $\phi_{(1,3)}$ couple directly to the SM fermions and the size of their vevs are limited, while the $v_{(a,b)}$ only enter the masses at loop level and their values can be correspondingly larger. Provided that $v_a \sim v_b \gg v_{(1,3)}$, only diagrams with two or more ϕ_1, closed by the quartic coupling $\lambda_{1ab}\,\phi_a^\dagger\,\phi_b^\dagger\phi_1^2$ can give a contribution to $(g-2)_\ell$ with the required enhancement. Then, the total masses are,

$$\begin{aligned} m_\mu &= g_\mu^3\frac{v_H}{\sqrt{2}}\epsilon_1^2\left[\left(\frac{\epsilon_3}{\epsilon_1}+1\right)+\frac{\lambda_{1ab}}{16\pi^2}\frac{\epsilon_a^2}{\epsilon_1^2}I_m^\times(x_\phi)\right] \\ &\sim g_\mu^3\frac{v_H}{\sqrt{2}}\epsilon_1^2\left[-1+\frac{\lambda_{1ab}}{16\pi^2}\frac{\epsilon_a^2}{\epsilon_1^2}I_m^\times(x_\phi)\right], \end{aligned} \tag{5.24}$$

$$\begin{aligned} m_e &= g_e^4\frac{v_H}{\sqrt{2}}\epsilon_1^2\epsilon_3\left[\left(2\,\frac{\epsilon_3}{\epsilon_1}+1\right)+\frac{\lambda_{1ab}}{16\pi^2}\frac{\epsilon_a^2}{\epsilon_1^2}I_m^\times(x_\phi)\right] \\ &\sim 2\,g_e^4\frac{v_H}{\sqrt{2}}\epsilon_1^3\left[3-\frac{\lambda_{1ab}}{16\pi^2}\frac{\epsilon_a^2}{\epsilon_1^2}I_m^\times(x_\phi)\right], \end{aligned} \tag{5.25}$$

where $\epsilon_{(1,a)} = v_{(1,a)}/M_\chi$, we assume a common mediator mass M_χ to simplify the discussion and, in the second equality, we have taken $v_3 \sim -2v_1$. In this equation we can see that, as we said above, it is the presence of v_3 which provides the negative relative sign and different cancellation in m_μ and m_e. Now, the corresponding contributions to $(g-2)_\ell$ read as

$$\Delta a_\mu \sim g_\mu^3\,\frac{\lambda_{1ab}}{8\,\pi^2}\,\frac{v_H}{\sqrt{2}}\,\frac{m_\mu}{M_\chi^2}\,\epsilon_a^2\,I_{\Delta a}^\times(x_\phi)\,, \tag{5.26}$$

$$\Delta a_e \sim -2\,g_e^4\,\frac{\lambda_{1ab}}{8\,\pi^2}\,\frac{v_H}{\sqrt{2}}\,\frac{m_e}{M_\chi^2}\epsilon_a^2\,\epsilon_1\,I_{\Delta a}^\times(x_\phi)\,. \tag{5.27}$$

M_χ	m_{S_1}	m_{S_2}	m_{S_3}	m_{S_4}	m_{P_1}	m_{P_2}	m_{P_3}	m_{P_4}	v_1	v_3	$v_{(a,b)}$	g_e
1658	123	337	1245	1430	611	23	18	18	42	-84	262	0.72
λ_1	λ_3	$\lambda_{(a,b)}$	λ_{13}	$\lambda_{1(a,b)}$	$\lambda_{3(a,b)}$	λ_{ab}	λ'_{13}	λ_{1ab}	$\mu_{(1,3)}$	$\mu_{(a,b)}$	$\mu'_{(a,b)}$	g_μ
5.93	3.31	6.54	6.08	0.97	-0.31	1.82	0.65	-2.50	122	1010	9	0.85

TABLE 5.2: Example of a benchmark point. The spectrum mass parameters are given in GeV. The combination of parameters provides $\Delta a_\mu = 1.6 \times 10^{-9}$ and $\Delta a_e = -1.8 \times 10^{-13}$ with a relative size of the loop contributions $(c_e, c_\mu) = (7.1, 1.6)$.

The minimization of the scalar potential requires $\lambda_{1ab} < 0$ and the loop function is also $I_m^\times(x_\phi) < 0$, so the radiative diagram gives a positive contribution to the mass. From Eqs.(5.26) and (5.27) one sees that, to obtain $\text{Sign}(\Delta a_\mu) = -\text{Sign}(\Delta a_e)$ in the physical basis, we need the following condition to be satisfied

$$\frac{1}{\sqrt{3}} < \frac{4\pi}{\sqrt{\lambda_{1ab} I_m^\times(x_\phi)}} \frac{\epsilon_1}{\epsilon_a} < 1\,. \tag{5.28}$$

An example of a set of numerical values of the parameters giving a global minimum, the corresponding vevs, and the resulting scalar mass spectrum are shown in Table 5.2. Notice that as expected there are two light pseudoscalars, i.e. the pseudo Nambu-Goldstone bosons, with mass of the order of the explicit $U(1)_f$ breaking, and a third pseudoscalar which is instead light because its mass is controlled by the small vev v_1.

5.4 Phenomenological implications

We have seen that to explain the discrepancies in the muon and electron anomalous magnetic moments through a low scale flavor symmetry, a relatively light flavon and mediator sector is required. In this section we discuss the phenomenology of these light particles at colliders and precision experiments. Rather than focusing on the specific toy model presented in Section 5.3, we discuss the general features and phenomenological consequences of the mechanism outlined in Section 5.2.

In Figures 5.3 and 5.4, we can see the requirements on the masses and the vacuum expectation values needed to reproduce the anomalous magnetic moments through this mechanism, irrespective of the details of the model, as symmetries, charges, and scalar potential. The figure shows that we can successfully reproduce $(g-2)_\mu$ at the 2σ level with a mediator mass up to 5.7 TeV, although this implies that $c_\mu = 10$, i.e. a cancellation of the tree-level and radiative contributions to the muon mass with a

tuning of 10%. In the case of $(g-2)_e$ at 2σ the maximum allowed mediator mass is 2.5 TeV with a 10% tuning.

If we take both values at 2σ, we can see that we relax both the electron and muon discrepancies with $M_\chi \simeq 2.5$ TeV and $x_\phi \simeq 0.6$. This implies $c_e = 10$ and $c_\mu \in [2.2, 6.9]$, where the c_μ range reflects the 2σ range in Eq.(5.2). Then, the cancellation is larger for the electron that for the muon and, as expected, a smaller degree of cancellation would imply a lighter mediator. For instance, to reproduce the central values with $M_\chi = 1$ TeV and $x_\phi = 1$, it would require $c_\mu = 1.1$ and $c_e = 7.7$. Therefore, our explanation of the muon and electron discrepancies in the anomalous magnetic moments at two sigmas has a definite prediction: we expect vector-like fermions with the quantum numbers of right-handed and/or left-handed SM leptons with mass below 2.5 TeV.

The scalar sector is more model dependent, as the exact spectrum depends on the minimization of the scalar potential as exemplified in Appendix E.1 for the toy model. We can however outline some general features, based on the discussion in Section 5.2. Figures 5.3 and 5.4 show that for our mechanism to work we need: (i) a hierarchy between the $U(1)_f$-breaking vevs with those ("v_1") entering the tree-level mass diagrams smaller than those ("v_a") controlling the radiative mass and the contributions to $(g-2)_\ell$, i.e. $v_1 < v_a$; (ii) the bilinear terms in the scalar potential μ_ϕ of the flavons coupling to leptons of the same order or smaller than the mediator mass M_χ, unless $v_1 \ll v_a$. It is thus reasonable to expect at least one scalar and/or pseudoscalar to be much lighter than the mediators. This is indeed the case in the explicit example shown in Table 5.2, where the scalar spectrum lies in the 10 GeV–2 TeV range. The light states have in particular to come mostly from the flavons involved in the FN diagram, thus coupling to light leptons, that in Section 5.2 we denoted as ϕ_1. Besides, there must be one or more pseudo-Goldstone bosons whose mass is controlled by explicit $U(1)_f$-breaking terms and thus naturally — although not necessarily — light. Given the above discussion, here we focus on the phenomenology of scalar states with a substantial component of the flavon ϕ_1 entering the tree-level FN diagrams that are in general expected to have mass of $\mathcal{O}(100)$ GeV or lighter.

From Figure 5.1, one can see that the coupling $y_{\phi\ell}$ of a physical state in ϕ_1 to $\ell_L \ell_R$ is proportional to the FN contribution to the lepton mass:

$$y_{\phi\ell} \approx n_\phi \frac{m_\ell^{\rm FN}}{v_1}, \tag{5.29}$$

where n_ϕ is the number of ϕ_1 insertions in the diagram. Even considering the maximal tuning we allowed, $m_\ell^{\rm FN} = 10\, m_\ell^{\rm exp}$ (i.e. $c_\ell = 10$), the ratio $m_\ell^{\rm FN}/v_1$ provides a

substantial suppression to the couplings to electrons and muons. Indeed, numerically the couplings result

$$y_{\phi e} \approx 2 \times 10^{-4} \left(\frac{n_\phi}{2}\right) \left(\frac{c_e}{10}\right) \left(\frac{50\,\text{GeV}}{v_1}\right), \tag{5.30}$$

$$y_{\phi \mu} \approx 4 \times 10^{-2} \left(\frac{n_\phi}{2}\right) \left(\frac{c_\mu}{10}\right) \left(\frac{50\,\text{GeV}}{v_1}\right). \tag{5.31}$$

The flavon couples preferably to the heaviest lepton, in our case the muon. Of course, it would be the tau if the same flavon were involved in the generation of the tau mass. As a consequence, if produced at colliders either directly or through decays of the mediators, our flavon would decay as $\phi_1 \to \mu^+\mu^-$ (or $\tau^+\tau^-$) with a branching ratio close to 100%. A ϕ_1 lighter than about 200 GeV could appear as a di-muon (or di-tau) resonance at LEP: $e^+e^- \to \phi_1 \to \mu^+\mu^-$. However, the production cross section depends on the small coupling to electrons and, due to limited statistics, searches for such kind of di-fermion resonances performed by LEP experiments are not sensitive to couplings $y_{e\phi} \lesssim 10^{-2}$ [57]. For flavons substantially heavier than the maximum LEP center-of-mass energy (209 GeV), bounds on the 4-lepton contact interaction [58] translate into a limit $y_{e\phi}\, y_{\mu\phi} \lesssim 5 \times 10^{-3}\, (m_\phi/400\,\text{GeV})^2$, several orders of magnitude above our typical values shown in Eq.(5.30). It would be interesting to assess the sensitivity of proposed future leptonic colliders — such as the ILC, CLIC, CEPC, and FCC-ee, see e.g. [59] — to leptonic flavons, a question that we defer to future work.
The FN mediators we considered are heavy vector-like leptons with the quantum numbers of the SM lepton singlets, although realizations of our mechanism involving also or exclusively SU(2) doublet mediators are conceivable. In either case, these new heavy fermions can be abundantly produced at the LHC via the electro-weak Drell-Yan process $pp \to Z^*/\gamma^* \to \chi^+\chi^-$, plus modes involving the neutral states in case of doublet mediators. In general, vector-like leptons mix with the SM leptons, hence the charged states can decay to light leptons and SM bosons: $\chi^\pm \to Z\,(h)\,\ell^\pm$, see e.g. [60]. In our case a more direct decay mode involves lighter flavon states: $\chi^\pm \to \phi_1\,\ell^\pm$, where again with ϕ_1 we denote a flavon appearing in FN diagrams. Depending on the FN charge of a given mediator, decays of this kind may occur through a renormalizable $\mathcal{O}(1)$ coupling, or again through an effective coupling arising from mixing of different mediators involving the insertion of a certain number of flavon and/or Higgs, as one can see from FN diagrams such as in Figure 5.5. As in general a fewer number of vev insertion is needed than for the decays to SM particles, we expect that this mode will be always dominant. The exact quantum numbers of a given mediator will also determine which lepton the mediator preferably decays

into. Considering that as discussed above flavons decay to pairs of the heaviest lepton they couple to, the typical signature of this kind of models at the LHC consists of a multi-lepton final state such as:

$$pp \to \chi^+\chi^- \to \phi_1(\to \mu^+\mu^-)\,\ell^+\,\phi_1(\to \mu^+\mu^-)\,\ell^-, \tag{5.32}$$

where $\ell = e, \mu$ and the di-muon invariant mass can reconstruct the mass of the ϕ_1 state. Of course for models involving the third generation, decay chains of this kind involving taus are possible and, in particular, flavons coupling to a FN diagram for the tau would mostly decay into $\tau^+\tau^-$.

Searches based on multi-lepton final states have been performed by the LHC collaborations [61–64], and employed to constrain a variety of new-physics models. In particular the analysis in [63] was interpreted in terms of production of third generation vector-like lepton doublets decaying to SM gauge/Higgs bosons and taus/tau neutrinos. A limit on the mass of the vector-like lepton $\gtrsim 800$ GeV was obtained. We expect that reinterpreting this and other multi-lepton searches in terms of the vector-like lepton production and decay chain shown in Eq.(5.32) would yield a comparable limit, possibly stronger, in the 1 TeV ballpark, if no taus or neutrinos are present in the final state. An optimized search taking full advantage of the spectacular six-lepton signature in Eq.(5.32) should further increase the sensitivity.

Finally, we conclude this section by commenting about possible low-energy probes of our setup. The most obvious observables that could test a combined explanation of both electron and muon $g-2$ are LFV processes and the electron EDM. In fact, the suppression of LFV processes does not need to be complete as in the toy model of Section 5.3, and any deviation from a perfect flavour alignment of the dipole coefficients $C_{\ell\ell'}$ in Eq.(5.3) could be observed by searches for LFV processes, cf. [36] for status and prospects of these experiments. The same diagrams giving rise to $(g-2)_e$ can contribute to the electron EDM (eEDM). In terms of the usual effective operators such contribution reads

$$d_e = \frac{\mathrm{e}\, m_e}{4\pi^2}\,\mathrm{Im}(C_{ee}). \tag{5.33}$$

The latest experimental limit [65] then implies:

$$d_e < 1.1\times 10^{-29}\, e\,\mathrm{cm} \;\Rightarrow\; |\mathrm{Im}(C_{ee})| < 6\times 10^{-7}\,\mathrm{GeV}^{-2}. \tag{5.34}$$

Comparing this with Eq.(5.5), we can see that the suppression of the imaginary part of C_{ee}, thus of the overall CP-violating phase of the $(g-2)_e$ diagram, with respect to

the real part must be at the percent level. Therefore, unless the CP-violating phase is exactly zero, as it is the case if all new couplings are real, the eEDM is an observable where a non-standard $(g-2)_e$ can be tested, cf. a related discussion in [24].

5.5 Conclusions

We have proposed a new mechanism to accommodate the experimental $(g-2)_\ell$ ($\ell = e, \mu$) discrepancies within the framework of low-scale flavor symmetry models. In these flavour models, that generate the Yukawa couplings through a Froggatt-Nielsen mechanism, the presence of quartic couplings between flavons can always act to close the loop of two scalar flavons that contribute to the mass at tree level, and thus both give a radiative correction to the mass and generate a contribution to the magnetic moment. We stress that a sizeable contribution of the anomalous magnetic moment, as required by the observed discrepancies, gives necessarily a contribution to the mass.

In order to obtain a sizable $g-2$ correction, compatible with the present discrepancies, we introduce a nontrivial quartic coupling with a second flavon, that acquires a large VEV though does not participate to the tree level masses. The radiative mass receives the same enhancement and contributes significantly to the mass generation; this sets a limit on the size of the $g-2$ contribution. The FN and radiative diagrams, with opposite signs, contribute to the electron and muon masses through a cancellation that accommodates the experimental difference in sign between the electron and muon magnetic moment discrepancies and, at the same time, contributes to satisfy the experimental limit on searches of vector-like mediators.

We show that our mechanism can provide a simple explanation of the discrepancies of the muon $(g-2)_\mu$ and the electron $(g-2)_e$, simultaneously in a large viable parameter space, with predicted mediator masses as large as $M_\chi \in [0.6, 2.5]$ TeV. We give an example of how this can be achieved in a toy model based on a $U(1)_f$ flavor symmetry. The application to a complete model, including the tau, quarks and neutrino sectors and the study of its phenomenological consequences in flavor physics is left to future works.

References

[1] J. Albrecht et al., *Int. J. Mod. Phys.* **2018**, *A33*, 1830016, arXiv: 1806.05010 [hep-ex].

[2] Y. Li, C.-D. LÃŒ, *Sci. Bull.* **2018**, *63*, 267–269, arXiv: 1808.02990 [hep-ph].

[3] S. Bifani et al., *J. Phys.* **2019**, *G46*, 023001, arXiv: 1809.06229 [hep-ex].

[4] G. Bennett et al., *Phys. Rev. D* **2006**, *73*, 072003, arXiv: hep-ex/0602035.

[5] M. Davier et al., *Eur. Phys. J. C* **2011**, *71*, [Erratum: Eur.Phys.J.C 72, 1874 (2012)], 1515, arXiv: 1010.4180 [hep-ph].

[6] M. Davier et al., *Eur. Phys. J. C* **2017**, *77*, 827, arXiv: 1706.09436 [hep-ph].

[7] A. Keshavarzi et al., *Phys. Rev.* **2018**, *D97*, 114025, arXiv: 1802.02995 [hep-ph].

[8] T. Blum et al., *Phys. Rev. Lett.* **2018**, *121*, 022003, arXiv: 1801.07224 [hep-lat].

[9] F. Campanario et al., *Phys. Rev. D* **2019**, *100*, 076004, arXiv: 1903.10197 [hep-ph].

[10] M. Davier et al., *Eur. Phys. J. C* **2020**, *80*, 241, arXiv: 1908.00921 [hep-ph].

[11] S. Borsanyi et al., **2020**, arXiv: 2002.12347 [hep-lat].

[12] M. Passera et al., *Phys. Rev. D* **2008**, *78*, 013009, arXiv: 0804.1142 [hep-ph].

[13] A. Crivellin et al., **2020**, arXiv: 2003.04886 [hep-ph].

[14] J. Grange et al., **2015**, arXiv: 1501.06858 [physics.ins-det].

[15] M. Lindner et al., *Phys. Rept.* **2018**, *731*, 1–82, arXiv: 1610.06587 [hep-ph].

[16] T. Moroi, *Phys. Rev. D* **1996**, *53*, [Erratum: Phys.Rev.D 56, 4424 (1997)], 6565–6575, arXiv: hep-ph/9512396.

[17] S. P. Martin, J. D. Wells, *Phys. Rev.* **2001**, *D64*, 035003, arXiv: hep-ph/0103067 [hep-ph].

[18] D. Stockinger, *J. Phys. G* **2007**, *34*, R45–R92, arXiv: hep-ph/0609168.

[19] M. Endo et al., *JHEP* **2014**, *01*, 123, arXiv: 1303.4256 [hep-ph].

[20] M. Endo et al., *JHEP* **2020**, *04*, 165, arXiv: 2001.11025 [hep-ph].

[21] G. F. Giudice et al., *JHEP* **2012**, *11*, 113, arXiv: 1208.6583 [hep-ph].

[22] R. H. Parker et al., *Science* **2018**, *360*, 191, arXiv: 1812.04130 [physics.atom-ph].

[23] H. Davoudiasl, W. J. Marciano, *Phys. Rev.* **2018**, *D98*, 075011, arXiv: 1806.10252 [hep-ph].

[24] A. Crivellin et al., *Phys. Rev.* **2018**, *D98*, 113002, arXiv: 1807.11484 [hep-ph].

[25] J. Liu et al., *JHEP* **2019**, *03*, 008, arXiv: 1810.11028 [hep-ph].

[26] X.-F. Han et al., *Phys. Rev.* **2019**, *D99*, 095034, arXiv: 1812.02449 [hep-ph].

[27] M. Endo, W. Yin, *JHEP* **2019**, *08*, 122, arXiv: 1906.08768 [hep-ph].

[28] M. Abdullah et al., *Phys. Rev.* **2019**, *D100*, 115006, arXiv: 1907.08109 [hep-ph].

[29] M. Bauer et al., **2019**, arXiv: 1908.00008 [hep-ph].

[30] M. Badziak, K. Sakurai, *JHEP* **2019**, *10*, 024, arXiv: 1908.03607 [hep-ph].

[31] A. E. CÃ¡rcamo HernÃ¡ndez et al., **2019**, arXiv: 1910.10734 [hep-ph].

[32] G. Hiller et al., **2019**, arXiv: 1910.14062 [hep-ph].

[33] C. Cornella et al., *JHEP* **2020**, *01*, 158, arXiv: 1911.06279 [hep-ph].

[34] M. Endo et al., **2020**, arXiv: 2002.05948 [hep-ph].

[35] S. Jana et al., **2020**, arXiv: 2003.03386 [hep-ph].

[36] L. Calibbi, G. Signorelli, *Riv. Nuovo Cim.* **2018**, *41*, 71–174, arXiv: 1709.00294 [hep-ph].

[37] A. Baldini et al., *Eur. Phys. J. C* **2016**, *76*, 434, arXiv: 1605.05081 [hep-ex].

[38] L. Calibbi et al., *JHEP* **2018**, *07*, 046, arXiv: 1804.00009 [hep-ph].

[39] C. D. Froggatt, H. B. Nielsen, *Nucl. Phys.* **1979**, *B147*, 277–298.

[40] M. Leurer et al., *Nucl. Phys.* **1993**, *B398*, 319–342, arXiv: hep-ph/9212278 [hep-ph].

[41] M. Leurer et al., *Nucl. Phys.* **1994**, *B420*, 468–504, arXiv: hep-ph/9310320 [hep-ph].

[42] N. Haba et al., **2020**, arXiv: 2002.10230 [hep-ph].

[43] A. Czarnecki, W. J. Marciano, *Phys. Rev.* **2001**, *D64*, 013014, arXiv: hep-ph/0102122 [hep-ph].

[44] H. Okada, K. Yagyu, *Phys. Rev.* **2014**, *D89*, 053008, arXiv: 1311.4360 [hep-ph].

[45] M. Bauer, M. Neubert, *Phys. Rev. Lett.* **2016**, *116*, 141802, arXiv: 1511.01900 [hep-ph].

[46] E. Coluccio Leskow et al., *Phys. Rev.* **2017**, *D95*, 055018, arXiv: 1612.06858 [hep-ph].

[47] A. Crivellin et al., *Phys. Rev.* **2018**, *D97*, 015019, arXiv: 1706.08511 [hep-ph].

[48] I. DorÅ¡ner et al., **2019**, arXiv: 1910.03877 [hep-ph].

[49] L. Calibbi et al., **2019**, arXiv: 1912.02676 [hep-ph].

[50] A. Crivellin et al., **2019**, arXiv: 1912.04224 [hep-ph].

[51] W. Altmannshofer et al., **2020**, arXiv: 2002.01400 [hep-ph].

[52] I. Bigaran, R. R. Volkas, **2020**, arXiv: 2002.12544 [hep-ph].

[53] L. Calibbi et al., *JHEP* **2012**, *06*, 018, arXiv: 1203.1489 [hep-ph].

[54] L. Calibbi et al., *JHEP* **2012**, *07*, 004, arXiv: 1204.1275 [hep-ph].

[55] D. Das et al., *Phys. Rev.* **2017**, *D95*, 035001, arXiv: 1607.06827 [hep-ph].

[56] M. L. López-Ibáñez et al., *JHEP* **2017**, *11*, [Erratum: JHEP 04, 015 (2018)], 162, arXiv: 1710.02593 [hep-ph].

[57] M. Tanabashi et al., *Phys. Rev.* **2018**, *D98*, 030001.

[58] S. Schael et al., *Phys. Rept.* **2013**, *532*, 119–244, arXiv: 1302.3415 [hep-ex].

[59] R. K. Ellis et al., **2019**, arXiv: 1910.11775 [hep-ex].

[60] N. Kumar, S. P. Martin, *Phys. Rev.* **2015**, *D92*, 115018, arXiv: 1510.03456 [hep-ph].

[61] G. Aad et al., *JHEP* **2015**, *09*, 108, arXiv: 1506.01291 [hep-ex].

[62] M. Aaboud et al., *Phys. Rev.* **2018**, *D98*, 032009, arXiv: 1804.03602 [hep-ex].

[63] A. M. Sirunyan et al., *Phys. Rev.* **2019**, *D100*, 052003, arXiv: 1905.10853 [hep-ex].

[64] A. M. Sirunyan et al., **2019**, arXiv: 1911.04968 [hep-ex].

[65] V. Andreev et al., *Nature* **2018**, *562*, 355–360.

Appendix A

A.1 Rotation to the Physical basis

A.1.1 Canonical rotation

In general the matter fields do not have canonical wave functions (kinetic terms). To obtain canonical kinetic terms, i.e. the Käler metric K is the identity, we have to redefine the fields $\psi \to T\widehat{\psi}$ to go to the canonical basis

$$\psi^\dagger K \psi = \widehat{\psi}^\dagger (T^{-1})^\dagger K T^{-1} \widehat{\psi} = \widehat{\psi}^\dagger \widehat{\psi} \tag{A.1}$$

thus the rotation must be the square root of the Käler metric $T = K^{1/2}$ so that $K = T^\dagger T$ [42, 43]. It is always possible to write an Hermitian matrix as $K = T^\dagger T$ in terms of an upper triangular T matrix,

$$K = T^\dagger T = \begin{pmatrix} T_{11} & 0 & 0 \\ T_{12}^* & T_{22} & 0 \\ T_{13}^* & T_{23}^* & T_{33} \end{pmatrix} \begin{pmatrix} T_{11} & T_{12} & T_{13} \\ 0 & T_{22} & T_{23} \\ 0 & 0 & T_{33} \end{pmatrix} . \tag{A.2}$$

The equation is easy to solve

$$T_{11} = \sqrt{Y_{11}} \quad , \quad T_{12} = \frac{Y_{12}}{\sqrt{Y_{11}}} \quad , \quad T_{13} = \frac{Y_{13}}{\sqrt{Y_{11}}}, \tag{A.3}$$

$$T_{22} = \sqrt{Y_{22} - \frac{Y_{12}^2}{Y_{11}}} \quad , \quad T_{23} = \frac{Y_{23}Y_{11} - Y_{13}Y_{12}}{\sqrt{Y_{22}Y_{11}^2 - Y_{11}Y_{12}^2}}, \tag{A.4}$$

$$T_{33} = \sqrt{Y_{33} - T_{23}^2 - T_{13}^2}\,. \tag{A.5}$$

The inverse of this upper triangular matrix is also upper triangular, and it is also easily obtained.

A.1.2 Yukawa diagonalization

In the case that the entries in the Yukawa matrices Y have a hierarchical structure, with Y_{33} being the largest entry, a useful analytic expression for the diagonalizing matrices $V_{L,R}$ is readily obtained [44]. This has been used to derive many of the analytic expressions used in this thesis. The Yukawa matrices can be diagonalized, $V_L^\dagger Y V_R$, by three successive rotations in the (2,3), (1,3) and (1,2) sectors (denoted by s_{23}, s_{13} and s_{12})

$$V_L = \begin{pmatrix} 1 & -s_{12} & 0 \\ s_{12} & 1 & 0 \\ 0 & 0 & 1 \end{pmatrix} \begin{pmatrix} 1 & 0 & -s_{13} \\ 0 & 1 & 0 \\ s_{13} & 0 & 1 \end{pmatrix} \begin{pmatrix} 1 & 0 & 0 \\ 0 & 1 & -s_{23} \\ 0 & s_{23} & 1 \end{pmatrix}, \tag{A.6}$$

$$V_R = \begin{pmatrix} 1 & 0 & 0 \\ 0 & 1 & s'_{23} \\ 0 & -s'_{23} & 1 \end{pmatrix} \begin{pmatrix} 1 & 0 & s'_{13} \\ 0 & 1 & 0 \\ -s'_{13} & 0 & 1 \end{pmatrix} \begin{pmatrix} 1 & s'_{12} & 0 \\ -s'_{12} & 1 & 0 \\ 0 & 0 & 1 \end{pmatrix}. \tag{A.7}$$

Defining $\Delta s_{ij} = s^d_{ij} - s^u_{ij}$, the CKM matrix is given by

$$V_{\rm CKM} = \begin{pmatrix} 1 & \Delta s_{12} + s^u_{13}\Delta s_{23} & \Delta s_{13} - s^u_{23}\Delta s_{23} \\ -\Delta s_{12} - s^d_{13}\Delta s_{23} & 1 & \Delta s_{23} + s^u_{12}\Delta s_{13} \\ -\Delta s_{13} + s^d_{12}\Delta s_{23} & -\Delta s_{23} - s^d_{12}\Delta s_{13} & 1 \end{pmatrix}. \tag{A.8}$$

Assuming the off-diagonal elements are small relative to the on-diagonal ones in each step of the diagonalization leads to the perturbative relation for the small mixing angles given by

$$s_{23} \simeq \frac{Y_{23}}{Y_{33}} + \frac{Y_{32}Y_{22}}{Y_{33}^2} \quad , \quad s_{13} \simeq \frac{\widetilde{Y}_{13}}{Y_{33}} + \frac{\widetilde{Y}_{31}Y_{11}}{Y_{33}^2} \quad , \quad s_{12} \simeq \frac{\widetilde{Y}_{12}}{\widetilde{Y}_{22}} + \frac{\widetilde{Y}_{21}Y_{11}}{\widetilde{Y}_{22}^2}, \tag{A.9}$$

$$s'_{23} \simeq \frac{Y_{32}}{Y_{33}} + \frac{Y_{23}Y_{22}}{Y_{33}^2} \quad , \quad s'_{13} \simeq \frac{\widetilde{Y}_{31}}{Y_{33}} + \frac{\widetilde{Y}_{13}Y_{11}}{Y_{33}^2} \quad , \quad s'_{12} \simeq \frac{\widetilde{Y}_{21}}{\widetilde{Y}_{22}} + \frac{\widetilde{Y}_{12}Y_{11}}{\widetilde{Y}_{22}^2}, \tag{A.10}$$

where the successive rotations produce elements $\widetilde{Y}$

$$\begin{aligned} \widetilde{Y}_{22} &\simeq Y_{22} - \frac{Y_{23}Y_{32}}{Y_{33}}, \\ \widetilde{Y}_{13} &= Y_{13} - Y_{12}s'_{23} \quad , \quad \widetilde{Y}_{12} = Y_{12} - Y_{13}s'_{23}, \\ \widetilde{Y}_{31} &= Y_{31} - Y_{21}s_{23} \quad , \quad \widetilde{Y}_{21} = Y_{21} - Y_{31}s_{23}. \end{aligned} \tag{A.11}$$

A.1.3 Canonical normalization and rotation to CKM basis

To compare the MSSM contributions to the SM predictions, we have to rotate the Kähler to pass to the canonical basis, where the Kähler corresponds to the identity and the kinetic terms are canonical. Following Appendix A.1.1 this can be achieved through an upper triangular matrix $T^\dagger\, K_R\, T$, with T of the form

$$T \;=\; \begin{pmatrix} 1 - y_{3,a}\dfrac{\varepsilon_a^{2\alpha}}{2} & -y_{3,a}\,\varepsilon_a^{2\alpha} & -\dfrac{y_{3,a}}{\sqrt{1+y_{3,a}}}\left(e^{i(\gamma_a-\frac{\delta_a}{2})}\,r_a\,\varepsilon_a^{\alpha} \,+\, \varepsilon_a^{2\alpha}\right) \\ 0 & 1 - y_{3,a}\dfrac{\varepsilon_a^{2\alpha}}{2} & -\dfrac{y_{3,a}}{\sqrt{1+y_{3,a}}}\left(e^{i(\gamma_a-\frac{\delta_a}{2})}\,r_a\,\varepsilon_a^{\alpha} \,+\, \varepsilon_a^{2\alpha}\right) \\ 0 & 0 & \dfrac{1}{\sqrt{1+y_{3,a}}} \end{pmatrix}. \tag{A.12}$$

This upper triangular canonical transformation gives only sub-leading effects on the hierarchical structures of the Yukawas and trilinears and therefore can neglected in this qualitative discussion[1]. On the other hand, its effect on the soft mass matrices is a general 1-unit reduction in the degeneracy coefficients. The Yukawas are diagonalized by a bi-unitary transformation

$$Y'^{a} = P_{aL}^{*}\, V_L^{a\dagger}\, Y^a\, V_R^a\, P_{aR}\,, \tag{A.13}$$

where P_{aL}, P_{aR} are diagonal re-phasing matrices introduced to go to the SM phase conventions in the CKM matrix as shown below, while

$$V_L^a \;=\; V_R^{a*} \;=\; \begin{pmatrix} 1 - \dfrac{x_{1,a}^2}{2\,r^{2_a}\,x_{2_a}^2}\varepsilon_a^2 & e^{i\,(\gamma_a-\delta_a)}\dfrac{x_{1,a}}{r_a\,x_{2,a}}\varepsilon_a & e^{i\,\gamma_a}x_{1,a}\,\varepsilon_a^3 \\ -e^{-i\,(\gamma_a-\delta_a)}\dfrac{x_{1,a}}{r_a\,x_{2,a}}\varepsilon_a & 1 - \dfrac{x_{1,a}^2}{2\,r^{2_a}\,x_{2_a}^2}\varepsilon_a^2 & e^{i\,\delta_a}r_a\,x_{2,a}\,\varepsilon_a^2 \\ 0 & -e^{-i\,\delta_a}r_a\,x_{2,a}\,\varepsilon_a^2 & 1 \end{pmatrix}. \tag{A.14}$$

It can be easily checked that these two matrices diagonalize the Yukawa and respect unitarity up to $\mathcal{O}(\varepsilon_a^4)$. The CKM is defined in terms of the up and down-quark Left-rotation matrices as

$$V_{\rm CKM} \equiv P_{uL}^{*}\, V_L^{u\dagger}\, V_L^{d}\, P_{dL}. \tag{A.15}$$

[1] The only possible exception is the re-scaling of the third row and column

Given the expansion parameter in the up sector being three times smaller than in the down sector, we can convince ourselves that the $V_L^{u\dagger}$ part gives only higher order corrections to the LO structure, so in this qualitative discussion we can consider $V_{\rm CKM} \simeq V_L^d$. We can now make use of the re-phasing matrices P_{uL} and P_{dL} in order to make the 11, 22, 33, 12, 23 entries real in the CKM matrix. Looking at Eq.(A.14) we see that we need to get rid of $\theta_{12} = (\gamma_d - \delta_d), \theta_{23} = \delta_d$, which may can be achieved straightforwardly by

$$P_{dL} \;=\; P_{uL}^* \;=\; \begin{pmatrix} 1 & 0 & 0 \\ 0 & e^{i\,(\gamma_d - \delta_d)} & 0 \\ 0 & 0 & e^{i\,\delta_d} \end{pmatrix} . \tag{A.16}$$

Additionally, to keep real and positive Yukawa couplings after this rephasing, we must absorb these undesired phases in the right re-phasing matrices, as

$$P_{eR} \;=\; \mathrm{diag}\{e^{-i\,(2\gamma_e - \delta_e)}, e^{-i\,(\pi + \delta_e)}, 1\} \tag{A.17}$$

$$P_{uR} \;=\; \mathrm{diag}\{e^{-i\,\pi}, e^{-i(\gamma_d - \delta_d)}, e^{-i\,\gamma_d}\} \tag{A.18}$$

$$P_{dR} \;=\; \mathrm{diag}\{e^{-i\,(\pi + 2\gamma_d - \delta_d)}, e^{-i\,\gamma_d}, e^{-i\,\gamma_d}\}. \tag{A.19}$$

These same transformations must be performed on the soft-mass matrices. The results may be found in Section 2.3.

A.2 Gaugino-slepton-lepton interaction

The mass matrix of the *charginos* is written as

$$\begin{pmatrix} \overline{\widetilde{W}}_R^{\pm} & \overline{\widetilde{H}}_{uR}^{\pm} \end{pmatrix} \begin{pmatrix} M_2 & \sqrt{2}\, m_W\, c_\beta \\ \sqrt{2}\, m_W\, s_\beta & \mu \end{pmatrix} \begin{pmatrix} \widetilde{W}_L^{\pm} \\ \widetilde{H}_{dL}^{\pm} \end{pmatrix} , \tag{A.20}$$

where $s_\beta = \sin\beta$. This is diagonalized by two unitary matrices $U_{L,R}^c$, the eigenvalues are denoted by $m_{\widetilde{\chi}_A^{\pm}}$ with $A = 1, 2$. The mass eigenstates are called the charginos

$$\widetilde{\chi}_L^{\pm} = U_L^c \begin{pmatrix} \widetilde{W}_L^{\pm} \\ \widetilde{H}_{dL}^{\pm} \end{pmatrix} \quad , \quad \widetilde{\chi}_L^{\pm} = U_R^c \begin{pmatrix} \widetilde{W}_R^{\pm} \\ \widetilde{H}_{uR}^{\pm} \end{pmatrix} , \tag{A.21}$$

then $\widetilde{\chi}_A^{\pm} = \widetilde{\chi}_{AL}^{\pm} + \widetilde{\chi}_{AR}^{\pm}$ $(A = 1, 2)$ forms a Dirac fermion.
The mass matrix of the *neutralinos* is written as

$$\left(\widetilde{B}_L\, \widetilde{W}_L^0\, \widetilde{H}_{dL}^0\, \widetilde{H}_{uL}^0\right) \begin{pmatrix} M_1 & 0 & -m_Z\, s_W\, c_\beta & m_Z\, s_W\, s_\beta \\ 0 & M_2 & m_Z\, c_W\, c_\beta & m_Z\, c_W\, s_\beta \\ -m_Z\, s_W\, c_\beta & m_Z\, s_W\, s_\beta & 0 & -\mu \\ m_Z\, c_W\, c_\beta & -m_Z\, c_W\, s_\beta & -\mu & 0 \end{pmatrix} \begin{pmatrix} \widetilde{B}_L \\ \widetilde{W}_L^0 \\ \widetilde{H}_{dL}^0 \\ \widetilde{H}_{uL}^0 \end{pmatrix} \quad \text{(A.22)}$$

where $s_\beta = \sin\beta$, $c_\beta = \cos\beta$, $s_W = \sin\theta_W$ and $c_W = \cos\theta_W$. The mass matrix is diagonalized by a unitary matrix U^n. The mass eigenvalues are denoted by $m_{\widetilde{\chi}_A^0}$ (with $A = 1, \cdots 4$) and are called the neutralinos. They are defined as

$$\widetilde{\chi}_L^0 = U^n \begin{pmatrix} \widetilde{B}_L \\ \widetilde{W}_L^0 \\ \widetilde{H}_{dL}^0 \\ \widetilde{H}_{uL}^0 \end{pmatrix} . \quad \text{(A.23)}$$

Then $\widetilde{\chi}_A^0 = \widetilde{\chi}_{AL}^0 + \widetilde{\chi}_{AR}^0$ $(A = 1, \cdots, 4)$ forms a Majorana fermion. The relevant interaction Lagrangian for gaugino-slepton-lepton, in the mass basis, is written as

$$\mathcal{L}_{\text{int}} = \overline{\ell}_i \left(C_{iAX}^R P_R + C_{iAX}^L P_L\right) \widetilde{\chi}_A^- \widetilde{\nu}_{\ell_X} + \overline{\ell}_i \left(N_{iAX}^R P_R + N_{iAX}^L P_L\right) \widetilde{\chi}_A^0 \widetilde{\ell}_X + \text{h.c.} \quad \text{(A.24)}$$

where the coefficients are defined in terms of the rotation matrices as

$$C_{iAX}^R = -g U_{R,A1}^{c*}\, \delta_{iX} , \quad \text{(A.25)}$$

$$C_{iAX}^R = Y_{iX}^e\, U_{L,A2}^{c*} , \quad \text{(A.26)}$$

$$N_{iAX}^R = \frac{g}{\sqrt{2}} \left(U_{A1}^n\, \tan\theta_W + U_{A2}^n\right) V_{X,i}^{e*} - Y_{ij}^e U_{A3}^n V_{X,i+3}^{e*} , \quad \text{(A.27)}$$

$$N_{iAX}^L = -\sqrt{2}\, g\, \tan\theta_W\, U_{A1}^{n*}\, V_{X,i+3}^{e*} - Y_{ij}^e\, U_{A3}^{n*}\, V_{X,j}^{e*} . \quad \text{(A.28)}$$

A.3 Mass Insertion Approximation

Although the mass eigenstate basis is the natural basis for calculations of physical processes, for a qualitative analysis, it is often useful to have our expressions in the flavor basis. The standard strategy is an approximate diagrammatic method commonly referred to as the Mass Insertion Approximation (MIA) [45].

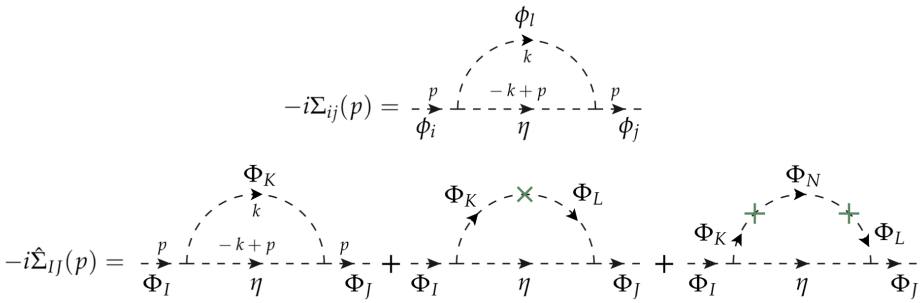

FIGURE A.1: The Feynman graphs for the scalar self energy in the mass eigenstate basis (top) and in the flavour basis (bottom).

The squared mass matrix, $\boldsymbol{M_{IJ}^2}$, of the flavour eigenstates Φ_I, are necessarily Hermitian but not aligned in general. The rotation to the mass basis ϕ_i is obtained by a unitary matrix U: $\Phi_I = U_{Ii}\,\phi_i$. We consider the example in which we want to approximate the scalar self-energy $-i\Sigma_{ij}$ in the mass eigenstate basis:

$$-i\hat{\Sigma}_{ij}(p) \;=\; \int \frac{d^4k}{(2\pi)^4}\frac{y_{jk}y_{li}}{(k-m_l^2)[(k-p)^2-m_\eta^2]} = \frac{i}{16\pi^2}\,y_{jk}y_{li}\,f(p;m_l^2,m_\eta^2) \tag{A.29}$$

In the standard MIA approach, this is done by writing

$$iU_{Jj}\,\Sigma_{ij}(p)\,U_{iJ}^\dagger = \hat{\Sigma}_{IJ}(p) \tag{A.30}$$

where $-i\hat{\Sigma}_{IJ}$ is the scalar self-energy in the flavour basis. To compute it, the flavor mass matrix $\boldsymbol{M_{IJ}^2}$ is decomposed into its diagonal and non-diagonal parts

$$\boldsymbol{M_{IJ}^2} = M_I^2\delta_{IJ} + \Delta_{IJ} \quad \text{with} \quad \Delta_{II} = 0\,. \tag{A.31}$$

where M_I^2 are the flavor masses and Δ_{IJ} are *the mass insertions*. The massive flavour propagators are defined by absorbing the diagonal part of the flavour mass matrix. The scalar self-energy $-i\hat{\Sigma}_{IJ}$ in the flavour basis is given by

$$\begin{aligned}
-i\hat{\Sigma}_{IJ}(p) \;&=\; \int \frac{d^4k}{(2\pi)^4}\frac{Y_{JK}Y_{LI}}{(k-p)^2-m_\eta^2}\left(\frac{\delta_{KL}}{k^2-M_K^2}+\frac{\Delta_{KL}}{(k^2-M_K^2)(k^2-M_L^2)}\right.\\
&+\; \left.\frac{\Delta_{KN}\Delta_{NL}}{(k^2-M_K^2)(k^2-M_N^2)(k^2-M_L^2)}+\cdots\right) \qquad \text{(A.32)}\\
&=\; \frac{i}{16\pi^2}Y_{JK}Y_{LI}\left(\delta_{KL}f(p;M_K^2,m_\eta^2)+\Delta_{KL}f^{\times}(p;M_K^2,M_L^2,m_\eta^2)+\right.\\
&+\; \left.\Delta_{KN}\Delta_{NL}\,f^{\times\times}(p;M_K^2,M_N^2,M_L^2,m_\eta^2)+\cdots\right) \qquad \text{(A.33)}
\end{aligned}$$

which as shown in Figure is essentially an expansion in terms of mass insertions. For the loop-functions f the MIA approximation writes

$$\begin{aligned} iU_{Kl}\, f(p; m_l^2, m_\eta^2)\, U_{lL}^\dagger &= \delta_{KL} f(p; M_K^2, m_\eta^2) + \Delta_{KL} f^{\times}(p; M_K^2, M_L^2, m_\eta^2) + \\ &+ \Delta_{KN}\Delta_{NL}\, f^{\times\times}(p; M_K^2, M_N^2, M_L^2, m_\eta^2 + \cdots)\,, \end{aligned} \tag{A.34}$$

which can be generalized to the case of an arbitrary n-point amplitude. However, this result, can be also obtained by a theorem of matrix analysis called the Flavor Expansion Theorem.

Appendix B

B.1 A_4 Group

The set of even permutations on four objects form a group, labeled A_4. This group can be generated by two elements S and T obeying the following relations

$$S^2 = (ST)^3 = T^3 = 1. \tag{B.1}$$

It has three independent one-dimensional representations $\mathbf{1}$,$\mathbf{1}'$,$\mathbf{1}''$ and one three-dimensional representation $\mathbf{3}$. The one-dimensional representations are given by:

$$\begin{aligned} &\mathbf{1} \quad S = 1 \quad T = 1 \\ &\mathbf{1}' \quad S = 1 \quad T = e^{i4\pi/3} = \omega^2 \\ &\mathbf{1}'' \quad S = 1 \quad T = e^{i2\pi/3} = \omega. \end{aligned} \tag{B.2}$$

The three-dimensional representation, in a basis where the generator T is diagonal, is given by:

$$T = \begin{pmatrix} 1 & 0 & 0 \\ 0 & \omega^2 & 0 \\ 0 & 0 & \omega \end{pmatrix} \quad , \quad S = \frac{1}{3}\begin{pmatrix} -1 & 2 & 2 \\ 2 & -1 & 2 \\ 2 & 2 & -1 \end{pmatrix}. \tag{B.3}$$

The multiplication rules between the various representations are:

$$\mathbf{1} \otimes \mathbf{1^{any}} = \mathbf{1^{any}} \quad , \quad \mathbf{1}' \otimes \mathbf{1}^{'} = \mathbf{1}^{''} \quad , \quad \mathbf{1}' \otimes \mathbf{1}'' = \mathbf{1} \quad , \quad \mathbf{1}'' \otimes \mathbf{1}'' = \mathbf{1}', \tag{B.4}$$

then, taking $\mathbf{3}_\alpha = (\alpha_1, \alpha_2, \alpha_3)$ and $\mathbf{3}_\beta = (\beta_1, \beta_2, \beta_3)$ as two generic triplets, we can write also

$$\mathbf{1} \otimes \mathbf{3}_\alpha = \mathbf{3}_\alpha \sim \begin{pmatrix} \alpha_1 \\ \alpha_2 \\ \alpha_3 \end{pmatrix} \quad , \quad \mathbf{1}' \otimes \mathbf{3}_\alpha = \mathbf{3} \sim \begin{pmatrix} \alpha_3 \\ \alpha_1 \\ \alpha_2 \end{pmatrix} \quad , \quad \mathbf{1}'' \otimes \mathbf{3}_\alpha = \mathbf{3} \sim \begin{pmatrix} \alpha_2 \\ \alpha_3 \\ \alpha_1 \end{pmatrix} \tag{B.5}$$

$$\mathbf{3}_\alpha \otimes \mathbf{3}_\beta = \mathbf{1} + \mathbf{1}' + \mathbf{1}'' + \mathbf{3}_S + \mathbf{3}_A \quad \text{with} \quad \begin{cases} \mathbf{1} \sim \alpha_1\beta_1 + \alpha_2\beta_3 + \alpha_3\beta_2 \\ \mathbf{1}' \sim \alpha_3\beta_3 + \alpha_1\beta_2 + \alpha_2\beta_1 \\ \mathbf{1}'' \sim \alpha_2\beta_2 + \alpha_1\beta_3 + \alpha_3\beta_1 \\ \mathbf{3}_S \sim \frac{1}{3}\begin{pmatrix} 2\alpha_1\beta_1 - \alpha_2\beta_3 - \alpha_3\beta_2 \\ 2\alpha_3\beta_3 - \alpha_1\beta_2 - \alpha_2\beta_1 \\ 2\alpha_2\beta_2 - \alpha_1\beta_3 - \alpha_3\beta_1 \end{pmatrix} \\ \mathbf{3}_A \sim \frac{1}{2}\begin{pmatrix} \alpha_2\beta_3 - \alpha_3\beta_2 \\ \alpha_1\beta_2 - \alpha_2\beta_1 \\ \alpha_1\beta_3 - \alpha_3\beta_1 \end{pmatrix} \end{cases} . \tag{B.6}$$

It is useful to note that the operation of complex conjugation acts as

$$\mathbf{1}^* \sim \mathbf{1} \quad , \quad (\mathbf{1}')^* \sim \mathbf{1}'' \quad , \quad (\mathbf{1}'')^* \sim \mathbf{1}' \quad , \quad \mathbf{3}^* \sim \begin{pmatrix} {\alpha_1}^* \\ {\alpha_3}^* \\ {\alpha_2}^* \end{pmatrix}, \tag{B.7}$$

so, for example, the product rule $(\mathbf{1}' \otimes \mathbf{3})^* = \mathbf{1}'' \otimes \mathbf{3}^*$.The reason for this is that $T^* = U_{23}^T T U_{23}$ and $S^* = U_{23}^T S U_{23} = S$ where U_{23} is the matrix that changes the 2nd and 3rd row and column.

B.2 S_3 Group

The group S_3 is defined by the possible permutations among three objects. One of its presentations is that given by the generators S and T satisfying the following relations

$$S^2 = (ST)^2 = T^3 = 1. \tag{B.8}$$

The number of irreducible representations is three: two one-dimensional, $\mathbf{1}$ and $\mathbf{1}'$, and one two-dimensional, $\mathbf{2}$. The generators in the one-dimensional representations

are given by:

$$\begin{array}{ll} \mathbf{1} & S=1 \quad T=1 \\ \mathbf{1}' & S=-1 \quad T=1 \end{array} \tag{B.9}$$

while, in the two-dimensional representation for the T-diagonal basis, they can be written as:

$$T=\begin{pmatrix} \omega & 0 \\ 0 & \omega^2 \end{pmatrix} \quad , \quad S=\begin{pmatrix} 0 & 1 \\ 1 & 0 \end{pmatrix}. \tag{B.10}$$

The tensor products between singlets and pseudosinglets are:

$$\mathbf{1}\otimes\mathbf{1^{any}}=\mathbf{1^{any}} \quad , \quad \mathbf{1}'\otimes\mathbf{1}'=\mathbf{1} \tag{B.11}$$

Considering two doublets, $\mathbf{2}_\alpha=(\alpha_1,\alpha_2)$ and $\mathbf{2}_\beta=(\beta_1,\beta_2)$, we can also write

$$\mathbf{1}\otimes\mathbf{2}_\alpha=\mathbf{2}_\alpha\sim\begin{pmatrix}\alpha_1\\ \alpha_2\end{pmatrix} \quad , \quad \mathbf{1}'\otimes\mathbf{2}_\alpha=\mathbf{2}\sim\begin{pmatrix}-\alpha_1\\ \alpha_2\end{pmatrix} \tag{B.12}$$

$$\mathbf{2}_\alpha\otimes\mathbf{2}_\beta=\mathbf{1}+\mathbf{1}'+\mathbf{2} \quad \text{with} \quad \begin{cases} \mathbf{1}\sim\alpha_1\beta_2+\alpha_2\beta_1 \\ \mathbf{1}'\sim\alpha_1\beta_2-\alpha_2\beta_1 \\ \mathbf{2}\sim\begin{pmatrix}\alpha_2\beta_2\\ \alpha_1\beta_1\end{pmatrix} \end{cases} \tag{B.13}$$

The operation of complex conjugation leaves the singlets unchanged but acts over the doublet as follows

$$\mathbf{2}^*\sim\begin{pmatrix}{\alpha_2}^*\\ {\alpha_1}^*\end{pmatrix}, \tag{B.14}$$

so that $\mathbf{2}^*$ transforms now as an anti-doublet with the matrices $(S^*,\, T^*)$.

B.3 A_5 Group

Here we present the matrix form of the A_5 and CP generators, $S_{\mathbf{r}}$ and $T_{\mathbf{r}}$, for each of the irreducible representations of the group: $\mathbf{r} = \mathbf{1}, \mathbf{3}, \mathbf{3'}, \mathbf{4}$ and $\mathbf{5}$ [46].

$$S_{\mathbf{1}} = e^{i\pi} \qquad T_{\mathbf{1}} = e^{i\frac{2\pi}{5}} \tag{B.15a}$$

$$S_{\mathbf{3}} = \frac{1}{\sqrt{5}}\begin{pmatrix} 1 & \sqrt{2} & \sqrt{2} \\ \sqrt{2} & -\varphi & 1/\varphi \\ \sqrt{2} & 1/\varphi & -\varphi \end{pmatrix} \qquad T_{\mathbf{3}} = \begin{pmatrix} 1 & 0 & 0 \\ 0 & e^{i\frac{2\pi}{5}} & 0 \\ 0 & 0 & e^{i\frac{8\pi}{5}} \end{pmatrix} \tag{B.15b}$$

$$S_{\mathbf{3'}} = -\frac{1}{\sqrt{5}}\begin{pmatrix} 1 & \sqrt{2} & \sqrt{2} \\ \sqrt{2} & 1/\varphi & -\varphi \\ \sqrt{2} & -\varphi & 1/\varphi \end{pmatrix} \qquad T_{\mathbf{3'}} = \begin{pmatrix} 1 & 0 & 0 \\ 0 & e^{i\frac{4\pi}{5}} & 0 \\ 0 & 0 & e^{-i\frac{4\pi}{5}} \end{pmatrix} \tag{B.15c}$$

$$S_{\mathbf{4}} = -\frac{1}{5}\begin{pmatrix} -\sqrt{5} & \varphi-3 & \varphi+2 & -\sqrt{5} \\ \varphi-3 & \sqrt{5} & \sqrt{5} & \varphi+2 \\ \varphi+2 & \sqrt{5} & \sqrt{5} & \varphi-3 \\ -\sqrt{5} & \varphi+2 & \varphi-3 & -\sqrt{5} \end{pmatrix} \quad T_{\mathbf{4}} = \begin{pmatrix} e^{i\frac{2\pi}{5}} & 0 & 0 & 0 \\ 0 & e^{i\frac{4\pi}{5}} & 0 & 0 \\ 0 & 0 & e^{i\frac{6\pi}{5}} & 0 \\ 0 & 0 & 0 & e^{i\frac{8\pi}{5}} \end{pmatrix} \tag{B.15d}$$

$$S_{\mathbf{5}} = \frac{1}{5}\begin{pmatrix} -1 & \sqrt{6} & -\sqrt{6} & -\sqrt{6} & -\sqrt{6} \\ \sqrt{6} & 2-\varphi & 2\varphi & 2(1-\varphi) & -(1+\varphi) \\ -\sqrt{6} & 2\varphi & 1+\varphi & 2-\varphi & 2(\varphi-1) \\ -\sqrt{6} & 2(1-\varphi) & 2-\varphi & 1+\varphi & -2\varphi \\ -\sqrt{6} & -(1+\varphi) & 2(\varphi-1) & -2\varphi & 2-\varphi \end{pmatrix} \quad T_{\mathbf{5}} = \begin{pmatrix} 1 & 0 & 0 & 0 & 0 \\ 0 & e^{i\frac{2\pi}{5}} & 0 & 0 & 0 \\ 0 & 0 & e^{i\frac{4\pi}{5}} & 0 & 0 \\ 0 & 0 & 0 & e^{i\frac{6\pi}{5}} & 0 \\ 0 & 0 & 0 & 0 & e^{i\frac{8\pi}{5}} \end{pmatrix}. \tag{B.15e}$$

The matrix form of the CP generator, $X_{0,\mathbf{r}}$, in the irreps $\mathbf{r} = \mathbf{1}, \mathbf{3'}, \mathbf{4}$ and $\mathbf{5}$ is:

$$X_{0,\mathbf{1}} = \mathbf{1} \qquad X_{0,\mathbf{3'}} = \begin{pmatrix} 1 & 0 & 0 \\ 0 & 0 & 1 \\ 0 & 1 & 0 \end{pmatrix} \tag{B.16a}$$

$$X_{0,\mathbf{4}} = \begin{pmatrix} 0 & 0 & 0 & 1 \\ 0 & 0 & 1 & 0 \\ 0 & 1 & 0 & 0 \\ 1 & 0 & 0 & 0 \end{pmatrix} \qquad X_{0,\mathbf{5}} = \begin{pmatrix} 0 & 0 & 0 & 0 & 1 \\ 0 & 0 & 0 & 1 & 0 \\ 0 & 0 & 1 & 0 & 0 \\ 0 & 1 & 0 & 0 & 0 \\ 1 & 0 & 0 & 0 & 0 \end{pmatrix}. \tag{B.16b}$$

For $\mathbf{r} = \mathbf{3}$, $X_{0,\mathbf{3}}$ has been specified in Eq.(3.10).

Appendix C

C.1 Boltzmann equations

Recall that the baryon asymmetry Y_B can be expressed as

$$Y_B = \frac{10}{31}\sum_\alpha Y_{\Delta_\alpha}, \tag{C.1}$$

where Y_{Δ_α} are the $B/3 - L_\alpha$ asymmetries for each active lepton species α. In the fully-flavoured scenario, these are simply the usual three lepton flavours, $\alpha = e, \mu, \tau$. Assuming hierarchical RH neutrinos and thermal leptogenesis, the lepton asymmetries are obtained by solving the Boltzmann equations

$$\begin{aligned}
\frac{dY_{N_i}}{dz} &= -2D\left(Y_{N_i} - Y^{\rm eq}_{N_i}\right), \\
\frac{dY_{\widetilde{N}_i}}{dz} &= -2D\left(Y_{\widetilde{N}_i} - Y^{\rm eq}_{\widetilde{N}_i}\right), \\
\frac{dY_{\Delta_\alpha}}{dz} &= 2\varepsilon^\alpha_{N_i} D\left(Y_{N_i} - Y^{\rm eq}_{N_i}\right) + 2\varepsilon^\alpha_{\widetilde{N}_i} D\left(Y_{\widetilde{N}_i} - Y^{\rm eq}_{\widetilde{N}_i}\right) + \frac{K^\alpha_{N_i}}{K_{N_i}} W \sum_{\alpha'} A_{\alpha\alpha'} Y_{\Delta_{\alpha'}} \quad ,
\end{aligned} \tag{C.2}$$

where $z = M_i/T$. As noted in Section 4.4, the factors D and W govern the decay and washout behaviour. In this appendix we make these explicit, noting how information about decays and scattering are incorporated. In particular, we follow [47].

The equilibrium number density for a given field f is denoted $Y^{\rm eq}_f$, and are functions of z. The RH (s)neutrino densities are given by

$$Y^{\rm eq}_{N_i} = Y^{\rm eq}_{\widetilde{N}_i} = \frac{45}{2\pi^4 g_*} z^2 \mathcal{K}_2(z), \tag{C.3}$$

where $g_* = 228.75$ is the effective number of degrees of freedom in the MSSM and $\mathcal{K}_2(z)$ the modified Bessel functions of the second kind. The (s)lepton distributions are given by

$$Y^{\rm eq}_\alpha = Y^{\rm eq}_{\widetilde{\alpha}} = \frac{45}{\pi^4 g_*}. \tag{C.4}$$

We now turn to the decay and washout factors, D and W. There are three classes of processes that contribute to the Boltzmann equations: (1) decays and inverse decays ($N \leftrightarrow L_\alpha H_u$), (2) $\Delta L = 1$ scatterings (e.g. $NQ \leftrightarrow L_\alpha t$) and (3) $\Delta L = 2$ processes ($L_\alpha L_\alpha \leftrightarrow \overline{H}_u \overline{H}_u$, $L_\alpha H_u \leftrightarrow \bar{L}_\alpha \overline{H}_u$). Following [48] and [47], in this analysis we include $\Delta L = 1$ scatterings involving neutrino and top Yukawa couplings, neglecting gauge boson-mediated processes, as well as thermal corrections, and all $\Delta L = 2$ processes. Then

$$D = zK_{N_i} f_1(z) \frac{\mathcal{K}_1(z)}{\mathcal{K}_2(z)}, \qquad W = \frac{z}{2} K_{N_i} f_2(z) \frac{\mathcal{K}_1(z)}{\mathcal{K}_2(z)} \frac{\Upsilon_{N_i}^{\mathrm{eq}} + \Upsilon_{\widetilde{N}_i}^{\mathrm{eq}}}{\Upsilon_{\alpha}^{\mathrm{eq}} + \Upsilon_{\widetilde{\alpha}}^{\mathrm{eq}}}. \tag{C.5}$$

The effects of $\Delta L = 1$ scatterings are encapsulated in the functions $f_1(z)$ and $f_2(z)$. These are discussed in [48] and [47], and we may approximate them by

$$f_1(z) \simeq f_2(z) \simeq \tfrac{z}{a} \left[\log\left(1 + \frac{a}{z}\right) + \frac{1}{a \log(M_i/M_h) z} \right] \left(1 + \tfrac{15}{8z}\right), \tag{C.6}$$

$$a = \frac{4\pi^2 g_{N_i} v_u^2}{9 m_t^2 \log(M_i/M_h)}, \tag{C.7}$$

where $M_h = 125$ GeV is the Higgs mass, $m_t \simeq 93$ GeV is the top mass (at the GUT scale, which is a reasonable approximation of the value at the leptogenesis scale for our purposes) and $g_{N_i} = 2$.

A is a numerical matrix describing flavour mixing, and is given in the n_F-flavour regime by

$$A = \begin{cases} \begin{pmatrix} -93/110 & 6/55 & 6/55 \\ 3/40 & -19/30 & 1/30 \\ 3/40 & 1/30 & -19/30 \end{pmatrix}, & n_F = 3 \\ \begin{pmatrix} -541/761 & 152/761 \\ 46/761 & -494/761 \end{pmatrix}, & n_F = 2 \\ -1, & n_F = 1 \end{cases}. \tag{C.8}$$

While the ratio of Bessel functions, $\mathcal{K}_1(z)/\mathcal{K}_2(z)$, is in principle well-behaved for all positive z, for computational efficiency and stability it may be convenient to use the approximations

$$\mathcal{K}_1(z) \approx \left(1 + \frac{15}{8z}\right)^{-1} \mathcal{K}_2(z) \approx \frac{1}{z} \sqrt{1 + \frac{\pi}{2} z} e^{-z}. \tag{C.9}$$

As described in Section 4.4, the decay factors are given by

$$K^{\alpha}_{N_i} = \frac{v_u^2}{m_* M_i}(\lambda_\nu^\dagger)_{i\alpha}(\lambda_\nu)_{\alpha i}, \qquad K_{N_i} = \sum_\alpha K^{\alpha}_{N_i}, \tag{C.10}$$

and the CP asymmetries by

$$\varepsilon^{\alpha}_{N_i} = \varepsilon^{\alpha}_{\widetilde{N}_i} = \frac{1}{8\pi}\sum_{j\neq i}\frac{\mathrm{Im}[(\lambda_\nu^\dagger)_{i\alpha}(\lambda_\nu^\dagger\lambda_\nu)_{ij}(\lambda_\nu^T)_{j\alpha}]}{(\lambda_\nu^\dagger\lambda_\nu)_{ii}} g\left(\frac{M_j^2}{M_i^2}\right). \tag{C.11}$$

where $g(x)$ is a loop function given by the sum of the vertex and the self energy contributions [47, 49]; in the MSSM,

$$g(x) = \sqrt{x}\left[\frac{2}{1-x} - \log\left(\frac{1+x}{x}\right)\right]. \tag{C.12}$$

In the limit of very hierarchical RH neutrino masses, i.e. $x \ll 1$ or $x \gg 1$, to good approximation,

$$g(x) = \begin{cases} -\dfrac{3}{\sqrt{x}}, & x \gg 1 \\ 2\sqrt{x}\left(1+\log\sqrt{x}\right), & x \ll 1 \end{cases}. \tag{C.13}$$

C.2 Seesaw with rank-one matrices

We consider here a more intuitive explanation of the texture zero remaining after seesaw, following the method employed for the model in [10], and presented in [11]. The Dirac and Majorana matrices are given in terms of four rank-1 matrices, expressed in terms of the VEV alignments of flavons $\phi_{a,b,c}$, where

$$\phi_a \propto (1,1,-1), \qquad \phi_b \propto (0,1,1), \qquad \phi_c \propto (0,0,1). \tag{C.14}$$

For notational simplicity, in tis appendix we use ϕ_i to refer simply to the direction of the VEV (rather than the field or VEV itself). We have

$$\begin{aligned} Y^\nu &= y_a^\nu(\square_{ab}+\square_{ba}) + y_b^\nu\square_b + y_c^\nu\square_c, \\ M_N &= M_a(\square_{ab}+\square_{ba}) + M_b\square_b + M_c\square_c, \end{aligned} \tag{C.15}$$

where

$$\square_{ab} = (\square_{ba})^T = \phi_a\phi_b^T, \qquad \square_b = \phi_b\phi_b^T, \qquad \square_c = \phi_c\phi_c^T. \tag{C.16}$$

We define another set of vectors $\widetilde{\phi}_{a,b,c}$, which are orthogonal to $\phi_{a,b,c}$, i.e.

$$\widetilde{\phi}_i^T \phi_j = \delta_{ij}, \qquad i,j = a,b,c. \tag{C.17}$$

An appropriate choice is

$$\widetilde{\phi}_a \propto (1,0,0), \qquad \widetilde{\phi}_b \propto (-1,1,0), \qquad \widetilde{\phi}_c \propto (2,-1,1), \tag{C.18}$$

and new rank-1 matrices $\widetilde{\square}_{ij} = \widetilde{\phi}_i \widetilde{\phi}_j^T$. The inverse of the Majorana mass matrix can then be decomposed in terms of the new matrices as

$$M_N^{-1} = \frac{1}{M_a}(\widetilde{\square}_{ab} + \widetilde{\square}_{ba}) - \frac{M_b}{M_a^2}\widetilde{\square}_a + \frac{1}{M_c}\widetilde{\square}_c. \tag{C.19}$$

Decomposing Y^ν and M_N as per Eqs. (C.15) and (C.19) and applying the seesaw formula, $m_\nu = -v_u^2 Y^\nu M_N^{-1} Y^{\nu T}$, we note that, due the orthogonality of the two sets of vectors, no new matrix structures appear. In particular, there are no mixed terms with ϕ_c, e.g. $\square_{ac}$, nor a structure $\square_a$, either of which would spoil the texture zero in m_ν. The light neutrino mass matrix in fact preserves the same structure as the other mass matrices in the model, i.e.

$$m_\nu = m_a(\square_{ab} + \square_{ba}) + m_b\square_b + m_c\square_c. \tag{C.20}$$

The parameters of the light neutrino mass matrix, m_a, m_b, m_c, are given in terms of $y^\nu_{a,b,c}$ and $M_{a,b,c}$ by

$$m_a = -\frac{v_u^2 y_a^{\nu 2}}{M_a}, \qquad m_b = m_a\left(2\frac{y_b^\nu}{y_a^\nu} - \frac{M_b}{M_a}\right), \qquad m_c = -\frac{v_u^2 y_c^{\nu 2}}{M_c}. \tag{C.21}$$

The above discussion holds true also when the first higher-order terms are introduced. These are given by the superpotential

$$\delta\mathcal{W}_Y = \bar{L}_{\nu,i} N_j H_u \left[\frac{g_d^\nu}{\Lambda^4}(\phi_b^i \phi_c^j + \phi_c^i \phi_b^j) S^2\right] + \bar{L}_{\nu,i} N_j H_u \left[\frac{g_e^\nu}{\Lambda^4}(\phi_a^i \phi_c^j + \phi_c^i \phi_a^j) S^2\right], \tag{C.22}$$

and modify Eq. (C.15) by

$$\delta Y^\nu = y_d^\nu(\square_{bc} + \square_{cb}) + y_e^\nu(\square_{ac} + \square_{ca}), \tag{C.23}$$

which preserves the texture zero. After seesaw, the main effect of these terms can be

absorbed into two additional parameters m_d and m_e and in corrections to the relations in Eq. (C.21). Note that the term dependent on y_e^ν gives rise to a $\square_a$ structure in m_ν, which spoils the texture zero, but appears only strongly suppressed by a factor $(y_e^\nu)^2/M_c$.

C.3 Analytic expression for the leptogenesis parameters

In this appendix we give the analytic expression for λ_ν, i.e. for the Dirac neutrino matrix in the basis where Y_e and M_N are diagonal, as well as for the decay factors $K^\alpha_{N_i}$ and the CP asymmetries $\varepsilon^\alpha_{N_i}$ entering in our numerical calculation.

The Yukawa and Majorana mass matrices share a unified symmetric and hierarchical texture zero,

$$M_\ell = \begin{pmatrix} 0 & a & a \\ a & b+2a & b \\ a & b & c+b-2a \end{pmatrix}, \qquad \ell = e, \nu, N, \tag{C.24}$$

where (a, b, c) stand for either $y^{\nu,e}_{a,b,c}$ or $M_{a,b,c}$. Given this complex symmetric structure with the hierarchy $a < b < c$, the diagonalizing matrices satisfy the relation

$$M'_\ell \equiv V_\ell^T M_\ell V_\ell \approx \text{diag}\left(|a^2/b|, |b|, |c|\right). \tag{C.25}$$

They can be approximated by

$$V_\ell^T = \begin{pmatrix} 1 - \frac{1}{2}\left|\frac{a}{b}\right|^2 & -\frac{a}{b}\left(1 - \frac{2a}{b}\right) & -\frac{2a^2}{bc} \\ \frac{a^*}{b^*}\left(1 - \frac{2a^*}{b^*}\right) & 1 - \frac{1}{2}\left|\frac{a}{b}\right|^2 & -\frac{b}{c} \\ \frac{a^*}{c^*} & \frac{b^*}{c^*} & 1 \end{pmatrix} P_\ell, \tag{C.26}$$

where $P_\ell = \text{diag}(e^{-i(2\gamma-\delta+\pi)/2}, e^{-i\delta/2}, 1)$ is a matrix of phases ensuring the eigenvalues in $\hat{M}_\ell$ are real and positive. With $a \sim \epsilon_\nu^3$, $b \sim \epsilon_\nu^2$, and $c \sim 1$, Eq. (C.26) is accurate (and unitary) to $\mathcal{O}(\epsilon_\nu^3)$, and preserves the (1,1) texture zero to $\mathcal{O}(\epsilon_\nu^4)$. Expanding V_ℓ as $V_\ell = (\mathbb{1} + \Delta V_\ell)P_\ell$, we split λ_ν into two parts, one which preserves Y^ν (up to rephasing) and a correction term $\Delta\lambda_\nu^*$, i.e.

$$\lambda_\nu^* \equiv V_e^T Y^\nu V_N = P_e(\mathbb{1} + \Delta V_e^T)Y^\nu(\mathbb{1} + \Delta V_N)P_N = P_e(Y^\nu + \Delta\lambda_\nu^*)P_N \tag{C.27}$$

where

$$\Delta\lambda_\nu^* \simeq \Delta V_e^T Y^\nu + Y^\nu \Delta V_N \simeq -\begin{pmatrix} y_a^\nu \frac{M_a}{M_b} + y_a^\nu \frac{y_a^e}{y_b^e} & y_b^\nu \frac{y_a^e}{y_b^e} & y_b^\nu \frac{y_a^e}{y_b^e} \\ y_b^\nu \frac{M_a}{M_b} & \mathcal{O}\left(y_a^\nu \frac{M_a}{M_b}\right) & y_c^\nu \frac{y_b^e}{y_c^e} \\ y_b^\nu \frac{M_a}{M_b} & \mathcal{O}\left(y_a^\nu \frac{M_a}{M_b}\right) & \mathcal{O}\left(y_b^\nu \frac{y_b^e}{y_c^e}\right) \end{pmatrix}, \tag{C.28}$$

having discarded the term $\Delta V_e^T Y^\nu \Delta V_N$. Notice that the corrections in $\Delta\lambda_\nu^*$ are typically of the order of Y^ν except in the 22,32 and 33 elements where they are smaller. They are never larger; in this sense λ_ν^* preserves the same hierarchy between the elements as Y^ν. Considering only the first term in Eq. (C.27), $\lambda_\nu^* \sim P_e Y^\nu P_N$, we can deduce for the decay factors:

$$K_{N_1} \sim \frac{v_u^2}{m_*}\left|\frac{y_a^{\nu 2} M_b}{M_a^2}\right| \begin{pmatrix} 0 \\ 1 \\ 1 \end{pmatrix}, \qquad K_{N_2} \sim \frac{v_u^2}{m_*}\left|\frac{y_b^{\nu 2}}{M_b}\right| \begin{pmatrix} \left|\frac{y_a^\nu}{y_b^\nu}\right|^2 \\ 1 \\ 1 \end{pmatrix}, \tag{C.29}$$

and for the CP asymmetries,

$$\begin{aligned} \varepsilon_{N_1} &\sim \frac{3}{8\pi}\left|\frac{y_b^\nu M_a}{M_b}\right|^2 \sin(2\omega_1) \begin{pmatrix} 0 \\ 1 \\ 1 \end{pmatrix}, \\ \varepsilon_{N_2} &\sim \frac{3}{16\pi}\left|\frac{y_c^\nu M_b}{M_c}\right| \begin{pmatrix} \left|\frac{y_a^{\nu 2}}{y_b^\nu}\right| \sin\omega_2 \\ |y_b^\nu| \sin\omega_2 \\ |y_c^\nu| \sin(\omega_2 - \delta_\nu) \end{pmatrix} + \frac{1}{4\pi}\left|\frac{y_a^\nu M_a}{M_b}\right|^2 \sin(2\omega_1) \begin{pmatrix} 0 \\ 1 \\ 1 \end{pmatrix}, \end{aligned} \tag{C.30}$$

where we have called $\omega_1 = [\gamma_N - \gamma_\nu - \delta_N + \delta_\nu]$ and $\omega_2 = [\delta_N - \delta_\nu]$ the leading order leptogenesis phases entering the N_1 and N_2 calculations respectively. Including also the leading-order contributions from $\Delta\lambda_\nu^*$, we obtain analytic approximations for the decay factors and CP asymmetries in terms of the input parameters of our analysis.

Defining $Q = |M_a y_b^\nu / (M_b y_a^\nu)|$, we have

$$\begin{aligned} K_{N_1} &\simeq \frac{v_u^2}{m_*} \left| \frac{y_a^{\nu 2} M_b}{M_a^2} \right| \left(1 - 2Q\cos\omega_1 + Q^2\right) \begin{pmatrix} \mathcal{O}\left(\frac{M_a}{M_b}\frac{y_a^e}{y_b^e}\right) \\ 1 \\ 1 \end{pmatrix}, \\ \varepsilon_{N_1} &\simeq \frac{3}{4\pi} \left| \frac{y_b^\nu M_a}{M_b} \right|^2 \frac{\sin\omega_1(\cos\omega_1 - Q)}{1 - 2Q\cos\omega_1 + Q^2} \begin{pmatrix} \mathcal{O}\left(\frac{M_a}{M_b}\frac{y_a^e}{y_b^e}\right) \\ 1 \\ 1 \end{pmatrix}, \end{aligned} \tag{C.31}$$

and, defining $Q_e = |y_a^e y_b^\nu / (y_b^e y_a^\nu)|$ and $\omega_{1,2}^e = \omega_{1,2}(N \to e)$,

$$\begin{aligned} K_{N_2} &\simeq \frac{v_u^2}{m_*} \left| \frac{y_b^{\nu 2}}{M_b} \right| \begin{pmatrix} \left|\frac{y_a^\nu}{y_b^\nu}\right|^2 \left(1 - 2Q_e\cos\omega_1^e + Q_e^2\right) \\ 1 \\ 1 \end{pmatrix}, \\ \varepsilon_{N_2} &\simeq \frac{3}{16\pi} \left| \frac{y_c^\nu M_b}{M_c} \right| \frac{1}{1 + 2\,\mathrm{Re}\left[\frac{y_a^\nu}{y_b^\nu}\right]} \begin{pmatrix} \left|\frac{y_a^{\nu 2}}{y_b^\nu}\right| \sin\omega_2(1 - 2Q_e\cos\omega_1^e + Q_e^2) \\ |y_b^\nu| \sin\omega_2 - \left|\frac{y_c^\nu y_b^e}{y_c^e}\right| \sin(\omega_2 + \omega_2^e) \\ |y_c^\nu| \sin(\omega_2 - \delta_\nu) \end{pmatrix}. \end{aligned} \tag{C.32}$$

Appendix D

D.1 Angles, phases and CP invariants of the PMNS

All the angles are in the first quadrant $\theta_{ij} \in [0, \pi/2]$ and can be extracted using the PMNS matrix elements as:

$$s^2_{12} = \frac{|V_{e2}|^2}{1-|V_{e3}|^2}, \qquad s^2_{13} = |V_{e3}|^2, \qquad s^2_{23} = \frac{|V_{\mu 3}|^2}{1-|V_{e3}|^2}\,. \tag{D.1}$$

We can define the Jarlskog invariant $J_{\rm CP}$ and similar CP invariants, called I_1 and I_2, for the Majorana phases:

$$J_{\rm CP} \equiv \mathrm{Im}\left[V_{e1}V^*_{13}V^*_{\tau 1}V_{\tau 3}\right] = c_{12}\,c_{23}\,c^2_{13}\,s_{12}\,s_{23}\,s_{13}\sin\delta\,, \tag{D.2}$$

$$I_1 \equiv \mathrm{Im}\left[V_{e2}V_{e2}V^*_{e1}V^*_{e1}\right] = s^2_{12}\,c^2_{12}\,c^4_{13}\,\sin\alpha\,, \tag{D.3}$$

$$I_2 \equiv \mathrm{Im}\left[V_{e3}V_{e3}V^*_{e1}V^*_{e1}\right] = s^2_{13}\,c^2_{12}\,c^2_{13}\,\sin\beta\,. \tag{D.4}$$

The Majorana phases can be derived from the numerical PMNS mixing matrix taking into account the unphysical phases described by the diagonal matrix that multiplies the $V_{\rm PMNS}$ from the left, $\mathrm{Diag}\{e^{i\delta_e}, e^{i\delta_\mu}, e^{i\delta_\tau}\}$. Those can be eliminated with a redefinition of the charged lepton fields. We can extract the Dirac and Majorana phases as

$$\delta = -\arg\left\{\frac{\frac{V_{e1}V^*_{e3}V^*_{\tau 1}V_{\tau 3}}{c_{12}c^2_{13}c_{23}s_{13}} + c_{12}c_{23}s_{13}}{s_{12}s_{23}}\right\},\ \alpha = 2\arg\left\{\frac{V_{e2}}{V_{e1}}\right\},\ \beta = 2\arg\left\{\frac{V_{e3}}{V_{e1}}\right\}. \tag{D.5}$$

For sake of completeness we report the values of the unphysical phases

$$\delta_e = \arg\{V_{e1}\} \quad \delta_\mu = \arg\left\{V_{\mu 3}e^{-i(\beta/2+\delta)}\right\} \quad \delta_\tau = \arg\left\{V_{\tau 3}e^{-i(\beta/2+\delta)}\right\}. \tag{D.6}$$

D.2 Bounds on Mass Insertions

Table D.1 collects the obtained intervals for the LL mass insertions after imposing all the constraints regarding lepton mixing and masses. Specifically, we report the off-diagonal elements of the soft mass matrix for LH sleptons divided by the MSUGRA parameter m_0^2, *i.e.* the value of the MI at the scale of flavor breaking, before RGE evolution. The allowed ranges are specified for each realization of the neutrino mass mechanisms analyzed in this work. In Section 3.5.2, the minimum of those intervals has been employed to constrain the MSUGRA plane $m_0 - M_{1/2}$ for a representative value of $\tan\beta = 10$.

Mechanism			δ_{12}^{LL}	δ_{13}^{LL}	δ_{23}^{LL}
I	$z = 0$	NH	$(3.9 \div 32) \times 10^{-5}$	$(3.9 \div 32) \times 10^{-5}$	$(3.9 \div 32) \times 10^{-5}$
	$x = 0$	IH	$(2.2 \div 9.2) \times 10^{-3}$	$(2.2 \div 9.2) \times 10^{-3}$	$(6 \div 26) \times 10^{-4}$
	$s = 0$	NH	$(1.3 \div 5.8) \times 10^{-3}$	$(1.3 \div 5.8) \times 10^{-3}$	$(1.1 \div 4.8) \times 10^{-3}$
		IH	$(1 \div 15) \times 10^{-3}$	$(1 \div 14) \times 10^{-3}$	$(1.5 \div 18) \times 10^{-3}$
II a-2	$f, g = 0$	IH	$(3.8 \div 21) \times 10^{-3}$	$(3.8 \div 21) \times 10^{-3}$	$(4.6 \div 23) \times 10^{-3}$
	$f, h_i = 0$	NH	$(3.3 \div 29) \times 10^{-3}$	$(3.3 \div 30) \times 10^{-3}$	$(2.7 \div 22) \times 10^{-3}$
		IH	$(3.4 \div 21) \times 10^{-3}$	$(3.4 \div 20) \times 10^{-3}$	$(4.5 \div 25) \times 10^{-3}$
	$h_r, g = 0$	NH	$(2.6 \div 14) \times 10^{-5}$	$(2.6 \div 14) \times 10^{-5}$	$(2.3 \div 12) \times 10^{-5}$
	$h_{r,2}, g = 0$	IH	$(5.8 \div 20) \times 10^{-3}$	$(5.8 \div 20) \times 10^{-3}$	$(1.3 \div 4.3) \times 10^{-3}$
	$h_{r,2}, h_i = 0$	IH	$(5.6 \div 19) \times 10^{-3}$	$(5.6 \div 19) \times 10^{-3}$	$(8.5 \div 26) \times 10^{-5}$
II c-2	$f_i, h_i = 0$	NH	$(2.7 \div 27) \times 10^{-3}$	$(2.7 \div 24) \times 10^{-3}$	$(0.9 \div 16) \times 10^{-2}$
		IH	$(4.8 \div 9.1) \times 10^{-3}$	$(4.8 \div 9.2) \times 10^{-3}$	$(9.4 \div 19) \times 10^{-3}$
	$f_i, f_r = 0$	NH	$(2.8 \div 22) \times 10^{-3}$	$(2.8 \div 21) \times 10^{-3}$	$(8.6 \div 86) \times 10^{-3}$
		IH	$(4.7 \div 8) \times 10^{-3}$	$(4.8 \div 8.1) \times 10^{-3}$	$(1.1 \div 1.9) \times 10^{-2}$
	$h_r, h_i = 0$	NH	$(6.1 \div 15) \times 10^{-3}$	$(6.1 \div 15) \times 10^{-3}$	$(6 \div 15) \times 10^{-3}$
	$h_r, f_r = 0$	NH	$(6.3 \div 22) \times 10^{-3}$	$(6.3 \div 23) \times 10^{-3}$	$(6.2 \div 22) \times 10^{-3}$
	$h_{r,2}, h_i = 0$	NH	$(8.1 \div 20) \times 10^{-3}$	$(8.1 \div 20) \times 10^{-3}$	$(0.8 \div 21) \times 10^{-6}$
	$h_{r,2}, f_r = 0$	NH	$(6.3 \div 22) \times 10^{-3}$	$(6.3 \div 23) \times 10^{-3}$	$(6.2 \div 22) \times 10^{-3}$

TABLE D.1: Obtained intervals for the LL mass insertions: δ_{12}, δ_{13}, δ_{23}. The allowed ranges are specified for each realization of the neutrino mass mechanisms analyzed in this work.

Appendix E

E.1 Minimization of the potential

In order to reduce the number of free parameters, we consider the following relations among coefficients: $\lambda_b \sim \lambda_a$, $\lambda_{(1,3)b} \sim \lambda_{(1,3)a}$, $\lambda_{3a} \sim (\lambda_{1a} + \lambda_{1ab})$, $\lambda_3 \sim (4\lambda_1 + 6\lambda_{13} - 11\lambda'_{13})/16$, $\mu_1 \sim \mu_3$, $\mu_b \sim \mu_a$, $\mu'_b \sim \mu'_a$. They are a total of 8 relations that reduce to 10 the number of free parameters in Eq.(5.21). We choose the following representation for the scalar fields after spontaneous symmetry breaking:

$$\phi_i = v_i + \sigma_i + i\varphi_i. \tag{E.1}$$

The minimization conditions of V in Eq.(5.21), with respect to σ_i read as

$$\begin{aligned}
\left\langle \frac{\partial V}{\partial \sigma_a} \right\rangle &= 2v_a \left[v_a^2 \left(2\lambda_a + \frac{v_b^2}{v_a^2}\lambda_{ab} \right) + v_1^2 \left(\lambda_{1a} + \frac{v_b}{v_a}\lambda_{1ab} \right) + v_3^2(\lambda_{1a} + \lambda_{1ab}) - \mu_a^2 - 2\mu_a'^2 \right] = 0 \\
\left\langle \frac{\partial V}{\partial \sigma_b} \right\rangle &= 2v_b \left[v_b^2 \left(2\lambda_a + \frac{v_a^2}{v_b^2}\lambda_{ab} \right) + v_1^2 \left(\lambda_{1a} + \frac{v_a}{v_b}\lambda_{1ab} \right) + v_3^2(\lambda_{1a} + \lambda_{1ab}) - \mu_a^2 - 2\mu_a'^2 \right] = 0 \\
\left\langle \frac{\partial V}{\partial \sigma_1} \right\rangle &= 2v_1 \left[2v_1^2 \left(\lambda_1 + \frac{v_3^2}{2v_1^2}\lambda_{13} + 3\,\frac{v_3}{2v_1}\lambda'_{13} \right) + 2v_a^2 \left(\lambda_{1a} + \lambda_{1ab} \right) - \mu_1^2 \right] = 0\,, \\
\left\langle \frac{\partial V}{\partial \sigma_3} \right\rangle &= 2v_3 \left\{ \frac{v_3^2}{2} \left[\lambda_1 + 2\left(\frac{v_1^2}{v_3^2} + \frac{3}{4} \right)\lambda_{13} + 2\left(\frac{v_1^3}{v_3^3} - \frac{11}{8} \right)\lambda'_{13} \right] + 2v_a^2 \left(\lambda_{1a} + \lambda_{1ab} \right) - \mu_1^2 \right\} = 0
\end{aligned} \tag{E.2}$$

where the symbol $\langle \cdots \rangle$ denotes that the fluctuating fields are taken to be zero. We obtain the required relations among vevs: $v_b \sim v_a$ and $v_3 \sim -2\,v_1$, while (v_1, v_a) in terms of the λs are given by

$$\begin{pmatrix}
v_1^2 = 0 & v_a^2 = 0 & V_0 = 0 \\
v_1^2 = \dfrac{\mu_1^2}{2\widetilde{\lambda}_1} & v_a^2 = 0 & V_1 = -\dfrac{5\mu_1^4}{4\widetilde{\lambda}_1} \\
v_1^2 = 0 & v_a^2 = \dfrac{\widetilde{\mu}_a^2}{\widetilde{\lambda}_a} & V_2 = -\dfrac{\widetilde{\mu}_a^4}{\widetilde{\lambda}_a} \\
v_1^2 = \dfrac{\mu_1^2 - 2\dfrac{\widetilde{\lambda}_{1a}}{\widetilde{\lambda}_a}\widetilde{\mu}_a^2}{2\widetilde{\lambda}_1 - 10\dfrac{\widetilde{\lambda}_{1a}^2}{\widetilde{\lambda}_a}} & v_a^2 = \dfrac{2\dfrac{\widetilde{\lambda}_1}{\widetilde{\lambda}_a}\widetilde{\mu}_a^2 - 5\dfrac{\widetilde{\lambda}_{1a}}{\widetilde{\lambda}_a}\mu_1^2}{2\widetilde{\lambda}_1 - 10\dfrac{\widetilde{\lambda}_{1a}^2}{\widetilde{\lambda}_a}} & V_3 = \dfrac{-\dfrac{\widetilde{\mu}_a^4}{\widetilde{\lambda}_a} - \dfrac{5\mu_1^4}{4\widetilde{\lambda}_1} + 5\dfrac{\widetilde{\lambda}_{1a}}{\widetilde{\lambda}_a\widetilde{\lambda}_1}\mu_1^2\widetilde{\mu}_a^2}{1 - 5\dfrac{\widetilde{\lambda}_{1a}^2}{\widetilde{\lambda}_a\widetilde{\lambda}_1}}
\end{pmatrix}, \tag{E.3}$$

where $\widetilde{\lambda}_1 = \lambda_1 + 2\lambda_{13} - 3\lambda'_{13}$, $\widetilde{\lambda}_a = 2\lambda_a + \lambda_{ab}$, $\widetilde{\lambda}_{1a} = \lambda_{1a} + \lambda_{1ab}/2$ and $\widetilde{\mu}_a^2 = \mu_a^2 + 2\mu_a'^2$. The only interesting minimum for us is the non-trivial case $v_1, v_a \neq 0$ with $v_1 \ll v_a$, so we require V_3 to be a global minimum. The 4×4 squared mass matrices of the CP-even and -odd bosons (S_i and P_i) are given by

$$\left(M_S^2\right)_{ij} = \frac{1}{2}\frac{\partial^2 V}{\partial\sigma_i \partial\sigma_j} \quad , \quad \left(M_P^2\right)_{ij} = \frac{1}{2}\frac{\partial^2 V}{\partial\varphi_i \partial\varphi_j}\,. \tag{E.4}$$

Using the potential in Eq.(5.21), these matrices acquire the following form

$$M_S^2 \simeq \begin{pmatrix} 2v_1^2(2\lambda_1 - 3\lambda'_{13}) & -v_1^2(-4\lambda_{13} + 3\lambda'_{13}) & 2v_a v_1 \widetilde{\lambda}_{1a} & 2v_a v_1 \widetilde{\lambda}_{1a} \\ -v_1^2(-4\lambda_{13} + 3\lambda'_{13}) & \frac{v_1^2}{2}(8\lambda_1 + 12\lambda_{13} - 21\lambda'_{13}) & -4v_a v_1 \widetilde{\lambda}_{1a} & -4v_a v_1 \widetilde{\lambda}_{1a} \\ 2v_a v_1 \widetilde{\lambda}_{1a} & -4v_a v_1 \widetilde{\lambda}_{1a} & 4v_a^2\lambda_a - \frac{v_1^2}{2}\lambda_{1ab} & 2v_a^2\lambda_a + \frac{v_1^2}{2}\lambda_{1ab} \\ 2v_a v_1 \widetilde{\lambda}_{1a} & -4v_a v_1 \widetilde{\lambda}_{1a} & 2v_a^2\lambda_a + \frac{v_1^2}{2}\lambda_{1ab} & 4v_a^2\lambda_a - \frac{v_1^2}{2}\lambda_{1ab} \end{pmatrix}, \tag{E.5}$$

$$M_P^2 \simeq \begin{pmatrix} -2v_a^2\lambda_{1ab} + 18v_1^2\lambda'_{13} & 3v_1\lambda'_{13} & v_a v_1 \lambda_{1ab} & v_a v_1 \lambda_{1ab} \\ 3v_1^2\lambda'_{13} & \frac{v_1^2}{2}\lambda'_{13} & 0 & 0 \\ v_a v_1 \lambda_{1ab} & 0 & 4\mu_a'^2 - \frac{v_1^2}{2}\lambda_{1ab} & -\frac{v_1^2}{2}\lambda_{1ab} \\ v_a v_1 \lambda_{1ab} & 0 & -\frac{v_1^2}{2}\lambda_{1ab} & 4\mu_a'^2 - \frac{v_1^2}{2}\lambda_{1ab} \end{pmatrix}. \tag{E.6}$$

The physical basis is the flavon mass basis

$$\sigma_j = (U_S)_{ij}\, S_i \quad , \quad \varphi_i = (U_P)_{ij}\, P_j, \tag{E.7}$$

defined where M_S^2 and M_P^2 are diagonal

$$M_S^2 \;\longrightarrow\; U_S^T\, M_S^2\, U_S = \text{diag}\left(m_{S_1}^2, m_{S_2}^2, m_{S_3}^2, m_{S_4}^2\right), \tag{E.8}$$

$$M_P^2 \;\longrightarrow\; U_P^T\, M_P^2\, U_P = \text{diag}\left(m_{P_1}^2, m_{P_2}^2, m_{P_3}^2, m_{P_4}^2\right). \tag{E.9}$$

with eigenvalues

$$m_{S_1}^2 \;\simeq\; 2v_1^2\left(2\lambda_1 - \lambda_{13} - \frac{9}{4}\lambda'_{13}\right) \;\;,\;\; m_{P_1}^2 \simeq -2\,v_a^2\left(\lambda_{1ab} + \frac{v_1^2}{2v_a^2}(\lambda_{1ab} - 18\lambda'_{13})\right), \tag{E.10}$$

$$m_{S_2}^2 \;\simeq\; 2\,v_1^2\left(2\widetilde{\lambda}_1 - \frac{5}{2}\frac{\widetilde{\lambda}_{1a}^2}{\widetilde{\lambda}_a}\right) \quad , \; m_{P_2}^2 \simeq v_1^2\frac{\lambda'_{13}}{2}, \tag{E.11}$$

$$m^2_{S_3} \simeq 2v_a^2\left(2\lambda_a - \lambda_{ab} - \frac{v_1^2}{2v_a^2}\lambda_{1ab}\right) \quad , \quad m^2_{P_{3,4}} \simeq 4\,{\mu'_a}^2\,, \tag{E.12}$$

$$m^2_{S_4} \simeq 2v_a^2\left(2\lambda_a + \lambda_{ab} + 10\,\frac{v_1^2}{v_a^2}\frac{\widetilde{\lambda}^2_{1a}}{\widetilde{\lambda}_a}\right). \tag{E.13}$$

where we have expressed $\mu^2_{1,a}$ with their value at the minimum using (E.3). The diagonalization matrices, U_S, U_P, at $\mathcal{O}(v_1/v_a)$ can be written as

$$U_S = \begin{pmatrix} \frac{2}{\sqrt{5}} & -\frac{1}{\sqrt{5}} & 0 & \frac{\sqrt{2}v_1}{v_a}\frac{\widetilde{\lambda}_{1a}}{\widetilde{\lambda}_a} \\ \frac{1}{\sqrt{5}} & \frac{2}{\sqrt{5}} & 0 & \frac{-2\sqrt{2}v_1}{v_a}\frac{\widetilde{\lambda}_{1a}}{\widetilde{\lambda}_a} \\ 0 & \frac{5\sqrt{2}v_1}{v_a}\frac{\widetilde{\lambda}_{1a}}{\widetilde{\lambda}_a} & -\frac{1}{\sqrt{2}} & \frac{1}{\sqrt{2}} \\ 0 & \frac{5\sqrt{2}v_1}{v_a}\frac{\widetilde{\lambda}_{1a}}{\widetilde{\lambda}_a} & \frac{1}{\sqrt{2}} & \frac{1}{\sqrt{2}} \end{pmatrix}, \; U_P = \begin{pmatrix} -1 & 0 & \frac{v_1}{\sqrt{2}v_a} & 0 \\ 0 & 1 & 0 & 0 \\ \frac{v_1}{\sqrt{2}v_a} & 0 & \frac{1}{\sqrt{2}} & -\frac{1}{\sqrt{2}} \\ \frac{v_1}{\sqrt{2}v_a} & 0 & \frac{1}{\sqrt{2}} & \frac{1}{\sqrt{2}} \end{pmatrix}. \tag{E.14}$$

The computation of the radiative diagram and the contribution to the anomalous magnetic moment in the flavon mass basis are given by

$$m_{\rm e}^{\rm RAD} = 2\,\frac{g_{\rm e}^4}{16\pi^2}\frac{v_H}{\sqrt{2}}\varepsilon_1\,\Delta I_m \quad , \quad m_{\mu}^{\rm RAD} = \frac{g_{\mu}^3}{16\pi^2}\frac{v_H}{\sqrt{2}}\,\Delta I_m, \tag{E.15}$$

$$\Delta a_e = 2\frac{g_{\rm e}^4}{8\pi^2}\frac{v_H}{\sqrt{2}}\frac{m_{\rm e}}{M_\chi^2}\varepsilon_1\,\Delta I_{\Delta a} \quad , \quad \Delta a_\mu = \frac{g_{\mu}^3}{8\pi^2}\frac{v_H}{\sqrt{2}}\frac{m_\mu}{M_\chi^2}\Delta I_{\Delta a}. \tag{E.16}$$

where we have defined

$$\Delta I = \sum_{i=1}^{4}\left[(U_S)^2_{1,i}\,I(x^2_{S_i}) \;-\; (U_P)^2_{1,i}\,I(x^2_{P_i})\right]. \tag{E.17}$$

In the case $M_\chi, \mu_{\phi,1} \gg m_\ell$, the loop functions are

$$I_m(x_\phi) = \frac{1 - x_\phi^2(1 - 2\log x_\phi)}{1 - x_\phi^2} \quad , \quad I_{\Delta a}(x_\phi) = \frac{1 - 4x_\phi^2 + x_\phi^4(3 - 4\log x_\phi)}{2(1 - x_\phi^2)^3}. \tag{E.18}$$

From Eq.(E.14) we see that, up to order $\mathcal{O}(v_1/v_a)$, we have $(U_S)_{1,i} = (2/\sqrt{5}, -1/\sqrt{5}, 0, 0)$ and $(U_P)_{1,i} = (-1, 0, 0, 0)$. Therefore, as already mentioned, in the calculation of $m_\ell^{\rm RAD}$ and Δa_ℓ only $S_{1,2}$ and P_1 play a significant role. The Eqs.(E.15) and (E.16) are very well approximated by the Mass Insertion Approximations of Eqs.(5.24-5.27).